Azulene-based Dyes for Dye Sensitised Solar Cells

Cowper, Paul

Award date:
2017

Awarding institution:
University of Bath

Azulene-based Dyes for Dye Sensitised Solar Cells

Paul Cowper

A thesis submitted for the degree of Doctor of Philosophy

University of Bath

Department of Chemistry

June 2017

..... *(date)*

..... (*signature*)

Science is the belief in the ignorance of experts.

RICHARD P. FEYNMAN

Contents

Achnowledgements

There are many people I would like to thank for their support, guidance and friendship over the course of my PhD. I would like to thank my supervisors Dr Simon Lewis and Dr Petra Cameron for giving me the opportunity to work with them over the last four years. I am extremely grateful for all of the help and guidance they have given me throughout my PhD and for their endless enthusiasm, even when things haven't gone to plan.

Thanks to Dr Gabriele Kociok-Köhn for running my X-ray crystal structures, Dr John Lowe and Dr Catherine Lyall for all their help with NMR, and Dr Anneke Lubben for her help with various mass spectrometry problems.

I would like to thank members of both the Lewis and Cameron groups past and present who have made my time in the labs most enjoyable and have been excellent colleagues and friends: Monika, Catherine, Julia, Anthony, Matthew, Toby, Ben, Simone, Afi, Kat, Tom, Shane, Ralf, Adam and Wentao.

Finally I would like to thanks my wife Claire for her unfailing support and encouragement in everything I do and my family for putting up with me all these years.

Declaration of Work Done in Conjunction with Others

The NOESY NMR spectrum discussed in section 4.3.1 was acquired by a fellow PhD student, Catherine Lyall.

The dye sensitised solar cells described in section 5.7.3 were fabricated and tested (with my assistance) by a fellow PhD student, Adam Pockett.

Much of the laboratory work to synthesise and characterise arylated azulene compounds to optimise the azulene sulfonium salt coupling reactions was undertaken by two project students, Michael Turton (MChem) and Yu Jin (MSc).

Abstract

This thesis studies the synthesis of azulene-based donor-π-acceptor organic dyes for application as the sensitising component of dye sensitised solar cells (DSSCs). Ruthenium (II) polypyridyl complexes have been widely studied and have been used to great success during the past 25 years; however, ruthenium is scarce and expensive. Ruthenium-free dyes have been the subject of intense research globally, and organic, metal-free dyes are attractive substitutes for ruthenium (II) sensitisers because of the wide availability of the starting materials and low cost.

Azulene is a simple, blue-coloured hydrocarbon with a ground-state dipole and a tendency for electron transfer between its seven- and five-membered rings. Its electronic and photo-physical properties and its ability to support a positive charge while remaining partially aromatic make it an interesting proposition for use in photovoltaic cells.

This thesis begins by discussing the rationale behind and design of DSSC sensitisers using azulene as the electron donor in a donor-electron rich π linker-acceptor push-pull dye structure. Extended Hückel molecular orbital calculations are used to identify potential molecular structures.

The thesis goes on to describe the synthesis of the identified target molecules to produce a range of azulene-based dyes over three separate iterations or generations, with the second and third generations designed to build on and enhance the dyes created in the earlier generations.

Electrochemical and spectroscopic studies are used to assess the suitability of the dyes synthesised for use in DSSCs and, for the first two generations, DSSCs are fabricated and evaluated to determine the effect of structural variations on photovoltaic efficiency.

Finally, a crystallography study examines the molecular structure of the azulene-based dyes and discusses the geometry of the molecules with reference to their use in DSSCs.

List of Abbreviations and Symbols

Chemical and experimental

Ac	acetyl
aq.	aqueous
Ar	aromatic
bipy	2,2'-bipyridine
Bu	butyl
conc.	concentrated
DMF	N,N-Dimethylformamide
DMSO	dimethylsulfoxide
Et	ethyl
FTO	fluorine-doped tin oxide
h	hour(s)
IPA	isopropanol
Me	methyl
min	minute(s)
O/N	overnight
rt/RT	room temperature
s	second(s)
sat.	saturated
t-/*tert*-	tertiary
TBAHFP	tetrabutylammonium hexafluorophosphate (NBu_4PF_6)
4-TBP	4-*tert*-butylpyridine

Electrochemical and photochemical

CE	counter electrode
CV	cyclic voltammetry/voltammogram
E_{CB}	conduction band energy
E_F	Fermi energy level
E_{VB}	valence band energy
E^0	standard electrode potential
$E^{0'}$	formal electrode potential
$E_{0\text{-}0}$	zero-zero transition energy
$E_{½}$	half wave potential
E_{pa}	Peak anodic (oxidation) potential

E_{pc}	peak cathodic (reduction) potential
eV	electron volt
HOMO	highest occupied molecular orbital
I_{pa}	peak anodic current
I_{pc}	peak cathodic current
LUMO	lowest unoccupied molecular orbital
NHE	normal hydrogen electrode
RE	reference electrode
SCE	saturated calomel electrode
SHE	standard hydrogen electrode
WE	working electrode

Analytical and techniques

COSY	correlation spectroscopy
d	doublet
dd	doublet of doublets
ESI-TOF	electrospray time-of-flight
HMBC	heteronuclear multiple-bond correlation spectroscopy HMQC heteronuclear multiple-quantum correlation spectroscopy
HRMS	high-resolution mass spectrometry
IR	infra-red
IPCE	incident photon to current efficiency
J	coupling constant
MALDI	matrix assisted laser desorption ionization
MHz	megahertz
m/z	mass to charge ratio
NMR	nuclear magnetic resonance
q	quartet
s	singlet
t	triplet
UV	ultraviolet
Vis	visible

Photovoltaic devices

AM	air mass
DSSC	dye-sensitized solar cell
FF	fill factor
I-V	current-voltage
J_{SC}	short-circuit current density
η	solar-to-power conversion efficiency
P_{in}	power input (solar power incident on the DSC)
P_{max}	maximum power point
PV	photovoltaic
V_{OC}	open-circuit photovoltage

1 Introduction

1.1 Renewable Energy

The human quality of life depends a great deal on the availability of energy. In the current age, most of the energy consumed by humans is derived from the combustion of fossil fuels in the form of natural gas, petroleum and coal. The problems associated with this are well known:

- Emissions from the combustion of fossil fuels cause damage to the environment, eg acid rain caused by sulfur dioxide released from coal fired power stations, and are blamed for causing or accelerating climate change through global warming;
- Fossil fuels are a finite resource. As the resources become more scarce the cost of extraction will escalate rapidly and subsequently so will the price of energy (and other dependant manufactured commodities);
- The dwindling fossil fuel resources are often concentrated in politically unstable areas of the world and therefore there are issues with security of supply to countries without natural reserves.

Nuclear fission has been used as an alternative to fossil fuel combustion since 1956 (Calder Hall, UK). Proponents of nuclear power claim that it can provide clean, safe and secure energy on a large scale. Emissions to the atmosphere (CO_2, SO_2) are very low compared to equivalent coal powered electricity generation and security of supply can be ensured by stockpiling fuel at the power station; however there are largely unresolved problems associated with dealing with the hazardous radioactive waste. In addition, notable nuclear accidents (eg Calder Hall, UK in 1957, Three Mile Island, USA in 1979, Chernobyl, Russia in 1986 and Fukushima, Japan in 2011) which caused widespread and long-lived radioactive contamination, have cast doubt on the safety of the technology. Opponents to nuclear power also cite the possibility of nuclear materials falling into the hands of terrorists as a potent risk.

Human quality of life may therefore be threatened unless alternative energy resources can be developed soon. Alternative energy sources include wind, waves, biofuel, biomass, hydroelectric and solar, all ultimately relying on energy from the

sun which is (at least for the next few billion years) regarded as an inexhaustible supply and, together with tidal energy and geothermal heat, are collectively known as renewable energy or just "renewables".

About 16% of global energy consumption comes from renewables,[1] with 10% from biomass (wood) used for traditional heating and 3.4% from hydroelectricity. Other renewables account for another 3%. Around 19% of electricity generation is via renewables, 16% of this being hydroelectricity and 3% others, chiefly wind power which is growing at 20% annually.

1.2 Energy from the Sun

Solar power is the conversion of sunlight into electricity, directly using photovoltaics (PV) or indirectly using concentrated solar power (CSP). CSP systems use lenses and mirrors to focus a large area of sunlight onto a small area where the concentrated energy is used to generate steam to drive turbines. PV systems convert light into electricity using the photovoltaic effect, a phenomenon related to the photoelectric effect, where photo-excited electrons remain within the irradiated material rather than being ejected from it. PV is the fastest growing renewable energy technology since 2004 when it overtook wind energy, with capacity doubling every two years since 2007.[2]

About 174 petawatts (PW) reaches the Earth's upper atmosphere from the Sun. Approximately 30% of this is reflected back into space with the rest being absorbed by clouds, oceans and land.[3] The total energy absorbed by the Earth is therefore approximately 439 exajoules (EJ) per hour, which in 2002 was more than the annual human energy consumption.[4] Solar energy therefore represents a huge resource that could provide large amounts of electrical energy if we could capture just a small fraction of it.

1.3 Photovoltaics

All current photovoltaic devices are built on the properties of semiconductors. Semiconductors are materials that have electrical properties that fall in between electrical insulators and conductors.

1.3.1 Insulators and Conductors[5]

Materials can be broadly classified into electrical insulators and conductors. A conductor is a material that contains moveable electric charges. In metals, the moveable charges are electrons, ie negative charges. Moveable positive charges occur as cations in electrolytes or as protons within the polymer electrolyte membrane of a fuel cell, for instance. Insulators are non-conducting materials with few mobile charges and therefore no or insignificant electric current.

The band structure of a solid material describes ranges of energy that an electron may have, ie are allowed, and ranges of energy that it may not have or are forbidden. Figure 1 shows a simple band diagram where the vertical axis represents a continuous range of energy states with the highest energy states at the top. E_V is the top of the valence band, E_C is the bottom of the conduction band and E_{VAC} is the vacuum energy, ie the energy at which an electron would be ejected from the surface. E_F is the Fermi level which denotes the energy state that has a 50% probability of being occupied by an electron. E_{ea} is the electron affinity which is the quantity of energy released when an electron is added to a neutral atom or molecule and ϕ is the work function of the material which is the energy required to remove an electron to a point immediately outside the solid surface. The energy range between E_V and E_C is the band gap E_g which contains forbidden energy states.

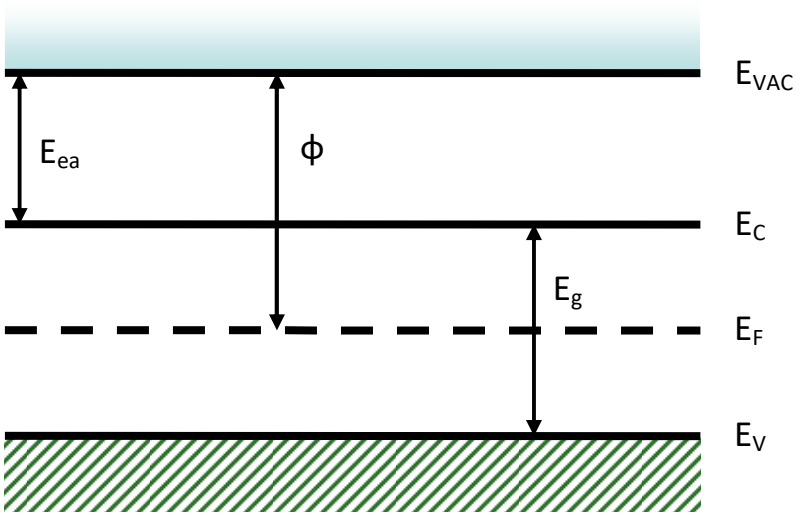

Figure 1. Simple band diagram

In the valence band, electrons are bound to individual atoms or molecules. To be a mobile charge carrier, an electron must be in the conduction band, where it may

travel through the crystal. For a metal, the Fermi level is in the conduction band, so that the band is partly filled. For an insulator, the Fermi level lies in the band gap, so the conduction band is essentially empty or contains very few occupied energy states.

1.3.2 Semiconductors

Semiconductors fall between electrical insulators and conductors, and have a narrower band gap than insulators. For semiconductors the Fermi level is in the band gap but because the band gap is narrower the electron energy distribution means, at temperatures greater than 0 K, some energy states in the conduction band are occupied and so become mobile charge carriers.

Because electrons can be thermally excited, the Fermi level is influenced by temperature and governed by the Fermi-Dirac distribution;[6] increasing the temperature raises the Fermi level and therefore increases the number of occupied states in the conduction band. Adding small quantities of impurities (doping) changes the number of charge carriers (electrons or holes) and therefore changes the Fermi level, resulting in increased mobile negative charge carriers in the conduction band or positive charge carriers in the valence band. Increasing the number of mobile charge carriers increases the electrical conductivity of the material.

Semiconductor materials form the foundation of modern electronic devices and appliances including computers, radios, televisions, mobile phones etc. and photovoltaic cells.

1.3.3 Photovoltaic Cells

Photovoltaic (PV) cells are a method of generating electrical power from solar energy using semiconductors that exhibit the photovoltaic effect. The photovoltaic effect is related to the photoelectric effect. In the photoelectric effect, electrons are ejected from the surface of the material following absorption of a photon, ie the photon must have sufficient energy to equal or exceed the work function of the material. In the photovoltaic effect, electrons are sufficiently excited to move from the valence to the conduction band but not to be ejected from the material, ie the photon must

have energy equal to or greater than the band gap energy, but less than the work function of the semiconductor.

Currently, the dominant PV technology uses silicon as the semiconductor material. Intrinsic (ie undoped) silicon is a poor conductor of electricity at room temperature.

1.3.4 Silicon p-n Junction

As already stated above, a semiconductor may be doped to introduce charge carriers into the crystal matrix. Silicon is in group four of the periodic table and has four valence electrons.

If silicon is doped with small quantities of an element from group three (usually boron is used), with three valence electrons, the resulting crystal lattice contains vacancies or holes (positive charge carriers) in the valence band creating p-type material. If silicon is doped with small quantities of an element from group five (usually phosphorus, arsenic or antimony), with five valence electrons, the resulting crystal lattice contains loosely bound electrons which don't incorporate easily into the diamond crystal structure. At temperatures above 50-100 K, these electrons (negative charge carriers) are almost all donated to the lattice as a whole and enter the conduction band. This is n-type material.

In n-type silicon the Fermi level is increased and lies closer to the conduction band and conversely, in p-type silicon the Fermi level is decreased and lies near the valence band (Figure 2).

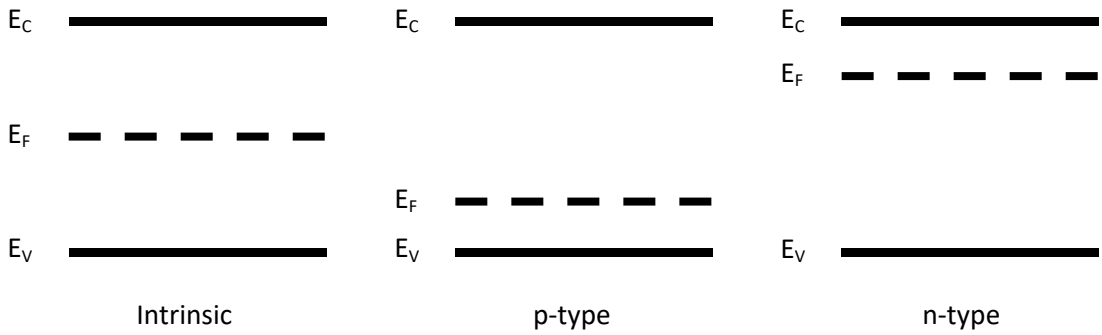

Figure 2. Fermi levels in intrinsic and doped semiconductors

When a junction is formed between p- and n-type semiconductor materials, the resulting charge carrier concentration gradients (high concentration of holes on the

p- side and high concentration of electrons on the n- side) cause diffusion of carriers to take place. Holes diffuse from the p- side to the n- side and electrons from the n- side to the p- side. This causes an electric field to be established which opposes the flow of charge carriers, and thus a state of equilibrium is reached. At equilibrium there is no net flow of charge carriers, ie the net current is zero. Because there has been separation of charges, there is a net potential difference across the junction, called the contact potential. This forms a built-in potential barrier, in that it is necessary for the maintenance of equilibrium at the junction. The region from which charge carriers have diffused in establishing the equilibrium is called the transition region (W) and since it contains few or no charge carriers it is also known as the depletion zone.

The contact potential causes the bands to separate; the valence and conduction bands are higher on the p- side of the junction than on the n- side, corresponding to the product of the electron charge (q) and the contact potential (V_0). The band separation is just enough to make the Fermi level constant across the junction (Figure 3).

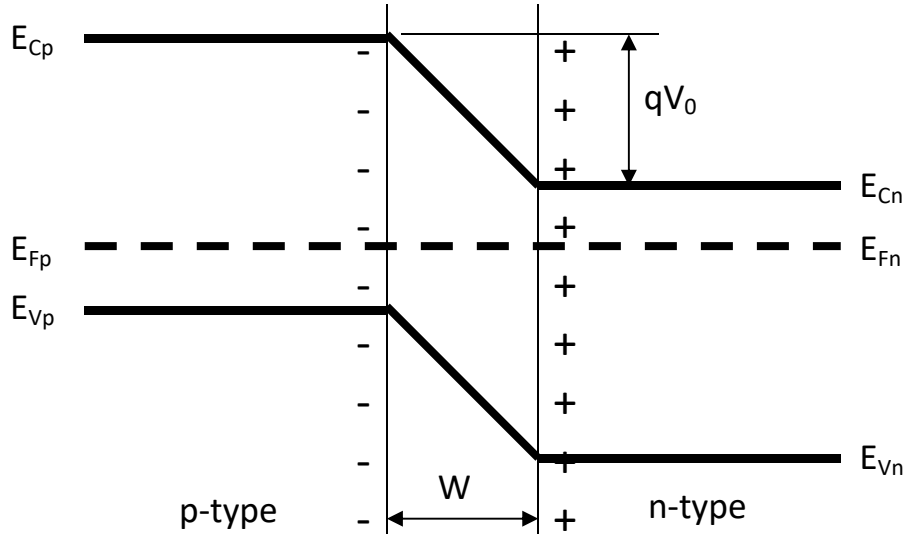

Figure 3. p-n Junction at equilibrium

A useful feature of the p-n junction is that electrons will flow freely in the n- to p- direction (conventional current flows p- to n-) when the n- region has a negative external voltage relative to the p- region (called forward bias), whereas virtually no electrons will flow if the potential is reversed. Applying a forward bias lowers the electrostatic potential at the junction whereas applying a reverse bias has the

opposite effect, raising the electrostatic potential. Electrons begin to flow from n- to p- once the applied forward bias is sufficient to overcome the contact potential. For silicon devices, this corresponds to a potential of less than 1 V.

1.3.5 Silicon PV Cells – 1st Generation

The most common silicon PV devices use single crystal silicon (c-Si) with a single p-n junction to create an electric field within the semiconductor, as described above. A schematic diagram showing the construction of a silicon PV cell is shown below (Figure 4).

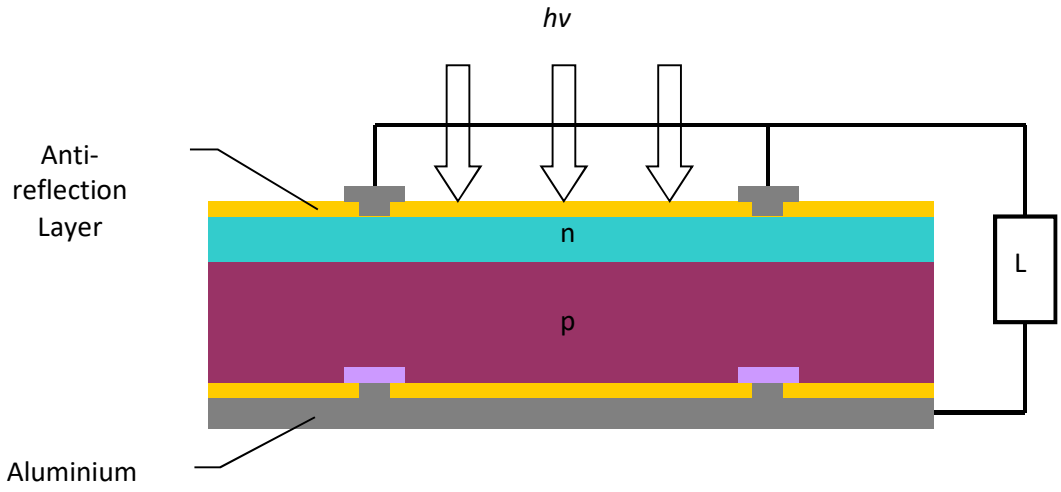

Figure 4. Silicon PV Cell cross-section

The lower aluminium sheet forms the anode which is connected to a layer of p type silicon via contact holes through an insulating layer. The n-type silicon is deposited on top of the p-type silicon and is just a few microns thick, so the area of the p-n junction is large compared with the volume of n-type silicon. In single crystal devices, which are the most efficient, the n-type layer is grown epitaxially onto a p-type substrate by chemical vapour deposition (CVD) pyrolysis of silane at about 1000 °C. With polycrystalline silicon (polysilicon or just 'poly') devices polysilicon is deposited by CVD at a relatively lower temperature of about 400 °C. The n- dopant is usually phosphorus, introduced by adding a small amount of phosphine to the silane stream. Metal contacts, through contact holes in a transparent protection and anti-reflection layer, form the cell cathode.

Photons incident on the n- region of the silicon cause electrons to be excited into the conduction band. The holes created in the n- region by photo-excitation drift

through the n- type silicon as minority carriers until they are swept across the p-n junction into the p- region. If the potential thus created in the n- region is sufficient to overcome the contact potential of the p-n junction, some excited electrons could also cross the junction into the p- region. Absorption of photons therefore creates a potential in the n- region with a magnitude up to the contact potential. This corresponds to the maximum open circuit voltage of the cell and can be used to drive electrons through a load (L) via the external circuit to the p region of the semiconductor. The electrons then combine with holes in the p region.

The current generated depends on the illuminated area but typically is in the 10-100 mA range for a junction with an area in the order of 1 cm^2.

1.3.6 Thin Film PV Cells - 2nd Generation

2nd generation solar cells are based on thin film technologies, eg amorphous silicon (a-Si), copper indium gallium selenide (CIGS) and cadmium telluride (CdTe). They also use a single p-n junction to create an internal electric field. They have a cost advantage over c-Si 1st generation cells, a wider range of applications and the possibility of using flexible substrates.[7]

The most established thin film technology is amorphous silicon (a-Si). The high costs of manufacturing equipment, pure gasses and energy used in manufacturing mean that the cost of a-Si is not much less than that of c-Si. Lab efficiencies of up to 13.5% have been achieved with module efficiencies of 5-6%.

For CdTe, lab efficiencies of 16.7% and module efficiencies of 10.9% have been reported; however drawbacks include toxicity and scarcity of materials. For CIGS, efficiencies of 19.9% in the lab and 13.5% in modules are possible.[8]

1.3.7 Dye Sensitised Solar Cells (DSSC) – Generation 2½?

3rd generation PV cells will potentially overcome the Shockley-Queisser limit[9] of 31-41% power efficiency for single bandgap devices. 3rd generation systems include multi-layer or tandem a-Si or a-GaAs. There is also a goal to reduce the production cost to < US$0.50 / W.

According to Hagfeldt *et al.*,[7] DSSCs can be considered as being between 2nd and 3rd generation solar cells, with the potential to become 3rd generation by utilising the nano-scale properties of the device. Presently, DSSCs offer several advantages including:

- Low production cost (ie cost of materials and processing) and low capital costs (ie cost of equipment);
- Possibility of lightweight and flexible cells by using non-rigid plastic substrates instead of glass;
- Transparency and multi-colour options leading to design opportunities in buildings and consumer goods;
- No scarce material usage with feedstock availability to enable mass production;
- Low toxicity materials;
- Good performance under real outdoor conditions (diffuse light and high temperatures) and outperforms competing devices for indoor applications;

DSSCs differ in their *modus operandi* from 1st and 2nd generation photovoltaics in that there is no p-n junction within the semiconductor material to create an internal electric field. Charge separation differs from the electron-hole generation mechanism described above and instead occurs via removal of an electron from a photo-exited dye molecule (oxidation) to the conduction band of a wide-bandgap semiconductor material (electron injection). The dye molecule is then rapidly regenerated (reduced) by transfer of an electron from a redox electrolyte with which it is in contact. An electrical potential is therefore created between the semiconductor and the electrolyte.

Peter[10] has described the driving force of DSSCs (and other PV devices) in terms of free energy changes and the effects of charge development at the semiconductor-electrolyte interface on the band structure of the semiconductor.

The construction of a typical DSSC is shown in Figure 5. Generation of photocurrent in a DSSC occurs when light is absorbed by the sensitiser dye which generates excited dye molecules with subsequent ultra-fast electron injection into the conduction band of the titanium dioxide. The injected electrons migrate through the interconnected network of sintered TiO_2 particles until they reach the conducting

glass substrate. The dye molecule, which has become oxidised by the electron injection process, is regenerated by electron transfer from the electrolyte iodide ions, generating I_3^- ions. The I_3^- ions diffuse to the platinum coated counter electrode (cathode) where they are reduced to I^- ions by electrons re-entering the cell from the external circuitry, completing the cycle.

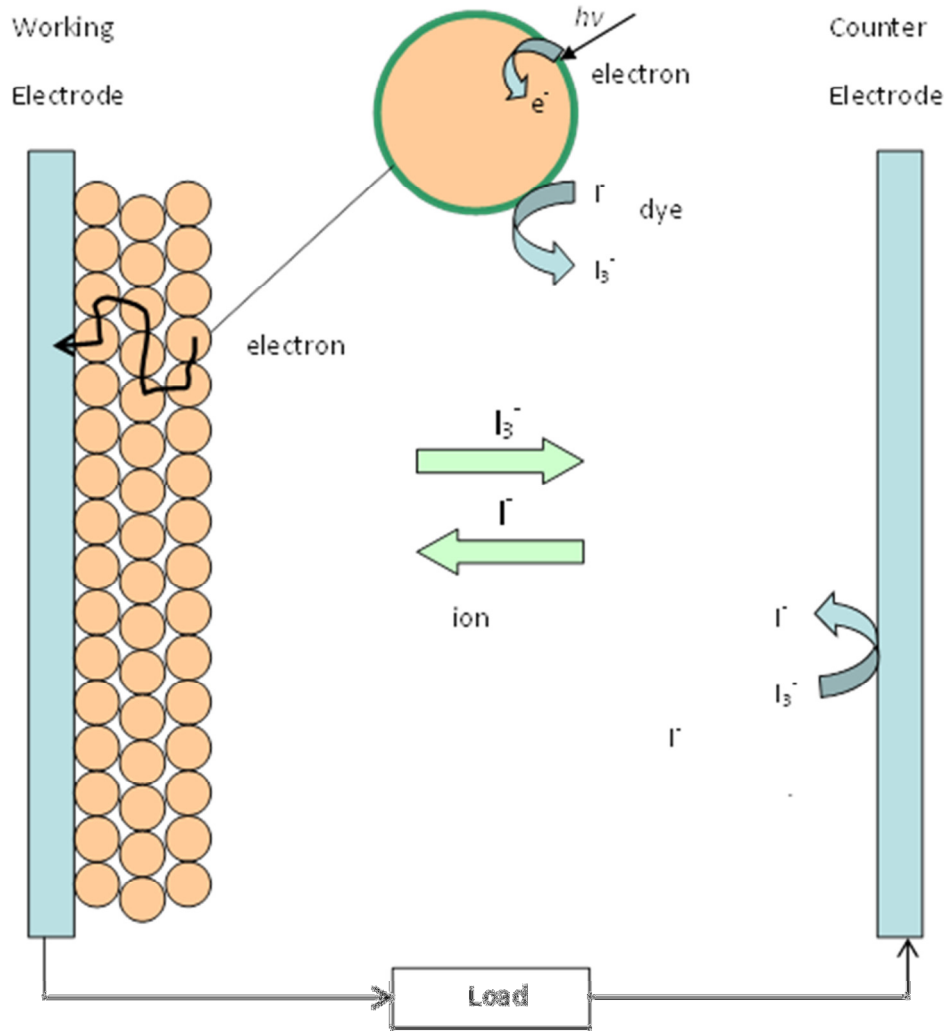

Figure 5. DSSC Cell

1.3.8 Dye Sensitisation of Semiconductors

The sensitisation of semiconductors using organic dyes dates back to the 19th century when dyes were first used in silver halide photographic emulsions to improve their spectral response. The mechanism of this system wasn't worked out until much later, however, after the development of quantum theory in the early part of the 20th century.

In 1937 Gurney and Mott at the University of Bristol applied quantum mechanics to "The Theory of the Photolysis of Silver Bromide and the Photographic Latent Image".[11] The authors describe how light quanta (photons) are absorbed by a photographic silver halide emulsion. Halide ions are oxidised following absorption of a photon and release an electron into the conduction band of the silver halide crystal. The free electron is then able to move through the crystal until it meets with a "speck" of elemental silver where it is trapped by falling into the lower energy conduction band of the metal. The then negatively charged silver metal attracts positive silver ions which are able to diffuse through the crystal. When a silver ion meets the silver metal it is reduced by the electron, thus causing the silver "speck" to grow.

The exposure to light of the silver halide emulsion creates a latent image comprising silver halide crystals containing small amounts of elemental silver. The silver metal then catalyses reduction of the entire silver halide crystal in the subsequent development process which generally employs a hydroquinone reducing agent.

Gurney and Mott reasoned that the mechanism of silver ion reduction must involve movement of electrons through the silver halide crystal because:

a. photon incidence onto a silver halide crystal must be random and uniformly distributed but resulting silver metal occurred in "specks" within the crystal rather than discrete atoms; and
b. it had been previously noted (Lehfeldt 1935) that photon absorption was accompanied by a photoelectric current.

AgCl and AgBr emulsions are sensitive only to light of wavelengths below 400 nm and 500 nm respectively, ie AgCl lacks sensitivity to green and red light (together making yellow) and AgBr lacks sensitivity to red. For pictures that correspond to human monochrome or colour perception therefore this sensitivity range must be extended. This is achieved through the use of dyes that are adsorbed onto the surface of the silver halide crystals. The adsorbed dyes perform the function of absorbing and transferring photonic energy to the silver halide crystals.

There are two basic mechanisms for sensitisation,[12] either:

a. An electron from an excited state of the sensitising dye tunnels through the energy barrier between the dye molecule and the surface of the silver halide crystal; or
b. The excitation energy of the sensitising dye is directly transferred to the silver halide.

Mechanism a. involves charge separation by oxidation of the dye molecule and "injection" of the removed electron into the conduction band of the silver halide crystal. Mechanism b. involves transfer only of the energy of excitation, ie the dye does not become oxidised; the excited dye molecule returns to its ground state and the excitation energy is transferred to the crystal where it causes an electron from a halide ion to enter the conduction band of the silver halide. Direct energy transfer may occur either via a dipole-dipole interaction (FRET) or an electron exchange (Dexter) route.

Kuhn et al[13] were able to differentiate between the two mechanisms by placing the sensitiser dye molecules at well-defined distances from the silver halide crystal surface through the use of fatty acid monolayers or extended alkyl side chains on the sensitising dyes. They found that both mechanisms are effective, but the proportions of each depended on the conditions and systems used.

Application of semiconductor dye sensitisation to solar power generation seems unlikely given the small amount of dye that can be in contact with a single crystal electrode and the subsequent low photocurrent that could be generated. In 1976 it was demonstrated[14] that using a porous microcrystalline layer of ZnO on top of the single crystal produced larger photocurrents due to the much larger surface area available for dye adsorption and light harvesting. However it wasn't until the seminal paper of O'Regan and Grätzel[15] in *Nature* fifteen years later that it was shown that an efficient (>7%) solar cell could be fabricated using a mesoporous layer of titanium dioxide sensitised with an adsorbed ruthenium dye complex. Since then, cells with efficiencies greater than 11% have been reported[16].

The best performing dyes used for DSSCs are still the ruthenium based complexes, eg N3 and N719 (Figure 6). Other types of dyes have also been investigated, including complexes of other transition metals (copper, cobalt, zinc) and many classes of organic, metal-free dyes.

1.4 Ru(II)-free Dyes for Dye Sensitised Solar Cells (DSSC)

1.4.1 Introduction

The best efficiencies for DSSCs have historically been reported with Ru(II) polypyridyl dyes.[17,18,19,20,21] Key examples include the well-established N3 and N719 dyes (Figure 6) and their functionalised derivatives.[22,23] These dyes have a wide absorption range from the visible to the near infrared and exhibit good thermal and chemical stability.

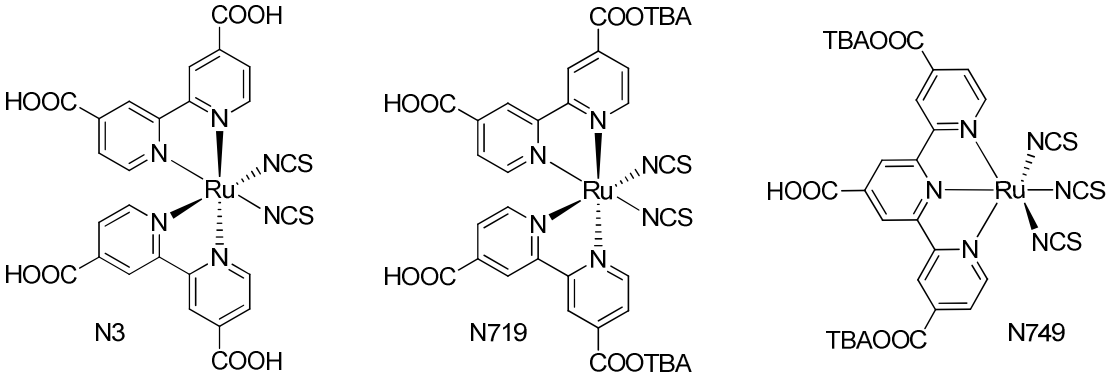

Figure 6. Ruthenium Dyes (TBA = tetrabutylammonium cation)

The most efficient and commonly used dyes include N719[24] and N749[25] (Figure 6). New series of Ru(II) polypyridyl dyes have been developed over recent years. The primary theme has been the addition of π-conjugated systems such as thiophene and its functionalised derivatives to one of the bipyridyl ligands, eg dye C101[18] (Figure 7). The effect of these additions is to increase and broaden absorption and also to induce a bathochromic shift towards the infra-red region of the spectrum where Ru(II) polypyridyl dyes are weak. Alternatively, the NCS ligands have been removed altogether using tridentate ligands, eg dye TF3[21] (Figure 7).

Ru(II)-based dyes are not suitable for cost-effective, environmentally-friendly photovoltaic systems because ruthenium is a rare and expensive metal which limits their wide application. Efficiencies of DSSCs based on Ru(II)-free dyes have, however, greatly improved recently. Many examples of dyes that exhibit outstanding efficiencies have been reported.[26,27,28,29,30] Most of these new dyes have extended conjugated systems and high molar extinction coefficients leading to good light-harvesting properties. This makes them good candidates for DSSCs based on liquid electrolytes other than the iodide/tri-iodide system used with Ru(II) based

dyes, eg Co(II)/Co(III)[31] and ferrocene/ferrocenium[32] electrolytes. Dyes with high extinction coefficients are required because the TiO_2 films need to be thinner to avoid electron/dye$^+$ recombination which leads to a reduction in cell voltages.

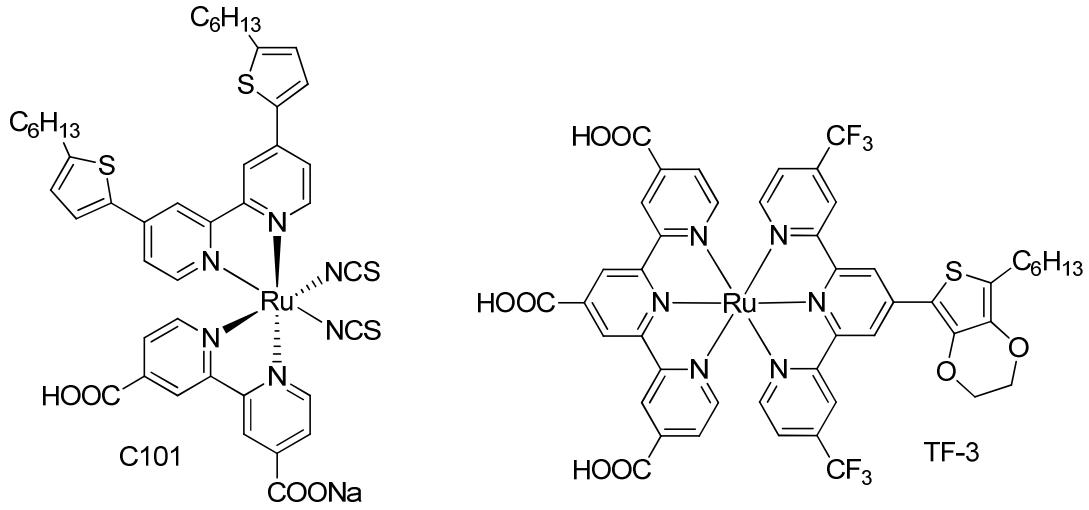

Figure 7. Ru(II) dyes with attached π-conjugated systems

Many classes of Ru(II)-free dyes have been reported for use in DSSCs, including porphyrins, phthalocyanines, squaraines and donor-(π linker)-acceptor (D-π-A) dyes. Some of these classes of dyes have been shown to function better in DSSCs based on electrolytes which are less corrosive than iodide/tri-iodide which may mean better long term DSSC stability.

1.4.2 Porphyrins and Chlorophyll Derivatives

Sometimes known as the "pigments of life", tetrapyrrolic dyes play an important role in processes such as oxygen transport (haemoglobin) and photosynthesis (chlorophyll). Porphyrins are also amongst the most efficient Ru(II)-free sensitisers for DSSCs. Porphyrins are fully conjugated aromatic macrocycles comprising four pyrrole units interconnected via methine bridging groups at their α carbon atoms. A metal atom (eg Fe, Mg, Cu or Zn) is generally (but not always) coordinated to the pyrrole nitrogen atoms in the centre of the ring. This basic structure may be modified to change its photophysical properties by adding substituents to the pyrrole rings or to the methine bridges. A carboxylic acid group is usually incorporated as the anchoring group.

Porphyrins show very strong absorption in the 400-450 nm region (Soret band) as well as absorptions in the 500-700 nm region (Q-bands). Efficiencies for porphyrin-

based DSSCs, however, have been low compared with Ru(II)-polypyridyl sensitised devices[33,34,35] due to relatively poor light harvesting properties. Elongation of the π conjugation and loss of symmetry result in broadening and bathochromic shift of the absorption bands, as well as an increased intensity of the Q bands relative to the Soret band. Bulky groups have also been added to reduce aggregation. Lin, Diau, Yeh *et al.* developed several such push-pull zinc porphyrins with efficiencies up to 11% for dye YD2[28] (Figure 8) under standard AMG 1.5 illumination. Diau *et al.* managed to further enhance this to 12.03% for dye YD2-*o*-C8[29] (Figure 8) which represents the highest efficiency published to date.

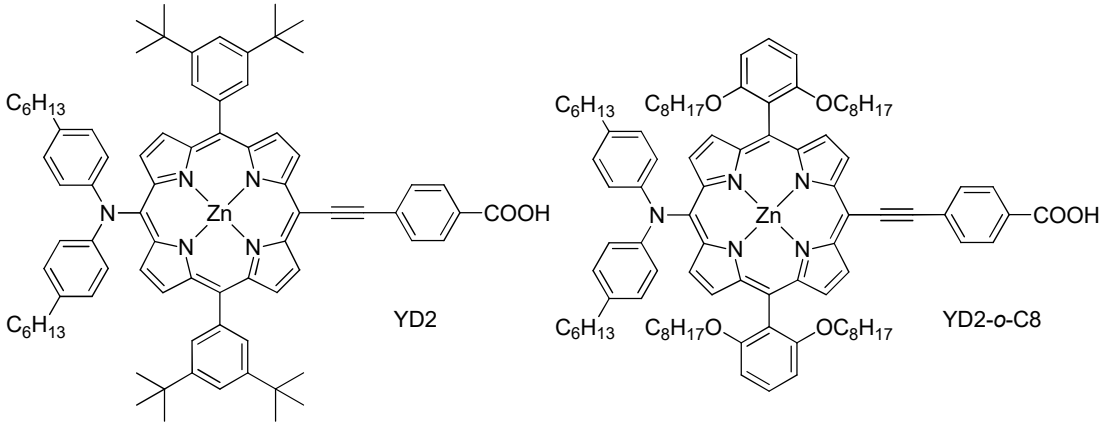

Figure 8. Molecular structure of push-pull porphyrin dyes YD2 and YD2-o-C8

Chlorophylls and related derivatives have been studied as sensitisers for DSSCs. The attraction of these compounds is clear; there are a large number known and their use could make large-scale production of DSSCs more economically viable. The highest chlorophyll DSSC efficiencies of 6.6% and 8.0% have been reported by Wang *et al.* with BChlorin-1[36] and Chlorin-3[37] (Figure 9).

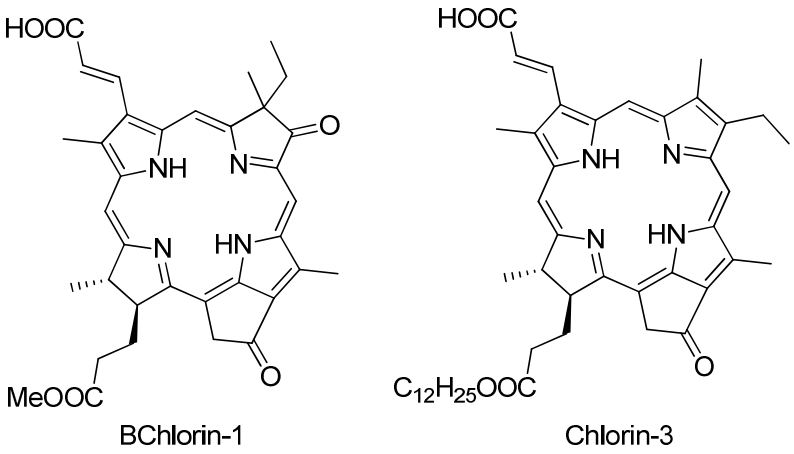

Figure 9. Molecular structures for BChlorin-1 and Chlorin-3 dyes

1.4.3 Phthalocyanines

Phthalocyanines are structurally related to porphyrins but with greater conjugation and absorb in the far red/near-IR region of the spectrum. They have extremely high extinction coefficients of over 10^5 M^{-1} cm^{-1} at around 700 nm giving them a bright cyan colour. Because they exhibit extremely good stability to light, they are widely used as pigments in paint and printing inks and as chromophores in textile dyes.

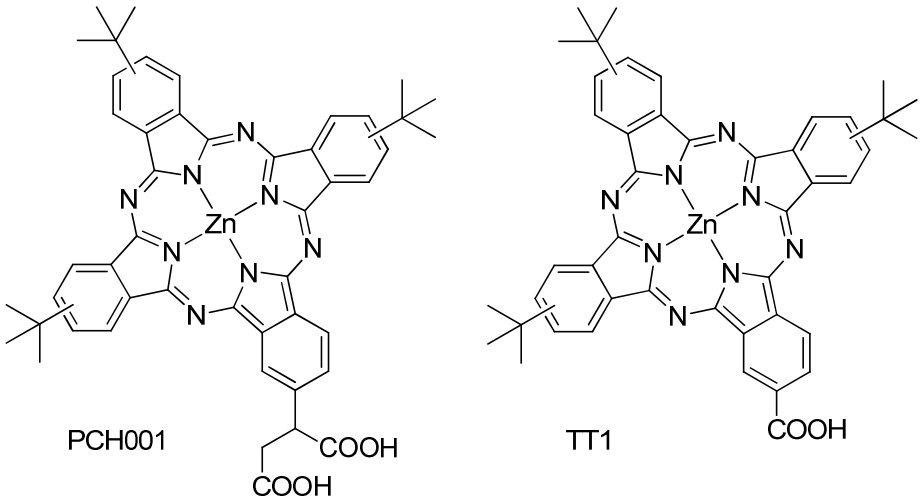

Figure 10. Molecular structures of PCH001 and TT1 dyes

Like porphyrins, until recently low efficiencies (< 1%) have been reported for phthalocyanine-based DSSCs.[3839] In 2007 Nazeeruddin *et al.* made a significant breakthrough with the development of zinc phthalocyanines with an efficiency of 3.05% (PCH001)[40] and Torres *et al.* developed a similar dye with efficiency of 3.52% (TT1)[41] (Figure 10). These dyes differ only in the number of carboxylic acid groups used to form the anchor group. Each has three bulky tertiary butyl groups to improve solubility and reduce aggregation. The unsymmetrical nature of these dyes improves the "directionality" of the excited state towards the anchoring group and so towards the TiO_2 substrate. This leads to improved DSSC electrical characteristics with IPCE values of over 80% at 700 nm.

Mori and co-workers achieved an efficiency of 4.6% with zinc phthalocyanine PcS6[42] (Figure 11), containing six 2,6-diphenylphenoxy groups designed to avoid aggregation even more effectively than the tert-butyl groups of TT1 and PCH001 (Figure 10). Addition of electron donating methoxy groups into the 4- position of the 2,6-diphenylphenoxy groups improved the photoresponse of PcS15 (Figure 11) over PcS6 and increased efficiency to 5.3%.[43]

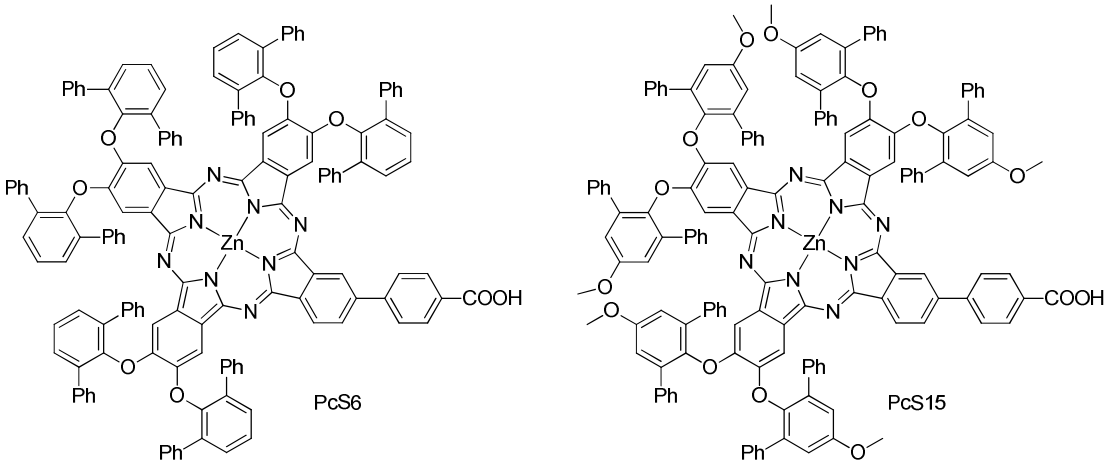

Figure 11. Molecular structure of PcS6 and PcS15 dyes

The best efficiency recorded so far for a phthalocyanine-based DSSC is 5.5% for TT40[44] (Figure 12). TT40 is similar to PcS6 but with a carboxyethynyl anchor group instead of the carboxyphenyl group of Pc56.

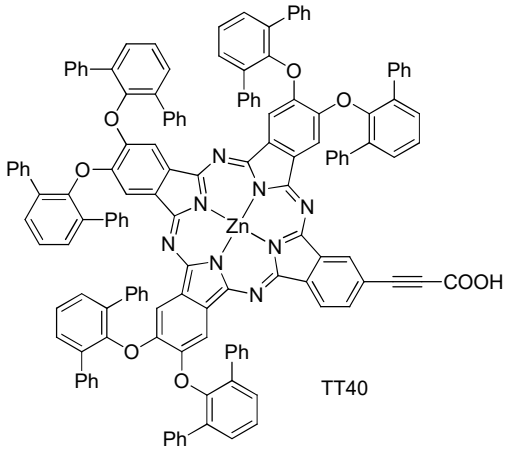

Figure 12. Molecular structure for TT40 dye

1.4.4 Coumarins, Indolines, Perylenes and Squarines

Other classes of Ru(II)-free dyes used in DSSCs include coumarins, indolines, perylenes and squarines. Coumarins were among the best early Ru(II)-free sensitisers with efficiencies of over 7% reported in 2003 by Arakawa *et al.*.[45] Hara *et al.* developed one of the most efficient coumarin dyes, NKX-2700,[46] with an efficiency of 8.2% (Figure 13).

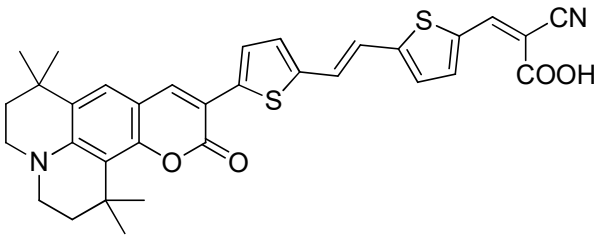

Figure 13. Molecular structure of coumarin dye NKX-2700

Indoline dyes have also been developed with high DSSC efficiencies up to 9.5%, eg dye D205[26] (Figure 14).

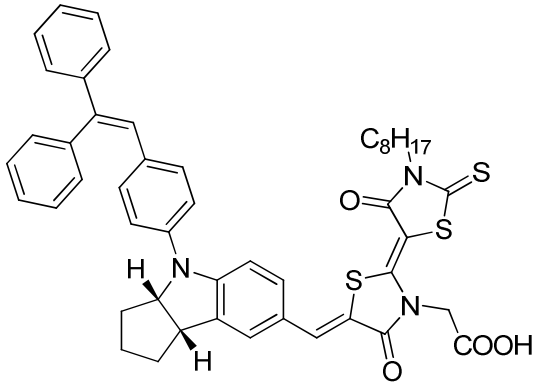

Figure 14. Molecular structure of indoline dye D205

Slightly lower efficiencies have been achieved with DSSCs based on perylene dyes. The best efficiency recorded is 6.8% for dye Perylene 1,[47] developed by Nazeeruddin *et al.* in 2008, bearing two thiophenol groups in the 1 and 6 positions (Figure 15).

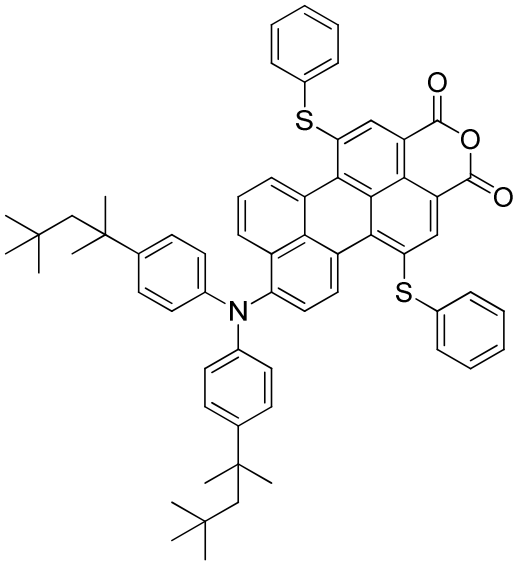

Figure 15. Molecular structure of perylene dye 1

Squaraines exhibit intense absorption bands in the far red/near infrared regions of the spectrum, similar to phthalocyanines. The best efficiency recorded for a squaraine-based DSSC is 6.74% for dye YR6,[48] developed by Nazeeruddin *et al.* in 2011 (Figure 16).

Figure 16. Molecular structure of squaraine dye YR6

1.4.5 Donor-[π Linker]-Acceptor (D-π-A) Dyes

D-π-A dyes, also known as push-pull dyes, comprise electron-donating and electron-withdrawing groups covalently linked via a π-conjugated spacer (Figure 17).

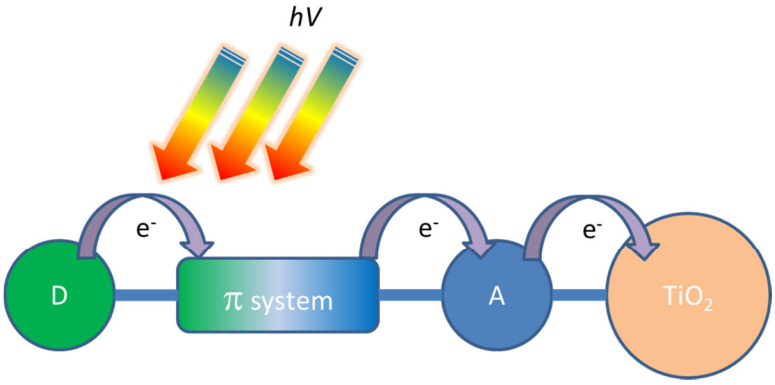

Figure 17. Structure of D-π-A dyes and the electron transfer processes following photon absorption

The photo-physical properties of D-π-A dyes are associated with an intra-molecular charge transfer from the donor to the acceptor group.[49] This transition engenders high molar extinction coefficient and singlet fluorescence via charge recombination. Extension of the π-conjugated system by adding electron donating or withdrawing groups can produce a shift in the HOMO and LUMO energy levels leading to changes in photo-physical properties. This means that the dyes can be "tuned" and so are considered to be a promising class of Ru(II)-free dyes for DSSCs.

Many different donors, π-conjugated linkers and acceptor groups have been investigated.[50] The most common D-π-A dyes comprise a triphenylamine donor, a thiophene-based linker and a cyanoacrylic acid acceptor. Wang *et al.* recorded an efficiency of 10.3% using the dye C219[27] (Figure 18), currently the record holder for metal-free organic dyes.

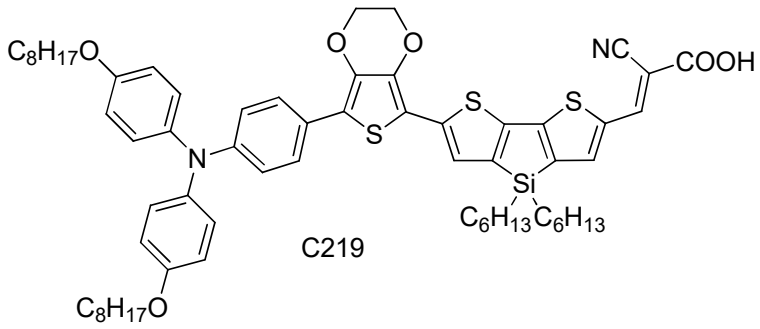

Figure 18. Molecular structure of D-π-A dye C219

1.4.6 Azulene Dyes

There are very few reports of azulene use in DSSCs and related research. Zhang *et al.* prepared and characterised four azulene based dyes, two from azulene (**1**) and two from guaiazulene (**2**)[51] (Figure 19). All four dyes have a cyanoacrylic acid acceptor / anchor group to attach the molecules to TiO_2 nanoparticles. With two of the dyes (Azu-1 and Guai-1) the anchoring group is attached directly to the azulene moiety; with the other two dyes (Azu-2 and Guai-2) there is an additional intervening vinyl linker group between the azulene moiety and the anchoring group.

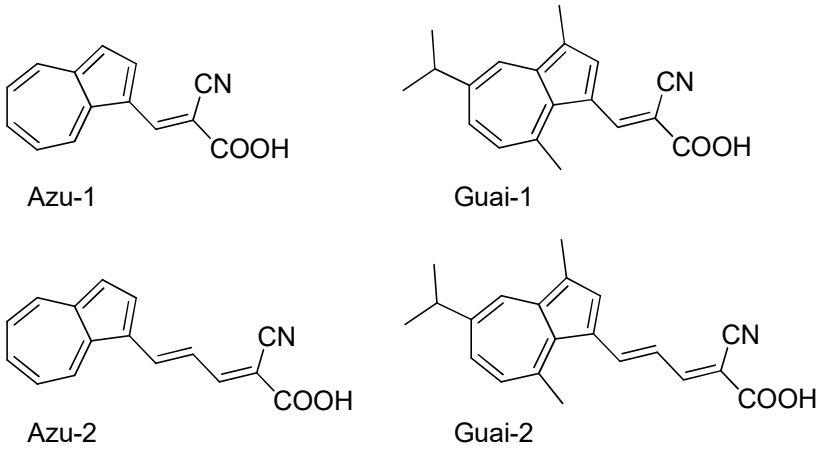

Figure 19. Azulene based dyes prepared by Zhang *et al.*

The intervening vinyl linker group increases the conjugation in the molecules and induces a bathochromic shift in the S_0-S_2 absorption band both in solution and

adsorbed onto TiO_2 films. DSSC efficiency was also greatly improved with the dyes containing the vinyl linker group, from 1.4% (Azu-1) and 1.7% (Guai-1) to 2.7% (Azu-2) and 2.8% (Guai-2).

The slightly better efficiency of the guaiazulene-based DSSCs compared with the azulene-based ones was ascribed to a reduction in the degree of aggregation due to steric hindrance of the alkyl side groups.

Piotrowiak and Galoppini studied the effect of linker groups in rigid-rod and tripodal azulene dyes on the absorbance spectrum of azulene chromophores.[122] They showed that a significant bathochromic shift in the S_0-S_2 transition resulted when azulene was substituted at the C-1 position with a p-ethynylenephenylene group (Figure 20).

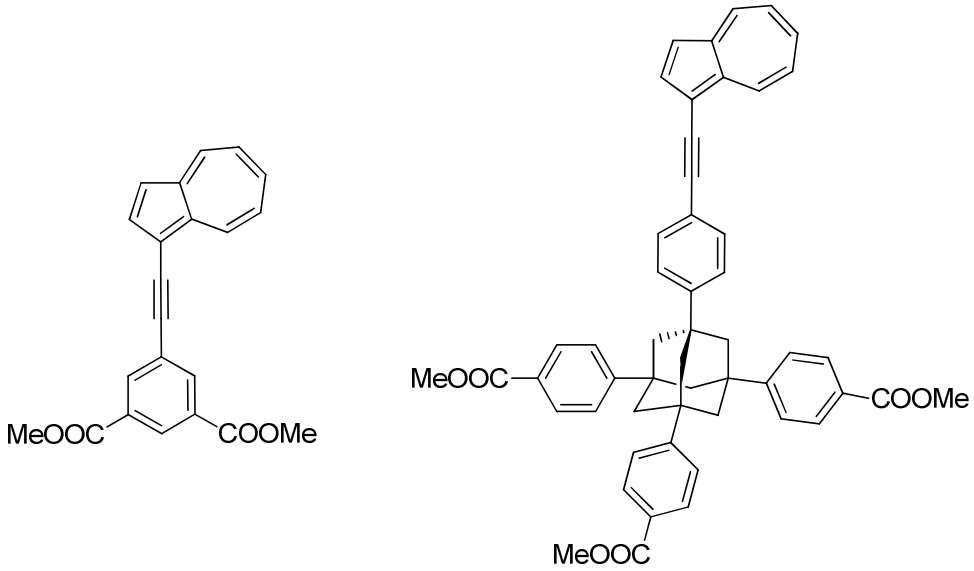

Figure 20. Rigid-rod and tripodal azulene dyes

No further significant shift was observed when the dyes were bound to TiO_2 nanoparticles, however. The authors suggested that this could mean weak electronic coupling of the dyes to the semiconductor surface. No results were reported for any DSSCs based on the dyes synthesised.

1.5 Azulene

Azulene (**1**) is a bicyclic, nonbenzenoid aromatic hydrocarbon and is an isomer of naphthalene. Azulenes have long been of interest to chemists due to their striking colours, interesting chemistry and unusual electronic properties. Azulene derivatives

may be used as advanced materials for optoelectronic[52] and electrochromic[53] devices, charge-transport[54] and nonlinear optics.[55] Some azulene derivatives have also been shown to have anti-inflammatory,[56] antiulcer,[57] and anticancer[58] properties.

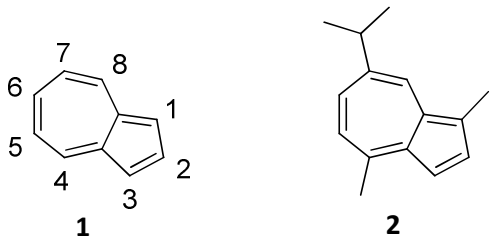

1 **2**

Figure 21. Azulene (1) and natural product Guaiazulene (2)

A blue colour has been observed during processing of certain essential oils for over 500 years.[59] Originally thought to be due to contamination from the copper apparatus used for distillations, the blue compound was found to be volatile and soluble in ethers. The generic name "azulene" was first applied to these oils by Piesse[60] in 1864 when he isolated guaiazulene (**2)** from the chamomile plant. In 1915, Sherndal[61] managed to purify Piesse's azulene sufficiently for elemental analysis and found it to have an empirical formula of $C_{15}H_{18}$, showing it was a deceptively simple hydrocarbon despite its blue colour. In 1936, over 70 years after its discovery, Pfau and Plattner[62] correctly assigned the structure of Piesse's azulene, which is now known as guaiazulene (**2**), and verified it via synthesis.

Azulene (**1**) is a conjugated, fused [5.3.0] ring system, bicyclic hydrocarbon. Although it is an isomer of naphthalene, its properties are very different because of the 5 + 7 ring arrangement.[63]

1.5.1 Electronic Structure and Colour

Huckel's rule predicts that conjugated rings with a number of π electrons equal to 4n+2, where n is an integer, will exhibit aromatic stabilisation. Like naphthalene, the 10 π electrons in azulene's fused ring system meet Huckel's 4n+2 rule for aromaticity, so the molecule as a whole is aromatic. If each ring is considered separately, ie as if in isolation, then the two rings of naphthalene both have six π electrons and so they also satisfy the 4n+2 rule. For conjugated rings with an odd number of π electrons, unusually stable carbocations and carbanions exist. With azulene, the seven membered ring would need to lose an electron to achieve

aromaticity (cf. tropylium cation), whereas the five membered ring would need to gain an electron to achieve aromaticity (cf. cyclopentadienide anion). Therefore if an electron is donated by the seven- to the five-membered ring then both rings can achieve aromaticity under the 4n+2 π electrons rule.

Unusually for a relatively simple hydrocarbon, azulene has a dipole moment of approximately one Debye[64] which supports the idea of electron transfer between the rings. This would imply that the five-membered ring is electron rich while the seven-membered ring is electron deficient. Resonance structures can be drawn that predict high electron densities at the C-1 and C-3 positions (Figure 22, right) and electron deficiencies at the C-4, C-6 and C-8 positions (Figure 22, left).

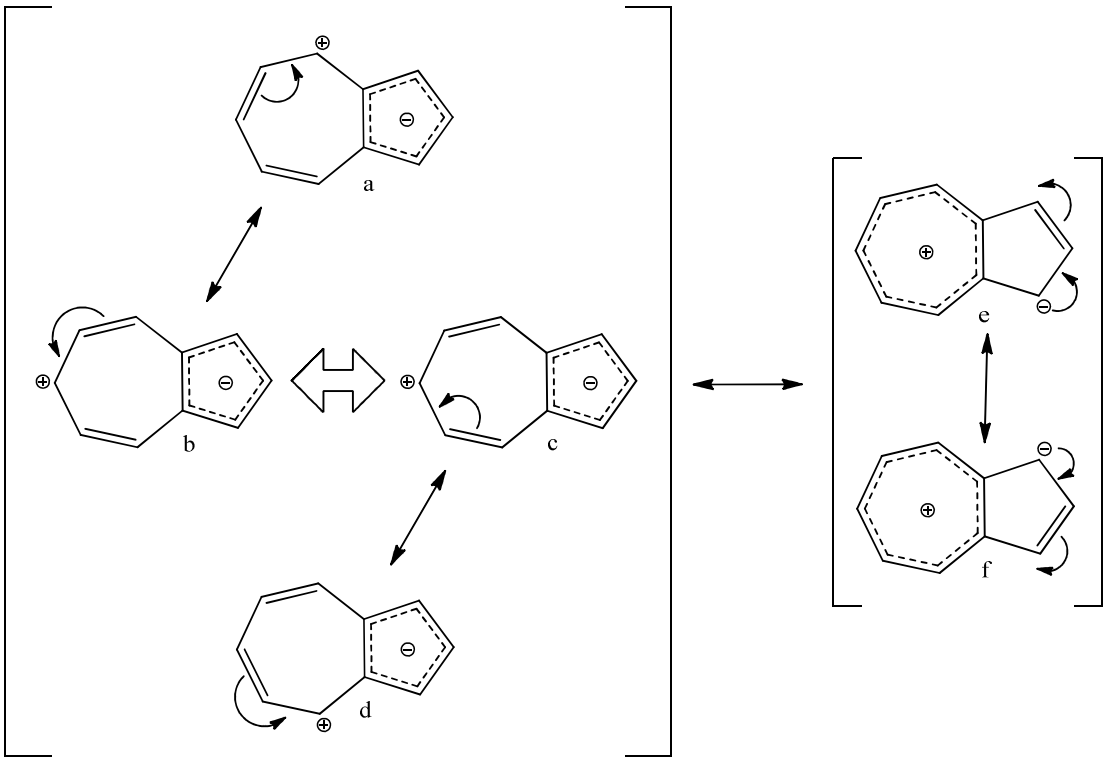

Figure 22. Azulene resonance structures

The calculations of Wheland and Mann[64] concur with this (Table 1).

Atom	q_r	Net charge (eu)
2	1.047	-0.047
1, 3	1.173	-0.173
9, 10	1.027	-0.027
4, 8	0.855	+0.145
5, 7	0.986	+0.014
6	0.870	+0.130

Table 1. Charge distribution in azulene[64]

Azulene is a non-alternant hydrocarbon (Figure 23, left, with two adjacent unstarred carbons at the ring junction) whereas naphthalene is an alternant hydrocarbon (carbons all alternating starred and unstarred).

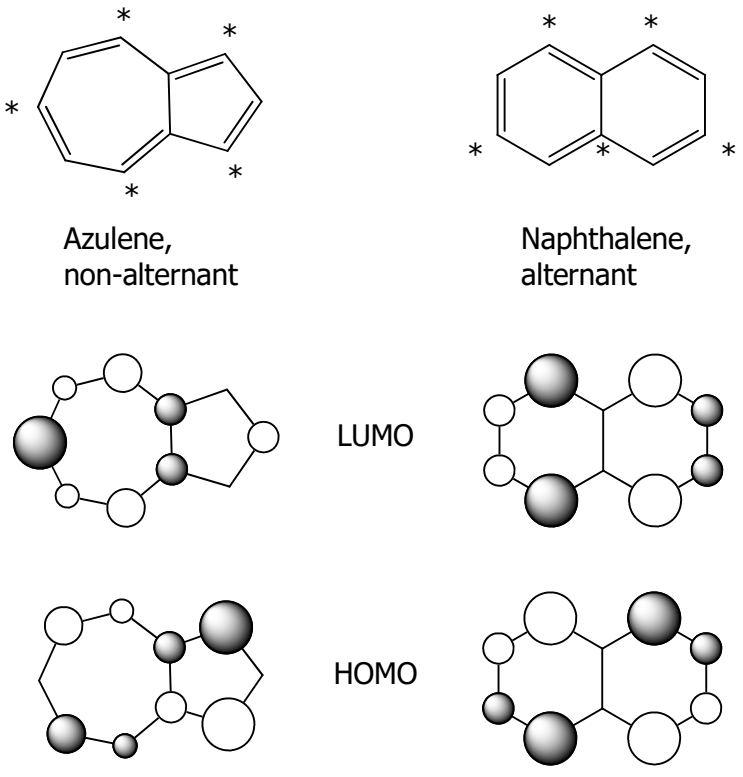

Figure 23. Non-alternant (top left) and alternant (top right) structures, with HOMO and LUMO orbitals below depicting nodes in azulene but not in naphthalene

According to Liu[63], this leads to HOMO nodes at C-2 and C-6 and LUMO (S_1) nodes at C-1 and C-3, causing relatively small repulsion between the two electrons occupying these orbitals, meaning a low $S_0 - S_1$ transition energy in the visible region. With naphthalene, the coefficient magnitude at different carbons is the same for HOMO and LUMO giving a high degree of overlap, and the two electrons occupy the same space with consequent high repulsion and higher transition energy in the UV. Therefore naphthalene is colourless but azulene, because the $S_0 - S_1$ transition corresponds to the green and red regions of the spectrum, is blue.

1.5.2 Substituent Effects

Substituents in the azulene moiety change its colour by changing the stability of the HOMO, LUMO and/or LUMO+1 orbitals. Changing the orbital stabilities alters their relative energy levels and the differences between them which in turn alters the absorption spectrum from the unsubstituted compound.

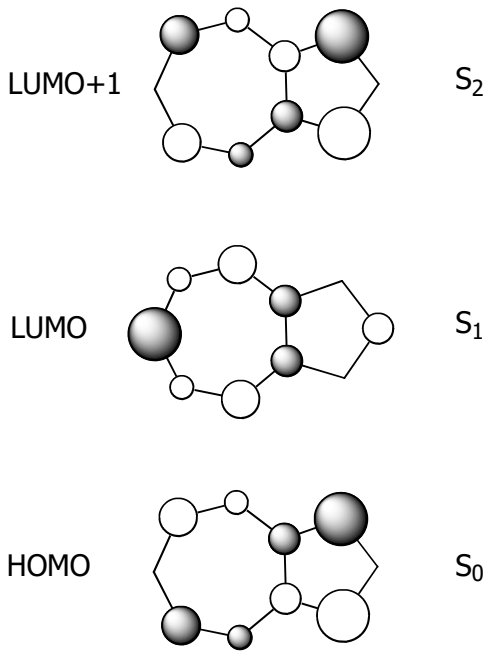

Figure 24. Electron densities for azulene ground and excited states

The effect on orbital stability depends on the carbon the substituent is attached to (odd or even numbered) and its electron donating or withdrawing nature. An electron donating group (EDG) attached to the C-1 position, which already has a high electron density in the HOMO and LUMO+1, lowers the HOMO and LUMO+1 stability, ie it increases their energy. The LUMO stability is essentially unaltered, so the energy gap between HOMO and LUMO is narrowed resulting in a bathochromic

(red) shift for the S_0 - S_1 transition. This makes the colour greener (ie blue instead of indigo).

Since the HOMO and LUMO+1 are both destabilised the energy gap between them remains similar to the unsubstituted compound. Adding an additional EDG substituent at the C-3 position compounds the HOMO and LUMO+1 destabilisation effect and produces a greater bathochromic $S_0 – S_1$ shift.

An electron withdrawing group (EWG) in the C-1 position has the opposite effect, stabilising the HOMO and LUMO+1 and increasing the energy gap between HOMO and LUMO. The resulting hypsochromic (blue) shift in the S0 – S1 transition makes the compound redder (violet to red instead of indigo).

Substitution at the C-5 position produces a similar effect, but to a lesser extent, because the seven membered ring is electron deficient.

The situation is reversed when substitution is at the C-2, C-4 or C-6 positions. In these cases the LUMO experiences the greatest effect because of the electron densities at those positions in the LUMO. EDGs will destabilise the LUMO, widening the HOMO – LUMO gap causing a hypsochromic $S_0 – S_1$ shift and making the compound appear redder. EWGs will stabilise the LUMO, causing a bathochromic $S_0 – S_1$ shift and a greener colour.

The substituent effects are summarised in Table 2.

	Substitution at	
	Odd numbered C	**Even numbered C**
EDG	Narrower energy gap, longer wavelength absorption	Wider energy gap, shorter wavelength absorption
EWG	Wider energy gap, shorter wavelength absorption	Narrower energy gap, longer wavelength absorption

Table 2. Effect of substitution on absorption spectrum

1.5.3 Reactivity

The reactivity of azulene is governed by the electronic charge distribution already discussed above. Like most aromatic compounds, azulene primarily undergoes electrophilic aromatic substitution. Nucleophilic aromatic substitution is also possible. Azulene reacts more readily with electrophiles and nucleophiles than most other aromatic compounds, often in the absence of a Lewis acid or catalyst.

The five-membered ring is very electron rich, especially at the C-1 and C-3 positions, so it is highly susceptible to electrophilic attack on these carbons and this is where electrophilic substitution takes place. The C-4, C-6 and C-8 positions are electron poor and are susceptible to nucleophilic attack. Nucleophilic substitution tales place at these positions. The C-2, C-5 and C-7 positions are much less reactive to either electrophiles or nucleophiles. This behaviour can be predicted from the resonance structures shown in Figure 22 above, providing a valence bond analysis for azulene's reactivity. MO theory can provide further insight.

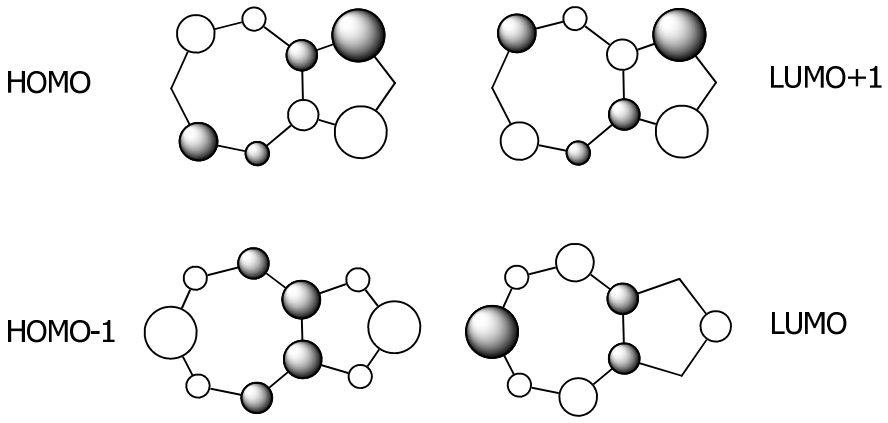

Figure 25. Azulene frontier molecular orbitals

In electrophilic aromatic substitution, the substrate acts as the nucleophile so the principle frontier orbital is the HOMO. In Figure 25 it can be seen that the HOMO electron density is greatest at the C-1 and C-3 positions, favouring electrophilic attack on these carbons over the others.

In nucleophilic aromatic substitution, the substrate acts as the electrophile and the principle frontier orbital is the LUMO where the wave function is concentrated on the C-4, C-6 and C-8 atoms.

From the MO analysis it is clear why the C-2, C-5 and C-7 positions exhibit low reactivity. Electrophilic attack on the C-2 position requires access to the HOMO-1 orbital and nucleophilic attack on C-5 and C-7 requires access to LUMO+1. The energy gaps between HOMO and HOMO-1 and between LUMO and LUMO+1 prevent significant reaction at these positions.

1.5.4 Common Reactions

Reactions at the C-1 and C-3 positions of azulene are similar to electrophilic aromatic substitution reactions of benzene. The comparatively increased nucleophilic nature of the C-1 and C-3 positions makes azulene more reactive than benzene with more facile reactions that often do not require Lewis acid catalysts.

Formylation can be achieved with the Vilsmeier-Haack reaction.[65] The reaction of a substituted amide (eg DMF) with phosphorus oxychloride gives a substituted chloroiminium ion, also called the Vilsmeier reagent. The initial product of reaction of the Vilsmeier reagent with azulene (**1**) is an iminium ion, which is hydrolysed to the aldehyde during workup (Scheme 1).

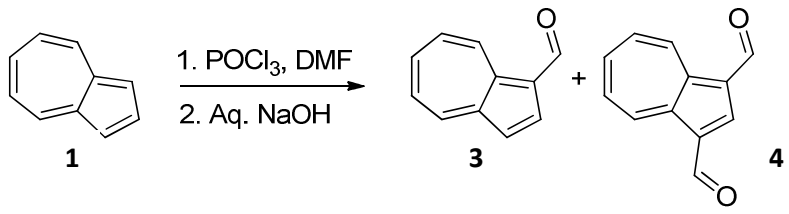

Scheme 1. Vilsmeier-Haack formylation

Alternatively, Treibs[66] has reported formylation of azulene (**1**) by reaction with trimethylorthoformate (**5**) using Friedel-Crafts conditions (Scheme 2).

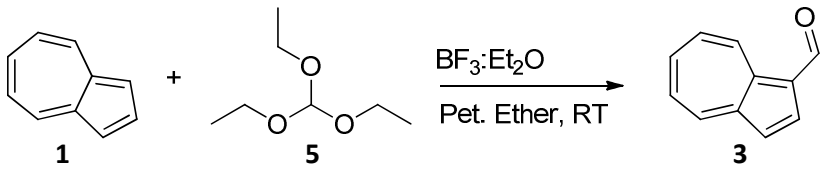

Scheme 2. Formylation under Friedel-Crafts conditions

Ketones are afforded by Friedel-Crafts acylation without requiring a Lewis acid for activation (Scheme 3).

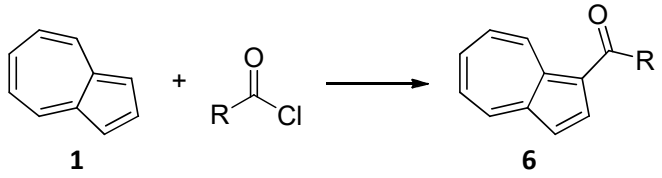

Scheme 3. Friedel-Crafts acylation

Facile halogenation is achieved using NCS (chlorination),[67,68,69] NBS (bromination)[68,69,70] or NIS (iodination)[69] in good yields. A Lewis acid catalyst is not required and exclusion of light avoids radical reactions with any alkyl side groups or the solvent (eg Scheme 4).

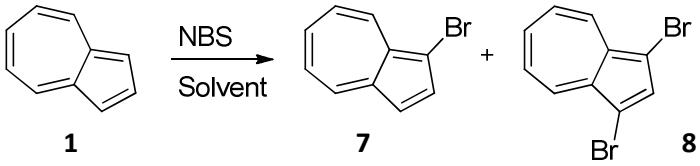

Scheme 4. Bromination

If two equivalents of the halogenating agent are used, the dihaloazulene will result. If only one equivalent is used, a mixture of unhalogenated starting material, mono- and dihalogenated product is formed. With bromination using NBS, we have found qualitatively that selectivity for the monobromo derivative depends on the solvent used, with THF and DCM being most selective for the mono- product and DMF the least selective.

Azulene forms azulenium salts on treatment with mineral acids showing that it does have basic character[71] (Scheme 5).

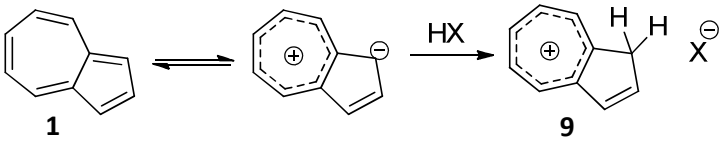

Scheme 5. Protonation of azulene

Salts can also be formed by azulenes with aprotic acids[72] which can lead to secondary products, eg dimerisation, when Friedel-Crafts catalysts are used.

Together with perchloric acid, azulene (**1**) will condense with aromatic aldehydes to form 1-(R-methy-1-ene)azulenium perchlorates[73] (Scheme 6).

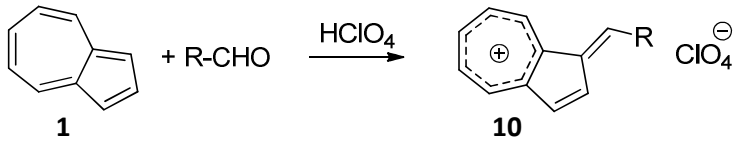

Scheme 6. Condensation with aldehyde

Because of their sensitivity to strong acids, azulenes cannot be nitrated using nitrating mixtures (eg mixed HNO_3 and H_2SO_4). However nitration can be achieved using acetyl,[74] copper[75] or urea[76] nitrates and also tetranitromethane in pyridine[77] (Scheme 7).

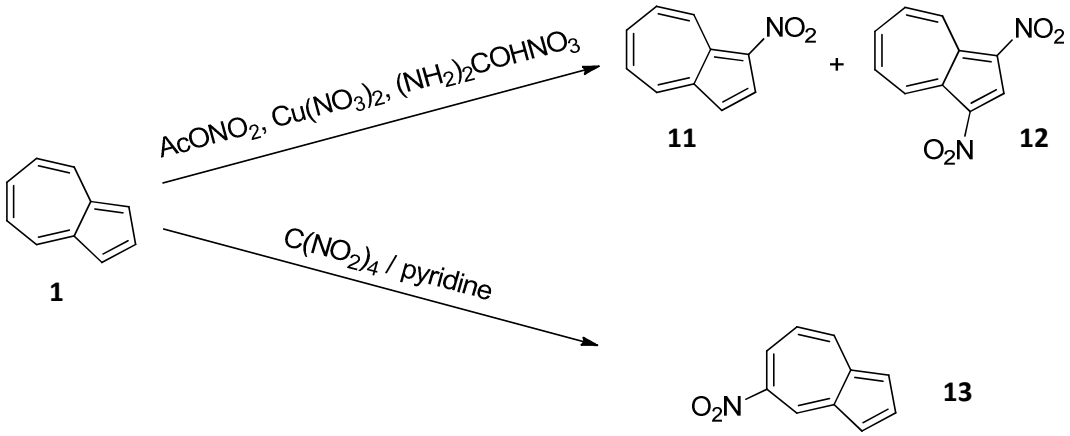

Scheme 7. Nitration of azulene

With urea nitrate both 1-mono- (**11**) and 1,3-dinitroazulenes (**12**) are formed but interestingly with tetranitromethane only 5-nitroazulene (**13**) is formed. If the 1- and 3- positions are both substituted then 5-nitroazulene (**13**) is formed in ~25% yield.

Nitrosation with nitrosyl perchlorate gives 1-nitrosoazulene (**14**)[78] (Scheme 8) which is unstable. The analogous nitroso-derivative of 4,6,8-trimethylazulene is considerably more stable.

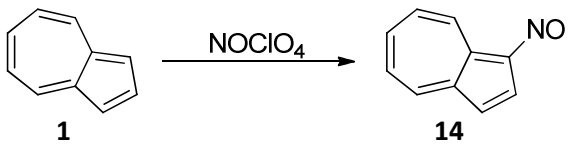

Scheme 8. Nitrosation of azulene

Azulene (**1**) and its 1(,3)-unsubstituted derivatives undergo azo coupling with diazonium salts to give high yields of azo dyes (**15**) (Scheme 9).[75,79]

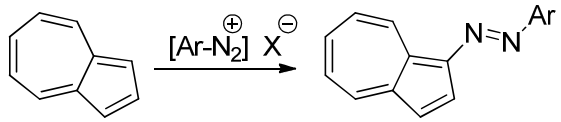

1 **15**

Scheme 9. Azo coupling with diazonium salt

Azulene (**1**) can be sulfonated by a solution of sulfuric acid in acetic anhydride to give the 1,3-disulfonic acid.[80] The mono-sulfonated adduct (**16**) has been synthesised by sulfonating with copper sulfate in acetic anhydride (Scheme 10).[81]

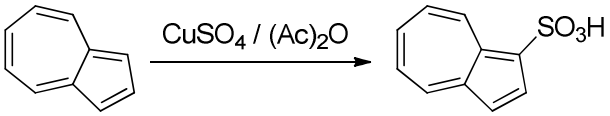

1 **16**

Scheme 10. Sulfonation with $CuSO_4$ in acetic anhydride

Azulene may be alkylated at the 1 and 3 positions using Friedel-Crafts conditions but yields are low due to the sensitivity of azulene to Lewis acids. The best yield of 5.6% was achieved with benzyl chloride.[82]

Nucleophilic aromatic substitution of azulene (**1**) is also possible. As predicted by the resonance hybrids and molecular orbital discussion above, nucleophilic attack takes place at the 4, 6, and 8 positions. Azulene (**1**) reacts with organolithium compounds affording addition products (**17**). Hydrolysis followed by dehydrogenation with chloranil yields 4-substituted azulenes (**18**) (Scheme 11).[83]

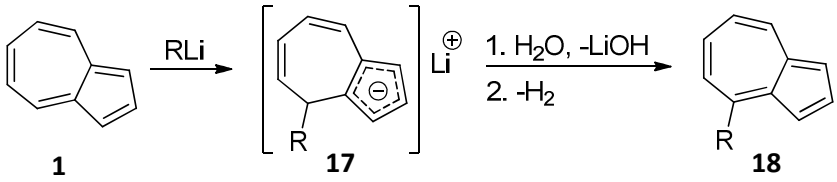

1 **17** **18**

Scheme 11. Nucleophilic substitution

4,8-disubstituted products can be synthesised by repeating the procedure.

An interesting observation is that the reaction of Grignard reagents with diethyl azulene-1,3-dicarboxylate does not affect the ester groups but instead forms 4-, 6-, and 2-substituted azulenes.[84] Generally esters react with two equivalents of a Grignard reagent giving a primary and a tertiary alcohol. Electron donation from azulene must attenuate the electrophilic character of the ester carbonyl groups sufficiently to prevent their attack by the Grignard reagent.

1.5.5 Azulene Synthesis

Several alkylated azulenes occur naturally including Guaiazulene (**2**) (1,4-dimethyl-7-isopropylazulene) and Chamazulene (**19**) (7-ethyl-1,4-dimethylazulene) which are constituents of some essential oils, mainly oil of guaiac and chamomile oil, from which they are obtained commercially. Vetivazulene (**20**) (4,8-dimethyl-2-isopropylazulene) is an isomer of Guaiazulene obtained from vetiver oil.

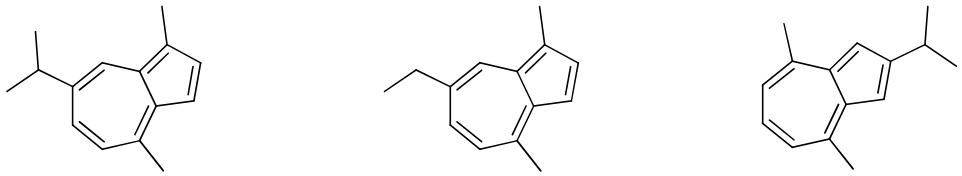

2 Guaiazulene

19 Chamazulene

20 Vetivazulene

Figure 26. Naturally occurring azulenes

Required substitution patterns that are not available in nature (this includes the parent molecule) must be synthesised either by introducing the substituents into a pre-formed azulene framework or by synthesising the framework with the substituents already in place. Due to the behaviour of azulene towards electrophiles and nucleophiles, some substitution patterns are difficult or impossible to access by direct methods.

Azulene itself has been synthesised by a number of methods, the principal ones are described below.

1.5.5.1 Pfau-Plattner

In 1937, Pfau and Plattner were the first to publish a synthesis of azulene starting from indane (**21**).[85] The first step is a Buchner ring expansion[86] using ethyldiazoacetate (**22**) to form a carbene. The carbene cyclopropanates the indane aromatic ring giving ester **23**. Hydrolysis of **23** gives the acid **24**, then simultaneous decarboxylation and dehydrogenation over a Pd/C catalyst yields azulene (**1**) (Scheme 12).

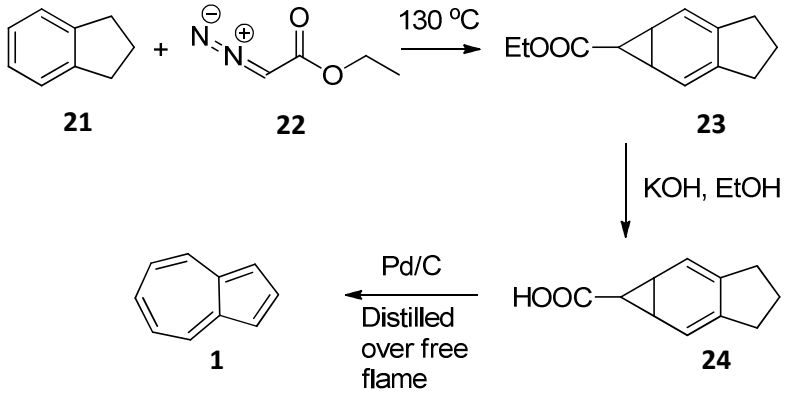

Scheme 12. Pfau Plattner azulene synthesis

Only low yields of azulene were obtained, attributed to the final high temperature dehydrogenation step. Substituted indane (**21**) has been used to synthesise substituted azulenes, eg Rao and Muthana synthesised 1-ethylazulene and 5-ethylazulene from 1-ethylindane and 5-ethylindane respectively.[87]

1.5.5.2 Zeigler-Hafner

The Zeigler-Hafner azulene synthesis (1955) involves annelation of a seven-membered ring onto a five-membered ring by ring closure of an unsaturated aminofulvene.[88] The synthesis begins by making the Zincke salt (**27**) from pyridine (**25**) and 1-chloro-2,4-dinitrobenzene (**26**). Treatment of **27** with dimethylamine and sodium methoxide results in nucleophilic attack by dimethylamine anion at a pyridine ring α carbon, followed by ring opening and nucleophilic attack by a further molecule of dimethylamine anion at the second pyridine α carbon giving **28**. Elimination of 2,4-dinitroaniline gives the unsaturated diamino salt **29**. Reaction of **29** with cyclopentadienide (Cp) yields the unsaturated aminofulvene **30** after elimination of dimethylamine. Further heating results in cyclisation and aromatisation by elimination of a second molecule of dimethylamine yielding azulene (**1**).

The Zeigler-Hafner synthesis seems to be complicated but it is a one-pot procedure with no purification of the intermediate compounds. Yield is claimed to be 51-59%. Substituted azulenes may be obtained through using substituted pyridine and / or cyclopentadiene starting materials.

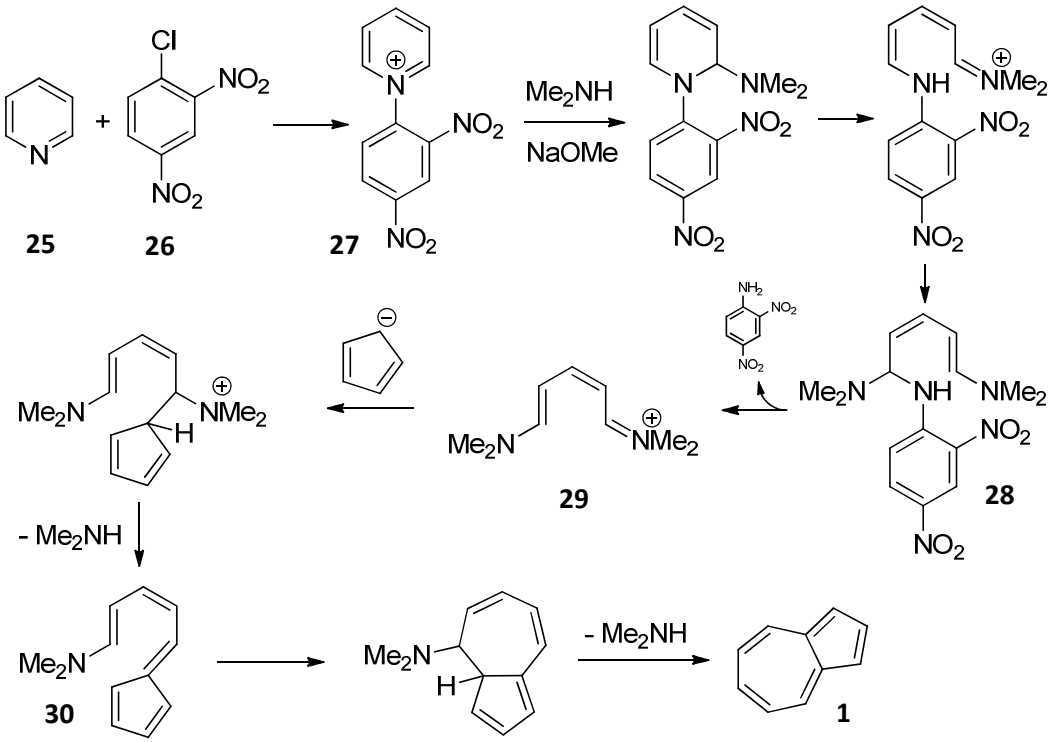

Scheme 13. Zeigler-Hafner azulene synthesis

1.5.5.3 Nozoe

The Nozoe azulene synthesis[89] (1955) forms polyfunctional azulene derivatives from reactive troponoid and activated methylene compounds such as malonitrile. The method is capable of producing unsubstituted through to heavily substituted azulenes in one-pot reactions with high yields.[90] One particular advantage is the ability to prepare azulenes with amino or hydroxyl groups at the C-2 position which can't be achieved by other methods. The amino or hydroxy groups at the C-2 position (W in Figure 27) strongly activate the C-4, C-6 and C-8 positions towards electrophiles, thus reversing the normal reactivity of these positions. Similarly, cyano or ester groups at the C-1 and C-3 positions also activate C-4, C-6 and C-8 towards electrophiles and activate the C-5 and C-7 positions towards nucleophiles, again reversing the normal azulene behaviour.

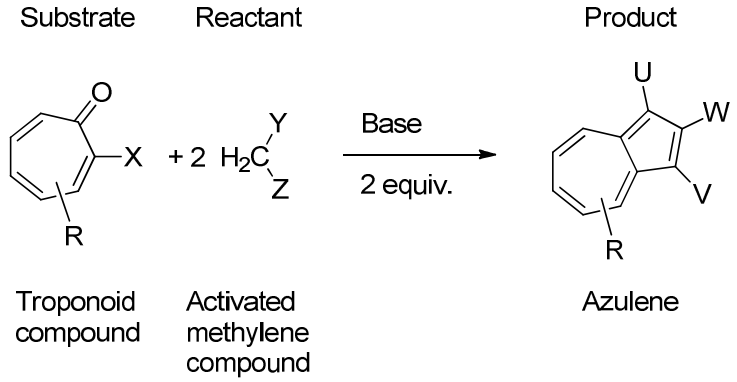

R = Alkyl (Me, Et, ^{i}Pr etc; X = Cl, Br, O-Ts, O-Me; W = NH_2 or OH

Figure 27. Nozoe azulene synthesis components[90]

Figure 27 depicts the generalised components of the reaction. The troponoid substrate is the electrophilic component with X forming the leaving group. Substituents R in the substrate will manifest in the seven-membered ring of the azulene product. The activated methylene reactant is the nucleophilic component. Groups Y and Z are electron withdrawing, thus rendering the methylene protons acidic. The base serves to aid with deprotonation of the activated methylene compound.

The Nozoe azulene synthesis proceeds in two stages. The first stage of the reaction of tropolone tosylate **31** with malonitrile is shown in Scheme 14.

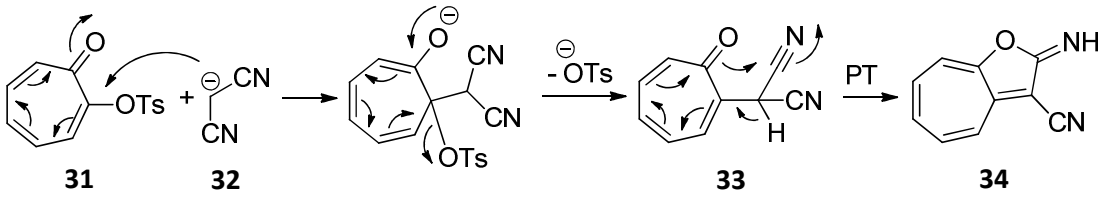

Scheme 14. Nozoe azulene synthesis - stage 1

Initial nucleophilic attack of **31** by malonitrile anion (**32**) with elimination of tosylate anion gives the tropone **33** which cyclises to the cycloheptafuran **34**.

In the second stage of the reaction (Scheme 15), a second molecule of malonitrile adds to **34** furnishing the conjugate base **35**. The proton of the introduced dicyanomethyl group is acidic due to the two electron withdrawing cyano groups and proton transfer to the basic amide leads to ring opening of **36**. Subsequent ring closure of **37** creates the five-membered ring giving the amide **38**. Proton transfer,

aromatisation of **39** by elimination of isocyanate (via isocyanic acid) and protonation of **40** yields the product, 2-aminoazulene-1,3-dinitrile (**41**).

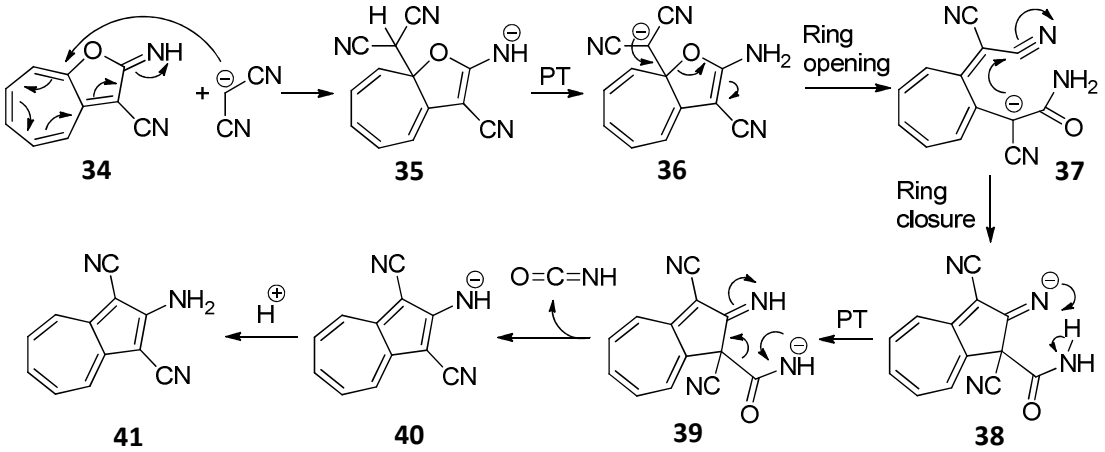

Scheme 15. Nozoe azulene synthesis - stage 2

The product azulene substituents may be varied by changing the reactant (activated methylene compound). Eg if diethylmalonate is used instead of malonitrile, the product will be diethyl 2-hydroxyazulene-1,3-dicarboxylate (**43**) (Scheme 16). If one equivalent of reactant is used it is possible to isolate the product of the first stage of the reaction. Subsequent treatment with a different reactant will result in mixed substituents at the azulene C-1 and C-3 positions.

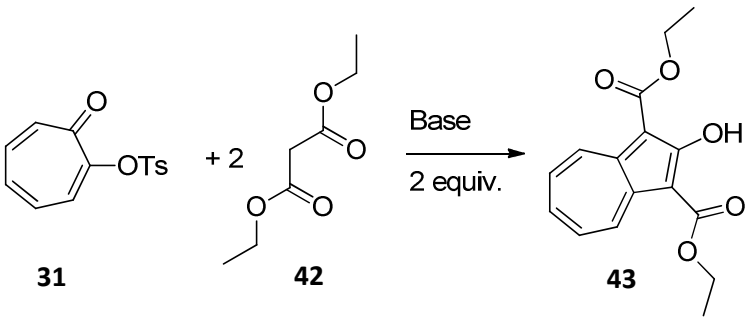

Scheme 16. Nozoe azulene synthesis variant

1.5.5.4 Hafner

The Hafner azulene synthesis[91] (1957) is a one-pot synthetic procedure for synthesising substituted azulenes through annelation of the seven-membered ring onto cyclopentadiene. Pyrillium salts serve as five carbon synthons. The method is especially useful for synthesising azulenes with substituents in the seven-membered ring.

Scheme 17 illustrates the synthesis of 4,6,8-trimethylazulene (**48**) by the Hafner azulene synthesis. The pyrylium salt **44** undergoes nucleophilic attack by the cyclopentadienide anion (Cp) (**45**) resulting in ring opening to give the intermediate compound **46**. Subsequent cyclisation and proton transfer creates the seven-membered ring. Elimination of water from **47** yields the product **48**.

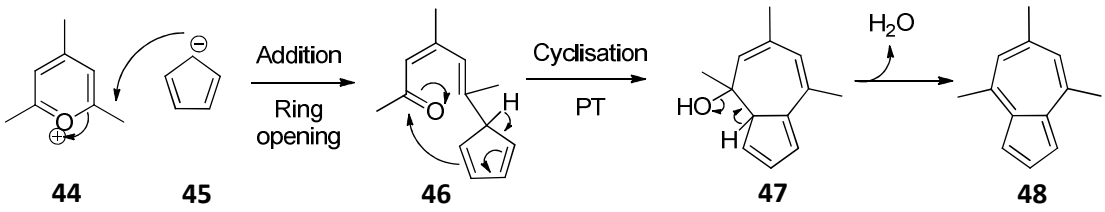

Scheme 17. Hafner azulene synthesis

A variety of substituted pyrylium salts are available or can be synthesised, enabling a range of azulene analogues with substituents in the seven-membered ring to be made.

1.5.5.5 Ring Expansion and Annelation

Several authors have published azulene syntheses based on the Buchner ring expansion reaction.[86] The Pfau-Plattner method (section 1.5.5.1 above) uses this reaction to expand the benzene ring of indane (**21**) to make the seven-membered ring of azulene. Other workers have used an intra-molecular Buchner ring expansion to expand a benzene ring while simultaneously annelating the five-membered ring thus creating the azulene framework in one step.

In 1980, Scott and co-workers published their remarkably short azulene synthetic protocol[92] (Scheme 18).

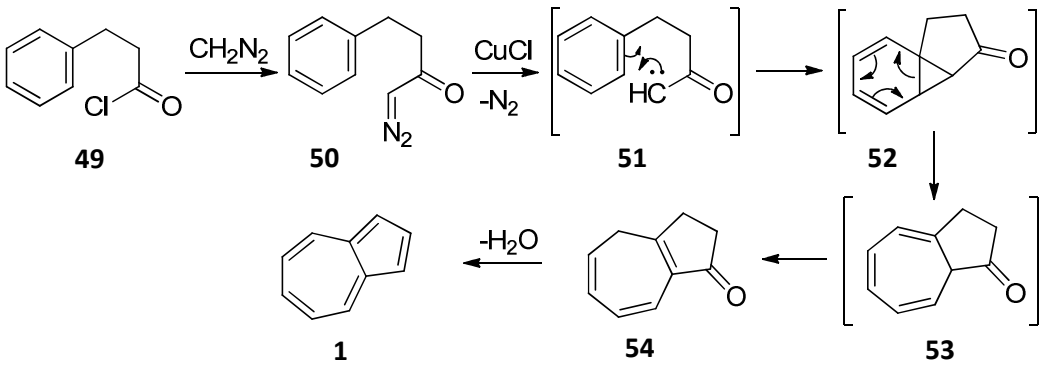

Scheme 18. Azulene synthesis via ring expansion and annelation

Diazomethane is reacted with 3-phenylpropionyl chloride (**49**) providing the diazoketone **50**. In the presence of cuprous chloride catalyst in refluxing benzene, **50** loses nitrogen generating the carbene **51** which undergoes the intra-molecular Buchner reaction to make tricyclic norcaradiene **52**. **52** then re-arranges to form the azulenone **53** which is unstable and isomerises to **54**. Dehydration of **54** by treatment with P_2O_5 and methanesulphonic acid under nitrogen at 60 °C yields azulene (**1**).

The azulenone **54** was found to undergo reactions with Grignard reagents to produce the corresponding alkylated tertiary alcohols. 1-alkylazulenes could then be produced by a dehydration and de-hydrogenation step, but with much lower yields. Electron withdrawing substituents in the phenyl ring of **49** are tolerated, with the exception of halogens, leading to azulenes substituted in the seven-membered ring.

Kane and co-workers published a similar method in 2001,[93] using 3-bromo-3-phenylpropionyl chlorides (**55**) to provide an appropriate leaving group (-Br) for the aromatisation step. This protocol results in unstable azulen-1-ol derivatives which need to be trapped, eg as acetate or triflate analogues, to prevent decomposition of the product. Following elimination of HBr from **57**, the ketone tautomerises to the enol form, which is trapped with acetic anhydride producing azulene-1-yl acetate (**58**) or with triflic anhydride to give the corresponding triflate (not shown).

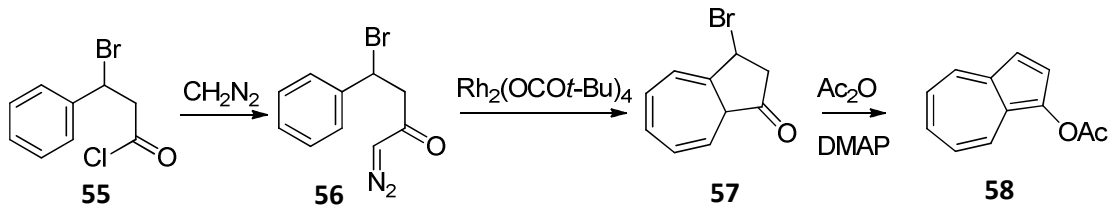

Scheme 19. Enhanced ring expansion and annelation

As with Scott's earlier synthesis, substituents in the phenyl ring of **55** manifest in the seven-membered ring of the azulene product. Electron donating and electron withdrawing groups are both tolerated, including halogens. In addition, the authors demonstrated that a substituent α to the carbonyl of **55** resulted in substitution at the azulene C-2 position.

1.5.5.6 [6 + 4] Cycloaddition Reactions

A most attractive route to azulene synthesis involves [6 + 4] cycloaddition reactions to annelate the seven membered ring to a fulvene derivative.[94,95] Typically 6-dimethylaminofulvene (**59**) or 6-acyloxyfulvenes[96] (**60**) are used as the six electron component and substituted 2-pyrones (**61**) or thiophene 1,1-dioxides (**62**), capable of extruding CO_2 or SO_2 from intermediate bridged products, serve as the four electron components (Figure 28).

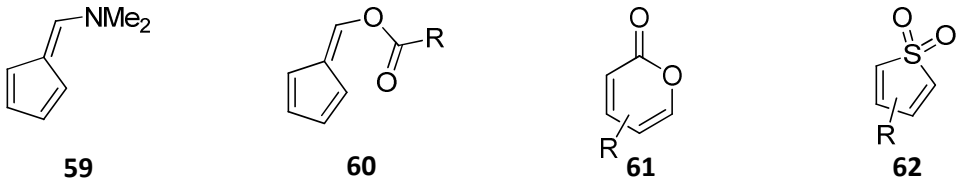

59 **60** **61** **62**

Figure 28. Azulene-forming [6 + 4] cycloaddition components

Substituents R present in the 2-pyrone or thiophene-1,1-dioxide component manifest in the seven-membered ring of the produced azulene compound. Scheme 20 illustrates the synthesis of azulene (**1**) from thiophene-1,1-dioxide (**63**) and 6-dimethylaminofulvene (**64**).

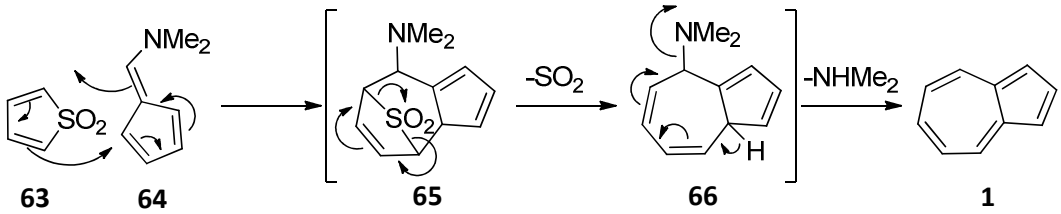

63 **64** **65** **66** **1**

Scheme 20. [6 + 4} cycloaddition azulene synthesis

The initial [6 + 4] cycloaddition reaction produces bridged intermediate **65** which spontaneously eliminates SO_2 to gives **66**. Aromatisation of **66** by elimination of $NHMe_2$ then affords azulene (**1**). According to Houk, the yield from such reactions is low (8 – 16%).[97] A much better yield (68%) of azulene was obtained from the reaction of 1-diethylaminobutadiene (**67**) with 6-(4-nitrobenzoyloxy)fulvene (**68**) (Scheme 21): With this reaction, the initial cycloaddition results in non-bridged intermediate **69** which spontaneously eliminates $NHEt_2$ giving intermediate **70**. **70** then aromatises by elimination of 4-nitrobenzoic acid (**74**) yielding the target molecule azulene (**1**).

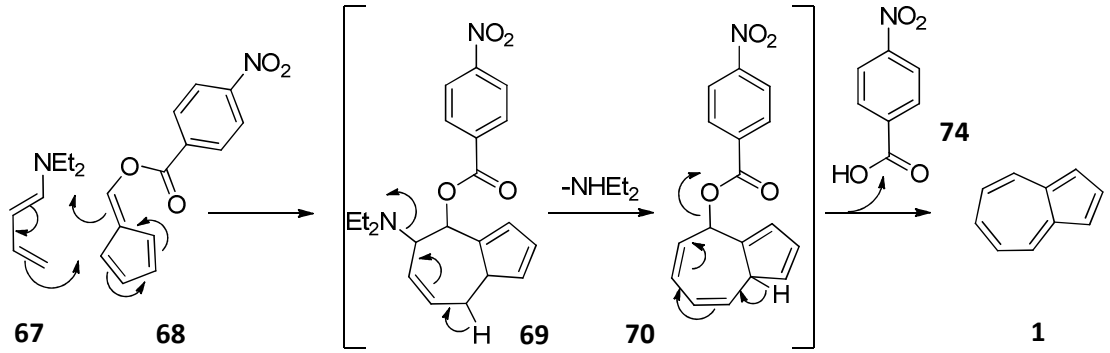

Scheme 21 - Houk [6 + 4] cycloaddition azulene synthesis

1.5.5.7 [2 + 2] Cycloaddition and Ring Expansion

Early attempts to prepare halogenated ketenes were unsuccessful and it was concluded that these ketenes were possibly formed but were unstable and polymerised under the reaction conditions. Subsequently it was demonstrated that halogenated ketenes may be generated *in situ* via the reaction of trichloroacetyl chloride with zinc or dichloroacetyl chloride with triethylamine and then trapped with unsaturated compounds to yield [2 + 2] cycloaddition products with four-membered rings (**71**).[98] Greene and Deprés then reported rapid, regioselective one-carbon ring expansion reactions of the produced 2,2-dichlorocyclobutanones (**71**) with diazomethane to give the corresponding 2,2-dichlorocyclopentanones (**72**).[99] Ready dechlorination with zinc and acetic acid yields the cyclopentanone analogues (**73**) (Scheme 22).

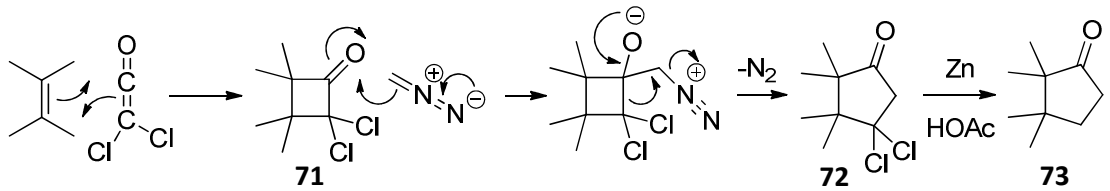

Scheme 22. [2 + 2] Cycloaddition and ring expansion

The route to substituted azulenes involves a [2 + 2] cycloaddition of dichloroketene with unsubstituted or 7-substituted cycloheptatrienes resulting in 2,2-dichlorocyclobutanones annelated to the seven membered ring.[100] The reaction of cycloheptatrienes (**75**) with one equivalent of dichloroketene gives mostly the mono cycloadduct **76** together with a small amount of the double addition product **77** (Scheme 23).

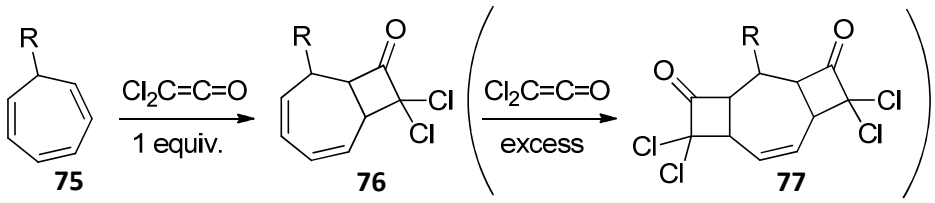

Scheme 23. [2 + 2] cycloaddition of dichloroketene to cycloheptetriene

Treatment of **76** with diazomethane gives the cyclopentanone analogues **78**. Treatment of **78** with DMF results in de-hydrochlorination[101,102] giving the enones **79**. Luche Reduction of the enones (sodium borohydride in the presence of cerium (3) chloride) selectively reduces the carbonyl group to the alcohols **80** which are dehydrated with Burgess reagent to **81**. Dehydrogenation of **81** with *p*-chloranil results in 1-chloroazulenes **82** (Scheme 24).

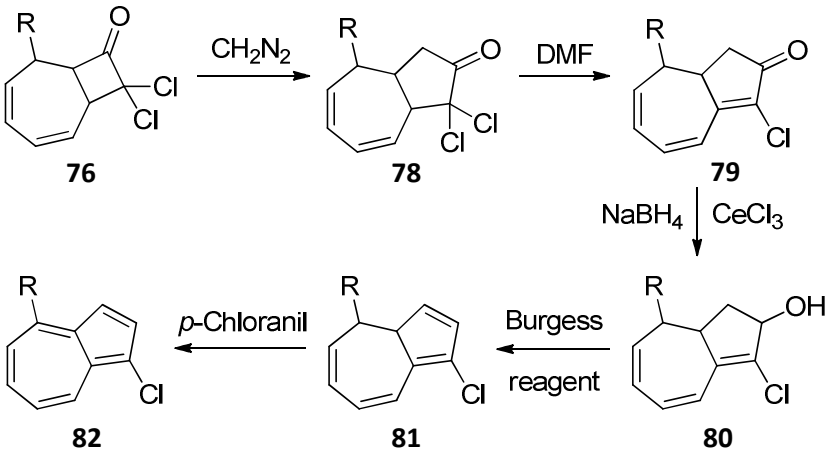

Scheme 24. Transformation of [2 + 2] cycloaddition product to Azulenes

The chlorine atom of **82** is a useful functional group for further transformations (eg cross-coupling reactions) or can be removed if not required using a Pd(0) catalysed reduction with PMHS [poly(methylhydrosiloxane)].[102] The authors demonstrated its utility in a Suzuki-Miyaura reaction to synthesise 1-methylazulenes.

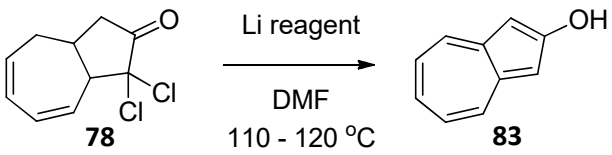

Scheme 25. 2-hydroxyazulene synthesis

Yokoyama, Shunji *et al* reported the reaction of the dichloroctclopentanone **78** (R = H) with lithium reagents (LiCl, LiBr or Li_2CO_3) in DMF at 110 – 120 °C which yielded 2-hydroxyazulene (**83**) directly in an isolated yield of 73%.[103] This is a valuable

discovery because 2-substituted azulenes are difficult to access by other means and the hydroxyl group is a useful synthetic handle that can be utilised, following conversion into eg. triflate or halogen,[104] in cross-coupling reactions.

2 Theory

2.1 Calculating DSSC Efficiency

To measure the performance or efficiency of a DSSC, the cell is illuminated using a light source with intensity and spectral distribution equivalent to "one sun" and a current-voltage (*I-V*) curve is measured with a potentiostat. "One sun" refers to a standardised set of light intensity conditions used for solar solar cell measurements known as "AM1.5". AM is the air mass coefficient which is the direct optical path length of sunlight through the Earth's atmosphere, expressed as a ratio relative to the path length vertically upwards. AM1.5, 1.5 atmosphere thickness, corresponds to a solar zenith angle of 48.2° and is useful for representing the overall annual average for mid-latitudes. One sun corresponds to a solar intensity of 1 KW m^{-2}.[105]

In order to calculate the solar to power conversion efficiency (η) of a DSSC, three key parameters are obtained from the *I-V* curve: the open-circuit voltage (V_{OC}); the short-circuit current density (J_{SC}); and the maximum power point (P_{max}) (Figure 29).

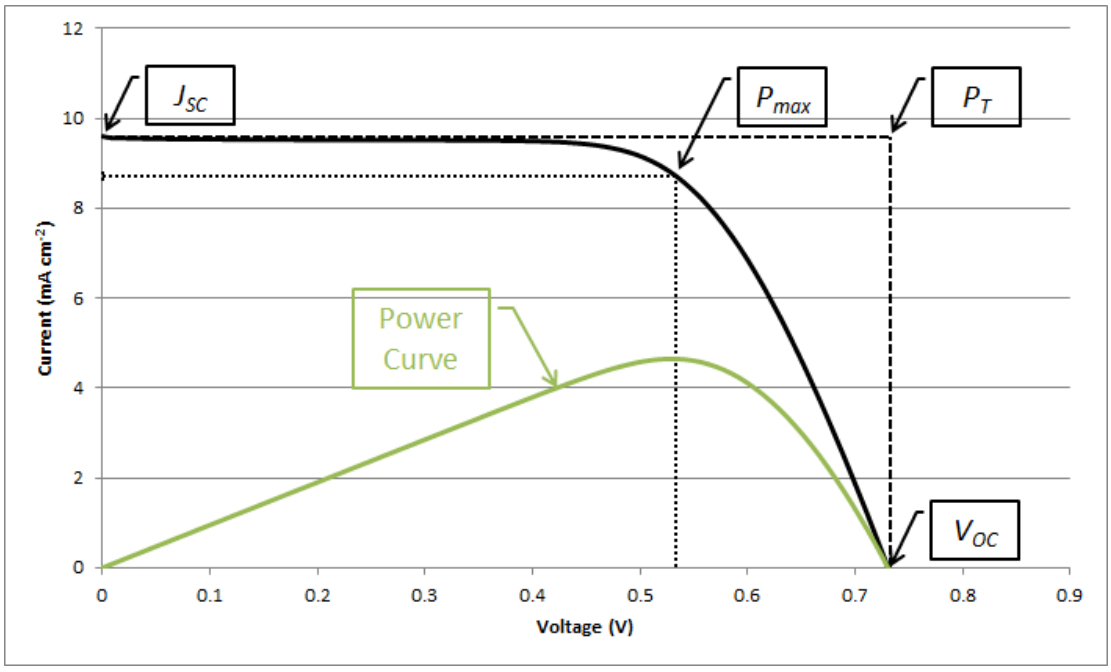

Figure 29. *I-V* curve with key parameters

The short-circuit current (I_{SC}) is the current through the solar cell when the voltage across the solar cell is zero (i.e., when the solar cell is short circuited). I_{SC} is the largest current obtainable from the DSSC. The short-circuit current density (J_{SC}) takes into account the DSSC area.

The open-circuit voltage (V_{OC}) is the maximum voltage available from a solar cell, and corresponds to the forward bias required to give zero current.

At both of the operating points corresponding to J_{SC} and V_{OC}, the power from the solar cell is zero. The product of J_{SC} and V_{OC} gives the DSSC theoretical power P_T (Equation 1).

$$P_T = J_{SC}V_{OC} \qquad \text{Equation 1}$$

P_{max} corresponds to the maxima in the product of current and voltage shown as the power curve line in Figure 29.

The fill factor (*FF*) is the ratio of P_{max} to the theoretical power P_T. (Equation 2). *FF* is the parameter which determines the maximum power available from a DSSC. It can be viewed as the "squareness" of the I-V curve, as shown by the dotted line in Figure 29. A low fill factor may be due to high internal DSSC resistance.

$$FF = \frac{P_{max}}{P_T} \qquad \text{Equation 2}$$

The overall power conversion efficiency (PCE or η) of the DSSC is determined as the fraction of incident power which is converted to electrical power. It is given by the ratio of P_{max} to the intensity of the incident light (P_{in}) (Equation 3)

$$\eta = \frac{P_{max}}{P_{in}} \qquad \text{Equation 3}$$

In a DSSC, the photovoltage arises as the difference between the Fermi energy level (E_F) of the semiconductor and the redox potential of the redox couple in the electrolyte (Figure 30). The Fermi level is defined as the energy state where the probability of being occupied by an electron is 0.5. In a semiconductor such as TiO_2, E_F is in the band gap close to the conduction band edge (E_C). In darkness, E_F and the redox couple potentials are equal; however, upon illumination electrons are injected into the TiO_2 conduction band and E_F is raised causing the splitting of energy levels shown in Figure 30. E_C and E_F are sensitive to the conditions at the TiO_2 surface. Their positions can be shifted in either direction through changes in the pH of the electrolyte or the presence of certain additives in the electrolyte.

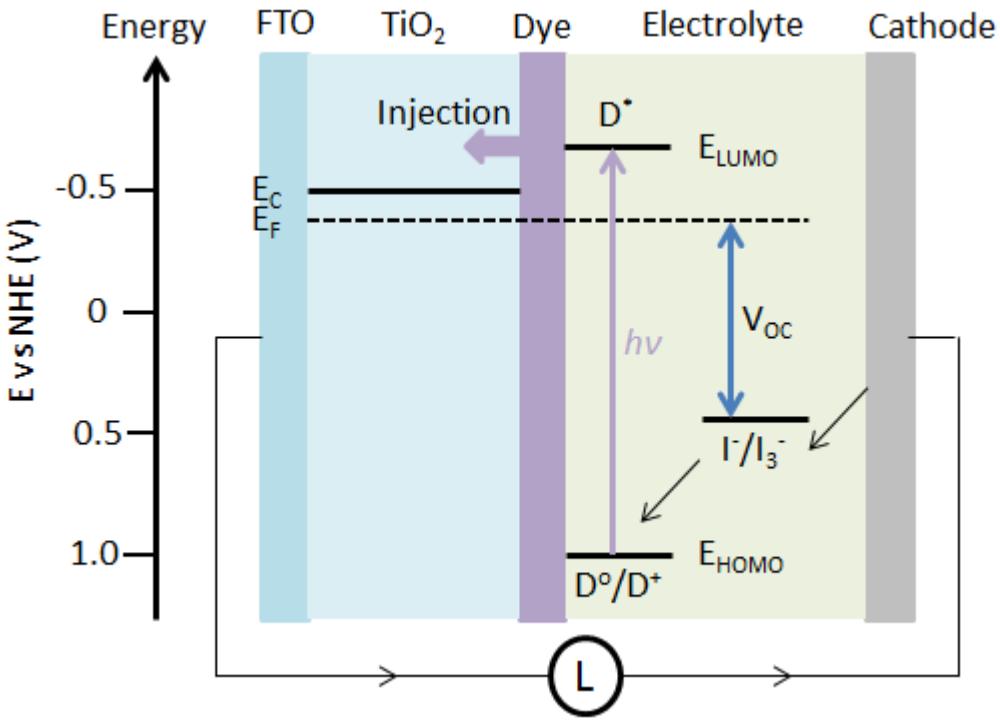

Figure 30. DSSC energy levels schematic and electron flow. Adapted from reference 106.

The level of current generated is influenced by a combination of factors:

- Light harvesting efficiency, which depends on the dye absorption efficiency (extinction coefficient) and TiO_2 nanoparticle surface coverage;
- Electron injection efficiency, which is linked to energy level matching between the dye excited state (D*) and the TiO_2 conduction band (E_C); and
- Charge collection efficiency following injection, which is the ratio of charges removed from the cell to those lost by re-combination with oxidised electrolyte redox couple.

In order to be suitable as a DSSC sensitiser, the dye ground (HOMO) and photo-excited (LUMO) energy levels must be appropriate as depicted in Figure 30:

- To ensure efficient electron injection, the photo-excited energy level (D*) must be sufficiently higher than the TiO_2 conduction band edge (E_C) which is ~-0.5 V vs. NHE; and
- To ensure that the oxidised species can be reduced back to the dye, the ground state energy level (D^o/D^+) must be sufficiently lower than the redox

potential of the electrolyte redox couple, which is ~0.4 V vs. NHE for the I^-/I_3^- couple.

2.2 Cyclic Voltammetry (CV)

Electrochemical measurements are used to study electron transfer reactions at an electrode surface.[107] CV is a potentiodynamic electrochemical measurement, typically carried out in a three-electrode setup comprising a working electrode (WE), a counter electrode (CE) and a reference electrode (RE). Electrolyte is usually added to the solution under analysis to ensure sufficient conductivity. The solvent, electrolyte and material composition of the working electrode determine the potential range that can be accessed during experiments. During experiments the solution is unstirred and the electrodes are immobile. The static nature of the method results in its characteristic diffusion-controller peaks.

Common materials for the working electrode include glassy carbon, platinum and gold, encased in a rod of inert insulator with a disk 2 mm in diameter exposed at one end. The counter electrode can be of any material that conducts current easily and is inert to the solution.

Current passes between the working and counter electrodes (via the analyte in solution) and the working electrode potential is measured relative to the reference electrode. The reference electrode is usually a half cell with a known redox potential that maintains a constant potential drop across its interface with the solution. Since (practically) no current passes via the reference electrode, its potential is regarded as being equal to that of the solution under analysis plus a constant (Equation 4).

$$E = (\theta_m - \theta_s) + constant \qquad \text{Equation 4}$$

In Equation 4, θ_m is the electrode (metal) potential and θ_s the solution potential. Because of problems with liquid junction potential drift, for experiments in non-aqueous solvents IUPAC recommends[108] the use of the ferrocene/ferrocenium (Fc/Fc^+) couple as an internal standard in conjunction with a simple inert metal electrode such as platinum wire.

Reduction or oxidation reactions occur at the working electrode surface as the species of interest either gains or loses an electron. Reactions at the counter

electrode are unimportant so long as it continues to conduct current well. To maintain the current the counter electrode will often oxidise or reduce the solvent or bulk electrolyte.

In a CV experiment, the working electrode potential is ramped linearly versus time until the set potential is reached. After the set potential is reached, the working electrode's potential is ramped in the opposite direction to return to the initial potential or ramped further until another set potential is reached followed by ramping in the original direction back to the starting potential. Potential ramping is therefore cyclic. The cyclic potential ramping may be repeated ("scanned") as many times as needed. The current at the working potential is recorded and plotted against the applied voltage to produce the cyclic voltammogram. Two principle factors influence the redox reaction:

1. the rate at which the species of interest reaches the electrode surface (mass transport); and
2. the rate of electron transfer between the reactant molecule and the electrode (kinetic effects)

Mass transport includes diffusion, convection and migration processes.[109] With CV, diffusion is the main contributing factor. Convection is avoided through the use of a static, unstirred solution although minimal natural convection will occur. Migration effects are due to the electric field which exists at the electrode / solution interface as a result of the drop in potential between the two phases. This exerts an electrostatic force on charged species present in the interfacial region and induces the movement of ions to or from the electrode. This tends to neutralise the electric field and hence changes the migratory flux. This varying rate of mass transport can make interpretation of results difficult.

Migratory effects can be neglected by use of a high concentration bulk electrolyte, eg 0.1 M tetrabutylammonium hexafluorophosphate (TBA PF_6 or TBAF), which helps to maintain electrical neutrality across the bulk solution. Electrolytic ion injection or removal at the electrode / solution interface causes a slight redistribution of the bulk electrolyte anions and cations near the interface maintaining near electrical neutrality in the entire interfacial space, except for a tiny region immediately

adjacent to the electrode. This ensures that electric fields do not build up as electroanalysis proceeds.

Diffusion is the movement of a species along a concentration gradient. The rate of diffusion at any point x is defined by Fick's first law of diffusion (Equation 5) where j is the diffusional flux (quantity of material diffusing through a unit area in mol.s^{-1}) for a species B; D_B is a diffusion coefficient (in m.s^{-1}).

$$j = -D_B \left(\frac{\delta[B]}{\delta x} \right) \qquad \text{Equation 5}$$

In a CV experiment, the applied potential is first ramped from an initial value to a set potential, as described above. If the ramp is from 0 V to increasingly positive values, once the redox potential of the electroactive species in solution has been exceeded electrons will begin to be transferred from it to the working electrode resulting in an anodic current. As the electrode potential becomes more oxidative, the rate constant of electron transfer will increase, resulting in increasing current so long as the concentration of electroactive species, B, at the electrode surface is replenished by diffusion from the bulk solution, reaching a peak anodic current at E_{PA} (Figure 31). Over time, however, a "diffusion layer" is established near to the electrode in which the concentration of B is reduced, leading to lower electron transfer rate and subsequently lower current. The response of the system is therefore diffusion limited.

Similarly, the concentration of oxidised species B^+ at the electrode surface will increase causing B^+ to diffuse away from the electrode into the bulk solution.

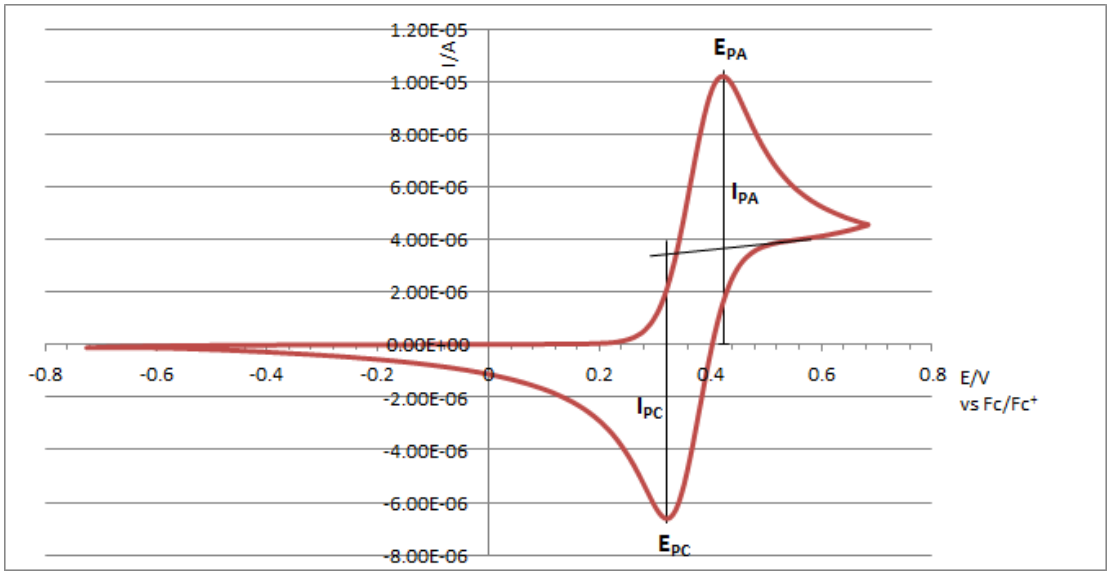

Figure 31. Cyclic Voltammogram showing oxidation and reduction waves.

During the reverse sweep, initially the electrode potential is higher than the redox potential of the electroactive species so oxidation will still occur at the "depleted" rate which will get gradually slower as the electrode potential becomes less oxidative. When the potential ramps below the redox potential of the electroactive species, electron transfer from B will cease and electron transfer to B^+ will begin, leading to a cathodic current. The rate constant of electron transfer from B^+ will increase as the electrode potential becomes less oxidative resulting in increased cathodic current so long as the concentration of B^+ is replenished by diffusion from the bulk solution, reaching a peak cathodic current at E_{PC} (Figure 31). When the concentration of B^+ becomes diffusion limited, the rate of electron transfer and subsequently the cathodic current will be diminished until B^+ becomes depleted at which point current ceases to flow.

The process of potential ramping with subsequent oxidation reaction and anodic current on the forward sweep followed by reduction of the oxidised species and cathodic current and the effect of diffusion limitation leads to the classic CV plot shape depicted in Figure 31 with oxidation and corresponding reduction "waves".

Nernst showed that the potential established at the electrode under equilibrium conditions is given by Equation 6:

$$E_e = E^\theta + \frac{RT}{nF} \ln \frac{[\mathrm{O}]}{[\mathrm{R}]} \qquad \text{Equation 6}$$

Where E_e is the equilibrium potential of the electrode, E^θ is the standard electrode potential, F is the Faraday constant, R is the ideal gas constant, T is the absolute temperature and n is the number of electrons transferred in the reaction. (Strictly, the concentrations in the Nernst equation should be replaced by activities. Equation 6 assumes that the activities of O and R are unity.)

At equilibrium the concentrations of O and R at the electrode surface are equal, so the equilibrium potential is equal to the formal electrode potential. The half wave potential, $E_{½}$, can be calculated from a CV as the mean of the peak anodic and cathodic current potentials (Equation 7):

$$E_{½} = \frac{E_{PA} + E_{PC}}{2} \qquad \text{Equation 7}$$

The half wave potential ($E_{½}$) is related to the formal potential (Equation 8) where D_R and D_O are the diffusion coefficients of R and O respectively:

$$E_{½} = E^\theta + \frac{RT}{nF} \ln \frac{D_R}{D_O} \qquad \text{Equation 8}$$

When the ratio of D_R and D_O is unity, then $E_{½}$ is equal to E^θ.

After mass transport, kinetic feasibility is the second factor which determines reactivity at an electrode surface. An electron transfer process is described as reversible, irreversible or quasi-reversible. To be ideally reversible,

- The magnitude of the oxidation and reduction wave peaks are equal;
- The difference between E_{PA} and E_{PC} is 59 mV for a one electron transfer process;
- The difference between E_{PA} and E_{PC} is independent of scan rate; and
- The peak currents are proportional to the square root of the scan rate.

Irreversible electrode kinetics may occur, for example, if the oxidised species B^+ has insufficient stability under the conditions of the experiment to survive long enough to be reduced back to the species B. When an electron is abstracted from a neutral molecule, the resulting entity is a radical cation which is a potentially very reactive species. If the radical cation oxidation product reacts with other molecules present (radical abstraction, addition to unsaturated bonds) or by fragmentation,

combination with other radicals or a combination of these reaction types, then it won't be available to reduce back to the original, unoxidised species *B* during the reverse sweep. If that is the case, then the CV will display an oxidation wave during the forward sweep, but no reduction wave or a greatly diminished reduction wave will be observed during the reverse sweep. In addition, on subsequent scans additional oxidation and / or reduction waves may appear providing evidence of new species appearing as a result of reactions or decomposition of the radical cation.

CV experiments may be used to estimate dye HOMO and LUMO energy levels. In a metal, the electrons occupy an effective continuum of energy states up to the Fermi Level (E_F). An electrical potential applied to the metal acts to increase or decrease the number of electrons and thus the populated energy states, which increases or decreases the energy of the Fermi Level. In Figure 32 (A) the metal electrode is in contact with molecules of dye. The Fermi Level of the electrode (metal) is between the HOMO and LUMO energy levels of the dye molecule. It is evident that for electrons to leave the metal to occupy the LUMO (reduce the dye) or for dye electrons to leave the HOMO to transfer to the metal (oxidise the dye) are both energetically unfavourable processes. If the energy in the metal is raised by applying a negative potential so that the metal Fermi level lies above the dye LUMO, however, then electron transfer into the dye LUMO becomes thermodynamically favourable (Figure 32 (B)).[110] Similarly, if the energy in the metal is reduced below the dye HOMO energy level, then transfer of an electron from the dye to the metal is favourable (Figure 32 (C)).

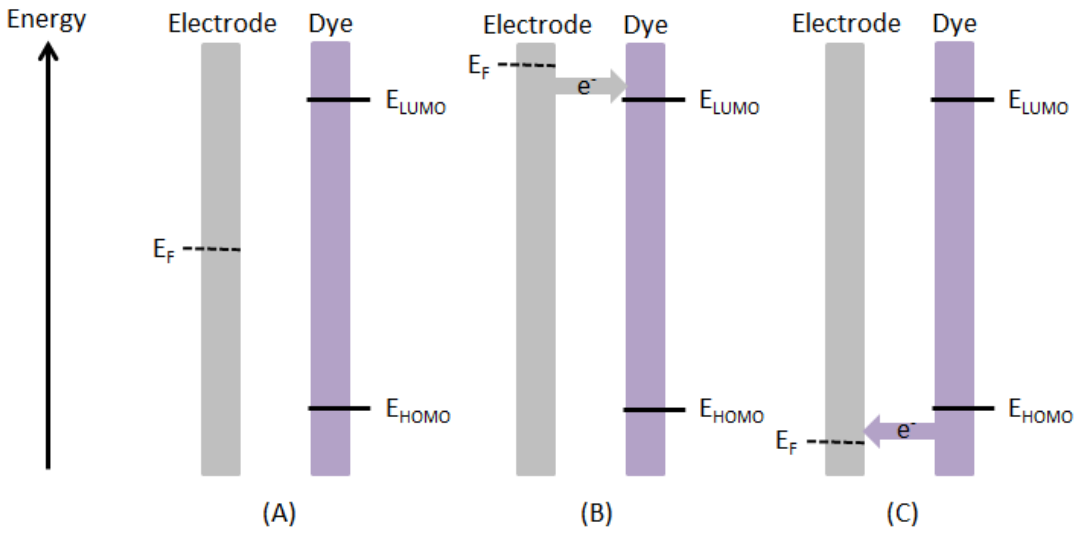

Figure 32. Energy level determination

The CV technique is therefore used to study the oxidation and reduction processes of compounds in solution. In this work, CV was used to estimate the HOMO energy levels of dyes and to determine if the dyes exhibited chemically reversible redox behaviour to give an indication of the stability of the oxidised dye radical cation in a DSSC.

2.3 UV/Vis Spectroscopy

The extent of absorption of light varies a great deal from one substance to another, with the probability of absorption being indicated by the Molar Extinction Coefficient (ε). As light is absorbed, the intensity of light entering the solution, I_{in}, is greater than the intensity of the emerging light, I_{out}, and there is an exponential relationship between their ratio (relative absorption) and the concentration c and path length l of the absorbing substance (Equation 9):

$$\frac{I_{out}}{I_{in}} = 10^{-\varepsilon cl} \qquad \text{Equation 9}$$

Taking logs to base 10 gives:

$$\log\left(\frac{I_{out}}{I_{in}}\right) = -\varepsilon cl \qquad \text{Equation 10}$$

Thus:

$$\log\left(\frac{I_{in}}{I_{out}}\right) = \varepsilon cl \qquad \text{Equation 11}$$

The left-land-side term is the absorbance, A, and the linear relationship between absorbance, concentration and path length is known as the Beer-Lambert law (Equation 12):

$$A = \varepsilon cl \qquad \text{Equation 12}$$

The units of ε are generally expressed as non-SI units for historic reasons, having being used in spectroscopy for many years:

- Concentration, c, has units of mol.L^{-1};

- Path length, *l*, has units of cm; and
- Absorbance, *A*, has no units since it is a logarithmic quantity.

Rearranging Equation 12 gives:

$$\varepsilon = \frac{A}{cl} \qquad \text{Equation 13}$$

So the units of ε are $cm^{-1}.(mol.L^{-1})^{-1} = L.mol^{-1}.cm^{-1}$.[111]

The magnitude of ε is a measure of the efficiency of light absorption, ie the greater ε is the higher the probability that a photon will be absorbed. For a given substance ε varies with the wavelength of the light used. A plot of ε against wavelength (λ) is known as the absorption spectrum of the substance (Figure 33). The principle use of absorption spectra is that they provide information as to the wavelength of maximum absorption (λ_{max}). In addition, the optical band gap (HOMO – LUMO) energy can be estimated by locating the onset of the absorption band, usually by extrapolation of the linear portion of the absorption band edge to intersect with the baseline. The band gap in *eV* is then calculated from:

$$eV = 6.242 \text{ x } 10^{18} \left(\frac{hc}{\lambda}\right) \qquad \text{Equation 14}$$

where h = Planck's constant, c = speed of light, λ = wavelength (m) and 6.242 x 10^{18} = conversion factor from Joules to *eV*. The conversion factor, h and c are all constants so conveniently:

$$eV = \frac{1240}{\lambda} \qquad \text{Equation 15}$$

where λ = wavelength (nm).

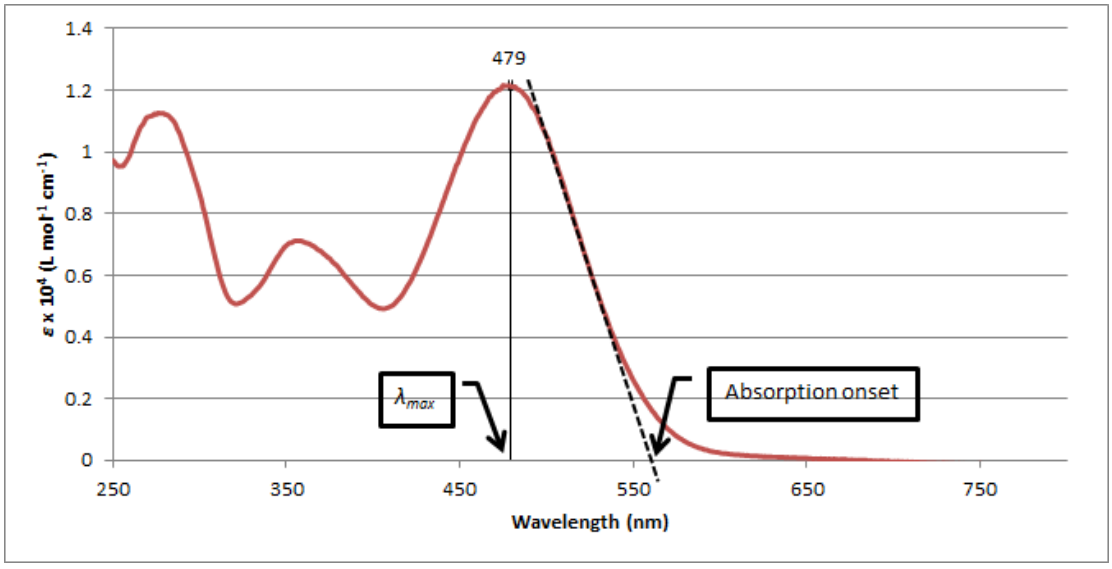

Figure 33. Dye UB-Vis absorption spectrum

To understand why the absorption onset is used to calculate the optical band gap, a consideration of the physical basis of light absorption is required.

The total energy of molecules comprises electronic energy (E_e) and energy due to vibrational (E_v) and rotational (E_v) nuclear motion (Equation 16):

$$E_t = E_e + E_v + E_r \qquad \text{Equation 16}$$

The energy gap between electronic states is much greater than that between vibrational states which are much greater than those between rotational states. Consequently, rotational states can be ignored when considering the effects of electronic transitions.

Absorption of ultraviolet and visible light results in electronic transitions which incorporate changes in both electronic and vibrational states (vibronic transitions). The Boltzmann distribution law describes the population of any series of energy levels at thermal equilibrium. If N_0 is the number of molecules in the ground state then the number in any higher energy level N_1 is given by Equation 17, where ΔE is the energy difference between the two levels, R is the gas constant and T the absolute temperature.

$$\frac{N_1}{N_0} = e^{\left(\frac{-\Delta E}{RT}\right)} \qquad \text{Equation 17}$$

According to the Boltzmann distribution law most molecules will be in the $v = 0$ vibrational state of the electronic ground state so most absorptions will occur from $S_0(v = 0)$ (Figure 34).

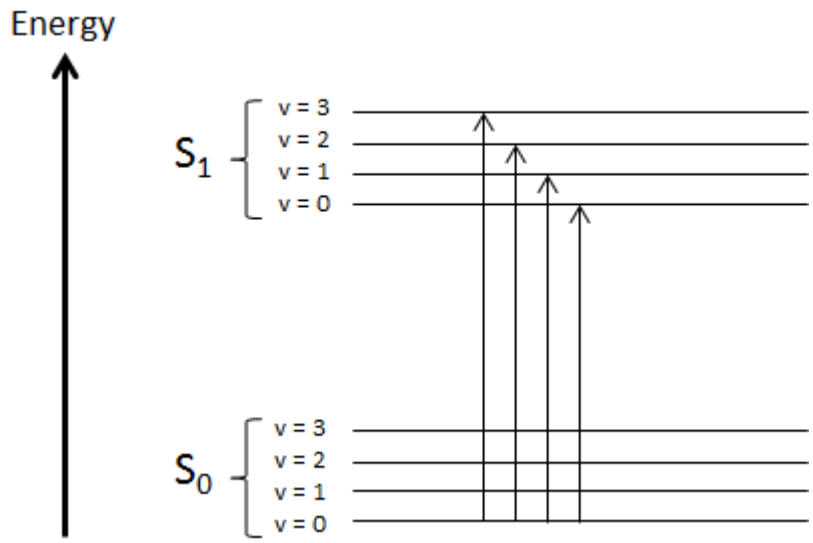

Figure 34. Electronic ground and first excited states with associated quantised vibrational energy levels for an organic molecule. (Reproduced from ref 111)

Therefore there are a range of possible transition energies from $S_0(v = 0)$ to the vibronic states $S_1(v = n)$. The transition $S_0(v = 0)$ to $S_1(v = 0)$, known as the 0-0 band, represents the S_0-S_1 electronic transition. It has the lowest ΔE and therefore the longest absorption wavelength and so is located at the onset of the absorption band. The characteristic absorption band "tail" is due to the few absorptions which occur from the higher vibrational levels of the electronic ground state.

Stretching vibrations of a molecular bond imply that the internuclear distance varies with time in an oscillatory fashion. At the ends of each oscillation, the nuclei are either slowing down, stationary (at the extremities) or accelerating, ie are moving slowly relative to each other. In mid-oscillation, the nuclei are moving quickly relative to each other with the greatest velocity occurring at the mid-point of the vibration. Therefore the nuclei spend most of their time close to the turning points of the vibrational motion. The most probable internuclear distance for a given vibrational quantum number, v, is given by the square of the associated wavefunction (Figure 35). This means that for higher vibrational energy levels, there is a greater probability of the molecule having a bond length at the two limits shown by the Morse curve.

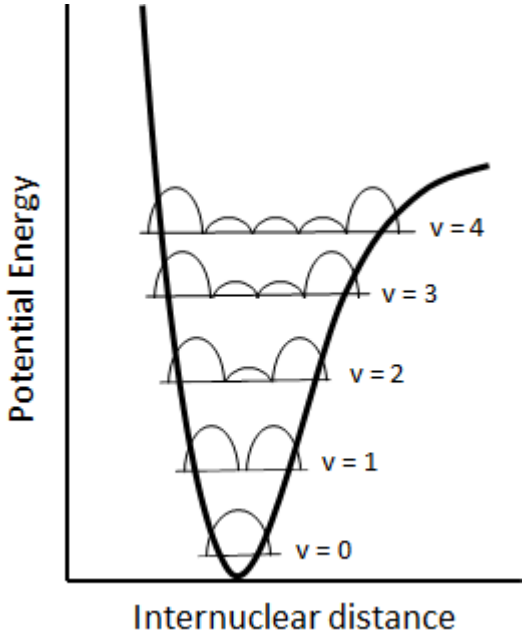

Figure 35. A Morse curve with vibrational probability functions for a series of vibrational quantum numbers. Adapted from reference 111

Nuclei move relatively very slowly on the timescales of electronic transitions, so during a transition the nuclei of the vibrating molecule can be assumed to be static. This is called the Franck-Condon principle which states that during an electronic transition, a change from one vibrational energy level to another will most likely occur if the two vibrational wavefunctions have more significant overlap.

The probability of photon absorption causing transitions between the vibrational levels in S_0 and S_1 is greatest, ie the absorption will be most intense, when the two states have similar internuclear separations and therefore the wavefunctions for the upper and lower vibronic states have greater overlap, called the Franck-Condon factor (Figure 36).

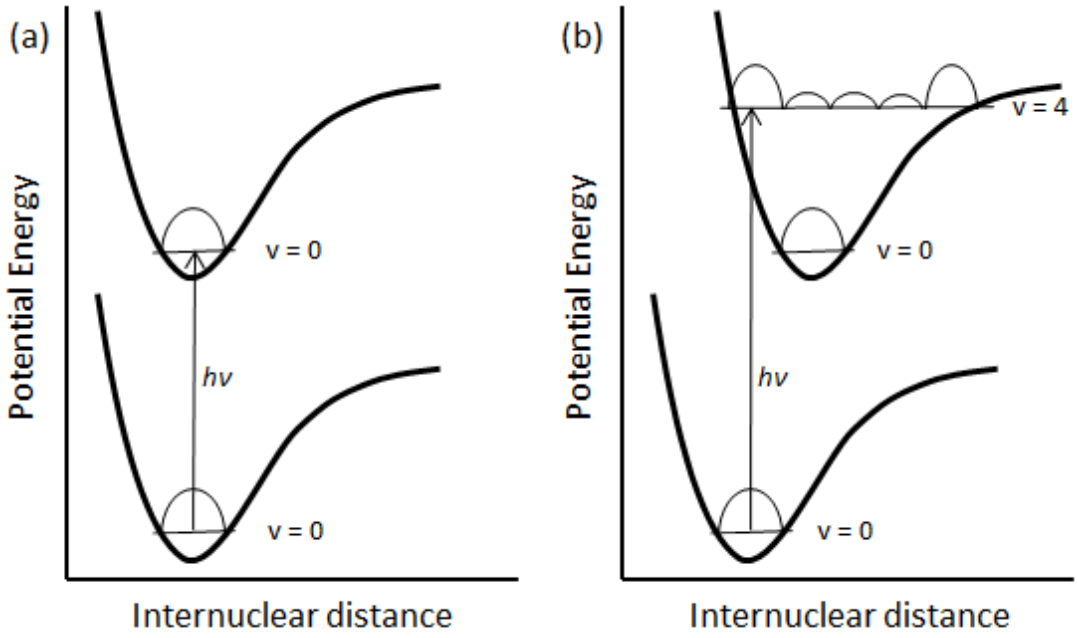

Figure 36. Electronic transitions with the greatest probability of absorption from S_0(v = 0). Adapted from reference 111.

In Figure 36 (a) both electronic states have similar geometries, shown by the minima of the Morse curves being coincident. The vibrational probability functions for S_0(v = 0) and S_1(v = 0) have the greatest overlap, ie the Franck-Condon factor for this transition is greatest, thus the v = 0 -> v = 0 transition will give rise to the most intense absorption. In Figure 36 (b) the excited state has a greater internuclear distance than the ground state. In this case, the vibrational probability functions for S_0(v = 0) and S_1(v = 4) have the greatest overlap so the v = 0 -> v = 4 absorption will be the most intense at a shorter wavelength than the v = 0 -> v = 0 transition.

With some organic compounds it is possible to discern the fine structure corresponding to the separate vibronic transitions eg anthracene,[112] however most have broad, featureless UV/Vis absorption spectra with the vibronic transitions merging into a smooth curve (Figure 37).

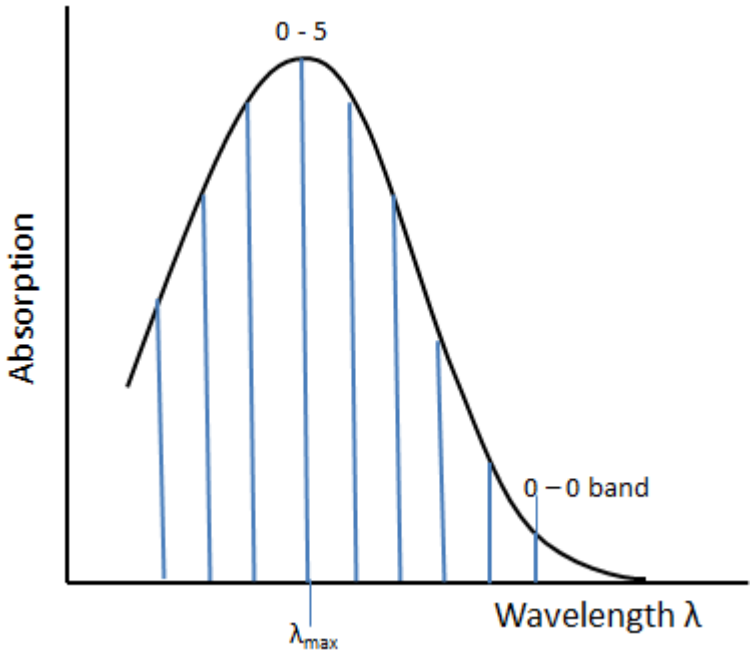

Figure 37. UV/Vis Absorption spectrum of organic compound comprising many vibronic transitions.

3 Dye Design

3.1 Introduction

The aim of this project was to design and synthesise dyes containing the azulene chromophore, characterise them and then to evaluate their performance as sensitisers in dye sensitised solar cells, with a view to improving the efficiency of the cells through structural modifications of the dyes.

As one of the crucial components of a DSSC, the photosensitising dye should exhibit some essential characteristics:

1. The dye absorption spectrum ideally should cover the entire visible spectrum and extend into the near-infrared (NIR) to maximise the absorbed energy;

2. The dye should have one or more anchoring groups to immobilise and bind it to the semiconductor surface;

3. The excited state energy of the dye should be higher than the conduction band edge of the semiconductor (n-type DSSCs) so that efficient electron injection from the dye into the semiconductor conduction band can take place;

4. The oxidised dye energy level must be more positive than the redox potential of the electrolyte to enable dye regeneration; and

5. The dye must be photo-, electrochemically and thermally stable to ensure that it survives the processes of DSSC fabrication and endures the continuous redox cycle associated with power generation long enough to provide a cell life of 15-20 years.

3.2 Anchor Group

DSSC sensitising dyes must have a suitable group that immobilises and couples the dye molecule to the oxide surface, known as the anchoring group. Dye molecules may be attached to a metal oxide substrate surface by a variety of mechanisms including covalent bonding, electrostatic interaction, hydrogen bonding, hydrophobic

interaction, van der Waals forces or physical entrapment.[113] Covalent bonding is almost exclusively used between dyes and TiO_2 surface atoms to provide strong coupling and device stability.

A variety of different anchor groups have been investigated, including phosphonic acids and carboxylic acids and their derivatives (esters, acid chlorides, carboxylate salts or amides).[113] Silanes, ethers, acetylacetonate and salicylates have also been employed.[114]

Carboxylic acid and cyanoacrylic acid groups are most frequently used for DSSC dyes. According to Polo and co-workers, six possible anchor modes have been identified: mono-dentate ester, bi-dentate chelating, bi-dentate bridging, mono-dentate and bi-dentate H-bonding, as well as mono-dentate coordination via the carbonyl group[113,115] (Figure 38).

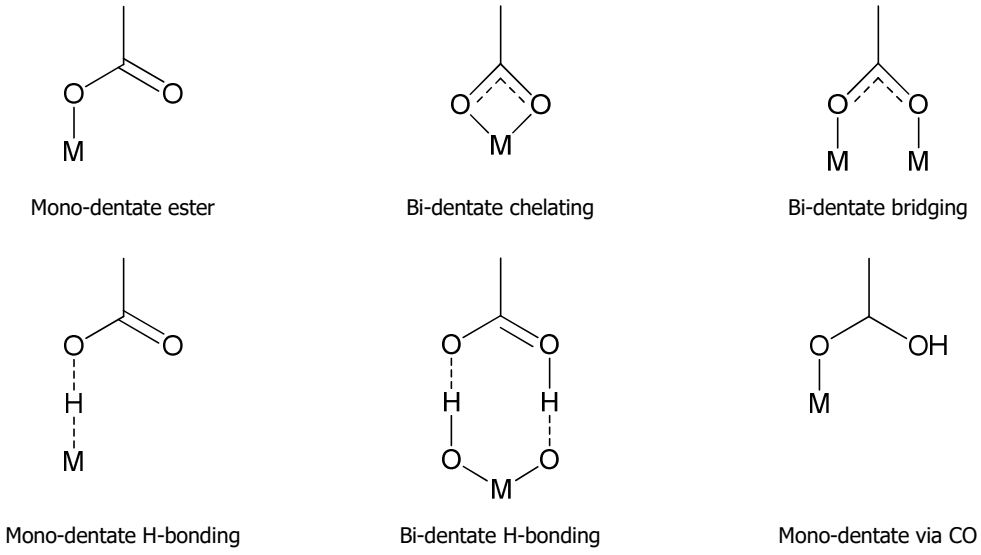

Figure 38. Possible Carboxylic Acid - Metal Oxide Binding Modes. Adapted from ref. 116

The amphoteric metal oxide nano-particle surface contains hydroxyl groups[117] which may be protonated by the carboxylic acid anchor group. The positively charged semiconductor surface then attracts the dye anion. Nucleophilic attack by the anion with elimination of water will result in the mono-dentate ester anchoring mode (Figure 38). The resulting covalent link is desirable, and may be augmented by further coordination and H-bonding.

Because of its excellent electron withdrawing capability, cyanoacrylic acid is used in most D-π-A dyes, whereas carboxylic acid anchors are usually used for transition metal complexes where metal-to-ligand-charge-transfer (MLCT) predominates.

The anchoring group may be either directly attached to the donor moiety or there may be a linking group in between them.

3.3 Linker Group

The linking group has two functions:

1. It increases the physical distance between the dye moiety and the TiO_2 substrate which should reduce the chance of charge recombination from TiO_2 to oxidised dye; and

2. It increases the conjugation chain length between the dye moiety and the electron acceptor (anchoring) group, which both intensifies and shifts the light absorption to longer wavelengths (bathochromic shift).

Linker groups for DSSC dyes are electron rich, π-conjugated moieties. A variety of functional units have been employed including vinyl, alkynyl, benzene, thiophene, furan, pyrrole, thienothiophene, benzothiadiazole,[118] 3,4-ethylenedioxythiophene (EDOT), 3-hexylthiophene (3HT), dithienothiophene, 4,4-dihexyl-4H-cyclopentadithiophene and 4,4-dihexyl-4H-silolodithiophene[119] (Figure 39).

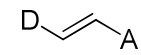

Vinyl

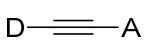

Alkynyl

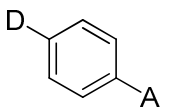

Benzene

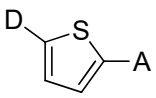

Thiophene

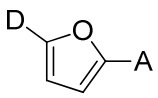

Furan

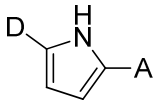

Pyrrole

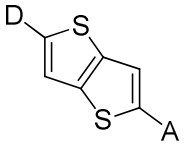

Thienothiophene

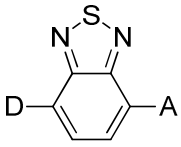

Benzothiadiazole

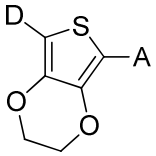

3,4-ethylenedioxy thiophene (EDOT)

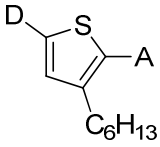

3-Hexyl thiophene (3HT)

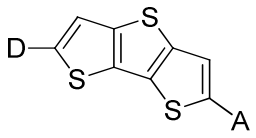

Dithienothiophene

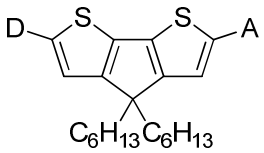

4,4-Dihexyl-4H-cyclopenta dithiophene

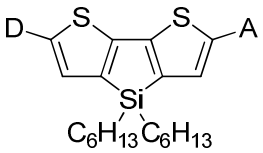

4,4-Dihexyl-4H-silolodithiophene

Figure 39. Dye π-linker example functional units

The units in Figure 39 are used individually, multiply (eg bithiophene) or in combinations to tune the photophysics and HOMO / LUMO energy levels of the resulting photo-sensitisers. For example, dyes C101 and TF-3 (Figure 7) use single thiophene and EDOT units respectively in their linkers; dyes YD2 and YD2-o-C8 (Figure 8) use a combined alkynyl with benzene ring; and dye C219 (Figure 18) employs an EDOT and 4,4-dihexyl-4H-silolodithiophene combination.

The proposed sensitisers bearing the azulene chromophores are therefore of the D-π-A type as described above (section 1.4.5 above). Thiophene was chosen as a starting point for the π-linker, attached to a cyanoacrylic acid group to anchor the dye to the surface of a TiO_2 nanoparticle (Figure 40).

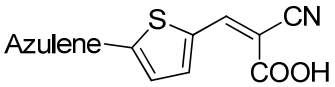

Figure 40. Azulene donor-thiophene linker-cyanoacrylic acid acceptor/anchor structure

The initial objective therefore was to synthesise, characterise and test (in DSSCs) sensitisers based on azulene with an attached 2-cyano-3-(thiophen-2-yl)acrylic acid group.

3.4 Molecular Orbital Models

In order that an electron becomes injected from an adsorbed sensitiser molecule into a TiO_2 nanoparticle it is necessary that, following photo-excitation, the electron density shifts from the azulene donor to the anchor group, from which rapid electron injection into the semiconductor conduction band takes place. Because of the different electron density distributions in the ground and excited states of azulene (section 1.5.1 above), the position of the linker/anchor group on the azulene framework will probably have a large effect on the performance of DSSCs based on the resulting photo-sensitisers.

In the ground state (HOMO, S_0) greatest electron density is located primarily on the C-1 and C-3 carbons in the five membered ring, with a node along the long axis of the molecule, resulting in the dipole moment and reactivity towards electrophiles already described (Sections 1.5 - 1.5.3). In the first excited state (LUMO, S_1), electron density shifts away from C-1 and C-3 to the C-4, C-6 and C-8 carbons in the seven membered ring, and to C-2 in the five membered ring, causing a reversal in the dipole moment. In the second excited state (LUMO+1, S_2), there is again a node along the long axis with primary electron density on the odd numbered carbons. Figure 41 depicts Extended Hückel MO calculations showing electron density distribution for azulene's ground and first two excited states.

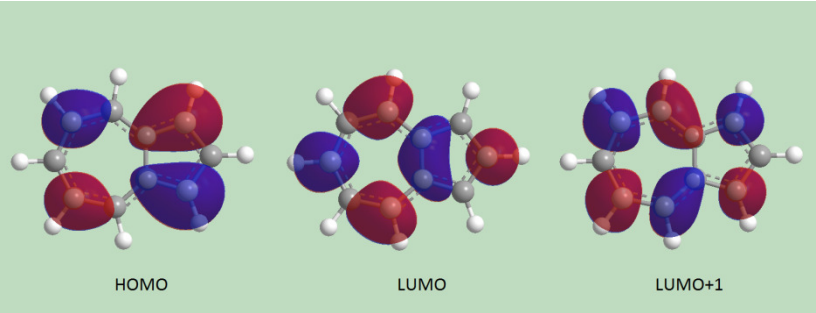

Figure 41. Azulene electron density distributions in ground and excited states

Similar electron density models can be calculated for postulated dyes. With the linker/anchor group attached to azulene at the C-1 (Figure 42) or C-5 (Figure 43) positions, the HOMO electron density distribution is mostly on the thiophene unit, ie the π linker. In the LUMO state, electron density shifts onto the azulene moiety (ie in the opposite direction to the anchor group and therefore the TiO_2 substrate), mostly on the seven membered ring in a pattern reminiscent of the azulene LUMO electron distribution.

Conversely, in the LUMO+1 state, the C-1 and C-5 positions of azulene are again electron rich and electron distribution is now shifted on to the thiophene unit and cyanoacrylic acid anchor group, ideally situated to enable electron injection into the TiO_2 substrate.

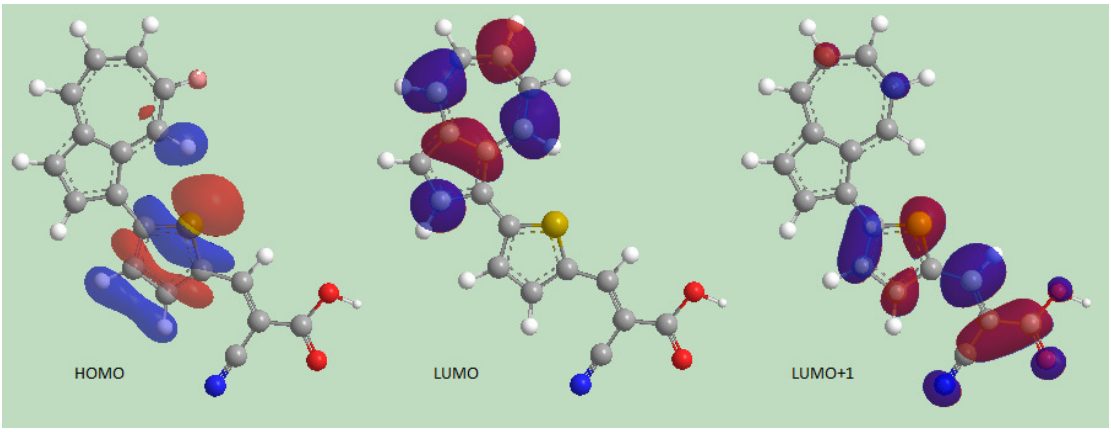

Figure 42. Orbital models for azulene substituted at C-1 with linker/anchor group

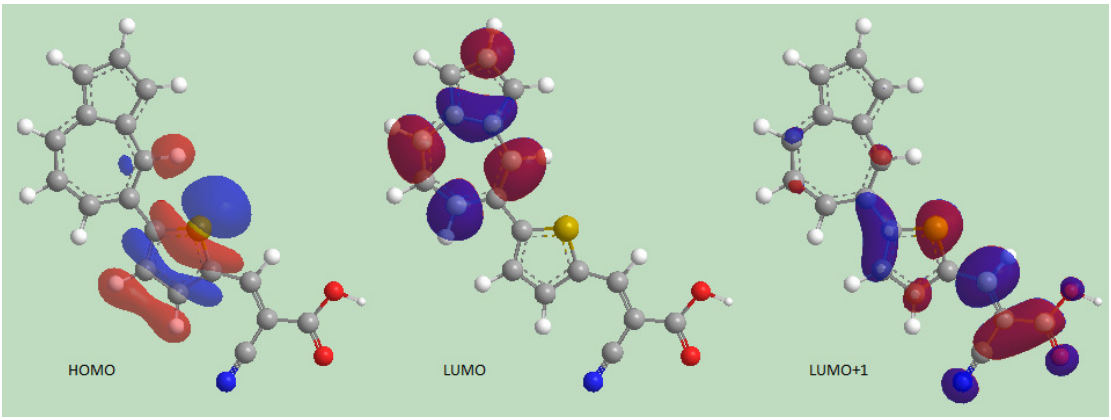

Figure 43. Orbital models for azulene substituted at C-5 with linker/anchor group

With azulene attached at the C-2 (Figure 44) and C-6 (Figure 45) positions to the linker/anchor group the models predict a similar but less extreme pattern of electron density shifts.

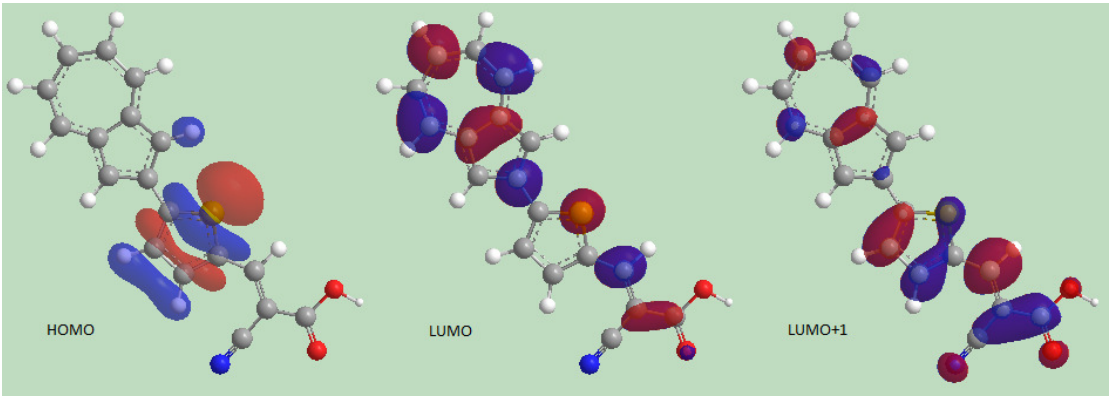

Figure 44. Orbital models for azulene substituted at C-2 with linker/anchor group

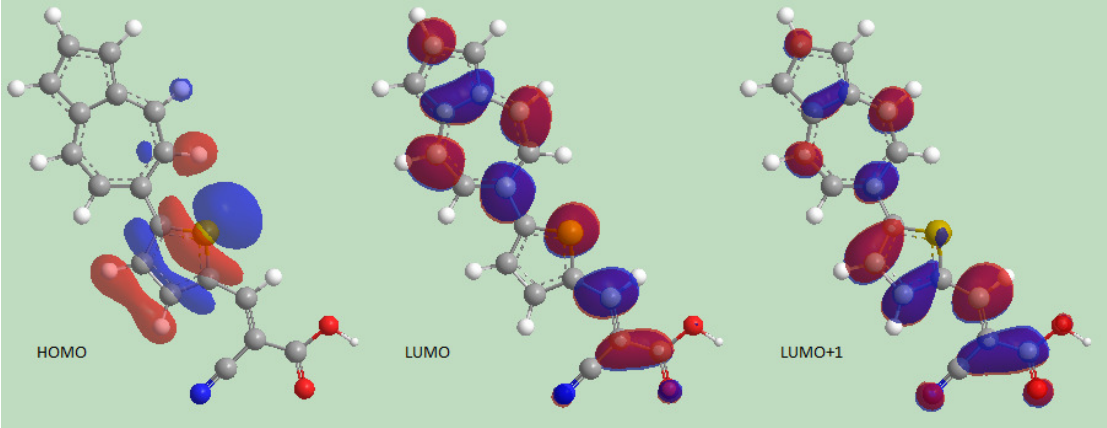

Figure 45. Orbital models for azulene substituted at C-6 with linker/anchor group

In these models, the HOMO electron density distribution is primarily on the thiophene linker, as was the case with the C-1 and C-5 substituted dyes. In the first excited state (LUMO) the electron density is distributed over most of the molecule, slightly favouring the azulene motif with the C-2 substituted dye. In the LUMO+1 the electron density is also distributed over the molecule, but with the greater density on the linker/anchor group.

The Extended Hückel molecular orbital model depicting the dye with azulene attached to the linker/anchor at the C-4 position does not follow the expected trend for substitutions at the even numbered carbon atoms (Figure 46). With this model the HOMO state electron density is fairly evenly distributed over the molecule, including the anchor group. The HOMO electron density distribution on the azulene moiety is similar to that of the LUMO states of the other dye models. The LUMO state electron density distribution is principally on the thiophene linker unit, similar to the HOMO state of the other dye models.

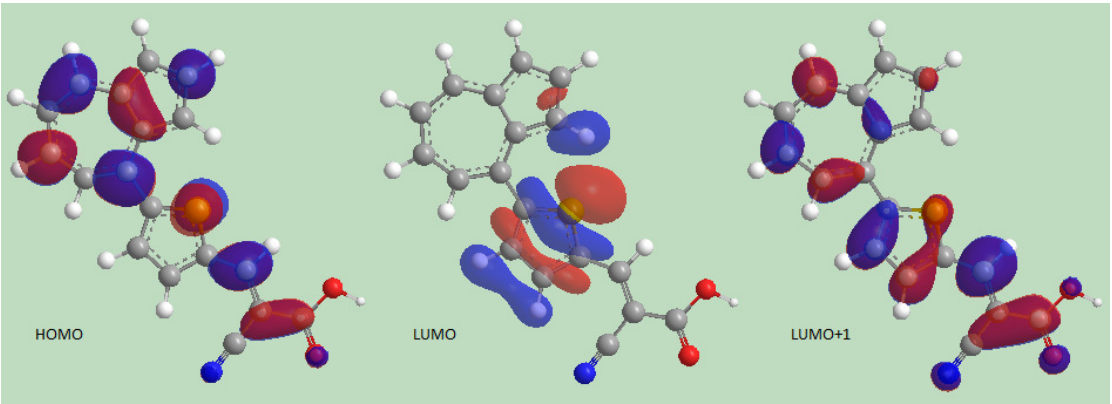

Figure 46. Orbital models for azulene substituted at C-4 with linker/anchor group

The LUMO+1 electron density is fairly evenly distributed over the molecule, and is similar to the other dyes with the linker/anchor attached to the azulene even numbered carbon atoms.

The models predict that electron density distributions for the C-1 and C-5 substituted azulene will be quite different to those for the C-2 and C-6 substituted derivatives. This could be rationalised from the electronic structure of azulene discussed above (section 1.5.1). The model for the C-4 substituted dye might be expected to be similar to the other dyes with the linker/anchor group attached to even-numbered carbon atoms (C-2 and C-6); however the model predicts that the electron density distributions for HOMO and LUMO energy levels are switched compared with the other dyes. If this is accurate then the C-4 attached dye is probably unsuitable as a DSSC sensitiser because the HOMO will be coupled to the TiO_2 substrate.

3.5 Excited States

The lifetime of the azulene S_1 state is very short, with non-emissive decay to the ground state occurring in less than 1 ps.[120] The S_2 state is long-lived, however, with a lifetime of ~1 ns and a fluorescence yield of 3-5%, and up to 20% with difluoroazulenes.[121] It therefore seems likely that electron injection will occur from the S_2 (LUMO+1) energy state rather than the LUMO.

In the UV/Vis spectrum of azulene (**1**), the S_0-S_1 transition (HOMO-LUMO) is a weak, broad absorption in the red/green region (λ_{max} = 580 nm, ε = 3.48 x 10^2 M^{-1} cm^{-1}),[121] and the S_0-S_2 transition (HOMO-LUMO+1) is a much stronger absorption in the near UV region (λ_{max} = 341 nm, ε = 4.01 x 10^3 M^{-1} cm^{-1}).[121] The S_0-S_2 transition would therefore be better at harvesting photons if it could be persuaded to absorb in the visible region.

All of the orbital models predict that there will be some electron density on the anchor group due to a shift between the HOMO and LUMO+1 following absorption of a photon of sufficient energy. The dyes with the linker/anchor group at azulene C-1 and C-5 show the highest electron density on the anchor group in the LUMO+1. In the LUMO, however, these dyes are predicted to have low electron density on the anchor group and high electron density on the azulene moiety, away from the TiO_2

surface. Since electron injection was expected to occur from the second excited state, attachment of the linker/anchor group at azulene C-1 or C-5 seemed to be appropriate. If efficient electron injection did not occur from the LUMO+1, then dyes with the linker/anchor group attached to an even-numbered carbon where electron density is highest in the LUMO may prove to be more successful.

Synthesis of azulenes substituted at the C-5 position is known to be difficult (see discussion section 1.5.3 above on page 27). The initial target molecule for synthesis and characterisation was therefore azulene with the linker/anchor group attached at the C-1 position, 3-(5-(azulen-1-yl)thiophen-2-yl)-2-cyanoacrylic acid, coded Az-1-tcaa (**84**) and variants with substituents at other positions in the azulene framework (Figure 47).

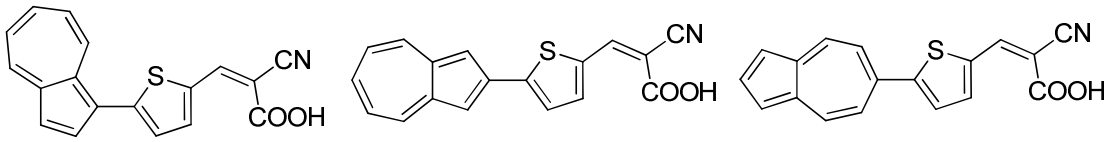

84– Az-1-tcaa **85**– Az-2-tcaa **86**– Az-6-tcaa

Figure 47. Molecular structures for proposed dyes Az-1-tcaa, Az-2-tcaa and Az-6-tcaa

This was to be followed by dyes with the linker/anchor group attached at C-2, 3-(5-(azulen-2-yl)thiophen-2-yl)-2-cyanoacrylic acid (**85**) and at C-6, 3-(5-(azulen-6-yl)thiophen-2-yl)-2-cyanoacrylic acid (**86**), coded Az-2-tcaa and Az-6-tcaa respectively.

4 Azulene Dyes – 1st Generation

4.1 Dye Az-1-tcaa (84) Proposed Synthetic Routes

Several synthetic routes were considered.

4.1.1 Cyanoacrylic Acid Anchor Group

The final stage in each proposed retrosynthesis is the attachment of the cyanoacrylic acid anchor group, which is conveniently achieved by Knoevenagel condensation of 5-(azulen-1-yl)thiophene-2-carboxaldehyde (**87**) with cyanoacetic acid (**88**) (Scheme 25).

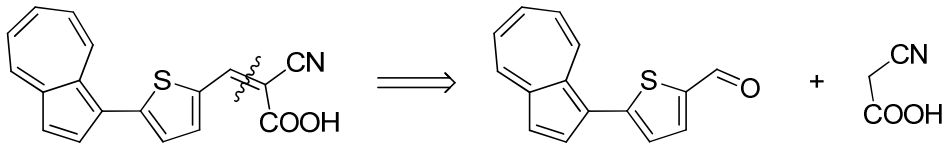

84 **87** **88**

Scheme 25. Retrosynthesis of Az-1-tcaa, final stage

4.1.2 Aldehyde Intermediate (87)

Several synthetic routes to **87** were considered.

4.1.2.1 Cross-Coupling Reactions

There have been some reports of transition metal catalysed cross-coupling reactions with azulene derivatives forming one of the coupling partners. In 2005 Lamberto et al[122] obtained a moderate yield (35%) of **91** with a Suzuki-type coupling of 1-bromoazulene (**7**) with **89**. The method used was in-situ generation of the 9-alkynyl-9-BBN coupling partner **90** from **89** using $(TMS)_2NLi$ to deprotonate the terminal alkyne and quenching of the resulting organo-lithium with 9-Methoxy-9-BBN. Coupling with **7** was achieved using $Pd(PPh_3)_4$ catalyst (Scheme 26).

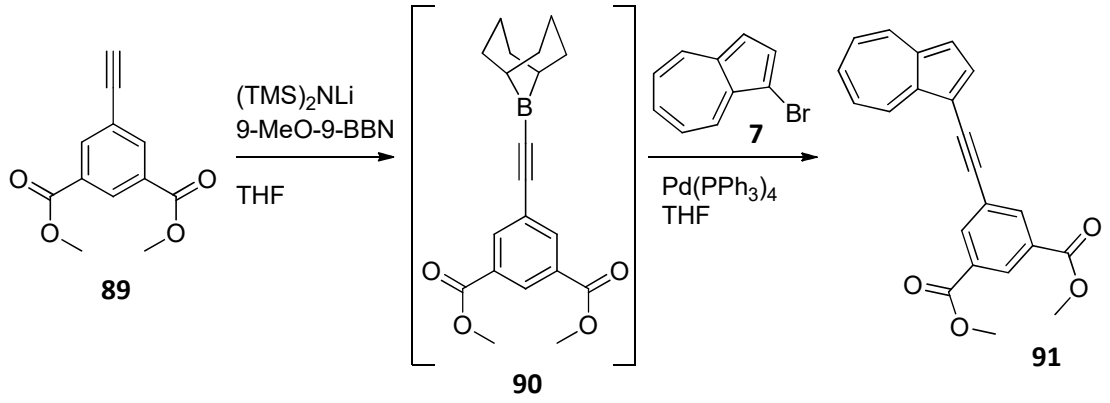

Scheme 26. Suzuki-type cross-coupling

They achieved a greater yield (100%!) with the Sonogashira cross-coupling of 1-iodoazulene (**92**) with tetramethylsilylacetylene (**93**). Following removal of the trimethylsilyl group a second Sonogashira cross-coupling reaction with **96** yielded **91** in 67% overall yield from azulene (Scheme 27).

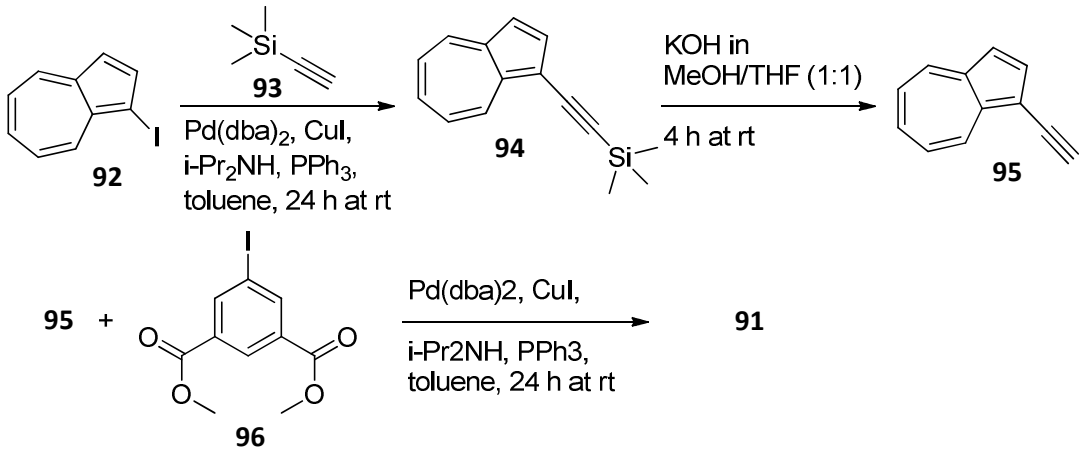

Scheme 27. Sonogashira cross-coupling

In 2002 Okujima et al[123] claimed to have created the first organometallic azulene reagents. 6-(tri-*n*-butylstannyl)azulenes (**97**) were prepared by a Pd(0) catalysed stannylation of 6-bromoazulenes (**98**) (Scheme 28).

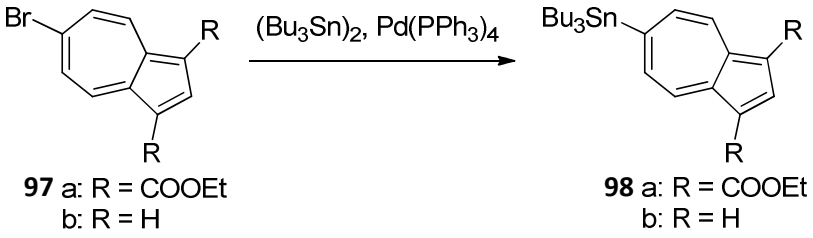

Scheme 28. Stannylation of 6-bromoazulene

The 6-(tri-*n*-butylstannyl)azulenes (**98**) were then used in Stille Pd(0) catalysed cross-coupling reactions with 4-halotoluenes (**99**) to give the coupled products (**100**) (Scheme 29).

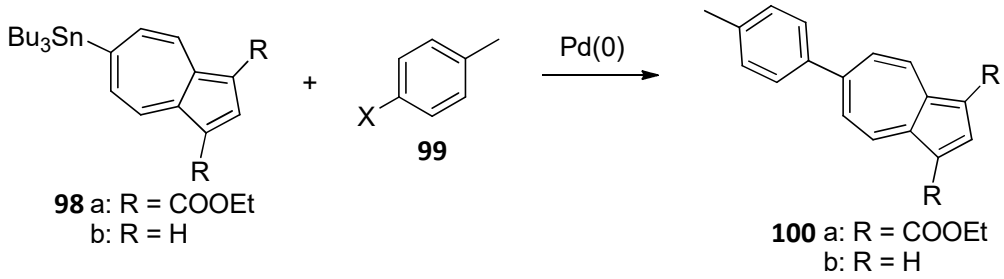

Scheme 29. Stille cross-coupling

Yields varied between 8% and 74%. 4-Tolylbromide gave better yields than the iodide, and adding caesium fluoride increased the yields significantly.

In 2004, Ito et al[124] synthesised 2-azulenylboronate (**103**) in 53% yield from 2-iodoazulene (**101**) by halogen–metal exchange using *n*-BuLi and subsequent quenching with 2-isopropoxy-4,4,5,5-tetramethyl-1,3,2-dioxaborolane (ITDB,**102**) (Scheme 30).

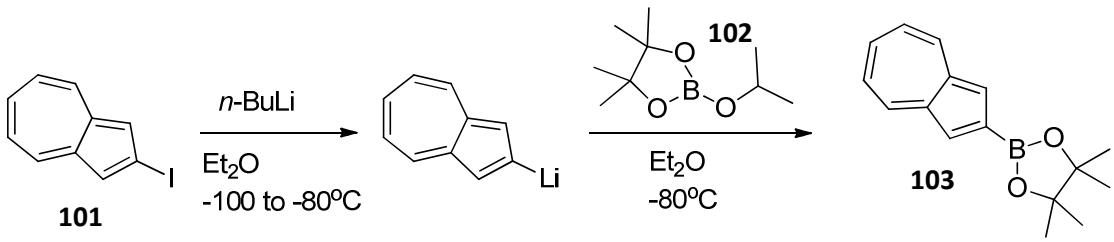

Scheme 30. Borylation of 2-iodoazulene

The 2-azulenylboronate (**103**) was then used in Suzuki-Miyaura cross-coupling reactions with a variety of aryl halides (Scheme 31).

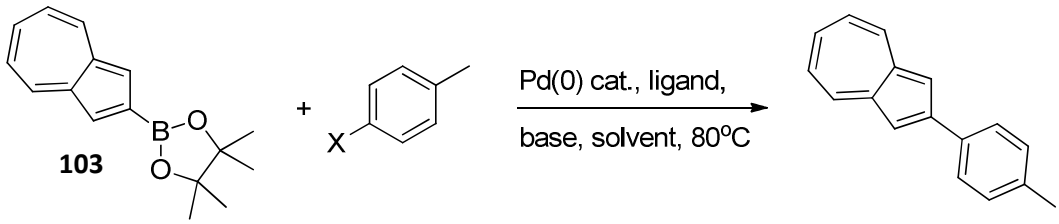

Scheme 31. Suzuki-Miyaura cross-coupling of 1-azulenylborates

Yields from 7% to 73% were recorded, with optimum yields achieved using bromoarenes, dba ligand and Cs_2CO_3 base in dioxane.

In 2001, Kane et al tried transition metal catalysed cross-coupling of 1-azulenyl triflate (**104**) which they had synthesised using a novel ring expansion and annulation method (see 1.5.5.5 above).[93] Attempts to utilize this compound in efficient coupling reactions with various organotin, boron, zinc, aluminium, copper, and magnesium reagents were not successful. Conditions which had proved successful in coupling reactions with the triflate derivative of 1-naphthol gave only uncharacterisable polymeric products in the case of the azulenyl triflate (**104**). Eventually successful coupling reactions were achieved using Buchwald's *o*-(dicyclohexylphosphino)biphenyl ligand in coupling reactions with B-alkyl- or B-aryl-9-BBN giving 1-ethylazulene (**105**) or 1-arylazulene in 56% and 60% yields respectively (Scheme 32).

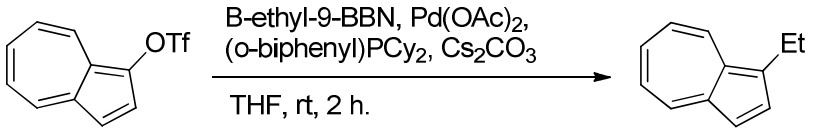

104 **105**

Scheme 32. Suzuki-Miyaura cross-coupling of 1-azulenyl triflate

In principle, synthesis of intermediate **87** should be achievable by a palladium catalysed cross-coupling reaction between an azulene (**106**) functionalised at the C-1 position with a halide or pseudo-halide group X, and an organometallic derivative of thiophene-2-carboxaldehyde functionalised at the C-5 (**107**) position, eg with boron (Suzuki-Miyaura), zinc (Negishi) or tin (Stille) (Scheme 33).

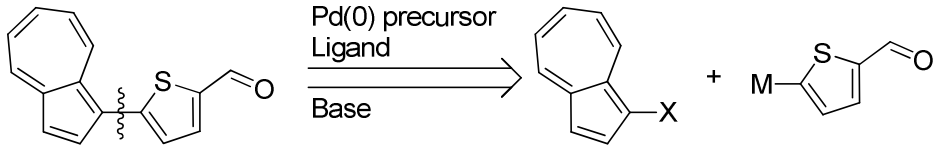

87 **106** **107**

Scheme 33. Cross-coupling retrosynthesis of intermediate 87

The various palladium catalysed cross-coupling reactions proceed via similar catalytic cycles involving oxidative addition of the organo-halide or pseudo halide to a palladium (0) / phosphine ligand complex. This results in a palladium (II) complex containing the fragmented electrophilic coupling partner as ligands. This is followed by a transmetallation or ligand exchange step where the second coupling partner is also attached to the palladium (II) complex. Reductive elimination of the product then re-generates the palladium (0) complex ready for the next catalytic cycle (Figure 48).

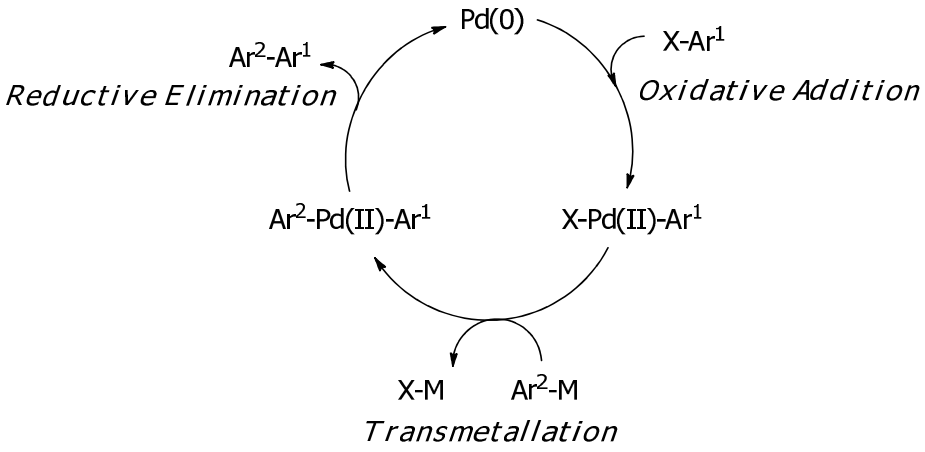

Figure 48. Pd(0) catalysed cross-coupling reaction catalytic cycle

Previous personal attempts at azulene arylation by Suzuki-Miyaura cross coupling reactions of 1-bromo-4,6,8-trimethylazulene (**108**) with methyl 5-(4,4,5,5-tetramethyl-1,3,2-dioxaborolan-2-yl)thiophene-2-carboxylate (**109**) proved to be unsuccessful, however, with no detectable product in the reaction mixture after extended reaction times (>24 hours) at elevated temperatures (refluxing toluene) (Scheme 34). In the oxidative addition step, the electron-rich palladium (0) complex reacts with the organohalide by nucleophilic attack; however the C-1 position of azulene is very electron rich making nucleophilic attack unfavourable, so it was assumed that this step in the cycle was failing.

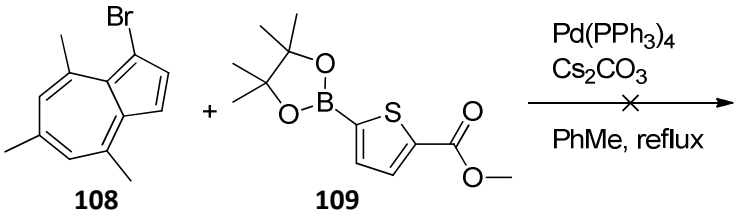

108 **109**

Scheme 34. Failed attempted Suzuki-Miyaura cross-coupling reactions

Of course, the coupling partners in a cross-coupling reaction may be reversed, ie the azulenic partner could be the organo-metallic compound (nucleophile) and the thiophene derivative the halide (electrophile). In this case oxidative addition would take place with the halo-thiophene derivative and transmetallation with the azuleno-metallic partner, which may be more successful than oxidative addition to electron-rich 1-bromoazulene.

Reports of azulene cross-coupling reactions in the literature are sparse. Kane *et al.*[93] reported similar difficulties with Suzuki-Miyaura cross-coupling of azulene-1-yl triflates, yielding uncharacterisable polymeric products in their case, but eventually

achieved moderate yields of 1-alkylated azulenes with the use of Buchwald's *o*-(dicyclohexylphosphino)biphenyl ligand.

The triflate substituent at the azulene C-1 position was created as a "side effect" of the method used to synthesise substituted azulenes via a ring-expansion and annulation route (Scheme 35).

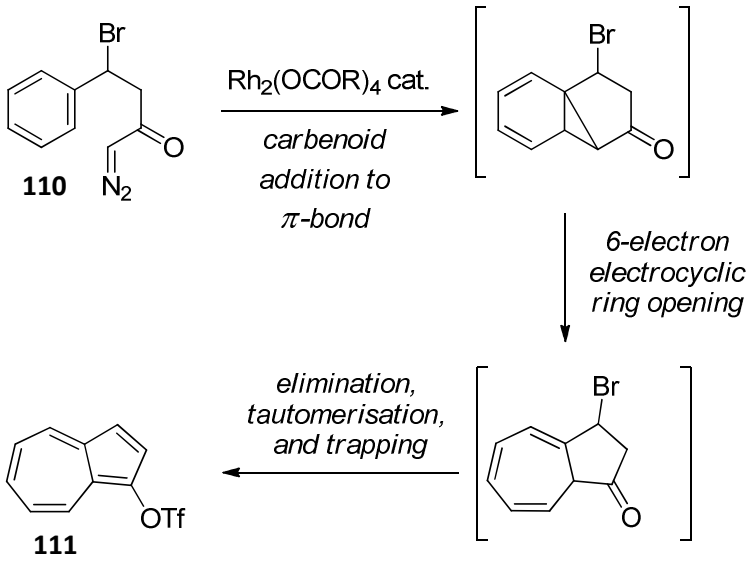

Scheme 35. Danheiser's ring expansion and annulation synthesis of azulene derivatives

In the final step of the synthesis, HBr is eliminated from the 5-membered ring giving the cyclic unsaturated ketone. The ring becomes aromatic by tautomerism (H on bridgehead C moves to carbonyl O). The triflate group is formed by trapping the 1-hydroxyl group thus formed with triflic anhydride. The authors found it necessary to trap the hydroxyl group because the azulen-1-ols initially formed were unstable and rapidly degraded or polymerised.

Deprés *et al*. briefly reported the Suzuki-Miyaura cross-coupling of 1-chloroazulene (**112**) with methylboronic acid in their paper describing a flexible route to azulene synthesis.[102] Again, the 1-chloro substituent was an artefact of the azulene synthesis used. For the cross-coupling reaction, the authors used reaction conditions developed by Buchwald *et al.* for efficient Suzuki-Miyaura cross coupling of unactivated aryl chlorides with boronic acids,[125] and obtained yields of 1-methylazulenes of up to 95%. A key part of the coupling reaction was the use of a specially designed ligand, dicyclohexyl(2',6'-dimethoxy-[1,1'-biphenyl]-2-yl)phosphine or "SPhos" (**113**) (Figure 49).

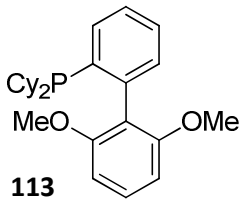

113

Figure 49. Buchwald's "SPhos" ligand

4.1.2.2 In-situ Thiophene Ring Synthesis

As an alternative to cross-coupling reactions, a synthetic route to **87** was devised via construction of the thiophene ring in-situ, rather than coupling a pre-formed thiophene derivative to a functionalised azulene compound (Scheme 36).

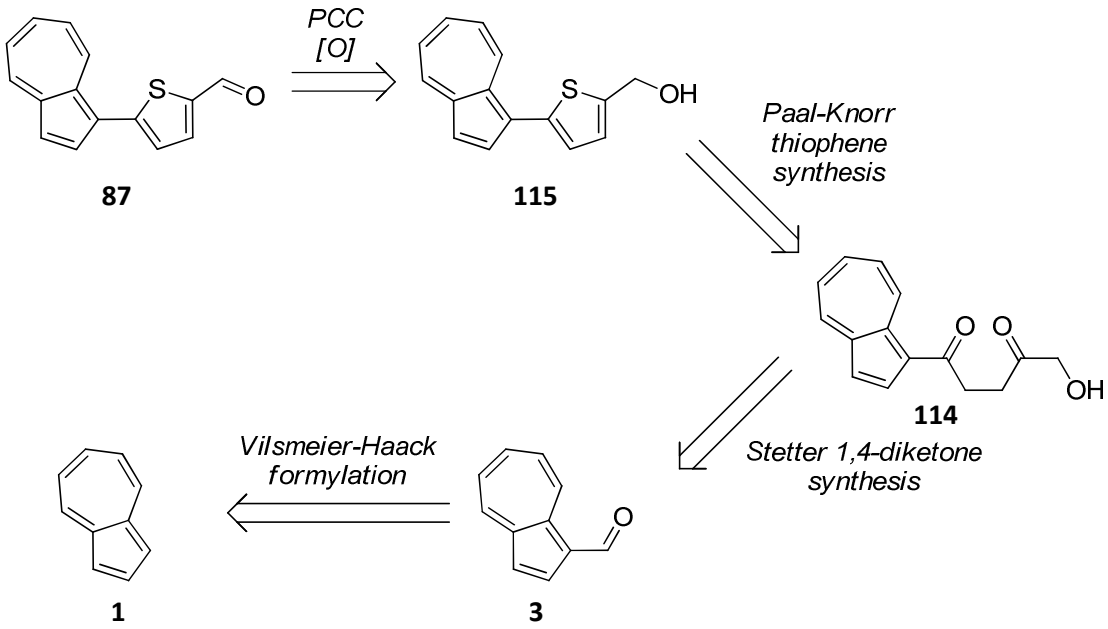

87 **115** **114** **1** **3**

Scheme 36. Retrosynthesis of intermediate 33 via Stetter and Paal-Knorr reactions

The well-known Paal-Knorr synthesis can be used to generate a thiophene ring from a 1,4-diketone by reaction with phosphorous pentasulphide or Lawesson's reagent (Scheme 37).

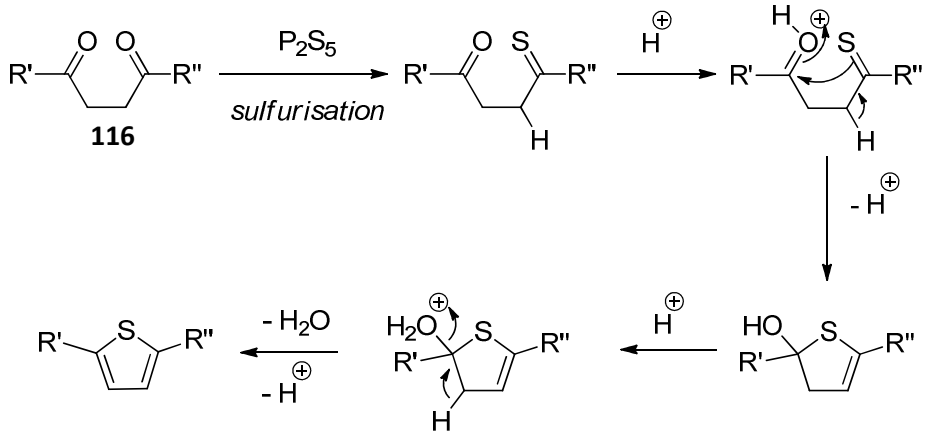

Scheme 37. Paal-Knorr thiophene synthesis

The 1,4-diketone (**116**) required for the Paal-Knorr reaction can be obtained by the Stetter reaction, which is a 1,4 addition reaction of an aldehyde with a Michael acceptor, eg an α,β-unsaturated ketone.[126] The reaction is catalysed by cyanide anion or thiazolium salt (**117**), which adds to and activates the aldehyde, reversing its polarity in an example of umpolung chemistry. The aldehyde is converted to a nucleophilic Breslow intermediate[127] (**118**) (Scheme 38).

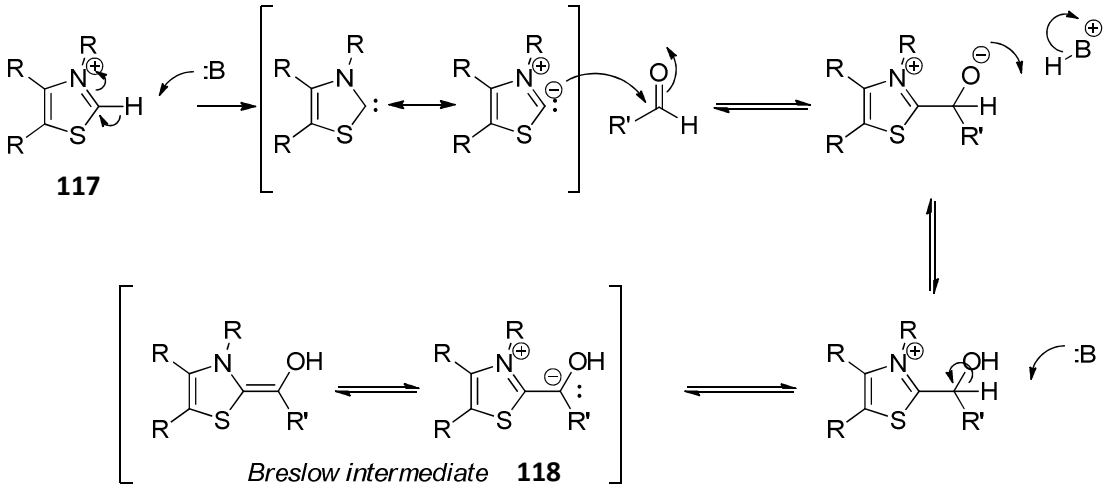

Scheme 38. Activation of aldehyde in Stetter reaction

The Breslow intermediate nucleophile then undergoes a 1,4 addition reaction with the Michael acceptor. Ultimately, the 1,4-diketone product of the Stetter reaction (**116**) is formed following elimination of the catalyst thiazolium ylide or cyanide ion (Scheme 39).

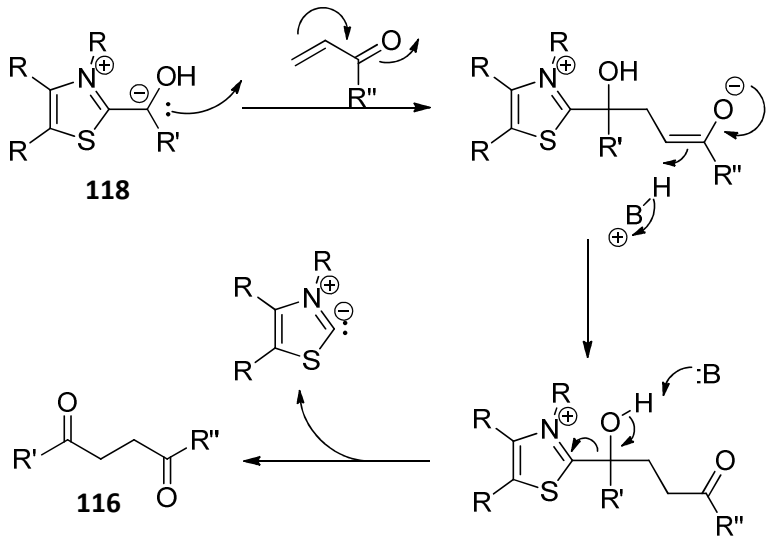

Scheme 39. 1,4 addition of activated aldehyde to Michael acceptor

For the synthesis of **87**, the aldehyde substrate for the Stetter reaction is provided by Vilsmeier-Haack formylation of the azulene starting material. The Vilsmeier reagent, a substituted chloroiminium ion (**119**), is generated by the reaction of phosphorous oxychloride with a substituted amide, eg dimethylformamide. An electron-rich aromatic substrate undergoes electrophilic attack by the Vilsmeier reagent to produce an iminium ion which is hydrolysed to the aldehyde during workup (Scheme 40).

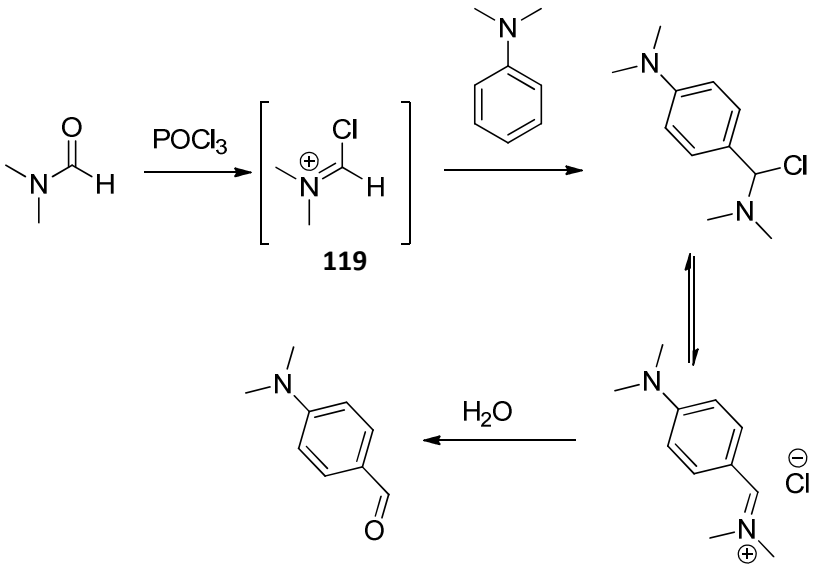

Scheme 40. Vilsmeyer-Haack formylation

4.1.2.3 Proposed Programmes

The avenues of research towards the goal of synthesising intermediate **87**, 5-(azulen-1-yl)thiophene-2-carboxaldehyde, were therefore as follows:

1. In-situ construction of the thiophene ring and α-formyl group via Stetter and Paal-Knorr reactions.

2. Cross-coupling of an azulenyl-1-metallic compound with 5-bromothiophene-2-carboxaldehyde; and

3. Suzuki-Miyaura cross-coupling of azulenyl-1-triflate or 1-chloroazulene with a boron functionalised thiophenecarboxaldehyde;

4.2 Dye Synthesis Discussion

4.2.1 4,6,8-Trimethylazulene

Due to the expense of purchasing azulene much of the trial work was conducted using 4,6,8-trimethylazulene (**48**) as the substrate, which can be made relatively cheaply via a modified version of the Hafner method[91] (see section 1.5.5.4 above for details of the Hafner azulene synthesis). **48** was prepared from 2,4,6-trimethylpyrylium tetrafluoroborate instead of the explosive perchlorate salt used in the literature.

The methyl groups of **48** were initially considered to be largely innocuous as far as reactivity was concerned. They are mildly electron donating and since they are attached to even-numbered azulene carbon atoms, slightly destabilise the LUMO resulting in a wider HOMO-LUMO gap (see section 1.5.1 above). This causes a hypsochromic shift in the absorption band which makes **48** a more purple (slightly redder) colour than azulene (**1**). The reactivity of **48** at the C-1, C-2 and C-3 positions was not expected to differ greatly from that of azulene.

4.2.2 In-Situ Thiophene Ring Synthesis

4,6,8-Trimethylazulene (**48**) was formylated using the Vilsmeier-Haack reaction to yield 4,6,8-trimethylazulene-1-carboxaldehyde (**120**) (Scheme 41).

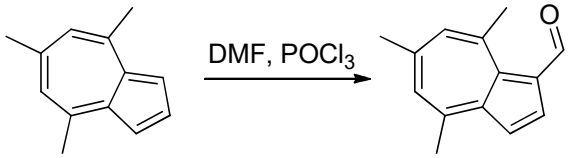

48 **120**

Scheme 41. Synthesis of 4,6,8-trimethylazulene-1-carboxaldehyde

This reaction proceeded smoothly and in good yield (81%). **120** was then used as the substrate for the Stetter reaction with the objective of synthesising the 1,4-diketone required for the Paal-Knorr thiophene synthesis (see section 4.1.2.2 above).

The target molecule **87** clearly has a formyl substituent on the thiophene α carbon. If this group or a precursor group that can be transformed into a formyl group is not introduced during the thiophene ring synthesis then it will be difficult or impossible to install it regioselectively afterwards, given that there would also be a highly reactive azulene moiety in the molecule. It is therefore necessary that the Michael acceptor component of the Stetter reaction be a compound incorporating such a group, eg 1-hydroxybut-3-en-2-one (**122**) which can be prepared from commercially available 2-butyne-1,4-diol (**121**)[128] (Scheme 42).

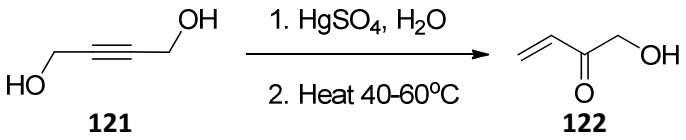

121 **122**

Scheme 42. Michael acceptor component for Stetter reaction

The Stetter reaction trials were carried out using methylvinylketone (**123**) as the Michael acceptor, however, to avoid possible complications wich may have been caused by the presence of a hydroxyl group. 3-Benzyl-5-(2-hydroxyethyl)-4-methylthiazol-3-ium (**124**) was employed as the catalyst with triethylamine base.

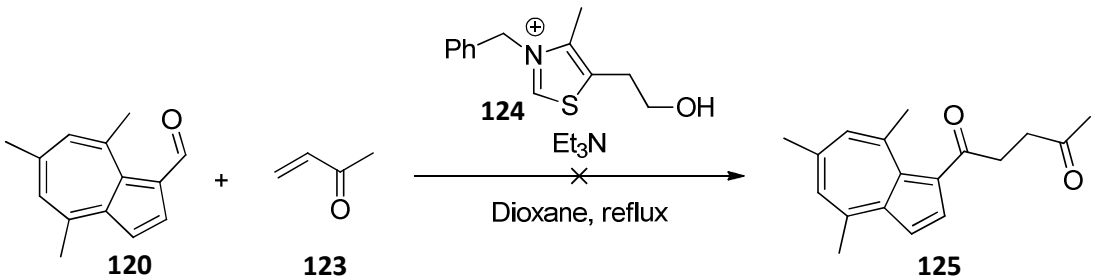

120 **123** **124** **125**

Scheme 43. Attempted Stetter reaction

Several attempts were made to synthesise 1-(4,6,8-trimethylazulen-1-yl)pentane-1,4-dione (**125**) by this method (Scheme 43), but unfortunately none of the desired product could be detected in the reaction mixture.

Possible reasons for the failure of the Stetter reaction are:

1. Instead of deprotonating the catalyst, the base may have deprotonated one of the methyl groups of **120**. The azulene C-4, C-6 and C-8 carbons are electron deficient (Figure 22, section 1.5.1 above) which renders the protons on the attached methyl groups more acidic and therefore more easily removed by base. This would have the effect of:

    a. Consuming the base leaving less or possibly none available for activating the thiazolium catalyst; and

    b. Increasing the electron density at the azulene C-1 and C-3 carbons of **120** (Scheme 44).

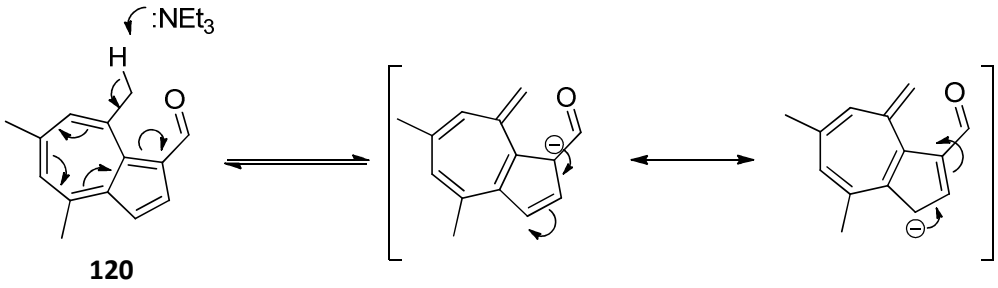

120

Scheme 44. Deprotonation of methyl group and resonance structures of resulting anion

2. The azulene C-1 (and C-3) carbons are very electron rich, attenuating the electrophilic nature of the aldehyde group in **120**, which would then be less likely to react with the nucleophilic catalyst. Ester groups at the azulene C-1 and C-3 positions are similarly affected and resist attack by Grignard reagents.[84]

Because of the failure of the Stetter reaction trials and the likelihood that the α-carbonyl attached to the azulene C-1 position is rendered inactive towards nucleophiles by electron donation, no further work was done on this avenue of research.

4.2.3 Metalated Azulene Compounds for Cross Coupling Reactions

Attempts were made to synthesise 1-borylated and 1-silylated azulene derivatives via lithiation of 1-bromoazulene (**7**) by halogen exchange reaction followed by quenching of the lithiated species (**126**) with an appropriate electrophile.

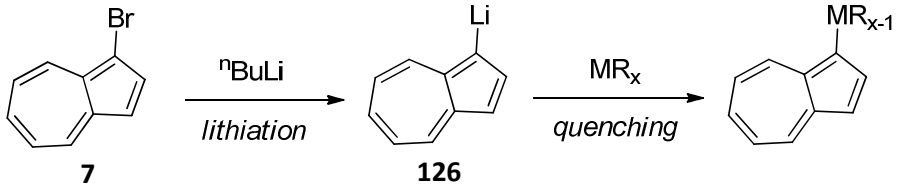

Figure 50. Synthetic approach to metalated azulene

Initial experiments were designed to produce 2-(azulen-1-yl)-4,4,5,5-tetramethyl-1,3,2-dioxaborolane (**127**) by quenching the lithiated azulene (**126**) with bis(pinacolato)diboron (B_2Pin_2).

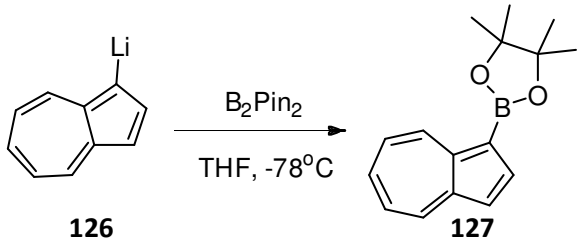

Scheme 45. Planned borylation of lithiated azulene

Azulene (**1**) was brominated using a single equivalent of *N*-bromosuccinimide (NBS) to give primarily 1-bromoazulene (**7**). It is impossible to avoid the production of some 1,3-dibromoazulene (**8**) as both the azulene C-1 and C-3 positions are susceptible to attack by electrophiles and the mono-brominated product is not deactivated sufficiently to prevent the second bromination. The crude reaction mixture therefore contained small (and equal) amounts of di-brominated and un-brominated azulene.

Because **7** is not sufficiently stable to purify by flash column chromatography, the crude reaction mixture was used immediately (following solvent removal) in the following lithiation stage without purification.

In the first lithiation attempt, no noticeable colour change was observed during the addition of *n*-BuLi to the crude reaction mixture from the bromination stage dissolved in THF at -78 °C. An appreciable colour change was expected because substitution of bromine for lithium would significantly change the electronics and

HOMO-LUMO gap of the molecule. Nor was any colour change observed with the addition of the B_2Pin_2. TLC analysis of the crude reaction mixture showed mostly 1-bromoazulene, suggesting that the lithiation step had failed.

The succinimide by-product of the bromination reaction with NBS has a pKa of ~9.5 and therefore easily deprotonated by the *n*-BuLi used in the lithiation reaction. Most of the n-BuLi used in the lithiation step would therefore be consumed by reacting with the succinimide by-product. In subsequent lithiation attempts an aqueous work-up of the bromination reaction crude including washing with sodium hydroxide solution was carried out prior to the lithiation step.

With the partially purified 1-bromoazulene crude, the colour of the reaction mixture during addition of n-BuLi changed from blue to green, indicating that the base was now reacting with **7**. On addition of the B_2Pin_2, there was a further colour change to dark grey-brown. TLC of the crude reaction mixture after workup showed several spots; the major spot was yellow with higher Rf than azulene or 1-bromoazulene, accompanied by several minor closely spaced brownish spots at lower Rf values. The TLC showed no sign of azulene or 1-bromoazulene. According to Crombie et al,[129] who synthesised this compound via a different route, the product should be dark purple, so it seems unlikely that the borylation reaction was successful.

An attempt was also made to synthesise a silylated azulene using a similar protocol to the attempted borylation. Following the bromination, work-up and lithiation steps chlorotrimethyl silane (TMSCl) was added to quench the lithiated azulene. In this experiment, after adding the *n*–BuLi in the lithiation step, the reaction mixture changed colour to yellow green, ie much yellower than before, suggesting that incomplete reaction had occurred and the green colour was due to a mixture of starting material (blue) and product of the lithiation step (probably yellow). After the TMSCl addition, the reaction mixture became cloudy due to a precipitate, possibly LiCl, but there was no further colour change until the mixture was allowed to warm to room temperature. During the warming period the mixture became dark grey-brown as it had with the attempted borylation reactions. TLC of the worked-up crude was similar to those from the attempted borylation reactions.

A test was done to determine the effect, if any, of *n*–BuLi on azulene (**1**), ie with no bromine substituent. The conditions used matched the lithiation steps above, ie

n–BuLi was added dropwise to a dry THF solution of azulene at -78°C. The solution remained blue, marginally greener than the starting material, and did not turn yellow. On addition of TMSCl, the original colour was immediately restored. TLC of the reaction mixture after warming to RT showed largely unreacted starting material.

Given that there was no sign of any starting material it seems likely that the lithium-halogen exchange reaction did occur. The assumption was made that the resulting azulenyl lithium species was not stable under the reaction conditions and decomposed before the quenching stage of the synthesis.

No further work was done on this avenue of research.

4.2.4 Azulenyl-1-triflate Synthesis

An attempt was made to replicate the synthesis of azulenyl-1-triflate using Kane's ring expansion and annelation method[93] (see section 1.5.5.5 above). The β-halodiazoketone starting material (Scheme 19) was derived from the corresponding cinnamic acid (**128**). Hydrobromination of the alkene double bond with a saturated solution of HBr in DCM in the presence of silica gel gave 3-bromo-3-phenylpropanoic acid (**129**). Subsequent treatment with oxalyl chloride to furnished the acid chloride **130** which reacted with diazomethane yielding the β-halodiazoketone **131** (Scheme 46).

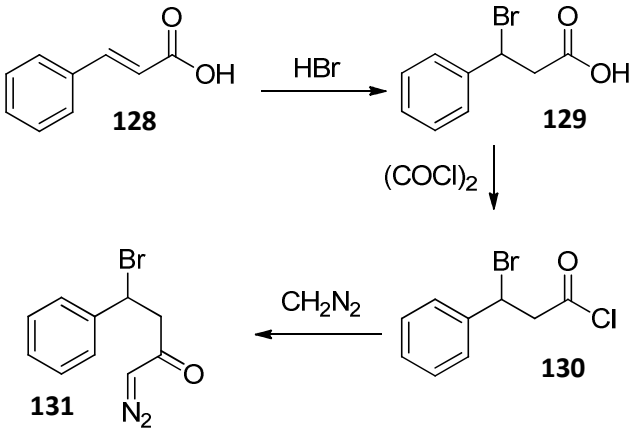

Scheme 46. β-halodiazoketone synthesis from cinnamic acid

Initial experiments were aimed at developing the hydrobromination reaction without the use of HBr gas according to the protocol developed by Kropp *et al.,*[130] which uses a silica gel surface mediated reaction of a HBr precursor and DCM solvent. The

HBr precursor used was bromotrimethylsilane, which reacts with the hydroxyl groups in silica gel to release HBr (Scheme 47).

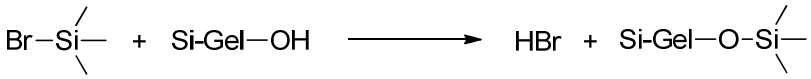

Scheme 47. Generation of HBr from $BrSiMe_3$ precursor

Several attempts were made to effect the hydrobromination reaction with 3,4-dimethoxycinnamic acid substrate. According to the Crombie,[129] electron-rich cinnamic acids were more easily hydrobrominated than electron deficient ones. The dimethoxy cinnamic acid should therefore be a reasonable test substrate; however while HBr (or some other highly corrosive substance) was clearly being generated in the reaction flask, none of the desired product was detected in the reaction mixtures.

4.2.5 Suzuki-Miyaura Cross-Coupling of 1-Chloroazulene with Boron Functionalised 2-Thiophenecarboxaldehyde

4.2.5.1 Azulenyl Coupling Partner (Electrophile)

1-Chloroazulene (**112**) was synthesised by the action of recrystallized *N*-chlorosuccinimide on azulene (**1**), similar to the synthesis of 1-bromoazulene (**7**) using NBS.

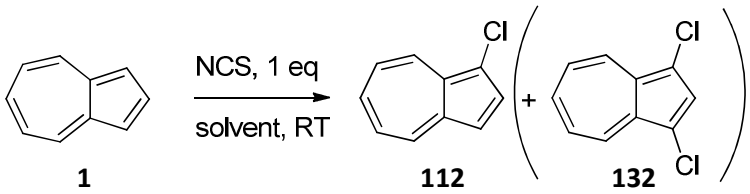

Scheme 48. Synthesis of 1-chloroazulene

The original solvent used was THF and the solid NCS was added portion-wise at regular intervals over a period of approximately ten minutes. A solution of NCS (or NBS) in THF rapidly becomes coloured, indicating the release of elemental chlorine (or bromine). Later experiments were carried out in dichloromethane (DCM); a solution of NCS (or NBS) in DCM remains colourless, so the DCM solution of NCS was added to the reaction dropwise via syringe. This allowed for a more controlled

addition of the halogenating agent and improved the selectivity for the mono-chlorinated product.

Initially, the work-up procedure used to remove the succinimide by-product when preparing 1-bromoazulene (**7**) was also used for the 1-chloroazulene work-up. The wash with aqueous NaOH seemed to degrade the 1-chloroazulene, however. Fortunately, 1-chloroazulene was found to be stable to purification by flash chromatography, so that technique was used to purify the product instead of the aqueous NaOH wash. The flash chromatography has the additional benefit of removing the unreacted azulene starting material and the unavoidable 1,3-dichloroazulene (**132**), yielding pure 1-chloroazulene.

4.2.5.2 Organoboron Coupling Partner

5-Formyl-2-thiopheneboronic acid (**138**) was the coupling partner originally chosen because the Buchwald group protocol[125] was developed to couple boronic acids. Since **138** is not commercially available a synthetic route was devised. Synthesis of **138** involves lithiation of thiophene-2-carboxaldehyde (**133**) and then quenching of the lithiated species with trimethylborate (**136**). Direct lithiation of **133** proved to be unsuccessful however due to reaction of the *n*–BuLi reagent with the carbonyl group of the aldehyde. It was therefore necessary to protect the aldehyde group prior to lithiation. The aldehyde was protected as a cyclic acetal (2-(thiophen-2-yl)-1,3-dioxolane (**135**)), using ethylene glycol (**134**) in refluxing toluene, catalysed by *p*-toluenesulphonic anhydride (TSAA). A Dean-Stark apparatus was used to remove the eliminated water from the reaction, driving it to completion. The product was purified by vacuum distillation. (Scheme 49)

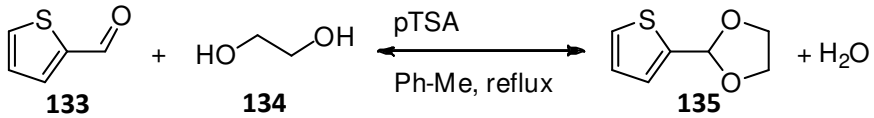

Scheme 49. 2-thiophenecarboxaldehyde protection

Lithiation of **135** with *n*-BuLi followed by quenching with **136** generated dimethyl (5-(1,3-dioxolan-2-yl)thiophen-2-yl)boronate (**137**), which hydrolysed to the unprotected product (**138**) on aqueous acid workup (Scheme 50).

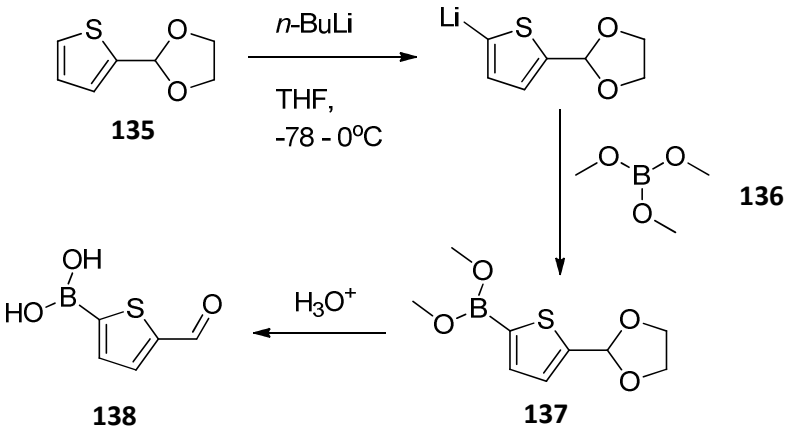

Scheme 50. Synthesis of 5-formyl-2-thiopheneboronic acid

In the initial cross-coupling reactions, **138** was used after aqueous workup without further purification. During the optimisation process, it was found that **138** could be recrystallised from a mixture of ethyl acetate and petroleum ether (40/60), and then subsequently that a more pure product could be obtained by recrystallisation from water. The ^{1}H NMR spectrum of **138** obtained by recrystallisation from water contained a lot of residual water, which was shown to be water of crystallisation by X-ray crystallography (Figure 51).[131]

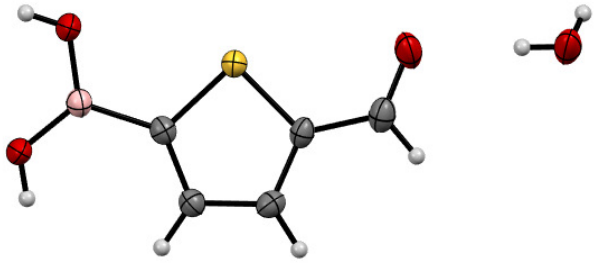

Figure 51. X-Ray crystal structure of 5-formyl-2-thiopheneboronic acid recrystallised from water

The water was successfully removed by treating an ethereal solution of the crystals with magnesium sulfate drying agent and then removing the ether *in vacuo* after filtering. The ^{1}H NMR spectrum was then free from water signal.

The ^{13}C NMR spectrum for **138** shows clear signals for four carbon atoms only (five expected). This is because signals for ^{13}C atoms next to a ^{11}B atom tend to be broadened. With aromatic boronic acids, the signal for the quaternary carbon atom bearing the boron atom is already weak and consequently is often difficult to discern from the background noise.[132]

4.2.5.3 Cross-Coupling Reaction

The first attempts at Suzuki-Miyaura cross-coupling of 1-chloroazulene (**112**) with 5-formyl-2-thiopheneboronic acid (**138**) were carried out using slightly modified conditions to those described by Buchwald et al.,[125] ie 1 equivalent of arylchloride, 1.5 equivalents of boronic acid and 2 equivalents of potassium phosphate base in toluene under nitrogen. The catalyst was formed in-situ from palladium acetate (4 mol%) and the SPhos ligand (**113**) (10 mol%). The catalyst loading was higher than that used by Buchwald et al. (0.003 – 1.0%) to increase the chances of producing some desired product. The initial reaction temperature chosen (RT to 50 °C) was lower than that used by Buchwald (90 to 110 °C) because azulene halides are rather unstable (Scheme 51).

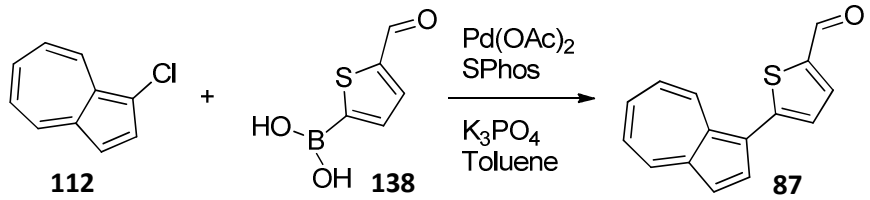

Scheme 51. Suzuki-Miyaura cross-coupling with modified Buchwald conditions

The reaction mixture changed colour from indigo to green during the initial 20 minutes while the temperature increased from RT to 50 °C. No further colour change was observed after stirring at 50 °C for an additional hour, or indeed for a further two hours at 70 °C and then 80 °C. TLCs showed much remaining starting material, but also an additional yellow spot with much lower Rf value.

Stirring was continued for a total of nine hours with no noticable change in colour and TLCs were hardly different from the ones taken during the first hour. After aqueous work-up and purification by flash chromatography, just over 20 mg of **87** was isolated corresponding to a yield of 6%. The product structure was confirmed by ^{1}H and ^{13}C NMR and mass spectrometry.

It appeared that the reaction had started well and that all the product that resulted was actually produced in the first 20 minutes or so (judging by the colour change and TLCs) but then the reaction stopped. After the initial approximately 20 minutes, further increases in temperature and extended reaction time were unfruitful. It was thought that either:

1. The catalyst was being deactivated, perhaps by contamination in the starting materials or by a reaction by-product; and/or
2. The boronic acid component was not stable under the reaction conditions and was undergoing protodeboronation.

The second of these hypotheses was partly supported by observation of a spot with the same R_f and appearance as 2-thiophenecarboxaldehyde in the reaction mixture TLCs. The same TLCs also showed a baseline spot of the correct colour for the boronic acid, however, indicating that at least some boronic acid remained when the reaction had terminated.

Further experiments were conducted with a view to increasing the product yield. The boronic acid starting material was further purified to eliminate possible contamination. This was accomplished by recrystallisation from hot ethyl acetate and petroleum ether.

Since the first reaction seemed to proceed at RT or slightly higher, subsequent experiments were performed at RT, with the hope that **138** would be more likely to survive if protodeboronation was the cause of the poor yield. Otherwise similar reaction conditions were employed except for the changes made in attempts to increase the conversion and yield.

5-formyl-2-thiopheneboronic acid (**138**) is almost insoluble in toluene but soluble in IPA (propan-2-ol) and THF. Coupling reactions were carried out in IPA and THF to see if the boronic acid solubility had a beneficial effect.

The reaction in THF was carried out under strictly anhydrous conditions using dry THF which had been sparged under argon for three hours immediately before use.

To test the hypothesis that the catalyst may have been deactivated, additional palladium acetate and SPhos ligand (equal to the original quantities) were added to the toluene and IPA reaction mixtures after several hours stirring. If the catalyst was becoming deactivated, addition of fresh catalyst may have kick-started the reaction at least for a short while, increasing the yield.

To test the hypothesis that **138** may be undergoing protodeboronation, an additional equivalent of **138** boronic acid was added to the toluene and IPA reaction

mixtures several hours after adding the additional catalyst. If the reaction was arrested because the boronic acid was becoming depleted through a competing reaction, adding more of the reagent should result in resumption of the reaction for a short period until it became depleted again.

With all three reactions (toluene, IPA and THF solvents), the turquoise reaction mixture colour noted previously was apparent within a few minutes of adding the respective solvent and stirring, and after 90 minutes stirring at RT the colour of all three was green. As before, TLCs showed much remaining blue starting material plus the yellow/green spot with lower R_f. Further TLCs at 90 minute intervals showed no discernible change and the colour of all three reactions remained constant.

Additional catalyst ($Pd(OAc)_2$ and SPhos) was added to the toluene and IPA reaction mixtures after stirring for ~16 hours. No further colour change or TLC change was apparent after stirring for an additional five hours, so catalyst deactivation seemed unlikely.

After adding the additional boronic acid reagent to the toluene and IPA reactions, no change in TLCs was apparent after stirring for a further nine hours, so boronic acid degradation seemed unlikely.

The yields from the initial coupling experiments are summarised below (Table 3).

Experiment	**Product Yield**	**1-Cl-Azulene recovered**
1: Toluene, RT to 100 °C	6.0%	-
2: Toluene, RT + added catalyst + extra **138**	8.8%	56%
3: IPA, RT + added catalyst + extra **138**	10.7%	65%
4: THF, anhydrous & sparged with Ar, RT	8.5%	59%

Table 3. Initial Suzuki-Miyaura coupling reactions

The yield was lowest from the first reaction which was run for an extended time at elevated temperatures, potentially degrading some of the product formed. The best product yield was achieved from the reaction in IPA; however the difference in yield between toluene, IPA and THF solvents is hardly significant. Also, it can be seen

that ~60% of the 1-chloroazulene starting material remained even after allowing many hours of reaction time and after adding additional catalyst and boronic acid coupling component in the case of experiments 2 and 3. Running the reaction under anhydrous, oxygen free conditions did not improve the yield. THF solvent seems to be no better or worse than toluene with respect to this reaction.

As already mentioned, a spot corresponding to the Rf and appearance of 2-thiophenecarboxaldehyde (2TC) was apparent in the reaction mixture TLCs. Some TLC tests were done with **138** in THF solution to determine when the thiophene-2-carboxaldehyde spot appears. The results are summarised below (Table 4).

Test	**Description**	**TLC Result**
1	**138** solution in THF, stir 30 mins @ RT	No 2TC spot seen
2	**138** + $Pd(Oac)_2$, stir 30 mins @ RT	Small 2TC spot
3	**138** + $Pd(OAc)_2$ + SPhos, stir 30 mins @ RT	Large 2TC spot

Table 4. 5-formyl-2-thiopheneboronic acid TLC tests

While based on subjective analysis, these results suggest that deborylation of **138** is catalysed by $Pd(OAc)_2$ and its catalytic efficiency is enhanced by the presence of the SPhos ligand.

References were found in the literature[133,134,135] describing a simple protection strategy for boronic acids for use in Suzuki-Miyaura cross-coupling reactions. The protocol involved treatment of the boronic acid with diethanolamine, a cheap intermediate used to make diethanolamides which are used in cosmetics and shampoos. If the low yield problem observed so far was due to protodeborylation of the boronic acid coupling partner (**138**) then protecting the boronic acid group may have a beneficial effect.

The protecting group was applied by adding a DCM solution of diethanolamine (**139**) to a DCM solution of **138** with stirring. The protected boronic acid then precipitated as the diethanolamine ester 8-(5-formylthiophen-2-yl)hexahydro-[1,3,2]oxazaborolo[2,3-b][1,3,2]oxazaborol-4-ium-8-uide (**140**) (Scheme 52).

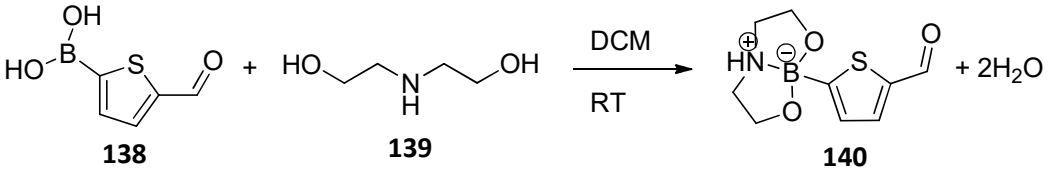

138 **139** **140**

Scheme 52. Protection of boronic acid with diethanolamine

The Suzuki-Miyaura cross-coupling reaction was then attempted using **140** as the organoboron coupling partner, with argon sparged 2-propanol as solvent and eliminating oxygen as far as possible. Unfortunately, the same pattern was observed as with the previous experiments; the reaction appeared to start but then arrested after a short time. TLCs were run after one hour reaction time, after a further 90 minutes and again after running over a long weekend. The TLCs were all identical and showed very little product formation.

Unfortunately, protection of the boronic acid with diethanolamine did not improve the yield of **87**.

Billingsley[136] found that Suzuki-Miyaura cross-coupling reactions of thiophene boronic acids catalysed by palladium (II) acetate and SPhos ligand may be adversely affected by the homo-coupled boronic acid by-product, which stopped the reaction and limited yields to approximately 7%. When an alternative ligand, dicyclohexyl(2',4',6'-triisopropyl-[1,1'-biphenyl]-2-yl)phosphine (**141**) or "XPhos" was employed, however, the reaction ran to completion.

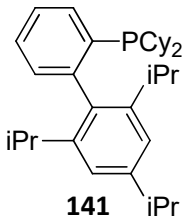

141

Figure 52. Molecular structure of "XPhos" ligand

Comparative Suzuki-Miyaura cross-coupling reactions between 1-chloroazulene (**112**) and 5-formyl-2-thiopheneboronic acid (**138**) with SPhos (**113**) and XPhos (**141**) ligands but otherwise identical conditions indicated (by observation of the colour change and by TLC) that the rate of coupling with XPhos was faster than with SPhos. The yield from the reaction with XPhos (10%) was also slightly higher than with SPhos (8.5%); however, both reactions arrested prematurely with much of the azulenyl starting material remaining.

A coupling reaction combining the most efficient solvent (2-propanol) and ligand (XPhos) from previous experiments but otherwise the same conditions to the previous cross-coupling reactions (same base, starting material stoichiometry, catalyst loading and reaction temperature) followed the same pattern as previously observed. Following aqueous work-up and purification by flash chromatography, an isolated yield of 12.2% of **87** was obtained and 75% of the 1-chloroazulene (**112**) starting material was recovered.

Although this latest result was twice the product yield of the initial cross-coupling experiments, most of the azulenyl starting material remained unconverted. Boronic acids are known to be unstable, suffering from protodeboronation and / or forming cyclic trimeric boroxines under the cross-coupling reaction conditions.[132] A popular alternative is to use boronic esters as surrogates for boronic acids.

The synthesis of the boronic acid starting material **138** was modified to yield the pinacol ester derivative instead, and because the acidic aqueous workup used to isolate **138** wasn't used in the synthesis of the boronic ester, the formyl group remained protected as the cyclic acetal, affording 2-(5-(1,3-dioxolan-2-yl)thiophen-2-yl)-4,4,5,5-tetramethyl-1,3,2-dioxaborolane (**142**) (Scheme 53).

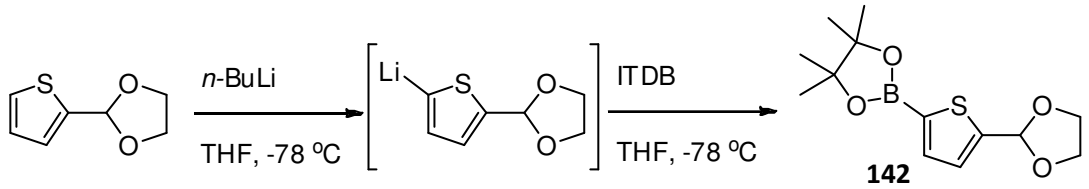

(ITDB = 2-Isopropoxy-4,4,5,5-tetramethyl-1,3,2-dioxaborolane)

Scheme 53. Synthesis of boronic acid pinacol ester coupling partner

142 was then used instead of **138** in a cross-coupling reaction with **112**, otherwise using the same reaction conditions as the previous best-yielding reaction with 2-propanol solvent and XPhos ligand to give 2-(5-(azulen-1-yl)thiophen-2-yl)-1,3-dioxolane (**143**) (Scheme 54).

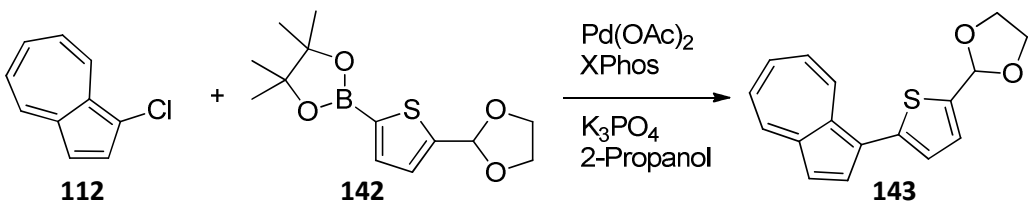

112 **142** **143**

Scheme 54. Suzuki-Miyaura cross-coupling reaction with boronic pinacol ester

After one hour stirring at room temperature, TLC monitoring showed several faint blue and green spots at lower Rf than the 1-chloroazulene (**112**) starting material. The situation did not change appreciably after stirring at room temperature for a total of 24 hours, at which point the reaction flask was placed in an oil bath and the temperature increased to 60 °C. After one hour at 60 °C TLC showed a much stronger green spot while the several blue spots had greatly diminished. Further TLC monitoring showed that the 1-chloroazulene (**112**) starting material was almost completely consumed after 3.5 hours stirring at 60 °C.

Following aqueous workup the cyclic acetal protection group was removed by stirring in wet acetone and catalytic *p*-TSA at 30 °C for two hours to afford **87** (Scheme 55).

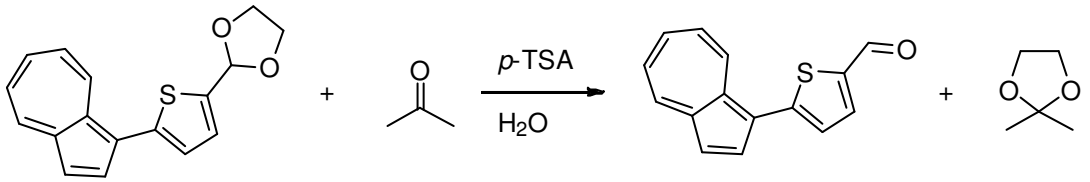

143 **87**

Scheme 55. Removal of cyclic acetal protection group

After purification by flash chromatography **87** was isolated as a green oil in 30.5% isolated yield. Subsequent repeat cross-coupling of **112** with **142** have been carried out entirely at 60 °C for 24 hours giving 43.5% isolated yield and at 70 °C for 3.5 hours giving 54% isolated yield after deprotection.

With a similar cross-coupling and de-protection sequence starting with 1-chloro-4,6,8-trimethylazulene (**144**) to produce the corresponding trimethyl-substituted analogue of **87**, 5-(4,6,8-trimethylazulen-1-yl)thiophene-2-carboxaldehyde (**146**) (Scheme 56), the cross-coupling reaction was completed in less than one hour at 60 °C with an overall isolated yield of 59% after de-protection and purification by flash chromatography.

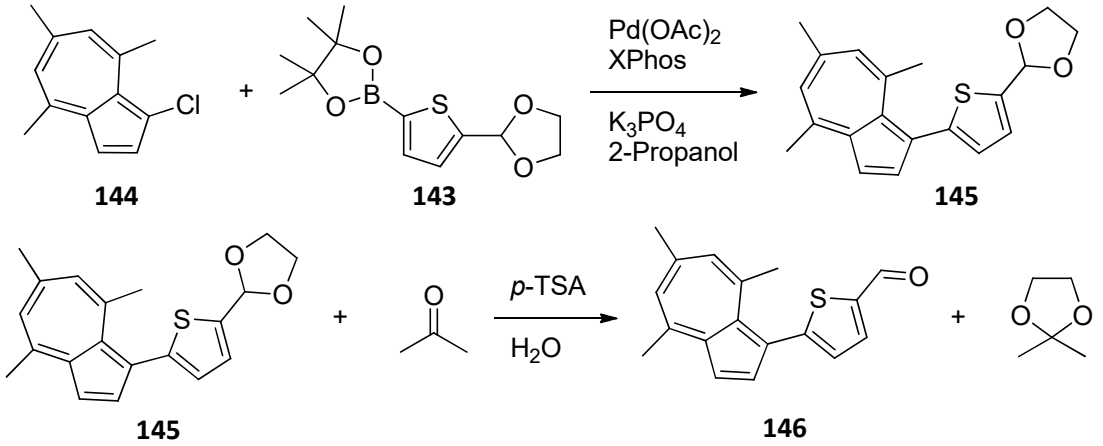

Scheme 56. Synthesis of 5-(4,6,8-trimethylazulen-1-yl)thiophene-2-carbaldehyde

4.2.5.4 Knoevenagel Condensation Reaction

The final step in the synthesis of dyes Az-1-tcaa (**84**) and the trimethyl analogue TMAz-1-tcaa (**147**) is the Knoevenagel condensation of the respective aldehyde intermediate (**87** and **146**) with cyanoacetic acid (**88**) to create the cyanoacrylic acid acceptor/anchor group (Scheme 57).

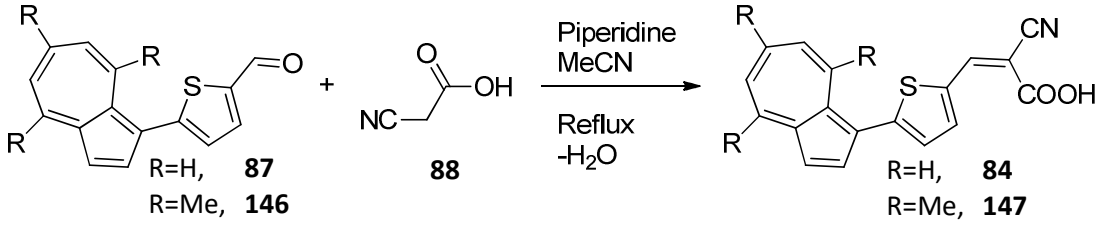

Scheme 57. Addition of cyanoacrylic acid anchor group

The Knoevenagel reaction is a modification of the aldol condensation reaction. The reaction is a nucleophilic addition of an activated hydrogen compound to a carbonyl group followed by elimination of a molecule of water. In this case, the electron withdrawing cyano- and carboxylic acid groups of **88** increase the acidity of ("activate") of the methylene group protons. Typically, the reaction is catalysed by a weak amine base such as piperidine (**148**) which serves to deprotonate **88** giving an enolate (**149**) which undergoes electrophilic attack by the aldehyde (**150**). Following protonation of the resulting alkoxide (**151**) by the protonated piperidine (and re-generation of the catalyst) giving **152**, base-catalysed elimination (E_1CB) of water yields the cyanoacrylic acid derivative (**153**) (Scheme 58).

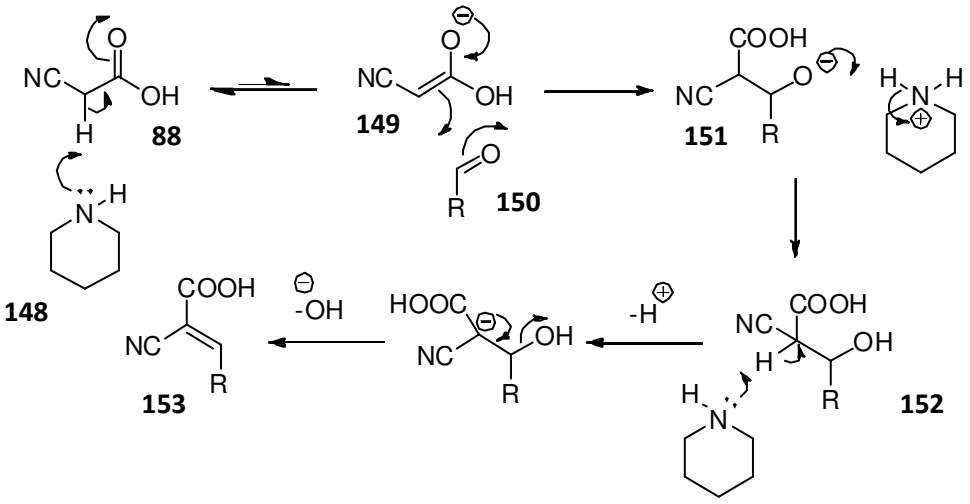

Scheme 58. Knoevenagel condensation reaction mechanism

The Knoevenagel reactions, carried out at reflux in acetonitrile with piperidine catalyst, proceeded slowly but relatively smoothly. A reaction time of 12-16 hours was necessary to consume all the aldehyde starting material with a 300% excess of cyanoacetic acid. The dyes were isolated by trituration with dichloromethane followed by recrystallisation from ethanol.

4.2.6 Azulene Dyes without Thiophene Linker

Two additional dyes, Az-1-caa (3-(azulen-1-yl)-2-cyanoacrylic acid) (**154**) and TMAz-1-caa (3-(4,6,8-trimethylazulen-1-yl)-2-cyanoacrylic) acid (**155**) (Figure 53), were synthesised without the thiophene linker group for comparison purposes to:

1. Determine the effect, if any, on the resulting DSSC performance; and

2. Benchmark the DSSC performance of Az-1-caa (**154**) against Zhang's Azu-1[51] dye which has exactly the same structure.

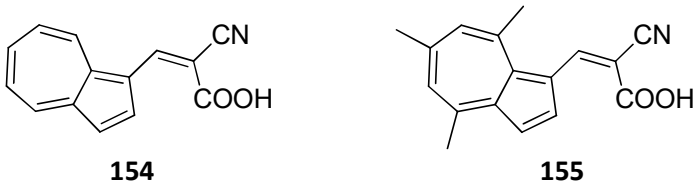

Figure 53. Molecular structures of Az-1-caa and TMAz-1-caa dyes

154 and **155** were synthesised in two steps:

1. Formylation of the respective parent azulene compound using the Vilsmeier-Haak reaction; followed by

2. Knoevenagel condensation of the resulting aldehydes with cyanoacetic acid in the presence of piperidine.

4.3 Dye Characterisation

4.3.1 NMR Spectroscopy

All of the dyes were characterised by ^{1}H and ^{13}C NMR. In addition a NOESY study on TMAz-1-tcaa (**147**) (Spectrum 1) enabled unequivocal assignment of the 1H NMR spectrum (Spectrum 2) for this dye.

The 'entry point' in the NOESY spectrum of **147** is the singlet corresponding to the vinylic proton (numbered 16 in Spectrum 1) which is highly de-shielded due to the combined effects of the electron withdrawing cyano and carboxylic acid groups and it manifests much further downfield than it would otherwise at 8.46 ppm. The characteristic upfield singlets of the three aryl methyl groups between 2.5 and 3.0 ppm are also useful markers in this molecule.

In the NOESY spectrum the peak at intersection (8.46, 7.96) ppm identifies the doublet of the thiophene ring proton (4). The peak at intersection (7.97, 7.18) identifies the doublet of the second thiophene ring proton (3). From the thiophene ring proton (3) (7.18 ppm), two further peaks (7.69, 7.18) and (7.18, 2.69) identify the azulene ring proton doublet (14) and methyl group singlet (22) respectively. The thiophene ring proton (3) interacts with both the methyl group (22) and the azulene ring proton (14) because of rotation about the azulene-thiophene bond. The remaining peaks correspond to:

(7.69, 7.41)* azulene ring proton doublets (14 and 15) respectively;

(7.41, 2.91)* azulene ring proton doublet (15) and methyl group singlet (20);

(7.29, 2.91)* methyl group singlet (20) and azulene ring proton singlet (10);

(7.29, 2.66)* azulene ring proton singlet (10) and methyl group singlet (21);

(7.23, 2.66) methyl group singlet (21) and azulene ring proton singlet (12);

(7.23, 2.69) azulene ring proton singlet (12) and methyl group singlet (22).

*=not labelled.

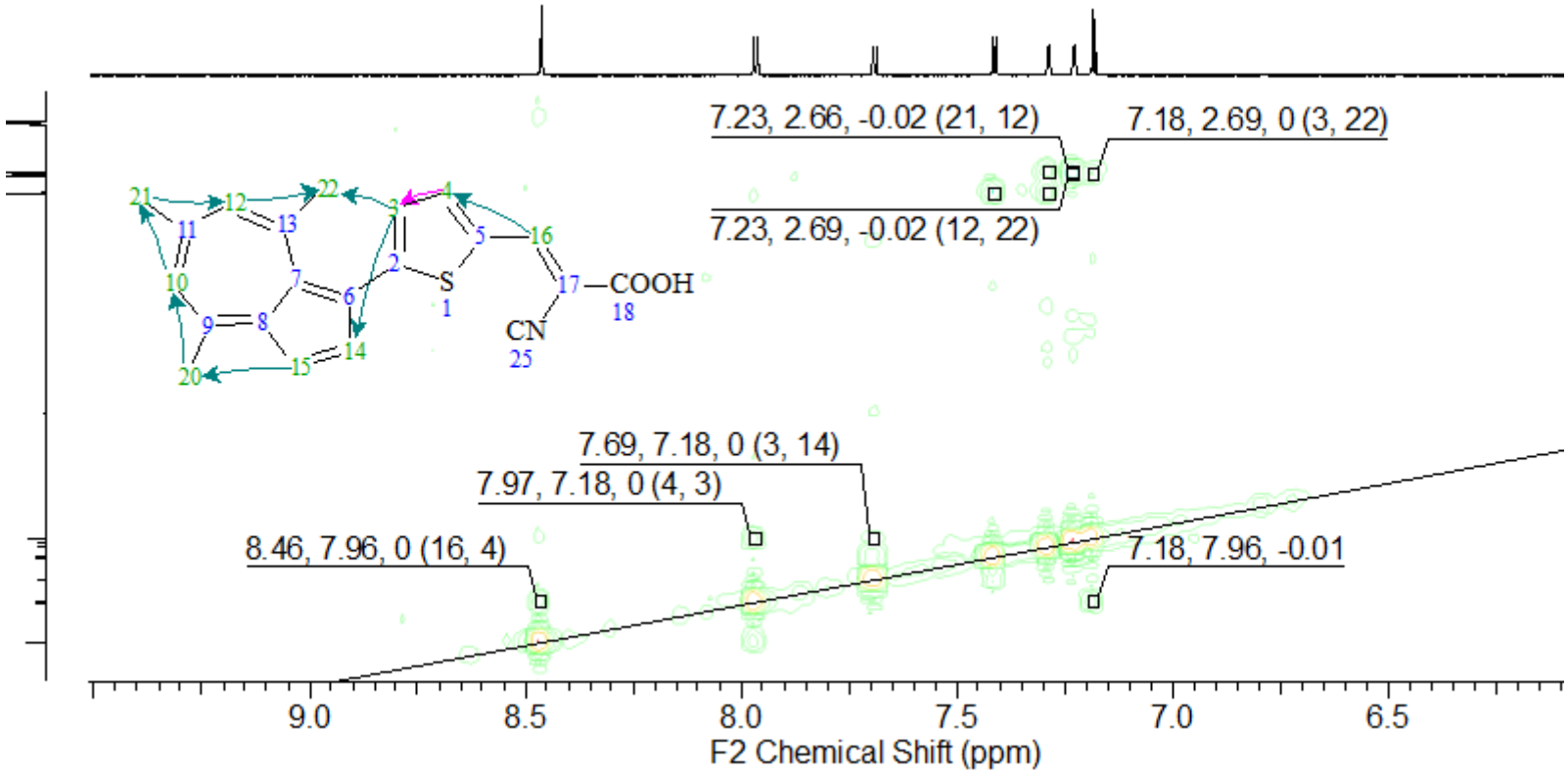

Spectrum 1. ^{1}H NMR NOESY (500 MHz, Acetone): TMAz-1-tcaa, 3-(5-(4,6,8-trimethylazulen-1-yl)thiophen-2-yl)-2-cyanoacrylic acid

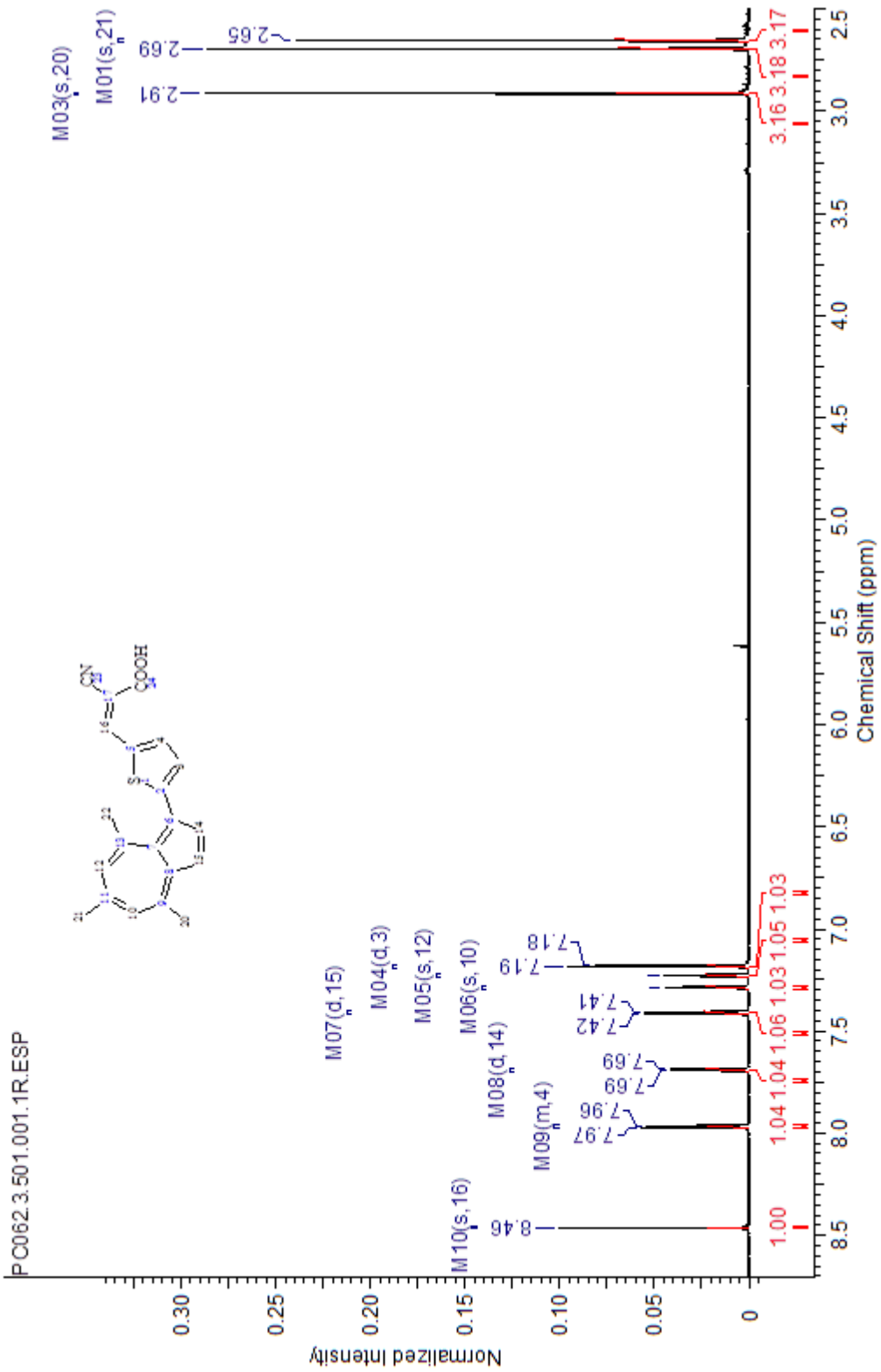

Spectrum 2. ^{1}H NMR (500 MHz, Acetone): TMAz-1-tcaa, 3-(5-(4,6,8-trimethylazulen-1-yl)thiophen-2-yl)-2-cyanoacrylic acid

4.3.2 UV-Vis Spectroscopy

4.3.2.1 Azulene and 4,6,8-Trimethylazulene

Spectrum 3 shows the UV/VIS absorption spectra of Azulene (Az) (1.0 mM) and 4,6,8-Trimethylazulene (TMAz) (0.4 mM) in acetonitrile. Both compounds have similar spectra.

The weak, broad absorption band 480 - 720 nm (Az) and 440 - 660 nm (TMAz) in the VIS is responsible for the perceived colour of the compounds. This absorption corresponds to the S0 – S1 transition and the λ_{max} is hypsochromic (blue shifted) by ~30 nm in TMAz compared with Az resulting in its redder hue. This concurs with the MO theory presented in section 1.5.2 above. The electron donating methyl groups attached to C-4, C-6 and C-8 in TMAz stabilise the HOMO, increasing the HOMO-LUMO gap and consequently increasing the frequency of absorption. The bandgap is estimated from the absorption onset, which is 700 nm (1.77 eV) for Az and 640 nm (1.94 eV) for TMAz.

There is a second much stronger absorption band in the near-UV at 302 – 360 nm (Az) and 315 – 370 nm (TMAz). This is assumed to correspond to the S0 – S2 transition and is slightly bathochromic (red shifted) by ~8 nm in TMAz compared with Az. In Figure 24 (section 1.5.2 above), it can be seen that electron densities in the HOMO and LUMO+1 are very similar, so substituents will have similar effects on their stabilities, ie the HOMO – LUMO+1 gap is not markedly affected and so the absorption occurs at similar wavelengths.

TMAz is more efficient at absorbing photons than Az and has a higher molar extinction coefficient, summarised in Table 5.

	S_0-S_1		**S_0-S_2**	
	λ (nm)	**ε (L.mol^{-1}.cm-1)**	**λ (nm)**	**ε (L.mol^{-1}.cm^{-1})**
Azulene (**1**)	576	1.631×10^2	340	1.918×10^3
4,6,8-Trimethylazulene (**48**)	544	4.660×10^2	348	4.638×10^3

Table 5. Molar extinction coefficients for azulene and 4,6,8-trimethylazulene

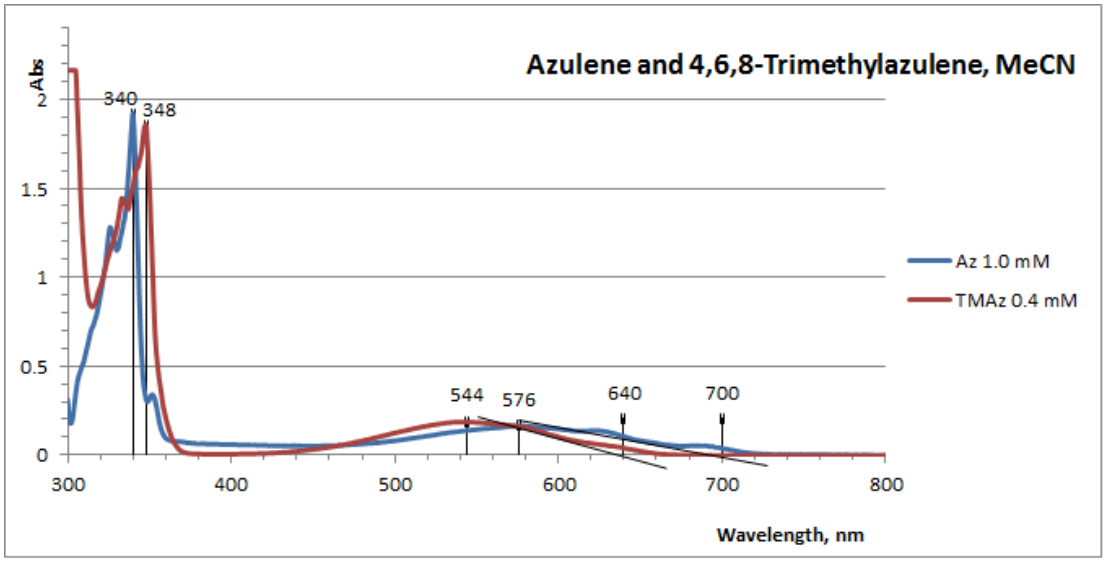

Spectrum 3. UV/Vis: Azulene (Az) and 4,6,8-Trimethylazulene (TMAz)

4.3.2.2 Azulene-based dyes

UV/VIS absorption spectra for the four azulene dyes synthesised were acquired: Az-1-caa (**154**) (Spectrum 4), Az-1-tcaa (**84**) (Spectrum 6), TMAz-1-caa (**155**) (Spectrum 5) and TMAz-1-tcaa (**147**) (Spectrum 7) at 0.025 mM in acetonitrile. Relevant data from the spectra are presented in Table 6.

The four spectra have similar features. The weak absorption in the VIS seen with the parent azulene compounds is still apparent at around 559 nm. The extinction coefficients for this band are increased 5-fold (Az-1-caa) and 11-fold (TMAz-1-caa) for the dyes without a thiophene linker group. It is difficult to estimate the effect of the thiophene linker group because of band overlap.

All four dyes exhibit an additional absorption band in the range 400 – 500 nm when compared with the parent azulene compounds. The band is more intensive (ie higher extinction coefficient ε at λ_{max}) for the dyes without a thiophene linker group (Az-1-caa and TMAz-1-caa) but is broader and bathochromic (red shifted) for the dyes with a thiophene linker group (Az-1-tcaa and TMAz-1-tcaa). The extinction coefficients for this band are summarised in Table 6.

In the near UV the dyes with thiophene linker differ markedly from those without. All the dyes have a peak at approx. 350 nm in the same region as the assumed S0 – S2 transition of the parent azulene compounds however the peak shapes are very different. The two dyes with thiophene linker (Az-1-tcaa and TMAz-1-tcaa) exhibit the beginnings of a further peak with onset at approx. 325 nm but this is absent in the dyes without thiophene linker.

Dye	**λ_{max} nm**	**ε L.mol^{-1}.cm^{-1}**	**λ_{onset} nm**	**E_g (opt) eV**
Az-1-caa (**154**)	423	3.952 x 10^4	460	2.70
TMAz-1-caa (**155**)	439	3.226 x 10^4	473	2.62
Az-1-tcaa (**84**)	473	3.026 x 10^4	547	2.27
TMAz-1-tcaa (**147**)	452	1.914 x 10^4	547	2.27

Table 6. UV/Vis data, 1st generation dyes

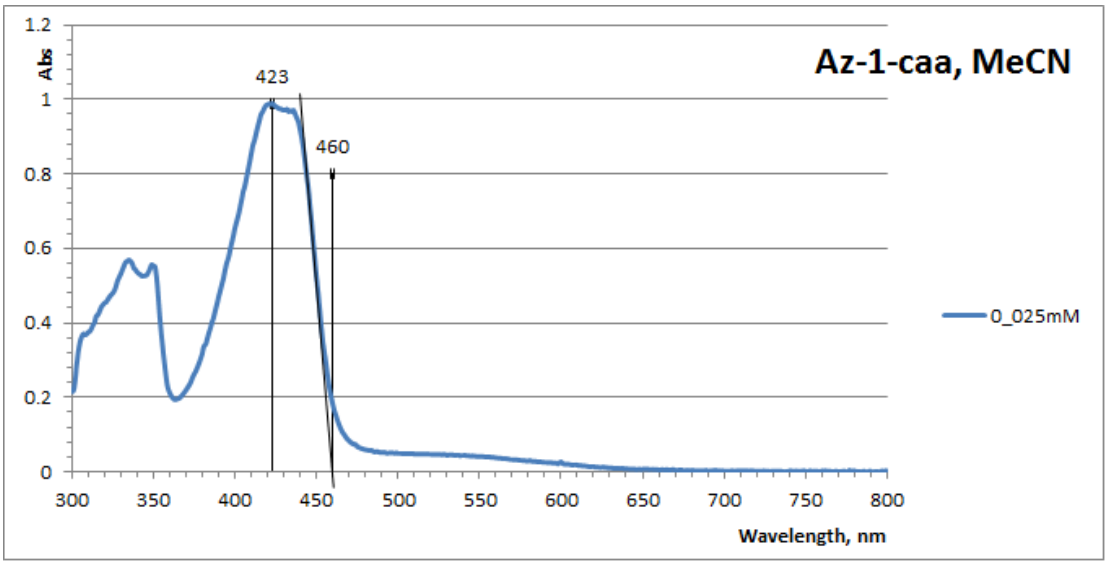

Spectrum 4. UV/Vis Az-1-caa (154) in acetonitrile.

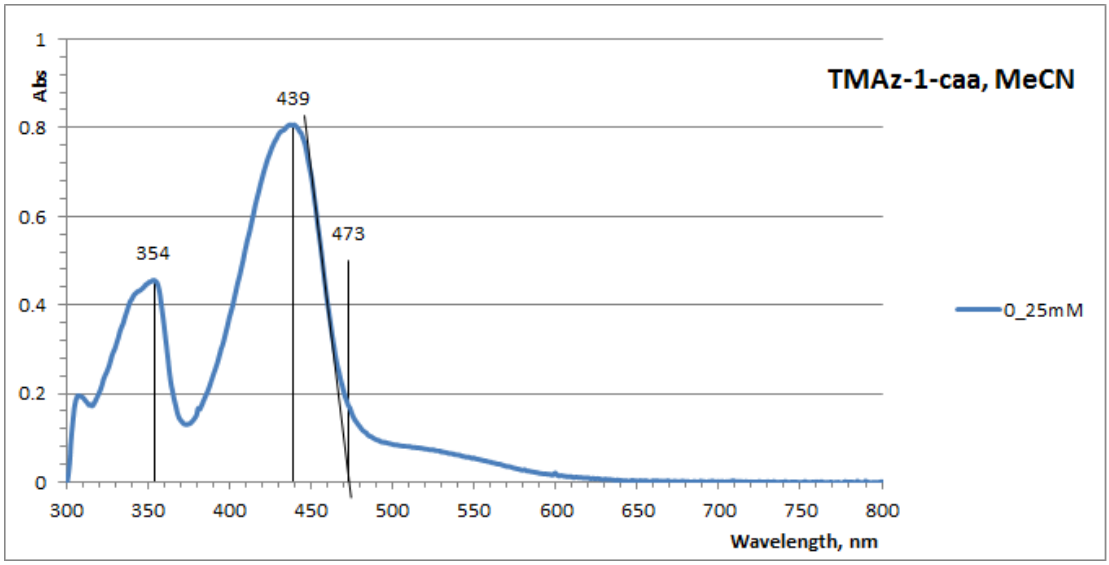

Spectrum 5. UV/Vis TMAz-1-caa (155) in acetonitrile.

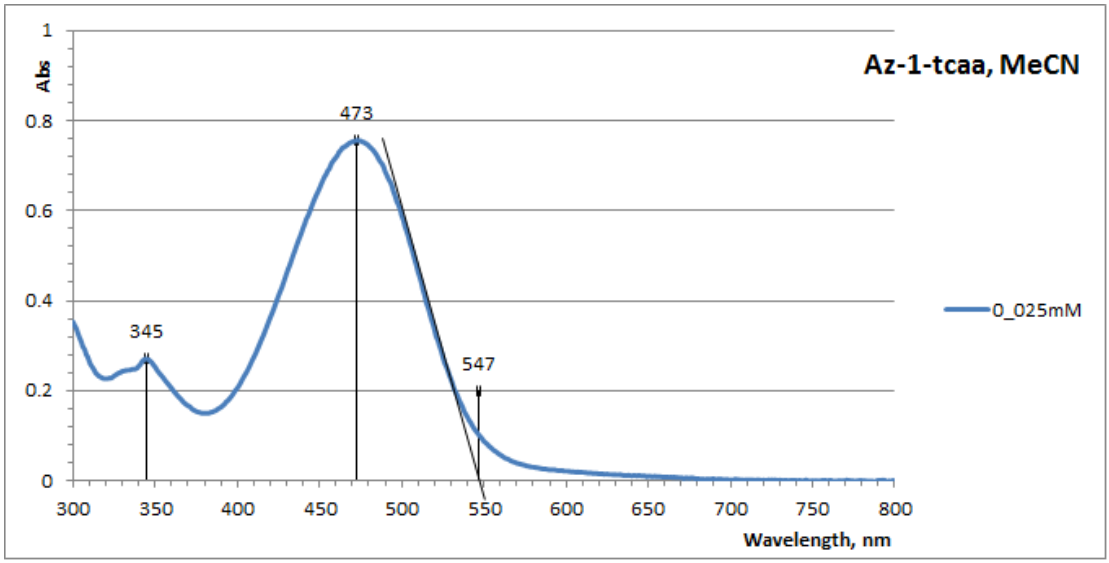

Spectrum 6. UV/Vis Az-1-tcaa (84) in acetonitrile.

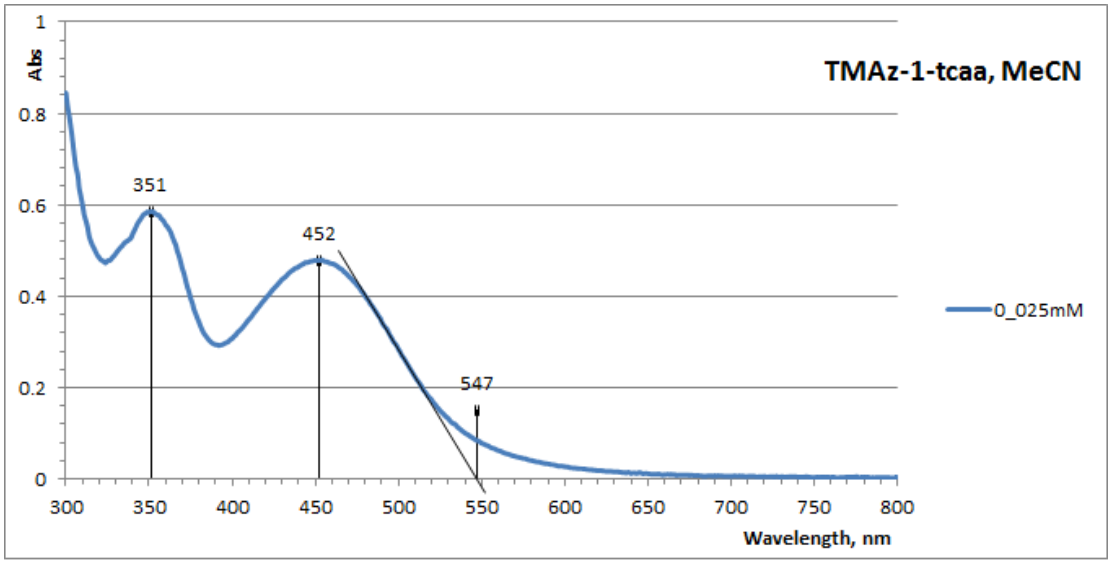

Spectrum 7. UV/Vis TMAz-1-tcaa (147) in acteonitrile

4.3.3 Infra-Red Spectroscopy

Infra-red spectra (thin film) were taken of the four dyes. Peaks corresponding to the carboxylic acid C=O and C–OH stretch, C≡N stretch and alkene C=C stretch can be assigned as follows (Table 7):

Functional group	**Wavenumber cm^{-1}**			
	Az-1-caa	**TMAz-1-caa**	**Az-1-tcaa**	**TMAz-1-tcaa**
C=O stretch	1659	1657	1676	1666
C–OH stretch	1247	1228	1238	1243
C≡N stretch	2208	2212	2211	2218
C=C stretch	1550	1545	1558	1572

Table 7. Infra-red spectra analysis summary

4.3.4 Electrochemistry

Cyclic voltammetry (CV) was used to determine the oxidation potentials of four azulene based dyes: Az-1-caa (**154**), Az-1-tcaa (**84**), TMAz-1-caa (**155**) and TMAz-1-tcaa (**147**) (Voltammogram 1 to Voltammogram 4). All CVs were run in dry THF with 0.1 M tetrabutylammonium hexafluorophosphate (Bu_4PF_6) supporting electrolyte at a scan rate of 100 $mV.s^{-1}$ (see section 8.2.20 below for details). Three scans were

taken for each run. The voltammograms show plots for the first and third scans only.

All the dyes exhibited at least one oxidation peak; however the oxidations were all irreversible so it was not possible to calculate the $E_{½}$ potentials. The peak oxidation potentials vs. Fc/Fc^+ are summarised below (Table 8).

Dye	**E_{pa1} mV**	**I_{pa1} µA**	**E_{pa2} mV**	**I_{pa2} µA**	**E_{ox} mV**	**HOMO V vs NHE**
Az-1-caa (**154**)	0.837	18.04	-	-	670	1.30
TMAz-1-caa (**155**)	0.697	12.98	-	-	540	1.17
Az-1-tcaa (**84**)	0.455	15.79	-	-	310	0.94
TMAz-1-tcaa (**147**)	0.455	9.22	0.566		320	0.95

Table 8. First generation dyes electrochemical data in THF (E/V vs. Fc/Fc^+)

The dyes with three methyl groups in the azulene 7-membered ring (TMAz-1-caa and TMAz-1-tcaa) have lower oxidation potentials than the unsubstituted analogues. This effect is more pronounced in the dyes without a thiophene linker (Az-1-caa and TMAz-1-caa).

The dyes without a thiophene linker (Az-1-caa and TMAz-1-caa) have significantly elevated oxidation potentials compared with the dyes with a thiophene linking unit (Az-1-tcaa and TMAz-1-tcaa). This suggests that the thiophene linker makes it easier to extract an electron from the dye molecule and that the resulting cation should be more stable (ie is less energetic).

The dye with methyl groups in the 7-membered ring and with a thiophene linking unit (TMAz-1-tcaa) exhibited two oxidation waves, neither being reversible (Voltammogram 4). This means that two electrons can be removed from this molecule, resulting in a dication.

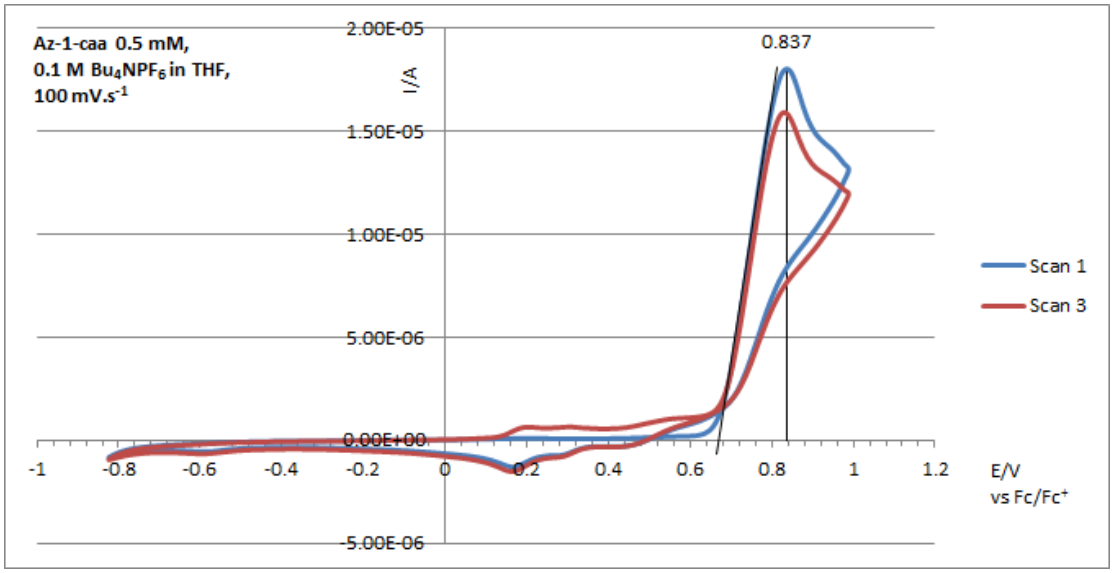

Voltammogram 1. Az-1-caa, 3-(azulen-1-yl)-2-cyanoacrylic acid (154)

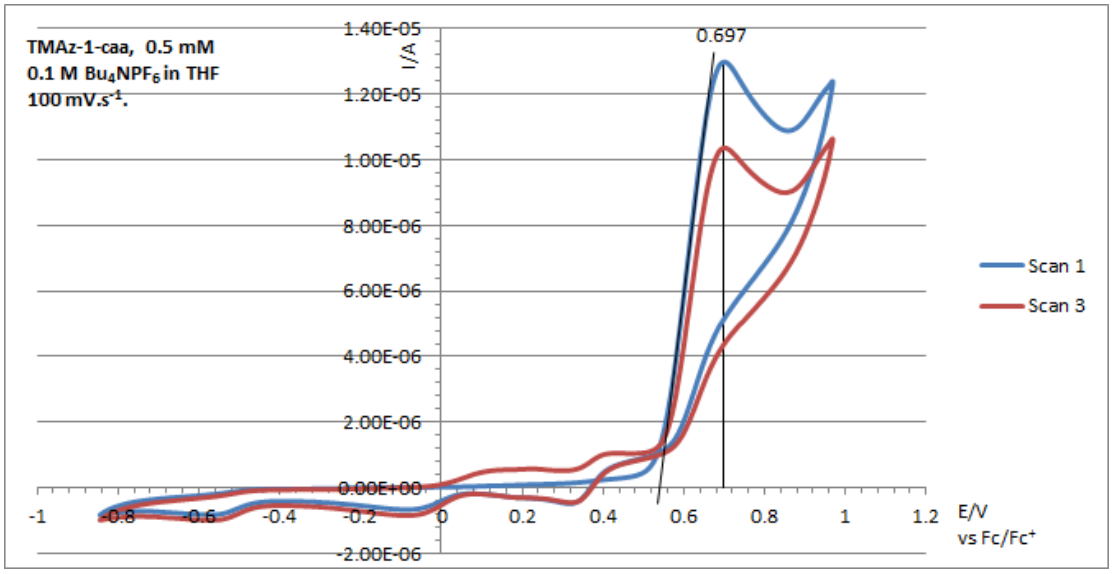

Voltammogram 2. TMAz-1-caa, 3-(4,6,8-trimethylazulen-1-yl)-2-cyanoacrylic acid (155)

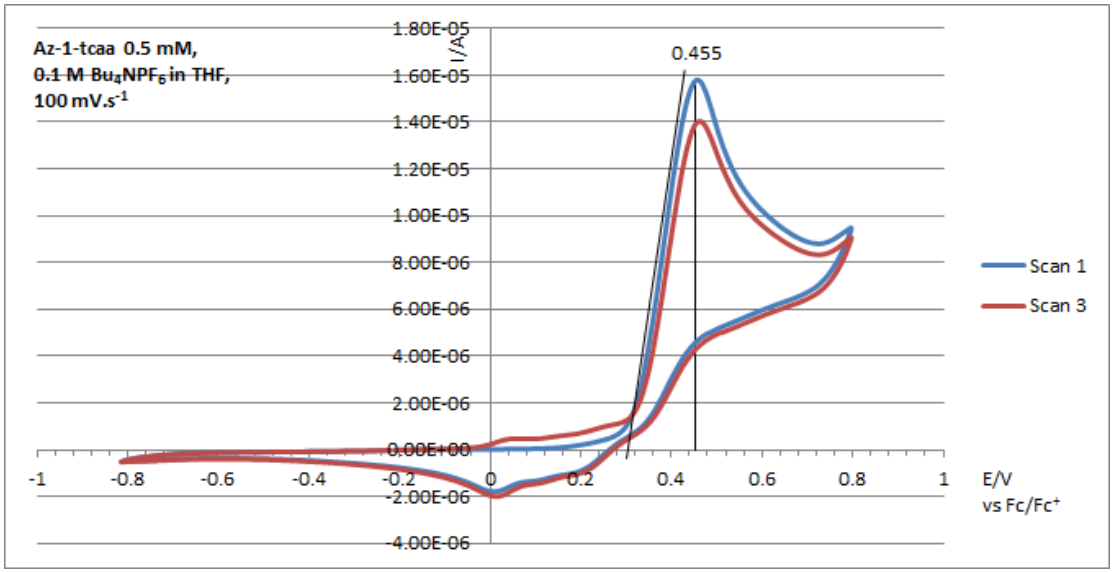

Voltammogram 3. Az-1-tcaa, 3-(5-(azulen-1-yl)thiophen-2-yl)-2-cyanoacrylic acid (84)

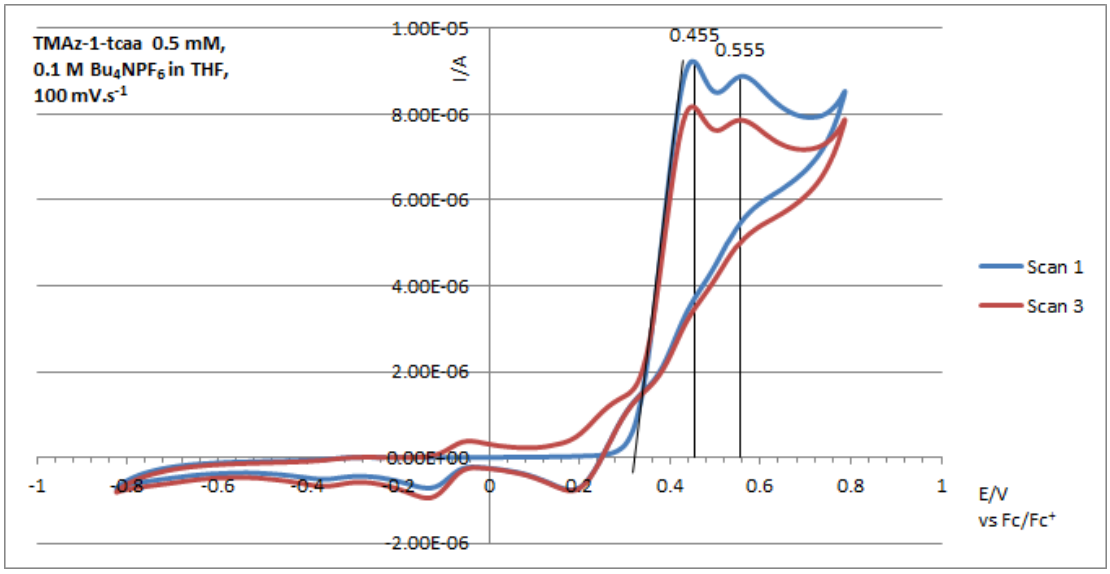

Voltammogram 4. TMAz-1-tcaa, 3-(5-(4,6,8-trimethylazulen-1-yl)thiophen-2-yl)-2-cyanoacrylic acid (147)

All of the CVs show that breakdown products are generated following oxidation of the dyes. This can be seen by comparing the traces of scan 1 (blue line) and scan 3 (red line) in each CV. With scan 1, there is no sign of any oxidation before the main oxidation peak begins, eg at approx. 0.3 V in Voltammogram 4. On subsequent scans, there is evidence of oxidation processes occurring at potentials lower than the main oxidation peak, eg in Voltammogram 4 two minor oxidation peaks can be seen at -0.049 V and 0.263 V vs Fc/Fc^{+}. These minor oxidation waves appear to be at least partially reversible since they have corresponding reduction waves.

Since the minor oxidation waves did not occur in the first scan, they must be due to species generated from the oxidised dye which is a radical cation (Scheme 59).

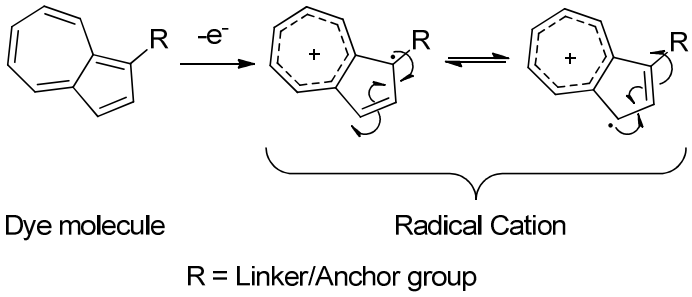

Scheme 59. Oxidation of dye molecule forming a radical cation

The radical cation is a very reactive species and may decompose or react with other molecules present eg solvent, other dye molecules (hydrogen abstraction) or other radicals (combination).

4.3.5 Crystallography

The crystal structure for TMAz-1-tcaa (**147**) (Figure 75, section 7.2 below) reveals a large torsional angle of 47.0(5)° between the azulene 5-membered ring and the thiophene ring, probably due to steric clash between the thiophene ring and the methyl group at the azulene C-8 position. This will hinder conjugation between the two rings, and may also hinder electron transfer from the azulene donor moiety to the cyanoacrylic acceptor/anchor group which in turn would limit the electron injection efficiency of the dye.

4.3.6 Dye Sensitised Solar Cells

Energy level data for the first generation dyes is summarised in Table 9. The ground state (D^0/D^+) potentials and band gap (E_g) values are taken from the electrochemistry (section) and UV/Vis spectrometry results (sections 4.3.4 and 4.3.2.2 above). Subtracting E_g from D^0/D^+ gives the excited state potential (Equation 18):

$$D^* = \frac{D^0}{D^+} - E_g \qquad \text{Equation 18}$$

Dye	$\frac{\mathbf{D^0}}{\mathbf{D^+}}$ **V vs NHE**	**E_g (opt) eV**	**D* V vs NHE**
Az-1-caa (**154**)	1.30	2.70	-1.40
TMAz-1-caa (**155**)	1.17	2.62	-1.45
Az-1-tcaa (**84**)	0.94	2.27	-1.33
TMAz-1-tcaa (**147**)	0.95	2.27	-1.32

Table 9. First generation dyes energy levels.

All of the first generation dyes clearly satisfy the energy level requirements to function as DSSC sensitisers. The excited state potentials provide an electron injection driving force of 0.82 to 0.95 V. and the redox potential of the ground state is 0.54 to 0.9 V. below that of the I^-/I_3^- couple used in the electrolyte.

Dye sensitised solar cells (DSSCs) were prepared using the general procedure (see section 8.4 below). The iodide/triiodide electrolyte used was a solution containing the following components in a mixture of acetonitrile and valeronitrile solvents (85:15):

Component	Concentration
Iodine	0.03 M
3-propyl-1-methyl-imidazonium iodide (ionic liquid)	0.60 M
Guanidine thiocyanate	0.10 M
tert-Butylpyridine	0.50 M

Table 10. DSSC electrolyte solution

The electrolyte recipe was one that had been used in the department for testing DSSCs based on a variety of dye types but optimised for ruthenium (II) based dyes. Two cells were prepared for each of the four azulene-based dyes. The cell efficiencies recorded were as follows:

Dye	Cell	Efficiency %
Az-1-caa (**154**)	01	0.0149
	02	0.0143
	Mean	0.0146
TMAz-1-caa (**155**)	03	n/a
	04	0.102
	Mean	0.102
Az-1-tcaa (**84**)	05	0.0214
	06	0.204
	Mean	0.1127
TMAz-1-tcaa (**147**)	07	n/a
	08	0.163
	Mean	0.163

Table 11. First generation dyes DSSC efficiencies

Not all of the cells worked; the cells with efficiency 'n/a' produced a negative open circuit potential (V_{oc}). This result usually implies that the cell is connected with reverse-polarity in the test apparatus, but with cells 03 and 07 a negative V_{oc} was reported whichever way the cells were connected.

On average, the dyes with thiophene linker (Az-1-tcaa and TMAz-1-tcaa) performed better than those without thiophene linker and the dyes based on 4,6,8-trimethylazulene (TMAz-1-caa and TMAz-1-tcaa) performed better than those based

on azulene (Az-1-caa and Az-1-tcaa). The best performing cell was cell 06, based on Az-1-tcaa.

4.4 Conclusions

A range of azulene-based dyes for DSSCs has been successfully synthesised with the linker/anchor group attached to the azulene C-1 position. Of the original synthetic routes that were devised to synthesise the aldehyde intermediate **87**, only the Suzuki-Miyaura cross-coupling of 1-chloroazulenes with boron-functionalised 2-thiophenecarboxaldehyde was successful. However, a versatile synthetic strategy has been developed that is capable of producing a wide range of dyes with different linker groups; this would not have been the case, for instance, with the in-situ thiophene synthesis via azulene formylation, Stetter and Paal-Knorr reactions. The only drawbacks to the developed strategy are:

1. The relative instability of the 1-chloroazulenes which means that they must be prepared and purified immediately before carrying out the Suzuki-Miyaura coupling reactions; and

2. The chlorination of azulenes with *N*-chlorosuccinimide (NCS) unavoidably results in a mixture of un-chlorinated starting material together with mono-chlorinated and di-chlorinated products. Because the parent azulene and the mono- and di-chlorinated analogues all have similar R_f values, they are difficult to separate using flash chromatography. This leads to wastage of the desired mono-chlorinated product due to contamination of some fractions with the undesired products.

The UV-Vis spectroscopy has shown that the light absorption of the dyes is satisfactory in terms of the region of the spectrum and the extinction coefficients of the dyes. A further broadening of and / or bathochromic shift in the absorption spectrum would probably be beneficial to improving the light harvesting efficiencies of the dyes.

The efficiency results from the DSSCs were disappointing. The efficiency achieved for the cells with Az-1-caa (**154**) dye (0.0146%) were much lower than the reported literature value (1.25%).[51]

The electrochemistry (cyclic voltammetry) study has indicated that the radical cation species that are generated by electron injection from a photo-excited dye molecule into the TiO_2 substrate in a DSCC may not be sufficiently stable to survive until they are reduced back to the ground-state dyes by the redox couple in the cell electrolyte. It is important that the radical cation species does not decompose or react with other molecules in order that a DSSC based on the dye has sufficient longevity to be useful.

5 Azulene Dyes – 2nd Generation

5.1 Introduction

The cyclic voltammetry study of the four dyes prepared so far has indicated that the compounds formed by oxidising the dye molecules (the radical cations) are not stable and may be decomposing or reacting with other molecules present. It may still be possible to make working DSSCs using these dyes; however in order to make DSSCs that have a long life it is important that the dyes are as stable as possible both in the dye and dye$^{\bullet+}$ states. The objective of the 2nd phase was therefore to synthesise dyes which had reversible electrochemistry through modifications to Az-1-tcaa and TMAz-1-tcaa designed to stabilise their oxidised states.

A literature search looking for azulene-based compounds with electrochemistry that exhibit reversible oxidation waves has suggested that both the azulene C-1 and C-3 positions must be substituted, preferably with substituents with steric bulk eg *tert*-butyl groups (**156**). Gerson *et al*. have reported that only radical cations substituted at the C-1 and C-3 positions were sufficiently persistent to be characterised by EPR spectroscopy, and *tert*-butyl groups were necessary to enable ENDOR and TRIPLE resonance studies.[137] The radical cations of 1,3-di-*tert*-butylazulenes persisted for 20-40 minutes at 273 -283 K.

The authors offered no explanation as to why the *tert*-butyl groups should confer stability to the azulene radical cation. 1,3-dimethylazulene radical cations were more stable than those of unsubstituted azulene, but were not so long-lived as the 1,3-di-*tert*-butylazulene ones. It is postulated that the *tert*-butyl groups shield the radical unpaired electron purely through their steric bulk, preventing the close approach of species that would otherwise be liable to react with the radical.

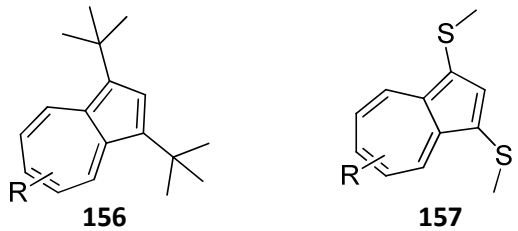

156 **157**

Figure 54. 1,3-di-tert-butyl- and 1,3-bis(methylthio)- azulenes

Shoji *et al*. have reported[138] that 1,3-bis(methylthio)azulenes (**157**) also exhibit reversible electrochemistry. The methylthio groups may also offer protection through steric "shielding"; however it is possible that the radical is delocalised onto the sulfur atoms. Resonance structures can be drawn showing possible delocalisation of the radical over both sulfur atoms and delocalisation of the positive charge too (Scheme 60).

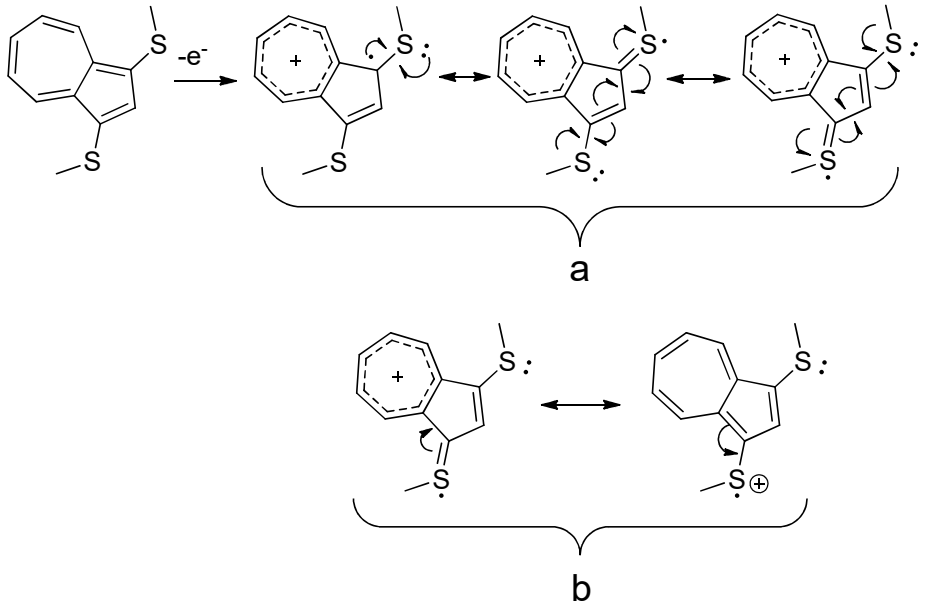

Scheme 60. 1,3-bis(methylthio)azulene: Delocalisation of a) radical and b) cation

Azulene compounds with a nitrone group conjugated to the C-1 and/or C-3 positions are reported by Becker to have reversible oxidation chemistry.[139] It is postulated that the radical formed by abstracting an electron is stabilised by delocalising it onto the nitrone group (Scheme 61).

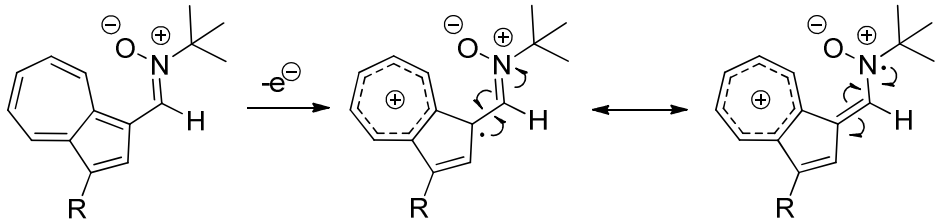

Scheme 61. Azulenyl radical stabilisation with nitrone group

The plan was to:

1. Reproduce the literature results by synthesising the relevant azulene derivatives and testing them using cyclic voltammetry; and

2. If reversible electrochemistry was achieved, synthesise and test analogues of Az-1-tcaa (**84**) and TMAz-1-tcaa (**147**) with *tert*-butyl, methylthio or nitrone groups in their C-3 positions.

5.2 Literature Compounds

5.2.1 1,3-Di-tert-butylazulene (160)

As already mentioned (section 1.5.4 above), azulene may be alkylated at the C-1 and C-3 positions using Friedel-Crafts conditions but azulene forms complexes with Lewis acids which can interfere with the reaction. Initial attempts at Friedel-Crafts alkylation using *tert*-butylchloride in DCM and $AlCl_3$ catalyst, while the reaction did proceed, were not successful in producing pure 1,3-di-*tert*-butylazulene (**160**) required for the cyclic voltammetry tests. Some mono-alkylated product **159** remained, even after extended reaction times. Since the Rf values of the mono- and di-alkylated products are almost identical, separating them by flash chromatography proved to be impossible.

Success was eventually achieved by following Hafner's method[140] using excess *tert*-butanol (**158**) and tetrafluoroboric acid catalyst in diethylether. After stirring at RT overnight, all starting material had been consumed. Following purification by flash chromatography, a pure sample of 1,3-di-*tert*-butylazulene was obtained after recrystallisation from petroleum ether.

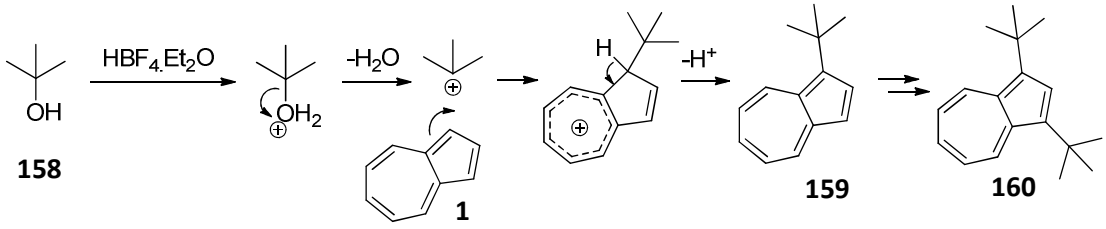

Scheme 62. Synthesis of 1,3-di-*tert*-butylazulene

A cyclic voltammogram of a 0.5mM solution of **160** in THF produced reversible oxidation wave with no evidence of decomposition products in the second and subsequent scans (Voltammogram 5). The tertiary butyl groups clearly do a good job of shielding the radical in the oxidised species.

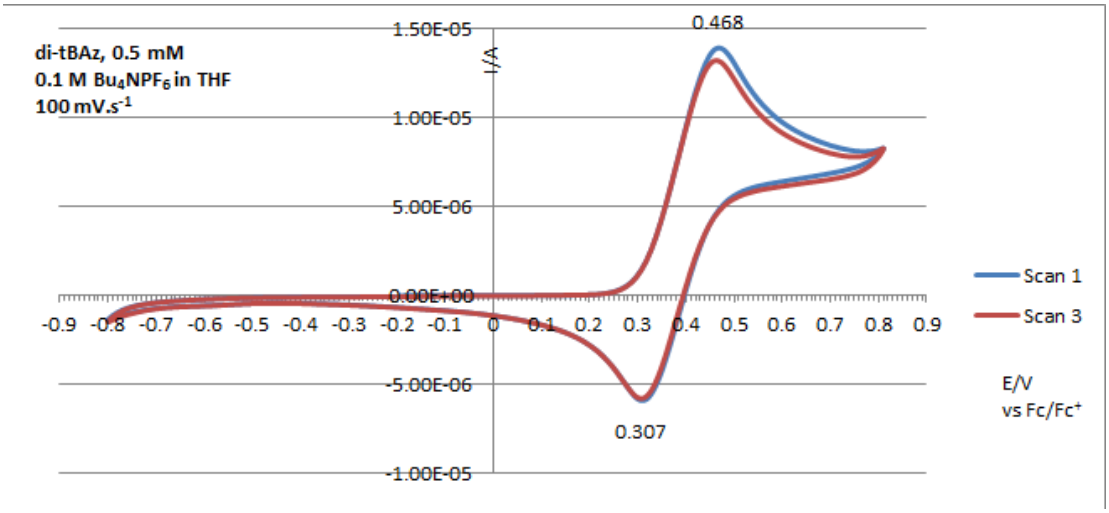

Voltammogram 5. 1,3-di-*tert*-butylazulene

5.2.2 1,3-Bis(methylthio)azulene (170)

This compound was synthesised according to the two-step method of Shoji *et al.*.[138] Azulene (**1**) was treated in the presence of dimethylsulfoxide (DMSO) with trifluoromethanesulfonic anhydride (triflic anhydride) (**166**). The DMSO is "activated" by **166**, an electrophile, generating dimethylsulfonium ditriflate (**167**). Azulene (**1**) undergoes electrophilic attack by **167**, giving 1-(dimethylsulfonium)azulene (**168**) following re-aromatisation. The sulfonium group deactivates the azulene towards electrophilic attack; however with a sufficiently electrophilic activating agent such as triflic anhydride, a second dimethylsulfonium group is installed at the C-3 position giving 1,3-bis(dimethylsulfonium)azulene. Since triflic anhydride was used as the activating agent, the counter ions are triflate ions (Scheme 63).

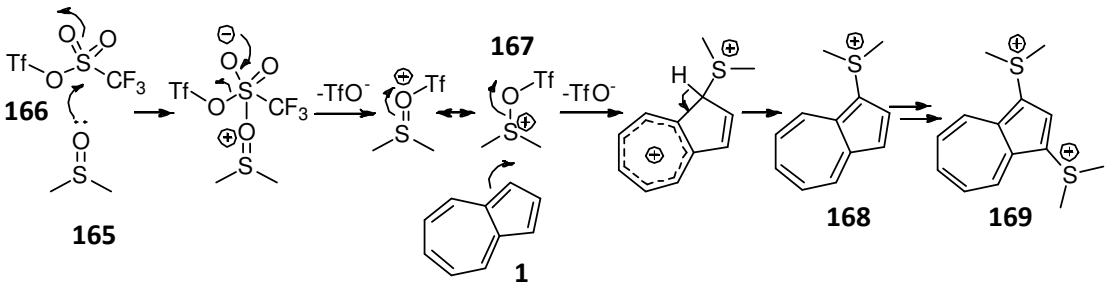

Scheme 63. Synthesis 0f 1,3-bis(dimethylsulfonium)azulene triflate

The second step was carried out after removing the solvent from the first step without any purification. The reaction mixture crude from step one was treated for

30 minutes with a 1:1 mixture of ethanol and triethylamine at reflux. One methyl group from each sulfonium group is removed from **169**, yielding **170** (Scheme 64).

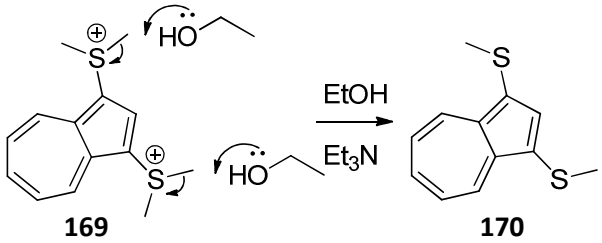

169 **170**

Scheme 64. Synthesis of 1,3-bi(methylthio)azulene

A cyclic voltammogram of a 0.5 mM solution of **170** in THF produced a near-perfect reversible oxidation wave with no evidence of decomposition products in the second and subsequent scans (Voltammogram 6). The traces from scan 1 and scan 3 are almost perfectly superimposed.

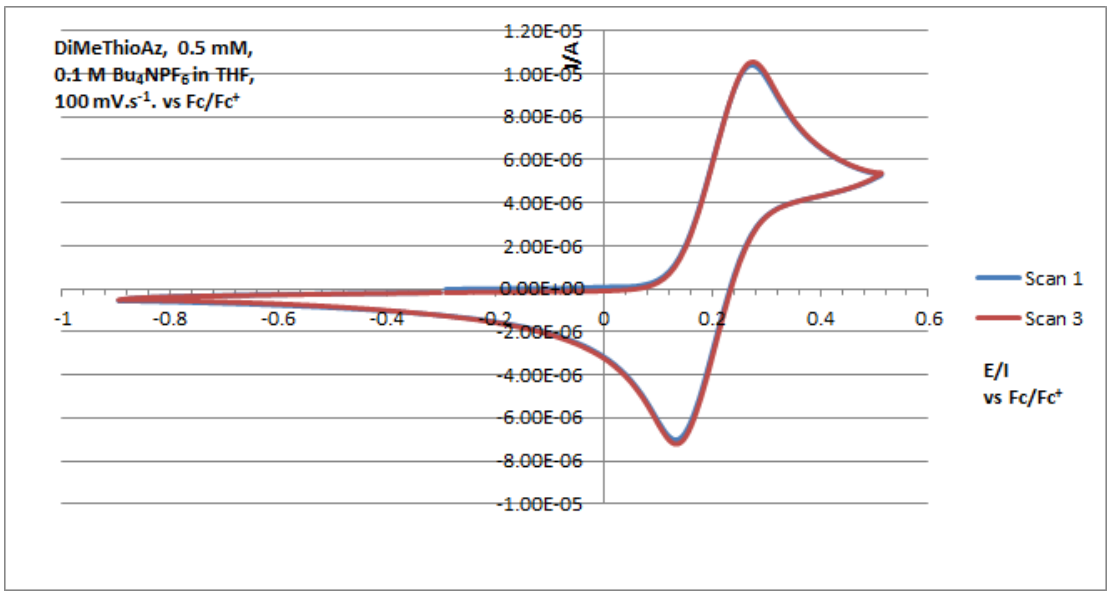

Voltammogram 6. 1,3-bis(methylthio)azulene

It is notable that the oxidation potential (the onset of the oxidation wave) is approximately 200 mV lower with **170** than it is with **160**, ie it is easier to remove an electron from **170** than **160**.

5.2.3 N-*tert*-Butyl-alpha-(7-isopropyl-4-methyl-3-ethoxycarbonyl-azulen-1-yl)nitrone (175)

The compound that Becker reported[139] to have reversible electrochemistry is derived from guaiazulene (**2**). The compound was synthesised in three steps. Purification by flash chromatography was required after each step.

In the first step, guaiazulene (**2**) was treated with oxalyl bromide in dry diethylether at RT according to the method of Treibs[141] giving acyl bromide **171**, which was directly esterified with ethanol to provide the violet ethyl ester **172**. In step two, **172** was oxidised with two equivalents of DDQ in aqueous acetonitrile at RT according to the method of Takase[142] affording the aldehyde **173**. Finally in step three, condensation of **173** with N-*tert*-butylhydroxylamine hydrochloride in pyridine at 95 °C yielded **175**.

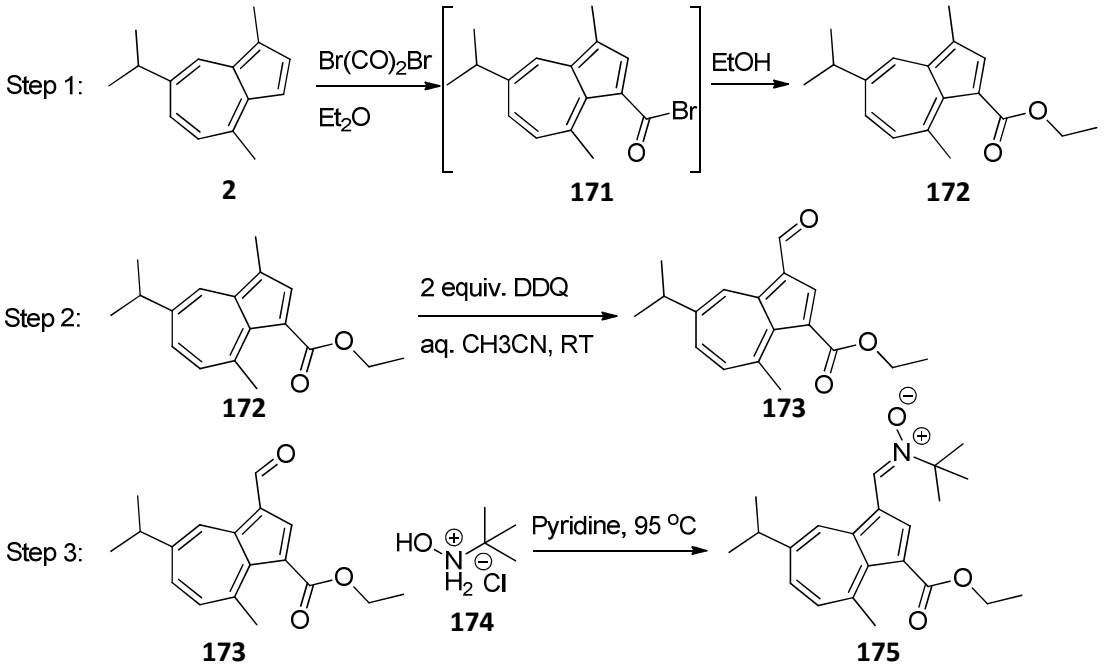

Scheme 65. Azulene-1-Nitrone synthesis

Initially, a modified procedure was followed for step one; oxalyl chloride was substituted for oxalyl bromide and THF for diethyl ether, because oxalyl chloride was available and there was a ready supply of dry THF in the laboratory. The use of oxalyl chloride instead of oxalyl bromide, however, had an unexpected consequence. While the ^{1}H NMR spectrum appeared to fit the structure of **172**, there was an extra unexplained signal in the ^{13}C NMR and the mass was ~28 Daltons higher than

expected. The product structure was therefore determined to be the ethyl oxoacetate **177**, obtained via the oxalylchloride **176**.

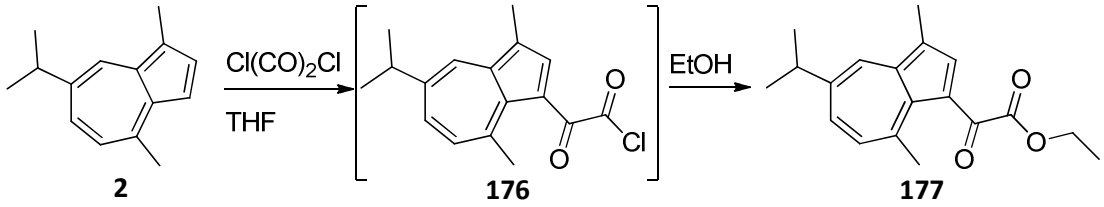

Scheme 66. Use of oxalyl chloride instead of bromide

Subsequently, the reaction was repeated using oxalyl bromide, but retaining the dry THF. This also had an unexpected consequence; the spectra showed an additional two signals in the ^{13}C NMR and four extra protons in the ^{1}H NMR over what was expected for **175**. The additional protons manifested as two triplets each integrating to two protons and a complex four proton multiplet. In addition, the mass was ~106 Daltons higher than expected and isotope analysis suggested the presence of a bromine atom. The structure was determined to be the 4-bromobutyl ester **180**. The 4-bromobutan-1-ol (**179**) required to form the ester is presumably generated by ring-opening addition of HBr to the THF solvent (Scheme 67).

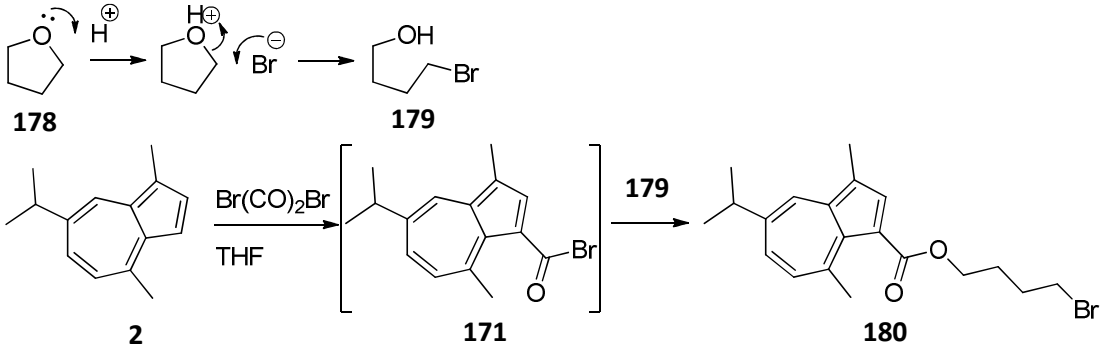

Scheme 67 - THF ring opening by HBr

Following Becker's protocol without substitution of reagents or solvent finally gave the required ethyl ester **172** which was subsequently taken forward to successfully synthesise **175**.

The cyclic voltammogram of **175** taken at 100 $mV.s^{-1}$, while not displaying any signs of decomposition products in the second and subsequent scans, did not display the reversible electrochemistry seen with **160** and **170** (Voltammogram 7).

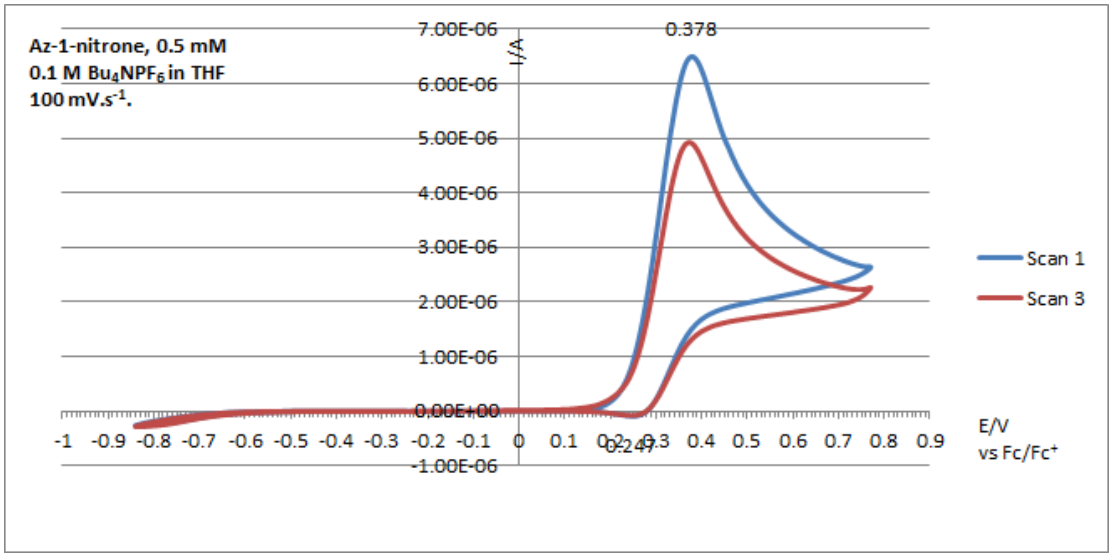

Voltammogram 7. Azulene-1-nitrone, 100 mV.s^{-1}

Further voltammograms were taken at higher scan rates (Voltammogram 8).

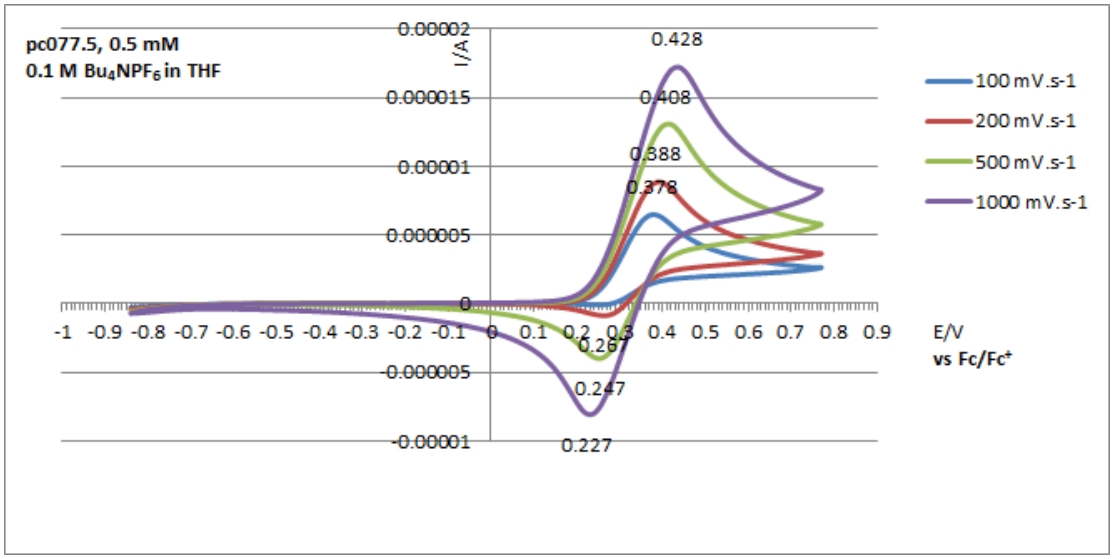

Voltammogram 8. Azulene-1-nitrone, various scan rates

As the rate of scanning increases, the reduction wave on the CV becomes more pronounced relative to the oxidation wave. This suggests that the nitrone group does offer some degree of protection or stabilisation of the radical cation, but the radical cations formed by extracting an electron are not so long lived as the ones formed from **160** and **170**.

5.2.4 Conclusions

Some stability was conferred to the azulene radical cations with all three of the groups tested, but the *tert*-butyl and methylthio groups clearly out-performed the nitrone group in this respect. It was also thought that the presence of a relatively labile nitrone group would make further substitutions and/or transformations during the dye synthesis much more difficult.

For these reasons a decision was made to synthesise dyes with *tert*-butyl and methylthio groups, but not with a nitrone group.

With the synthetic strategy developed to make the first generation dyes there are several opportunities for introducing the "shielding" group at the azulene C-1 (C-3) position:

- As the first step, before chlorination;
- After chlorination, prior to Suzuki-Miyaura cross-coupling to add the thiophene linker group;
- After Suzuki-Miyaura cross-coupling, either before or after removing the cyclic acetal aldehyde protecting group;
- As the final step after Knoevenagel condensation to add the cyanoacrylic acid anchor group.

The point at which the chosen groups may be introduced depends on:

1. The chemistry of the process used to perform the introduction and the resilience of existing groups to it;
2. The resilience of the introduced group to subsequent steps; and
3. Any effect of the new group on subsequent steps.

5.3 Dyes Bearing a *tert*-Butyl "Shielding" Group

The objective with this part of the project was to synthesise dyes of the structure depicted in Figure 55.

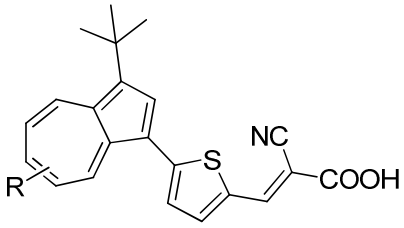

Figure 55. Dyes bearing a *tert*-butyl shielding group

Since the *tert*-butyl group is reasonably robust and relatively inert to the conditions all of the subsequent steps, introducing it as the first step of the synthesis appeared to be a good choice. In addition, the Friedel-Crafts conditions used to synthesise 1,3-di-tert-butylazulene (**160**) were quite harsh and the products from the intermediate steps of dye synthesis (1-chloroazulene **112**, aldehyde **87**) and the cyanoacrylic acid group of the dyes themselves are all susceptible to attack. An attempt was made to install the *tert*-butyl group into the aldehyde intermediate **87** to give **164** using the *tert*-butanol / HBF_4 method, but the reaction failed, with none of the desired product detected in the reaction mixture (Scheme 68).

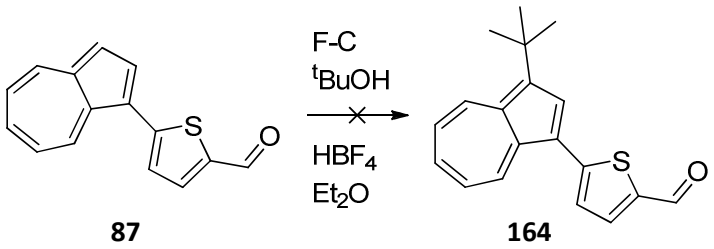

87 **164**

Scheme 68. Attempted Friedel-Crafts alkylation of aldehyde intermediate

The problem then was how to go about the synthesis of pure 1-*tert*-butylazulene (**159**). Previous experience had shown that mixtures of unsubstituted azulene, 1- and 1,3-di- *tert*-butyl azulenes are very difficult to separate since they all have very similar Rf values and tend to co-elute in flash chromatography.

Attempts to synthesise pure **159** by Friedel-Crafts reactions with carefully controlled conditions and equivalents of starting materials proved to be futile. With one equivalent of both azulene and alkylating agent (*tert*-butylchloride or *tert*-butanol) a mixture of unreacted starting material plus mono- and di- substituted products always resulted.

In principle, a small quantity of di-substituted product could be tolerated, since in the subsequent chlorination step it would remain unchlorinated and possibly removed in purification of that step. In any case, any unchlorinated material would

not participate in the Suzuki-Miyaura cross-coupling step and would then definitely be removed in purification of the coupled product.

Any unsubstituted azulene could not be tolerated, however, because it would probably end up in the final dye and result in poor electrochemistry. Also, precise characterisation of impure materials is not possible. A method of synthesising pure **159** was therefore necessary.

Attempts to synthesise **159** using cross-coupling reactions also proved to be futile, as expected, due to rapid ß-hydride elimination of isobutene (**183**) from the Pd^{II} complex **182** giving the Pd^{II} complex **184**. **182** is the product of oxidative addition of 1-chloroazulene to the Pd^{O} catalyst followed by transmetalation of the organo-metalic coupling partner. **184** then undergoes reductive elimination yielding azulene (**1**) and re-generating the Pd^{O} catalyst. (Scheme 69).

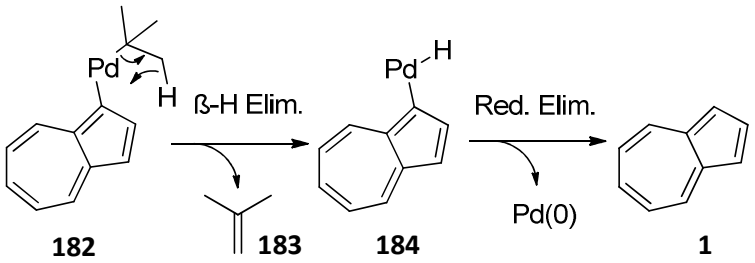

Scheme 69. Beta-hydride elimination of isobutene + reductive elimination of azulene

Both Suzuki-Miyaura and Negishi type reactions were tried with various ligands, organo-metalic coupling components and additives in an attempt to suppress the ß-H elimination but all these reactions failed; either there was no (useful) reaction at all, or azulene was the sole product. The Pd^{O}-catalysed cross-coupling reaction of 1-chloroazulene with *tert*-butylboronic acid turned out to be a very efficient (but expensive) method of de-chlorinating chlorinated azulene.

In 1962, Hafner and Moritz reported that when 1,3-di-*tert*-butylazulene was subjected to Vilsmeier formylation an excellent yield of 1-*tert*-butyl-3-formylazulene was obtained,[143] ie one *tert*-butyl group had been replaced (*ipso*-substitution) by a formyl group. More recently Shoji *et al*. reported[144] electrophilic *ipso*-substitution of 1,3,6-tri-*tert*-butylazulene via Vilsmeier formylation to give 1,6-di-*tert*-butyl-3-formylazulene. The authors went on to show that the formyl group could be removed by treatment with pyrrole in acetic acid, leaving 1,6-di-*tert*-butylazulene.

The *ipso*-substitution approach offered a solution to the problem of obtaining pure 1-*tert*-butyl azulene. The Friedel-Crafts alkylation using *tert*-butanol and HBF_4 etherate had already been used to synthesise 1,3-di-*tert*-butylazulene (**160**) with no contamination by unsubstituted azulene. *Ipso*-formylation to replace one of the *tert*-butyl groups would give **185**, a much more polar compound that would be easily separated from any unreacted starting material. Subsequent removal of the formyl group should afford 1-*tert*-butylazulene (**159**), also easily purified because of the difference in polarity compared to **185** (Scheme 70).

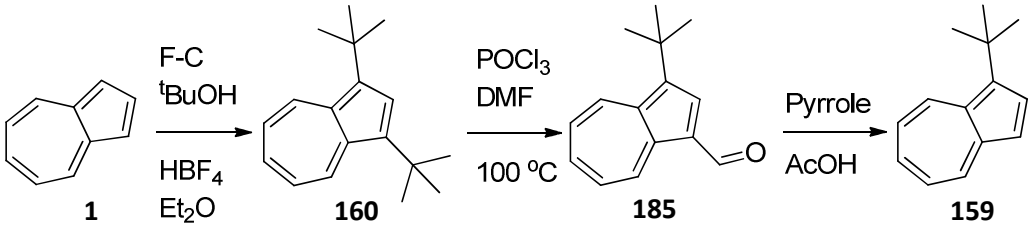

Scheme 70. Route to 1-*tert*-butylazulene

Vilsmeier formylation of 1,3-unsubstituted azulenes proceeds rapidly at room temperature; however more forcing conditions are required for the *ipso*-substitution reaction presumably because of the steric bulk of the *tert*-butyl groups. The *tert*-butyl group is able to act as a leaving group because of the relative stability of the *tert*-butyl cation (**187**). At the temperature of the reaction conditions employed, **187** dissociates into isobutene (**183**) and H^+ ion and is therefore removed from the reaction.

Electrophillic attack by the Vilsmeier reagent (**119**) gives Wheland intermediate **186**. Re-aromatisation is achieved when the *tert*-butyl cation (**187**) leaves **186** giving the iminium ion **188**. The electron-withdrawing iminium group de-activates the azulene ring towards further electrophilic attack, so multiple substitutions do not occur. **188** is hydrolysed to give **185** during workup (Scheme 71).

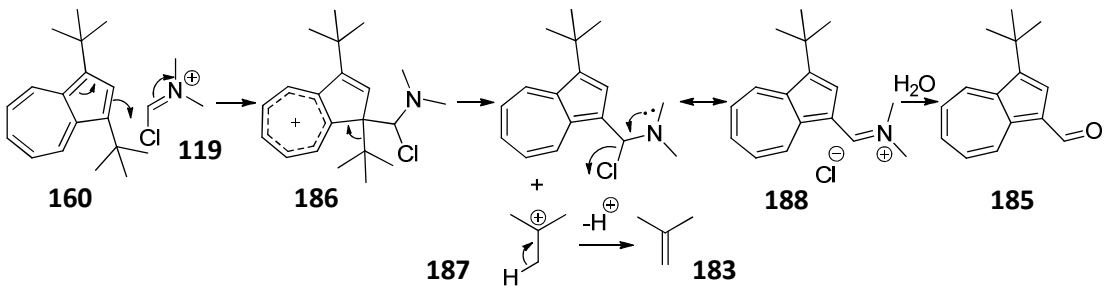

Scheme 71. Ipso-formylation of 1,3-di-tert-butylazulene

A small quantity (~8% yield) of 1,3-di-*tert*-butyl-5-formylazulene (**189**) (Figure 56) is also produced in this reaction, demonstrating that electrophilic substitution will occur in the azulene seven-membered ring if access to the C-1 and C-3 positions is restricted. The C-5 and C-7 positions have the highest electron density in the seven-membered ring in the ground state – see section 1.5.1 above.

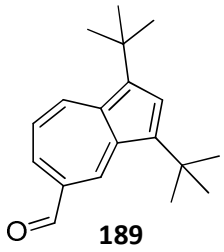

189

Figure 56. 1,3-di-*tert*-butyl-5-formylazulene

In the final step of the synthesis of **159**, **185** is treated with pyrrole in acetic acid, in accordance with the method of Shoji *et al*.[144] The authors offered no explanation of the mechanism of this reaction; it is presumed to be a variant of the *ipso*-substitution reaction, beginning with protonation of azulene C-3 to give the Wheland intermediate **190**. Pyrrole (**191**) is appreciably nucleophilic at the α–positions and undergoes electrophilic attack by **190** giving the alkoxide **192**. Re-aromatisation of the azulene core is achieved via 2-pyrrolecarboxaldehyde (**193**) leaving to furnish 1-*tert*-butylazulene (**159**) (Scheme 72). The synthesis of pure **159** was therefore achieved in three steps from azulene (**1**) in an overall yield of ~32%.

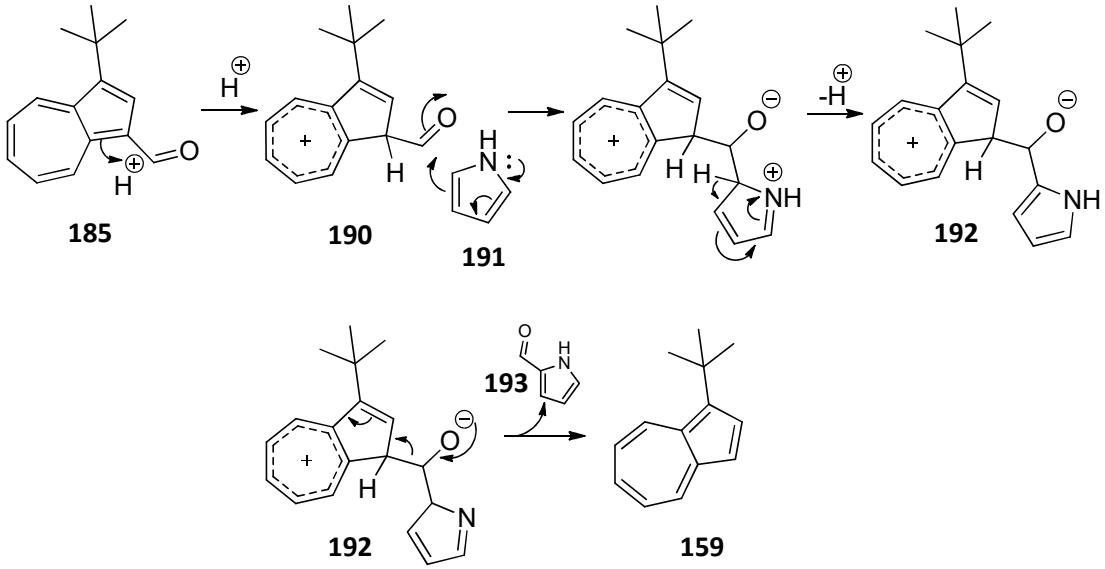

Scheme 72 - De-formylation of 1-*tert*-butyl-3-formylazulene

Unfortunately, the same methodology could not be used to synthesise 1-tert-butyl-4,6,8-trimethylazulene (**194**) from 4,6,8-trimethylazulene (**48**) because the Friedel-Crafts alkylation step failed completely (Scheme 73).

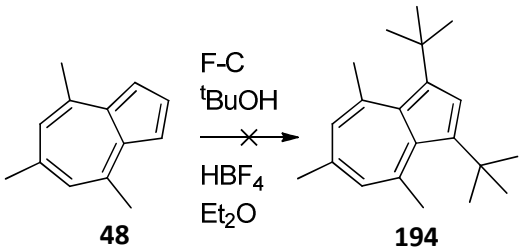

Scheme 73. Failed Friedel-Crafts with 4,6,8-trimethylazulene

On addition of HBF_4 etherate to the stirred solution of **48** in *tert*-butanol and diethyl ether, an almost colourless pale pink crystalline precipitate was formed. Stirring was continued at RT for an hour with no further apparent changes. During work-up, on neutralising the solution with 1M aq. NaOH, the ethereal layer immediately became deep purple in colour (colour of **48**). A ^1H NMR spectrum of the crude showed only the 4,6,8-trimethylazulene (**48**) starting material.

To make the aldehyde intermediate bearing the *tert*-butyl shielding group ready for Knoevenagel condensation to install the acceptor / anchor group, the Suzuki-Miyaura cross-coupling with **142** was carried out using the sulfonium salt adduct of **159**. The cross-coupling of azulenylsulfonium salts is discussed in section 5.6 below. The sulfonium salt coupling partner was prepared in a similar manner to 1-(dimethylsulfonium)azulene (**168**) (Scheme 76 below), but substituting tetrahydrothiophene-1-oxide (**161**) for DMSO. Thus, treatment of **159** in the presence of **161** with trifluoroacetic anhydride, followed by exchange of the counter ion affords 1-(3-*tert*-butylazulen-1-yl)tetrahydrothiophenium PF_6 (**162**) in high yield (Scheme 74).

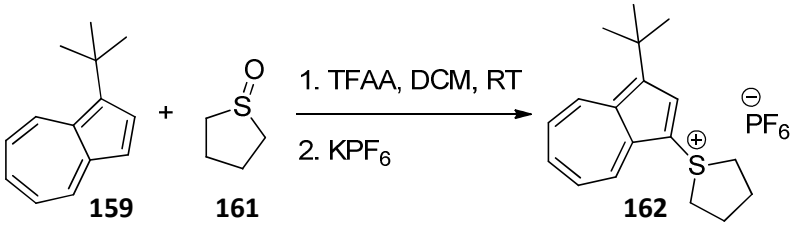

Scheme 74. Synthesis of 1-tert-butylazulene sulfonium salt

162 then undergoes Suzuki-Miyaura cross-coupling with **142** giving the cyclic acetal **163**. Deprotection in wet acetone with catalytic pTSA yields the aldehyde **164** (Scheme 75).

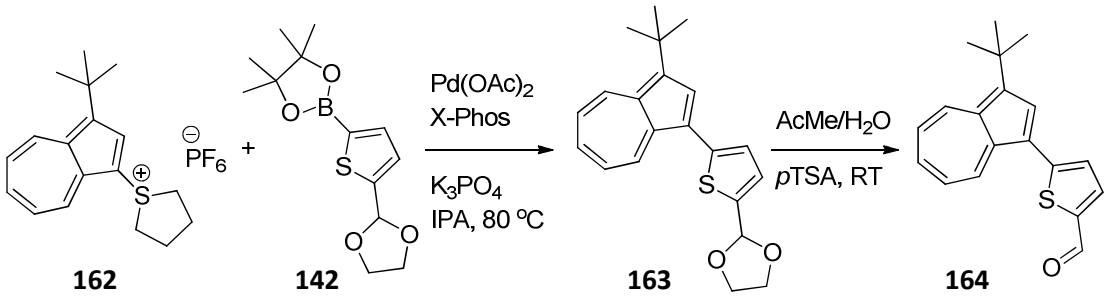

Scheme 75 - Synthesis of 5-(3-(tert-butyl)azulen-1-yl)thiophene-2-carboxaldehyde

5.4 Dyes Bearing a Methylthio "Shielding" Group

The objective with this part of the project was to synthesise dyes of the structure depicted in Figure 57.

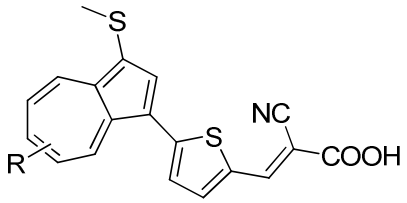

Figure 57. Dyes bearing a methylthio shielding group

Using the protocol of Shoji *et al.*,[177] the synthesis of 1- and 1,3-bis (methylthio)azulenes through the use of activated dimethyl sulfoxide (DMSO), via the respective sulfonium salts, is relatively straightforward. Previously, Balenkova *et al*. had reported that dimethylsulfonium ditriflate (DMSD), prepared by the reaction of triflic anhydride (Tf_2O) with DMSO can react with nonactivated arenes as a highly reactive electrophile to introduce sulfur-based substrituents.[145] With azulene substrates, Shoji *et al*. demonstrated that selective 1- (mono-) or 1,3- (di-) substitution could be achieved by using different activating electrophiles.

Thus, the use of excess DMSO with 2.4 equivalents of triflic anhydride leads to 1,3-bis(dimethylsulfonium)azulenes (see Scheme 63, section 5.2.2 above) whereas 1.2 equivalents of trifluoroacetic anhydride (TFAA) (**195**), a less powerful electrophile,

provides mono-substituted 1-(dimethylsulfonium)azulenes as the sole product. There was no reaction when acetic anhydride was used as the activating agent.

The reaction stops after the first substitution because the sulfonium group is electron withdrawing and therefore deactivates the azulene ring towards electrophiles (Figure 58). The dimethylsulfonium ditrifluoroacetate (**196**), formed by the reaction of DMSO and TFAA, is not sufficiently electrophilic to perform a second substitution on the deactivated azulene.

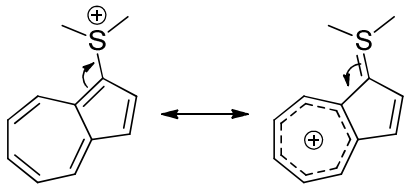

Figure 58. Deactivation of azulene ring by sulfonium electron withdrawing group

The mechanism of this reaction is similar to that for the reaction with triflic anhydride. Azulene (**1**) undergoes electrophilic attack by **196** giving the Wheland intermediate **197** which yields 1-(dimethylsulfonium)azulene (**168**) following re-aromatisation.

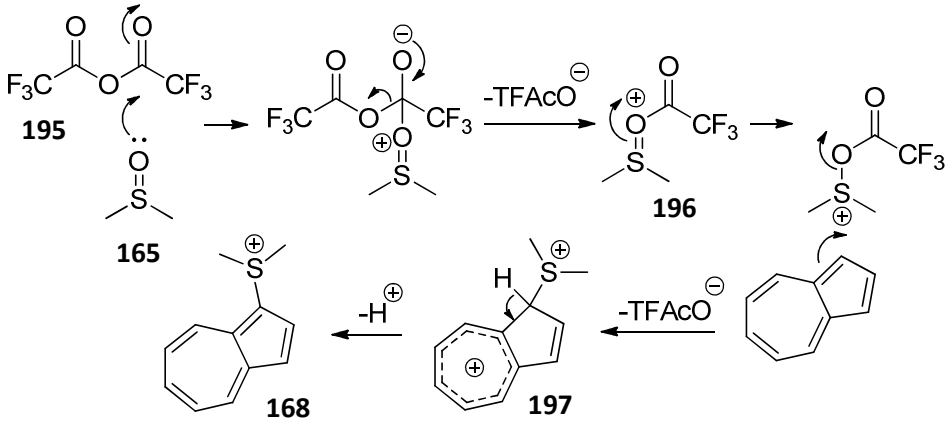

Scheme 76. Synthesis of azulene-1-dimethylsulfonium trifluoroacetate

Following solvent removal, treatment of **168** in a refluxing 1:1 mixture of ethanol and triethylamine yields 1-(methylthio)azulene.

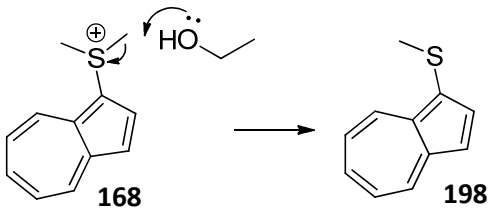

Scheme 77 - Synthesis of 1-(methylthio)azulene

The synthesis of 1-methylthioazulene was therefore achieved in two stages in an isolated yield of 96%. Unfortunately, however, attempted chlorination of **198** using *N*-chlorosuccinimide (NCS) resulted only in uncharacterisable tar. Likewise, attempted reaction of 1-chloroazulene (**112**) in the presence of DMSO with TFA Anhydride also failed (Scheme 78). It became apparent that adding the methylthio group in the early stages of the synthesis was not feasible due to the effect its presence had on the chlorination step or *vice-versa*.

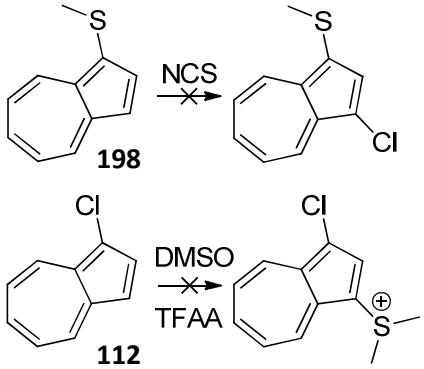

Scheme 78. Introduction of methylthio group in early stages unfeasible

Initial experiments to introduce the methylthio group into **87** (the aldehyde product after deprotection of the Suzuki-Miyaura cross-coupling reaction between **112** and **142**) using TFA anhydride as the DMSO activating agent showed no reaction. Replacing the TFA anhydride with triflic anhydride, however, resulted in successful installation of a dimethylsulfonium group, giving the sulfonium salt **199**, which was subsequently converted to methylthio group in refluxing ethanol : triethylamine (1:1) to furnish **200** in 65% overall yield. A similar protocol was used to synthesise the trimethyl analogue **202**, starting with **146** (Scheme 79).

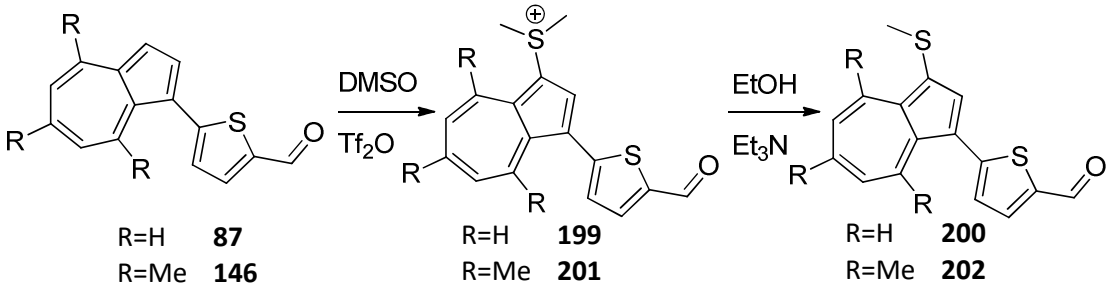

Scheme 79. Installation of methylthio group into aldehyde intermediate

5.5 Amino Acid Catalysed Knoevenagel Condensation

The dyes synthesised with *tert*-butyl and methylthio radical shielding groups (2nd generation) turned out to have much higher solubility in DCM than the analogues without such groups (1st generation). This meant that the method used to purify the 1st generation dyes - trituration in DCM followed by recrystallisation from ethanol - did not work for the 2nd generation dyes. Because of the higher solubility, the trituration step was not practical, since invariably all of the dye dissolved in only a small quantity of DCM solvent. Recrystallisation of the dyes directly from the Knoevenagel reaction crude was also impractical; crystals were never formed, and the fine particle precipitate that invariably resulted was always contaminated with unreacted starting material and other contaminants.

Attempts were made to purify the 2nd generation dyes by flash chromatography, eluting the silica gel column first with mixtures of ethyl acetate and petroleum ether to remove the less polar starting materials and by-products of reaction, then adding acetic acid to the eluent to elute the much more polar dyes with cyanoacrylic acid groups. Unfortunately the dyes were still contaminated with starting material, even after prolonged flushing of the column before adding the acetic acid. Presumably either starting material was trapped within particles of undissolved product or there was acid-catalysed retro-Knoevenagel reaction occurring in the column.

Analogues of the dyes were synthesised with methyl and *tert*-butyl ester groups instead of the carboxylic acid group by substituting the cyanoacetic acid in the Knoenenagel condensation with methylcyanoacetate or *tert*-butylcyanoacetate respectively. The idea was to synthesise the dyes in a form that could be purified by flash chromatography, then remove the protecting group with trifluoroacetic acid (Scheme 80).

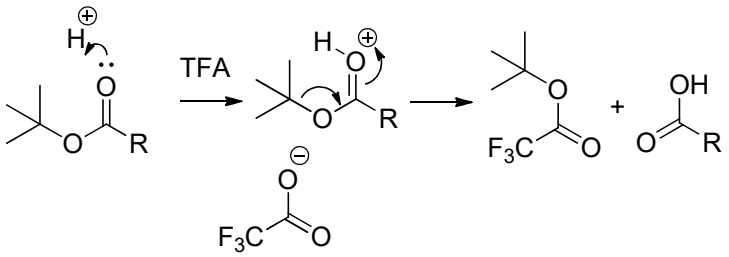

Scheme 80. Removal of *tert*-butyl protection group with TFA

The methyl dye ester was successfully purified by flash chromatography; unfortunately demethylation of the ester in trifluoroacetic acid failed. Purification of the *tert*-butyl dye ester by flash chromatography was not successful; TLCs of the fractions indicated the presence of an impurity with slightly higher Rf than the dye ester and there was a residue that remained on the base line. Re-purification by flash chromatography failed to remove the impurities.

An alternative to removing lots of impurities from a reaction mixture is to optimise the reaction conditions to minimise the formation of impurities that must be removed. Obviously if the proportion of impurities in the reaction mixture is reduced, by definition the yield of desired product will be increased. A literature survey revealed that while piperidine is by far the most popular catalyst used in Knoenenagel reactions, other catalytic systems have been used including pyridine, triphenylphosphine,[146] heterogeneous reconstructed hydrotalcite,[147] iridium(III) chloride and acetic anhydride,[148] carbamic acid ammonium salts,[149] iron(III)chloride,[150] zinc chloride[151] and ionic liquids.[152] Several authors have reported the use of amino-acids in Knoevenagel condensations under very mild conditions.[153,154,155] Zhu *et al*. and Prout had particular success with ß-alanine (3-aminopropionic acid) (3-APA) with 1,8-diazabicyclo(5.4.0)undec-7-ene (DBU) co-catalyst and ε-aminocaproic acid (6-aminocaproic acid) (6-ACA).

Experiments were carried out to determine if 3-APA and / or 6-ACA could be used to catalyse the Knoevenagel condensation of thiophene-2-carboxaldehyde (**133**), as a surrogate for the dye aldehyde intermediates, with cyanoacetic acid (CAA) (**88**).

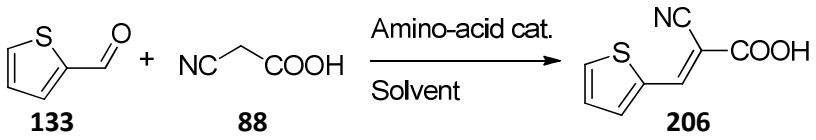

133 **88** **206**

Scheme 81. Amino-acid catalysed Knoevenagel reaction

Initially, the optimised conditions reported by Zhu[155] (ethanol solvent and 1 mol% DBU co-catalyst) were tested with 10% excess of **88** and 50 mol% of 3-APA, at a concentration of **133** ~1.7 M. After stirring for 1 hour at RT, the reaction mixture contained a solid mass of white crystalline material that was preventing the stirrer bar from moving. After adding additional ethanol to loosen and dissolve the solid mass, aqueous sulfuric acid (1 M, 10 mL) was added. The solid precipitate formed was filtered and washed with water. The product was confirmed as 2-cyano-3-(thiophene-2-yl)acrylic acid (**206**) by its NMR spectrum, which also confirmed that there were virtually no impurities. A yield of 74% was obtained.

The experiment was repeated, replacing the 3-APA with 6-ACA, while keeping all the other reagents and conditions as before. After stirring for 1 hour at RT, the reaction mixture had become cloudy but there was not the same mass of solid material as had been observed when 3-APA was used as the catalyst. Stirring was continued overnight. More product had clearly formed, but the stirrer bar was still able to rotate in the mixture.

The product was isolated as before by adding aqueous sulfuric acid, filtering and washing the precipitate with water. The product was confirmed to be **206** by NMR, obtained in 93% yield.

The lower yield obtained when 3-APA was used as the catalyst may have been due to the lack of stirring once the solid mass had formed and / or the extra reaction time that was allowed with the 6-ACA catalyst. Additional experiments were therefore undertaken with both catalysts using less concentrated reaction mixtures to ensure that the product remained in solution. The concentration of **133** was 0.166 M (ie $^{1}/_{10}$ of the first experiments); all other reagents were maintained in proportion. After stirring overnight at RT, TLCs indicated that a small quantity of starting material remained in each reaction mixture. The yield of product from the 6-ACA catalysed reaction (65%) was still higher than that obtained from the 3-APA catalysed one (58%); however both produced lower yields than the more concentrated reactions.

The success of the proof-of-concept experiments led to a series of experiments to further optimise the protocol using thiophene-2-carboxaldehyde as the substrate before attempting to use it in the final step of dye synthesis. The results are summarised below (Table 12).

Entry	**Catalyst**	**Catalyst Loading %**	**DBU %**	**CAA equiv.**	**Temp °C**	**Time**	**Yield %**
1	3-APA	50	1	1.1	RT	o/n	58
2	6-ACA	50	1	1.1	RT	o/n	65
3	3-APA	50	10	1.1	RT	o/n	55
4	6-ACA	50	10	1.1	RT	o/n	57
5	3-APA	50	1	2	RT	o/n	56
6	6-ACA	50	1	2	RT	o/n	51
7	3-APA	100	1	1.1	RT	o/n	36
8	6-ACA	100	1	1.1	RT	o/n	74
9	3-APA	25	1	1.1	RT	o/n	58
10	6-ACA	200	1	1.1	RT	o/n	57
11	6-ACA	100	1	1.1	RT	7 hr	70
12	6-ACA	100	0	1.1	RT	7 hr	61
13	Piperidine	2	0	1.1	RT	70 hr	35
14	6-ACA	100	1	1.5	RT	o/n	68
15	6-ACA	100	1	2	RT	o/n	74
16	6-ACA	100	1	4	RT	o/n	66
17	6-ACA	135	1	1.1	RT	o/n	67
18	6-ACA	135	1	1.5	RT	o/n	72
19	6-ACA	135	1	2	RT	o/n	69
20	6-ACA	100	1	1.1	50	3 hr	58
21	6-ACA	100	1	1.5	50	3 hr	75
22	6-ACA	100	0	1.5	50	3 hr	73

23	6-ACA	100	1	1.5	50	3 hr	69

Table 12. Amino-acid catalysed Knoevenagel reaction optimisation

Increasing the DBU loading so that its concentration was equivalent to the initial proof-of-concept experiments (entries 3 and 4) did not change the yield of product. Increasing the loading of CAA (**88**) while maintaining the catalyst loading (entries 5 and 6) likewise did not increase the product yield. Increasing the catalyst loading while maintaining the CAA loading (entries 7 and 8) had a contradicting effect; with the 3-APA catalyst the yield was significantly reduced, but with the 6-ACA catalyst the yield was significantly increased.

When the loading of 3-APA was halved to 25% the yield of product was equivalent to the run with 50% loading (entries 9 and 1). It is apparent that if the loading of 3-APA is increased beyond a threshold then yield is detrimentally affected. Similarly, the optimum loading of 6-ACA seems to be around 100%; at 135% (entries 17-19) the yield was slightly down but if increased to 200%, a lower yield resulted (entry 10).

To determine the effect of the DBU co-catalyst, two runs were made over a shorter time of 7 hours (approx. half of the overnight time), one with the same conditions that had produced the highest yield so far (entry 8), the other without the DBU co-catalyst (entries 11 and 12). Not surprisingly, both runs produced somewhat lower yields than the overnight run; the run without the DBU co-catalyst produced a slightly lower yield than the run with the co-catalyst but the difference was not dramatic.

Increasing the loading of CAA (entries 14-16 and 17-19) did not have a significant effect on yield even though some **133** could be detected by TLC in the reaction mixtures before isolating the product.

Increasing the temperature to 50 ^{o}C had a significant effect on the rate of reaction (entries 20 and 21); yields similar to the overnight runs were achieved in 3 hours (TLC showed only a trace of **133** remaining). A second trial with/without the DBU co-catalyst at 50 ^{o}C (entries 22 and 23) produced a slightly better yield without the DBU co-catalyst.

In summary, the best yields of **206** were achieved using the 6-ACA catalyst. The optimum loading was ~100%, with 1.1-1.5 equivalents of **88**. The DBU co-catalyst appeared to have no significant effect. Increasing the temperature to 50 °C had a significant effect on the rate of reaction (as expected) without affecting the yield.

The conditions from entry 22 were selected for trials with the dye aldehyde intermediates. The aldehyde intermediate **200** (0.166 M) was subjected to Knoevenagel condenation with **88** in the presence of 100 mol% of 6-ACA in ethanol at 50 °C. After stirring for 3.5 hours at 50 °C, TLC indicated that the starting material was consumed. The product was precipitated from solution by adding 1M aqueous sulfuric acid, washed with water and ice-cold ethanol and dried. The crude yield was 98%, but ^{1}H NMR revealed that the product **203** was contaminated with a trace amount of starting material. Recrystallisation from hot 2-propanol and water afforded a yield of 67% which was found to be pure by NMR.

The reaction was repeated, starting with **202** to give the dye **204** which was also successfully purified by recrystallisation from hot 2-propanol and water (Scheme 82).

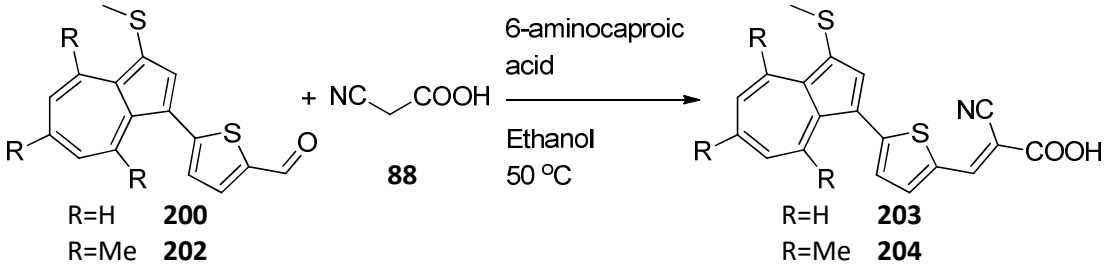

Scheme 82. Dyes with methylthio shielding group, final step

Similarly, the aldehyde **164** was reacted with **88** under the same conditions to give the dye **205** (Scheme 83). When the reaction was complete, aqueous sulfuric acid was added to the reaction mixture to precipitate the product. Unlike the previous reactions to make **203** and **204**, when the acid was added a tarry mass resulted instead of the expected filterable precipitate. The work-up procedure was therefore modified; the tarry mass was dissolved in DCM and washed with water. After removing the solvent, the crude product was re-crystallised from DCM/petroleum ether instead of hot 2-propanol/water which had been successful with **203** and **204**, but failed to produce crystals with **205**.

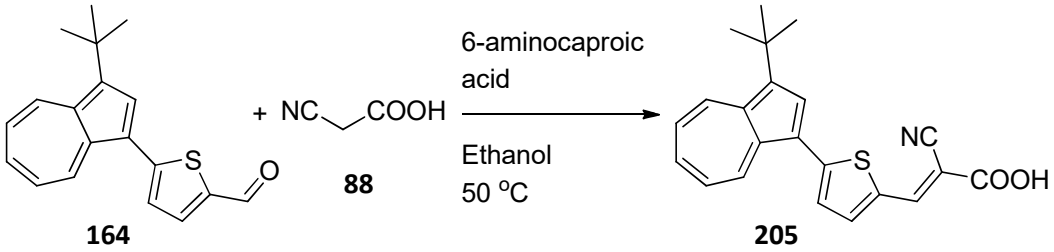

164 **88** **205**

Scheme 83. Dye with *tert*-butyl shielding group, final step

5.6 Azulenesulfonium Salts for Cross-Coupling

As already discussed (sections 1.5.4 and 4.1.2.1 above) the halogenation of azulene using electrophilic halogen sources is facile and the halogenated products have been shown to participate in cross-coupling reactions. However, this approach to the controlled introduction of substituents into the azulene skeleton suffers from serious drawbacks:

1. The treatment of azulene with one equivalent of *N*-halosuccinimide furnishes the required 1-haloazulene invariably in a mixture, requiring tedious separation and purification (where possible), with
    a. 1,3-dihaloazulene, as a consequence of the enhanced reactivity of the initial product, and
    b. unreacted starting material, since a proportion of the single equivalent of halogenating agent is consumed in making the di-substituted product;
2. The haloazulenes obtained are unstable to varying degrees
    a. Chloroazulenes have been shown to be stable to flash chromatography, but cannot be stored for long-term future use;
    b. Bromoazulenes are not stable to flash chromatography and degrade in a few hours out of solution;
    c. Iodoazulenes typically degrade on removal of the solvent from their solutions.

These problems of separation and stability have been commented on previously in several articles.[156] Attempts to mitigate the problems outlined above have been made, but these are usually compromises with their own restrictions. For example, crude mixtures of 1- and 1,3-di haloazulenes have been used in coupling reactions without purification, but with the consequence that doubly coupled products or higher oligomers also form, which also leads to purification issues. There are limited examples of the use of alternative azulene pseudo-halides, eg 1-trifloxyazulenes, but these coupling partners were also unstable and required specific reaction conditions.[93,129]

Liebeskind *et al*. reported the use of sulfonium salts as powerful electrophilic reagents for cross-coupling reactions,[157] but as far as could be determined they had

not previously been used in the context of azulene chemistry. In a subsequent article, Liebeskind *et al*. described efficient cross-coupling of electron rich and difficult benzylic and heterobenzylic partners.[158] Many heterobenzylic halides are too unstable to participate in transition metal catalysed cross couplings; for example, 2-chloromethylfuran must be stored in solution at -20 °C because neat samples decompose slowly, even at -20 °C.[159] Successful cross-coupling reactions, however, were achieved with sulfonium salt analogues. The parallels with haloazulenes and synergy with the work already completed for the synthesis of 1-methylthioazulene via the sulfonium salt (sections 5.2.2 and 5.4 above) led to a desire to explore the use of azulenesulfonium salts as reagents for cross-coupling reactions.

Liebeskind *et al*. used double alkylation of aromatic thiols to synthesise sulfonium salts; however this approach was discounted since 1-azulenethiol is itself unstable and difficult to access.[160] Instead, the protocol of Shoji *et al*.,[177] using a sulfoxide and electrophilic activating agent, was adapted to afford the tetrahydrothiophenium salts analogous to those used by Liebeskind *et al*.. Thus, azulene (**1**), in the presence of excess tetrahydrothiophene-1-oxide (**161**), treated with trifluoroacetic anhydride (TFAA) followed by anion exchange and recrystallisation, yielded the novel azulenylsulfonium salt **207** (Scheme 84).

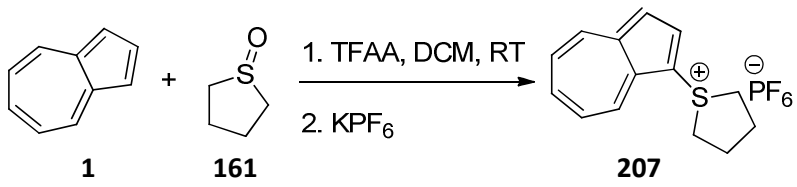

1 **161** **207**

Scheme 84. Synthesis of azlenyl-1-tetrahydrothiophium PF_6

207 is a purple crystalline solid with good stability; samples have been stored for months at ambient temperature and with no attempt to exclude air, moisture or light, without observing any degradation. In addition, no evidence of 1,3-disubstitution was observed, as expected, since **207** is much less electron rich than **1**.

Initial cross-coupling experiments were carried out using 4-tolylboronic acid (**208**) and the conditions reported by Liebeskind *et al*.;[157] however no cross-coupled product could be detected in the reaction mixture and the starting material was recovered (Scheme 85).

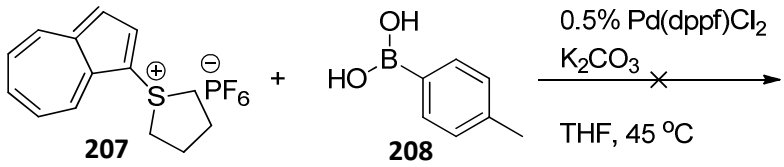

Scheme 85. Liebeskind's cross-coupling produced no reaction

When the conditions that have been developed for Suzuki-Miyaura cross-coupling of 1-chloroazulenes were employed, however, the cross-coupling reaction proceeded smoothly to give **209** in 60% yield.

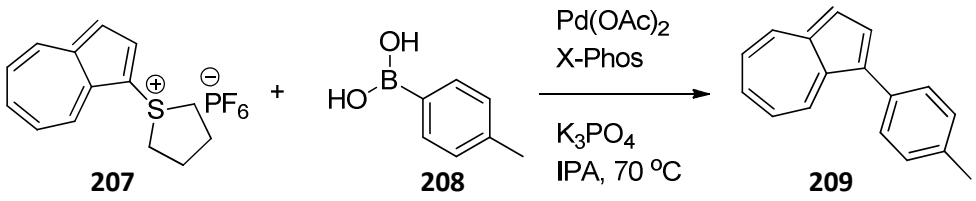

Scheme 86. Cross-coupling of azulenyl-tetrahydrothiophenium salt with 4-tolylboronic acid

Subsequently, a cross coupling reaction with 2-(5-(1,3-dioxolan-2-yl)thiophen-2-yl)-4,4,5,5-tetramethyl-1,3,2-dioxaborolane (**142**) followed by deprotection of **143** yielded the aldehyde **87** in 54% yield (Scheme 87).

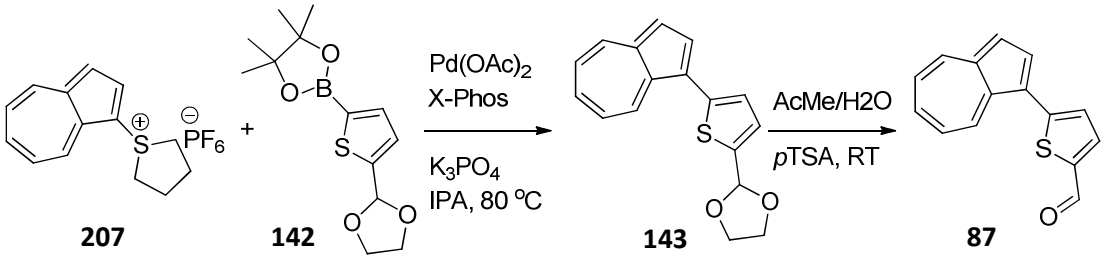

Scheme 87. Cross-coupling of azulenyl-tetrahydrothiophenium salt with borylated thiophene partner

Sulfonium salts were also prepared in high yield from 4,6,8-trimethylazulene (**48**) and 1-*tert*-butylazulene (**159**) by the same method to give **210** and **162** respectively (Figure 59).

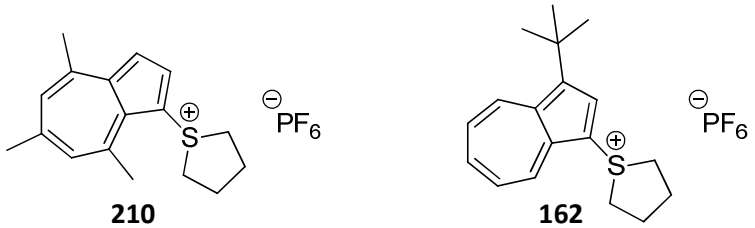

Figure 59. Sulfonium salts of alkyl- substituted azulenes

210 and **162** also participated in Suzuki-Miyaura reactions yielding the expected cross-coupled products. **210** is notable because of its bright scarlet colour; all of the other azulenesulfonium salts that were prepared are variations of deep purple.

The azulenesulfonium salts were therefore found to be direct replacements for the chloroazulenes that had previously been used in cross-coupling reactions during this project. Because of their facile preparation in high yield and purity and their convenience in storage and handling, azulenesulfonium salts were used for all subsequent cross-coupling reactions for the remainder of the project.

The discovery that azulenesulfonium salts participate in Suzuki-Miyaura cross-coupling reactions spawned an undergraduate MChem project and a postgraduate MRes project. Michael Turton carried out an optimisation study to discover the best combinations of solvent, base and ligands and Yu Jin performed many coupling reactions using the optimised conditions to discover the substrate scope. With the data gathered, a paper was prepared and accepted for publication in *Angewandte Chemie*, January 2016.[161] A copy of the paper is attached to this thesis.

5.7 Dye Characterisation

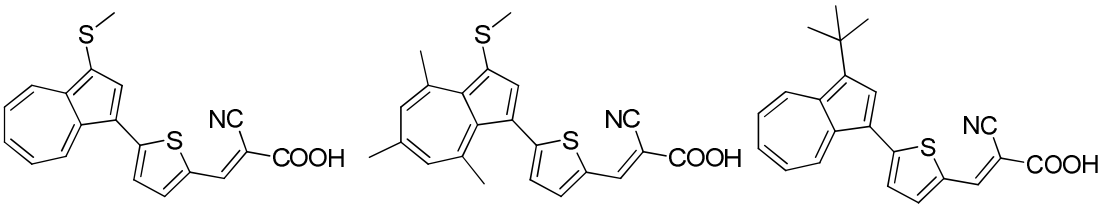

MeTAz-1-tcaa - **203** MeTTMAz-1-tcaa - **204** tBuAz-1-tcaa - **205**

Figure 60. Second generation dyes

5.7.1 Electrochemistry

The first generation dyes all exhibited non-reversible redox chemistry (Voltammogram 1 to Voltammogram 4 above), suggesting that the radical cations formed by oxidation of dye molecules did not survive long enough to be reduced back to the dye molecules. The longevity of DSSCs based on the first generation dyes is therefore compromised by the poor stability of the oxidised dye species.

Cyclic voltammograms (CVs) were acquired for each of the three 2nd generation dyes synthesised (Figure 60).

All three dyes show quasi-reversible redox chemistry (Voltammogram 9, Voltammogram 10 and Voltammogram 11). The radical cations produced by dye molecule oxidation clearly survive to be reduced back to the dye molecules as evidenced by the reduction waves in the reverse sweep which correspond to the oxidation waves in the forward sweep of the CVs. There is no sign of any decomposition products evident in the second and subsequent scans.

For all three dyes, the second and subsequent CV scans are almost exactly super-imposed (scan 1 and scan 3 are plotted for each dye), which indicates that there is little or no depletion of the dye species in the vicinity of the working electrode. This is in contrast with the first generation dye analogues (Az-1-tcaa, Voltammogram 3 and TMAz-1-tcaa, Voltammogram 4 above), where the magnitude of the oxidation waves diminish with each successive scan indicating that the dyes are being consumed.

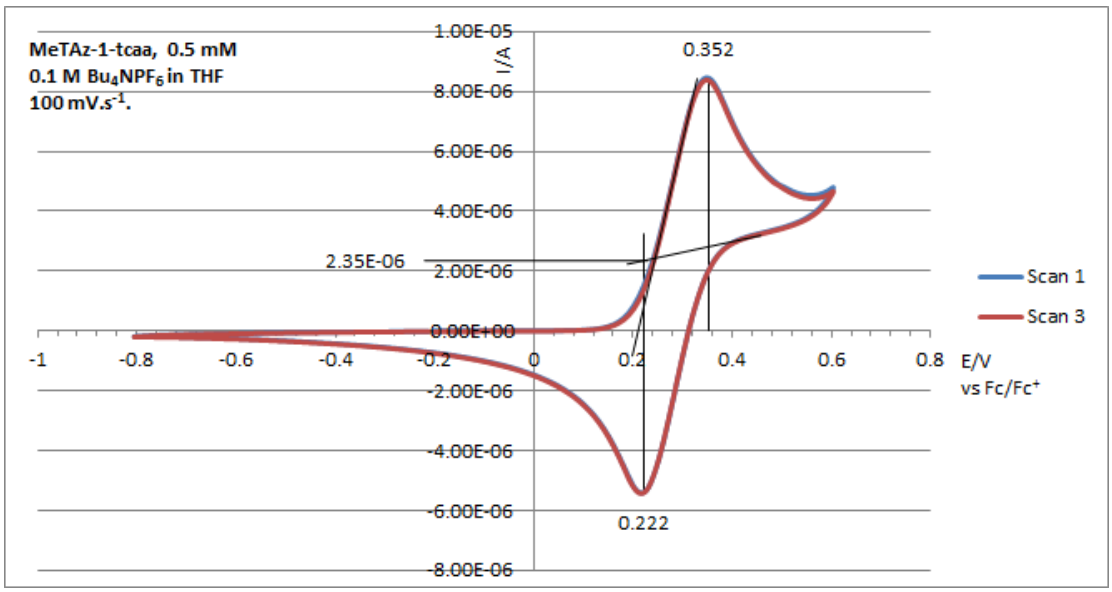

Voltammogram 9. CV of MeTAz-1-tcaa dye in THF

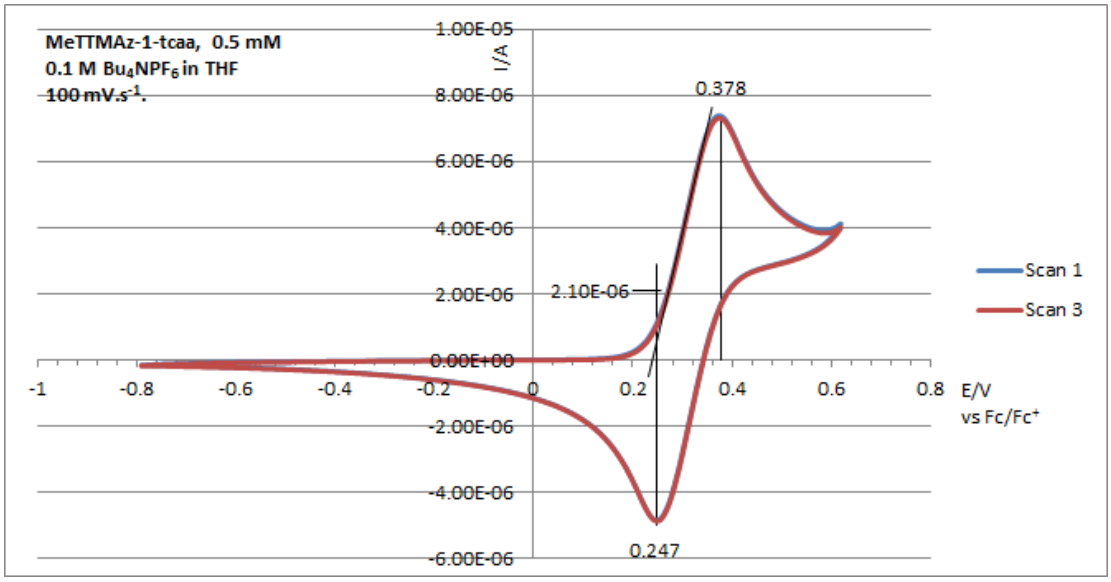

Voltammogram 10. CV of MeTTMAz-1-tcaa dye in THF

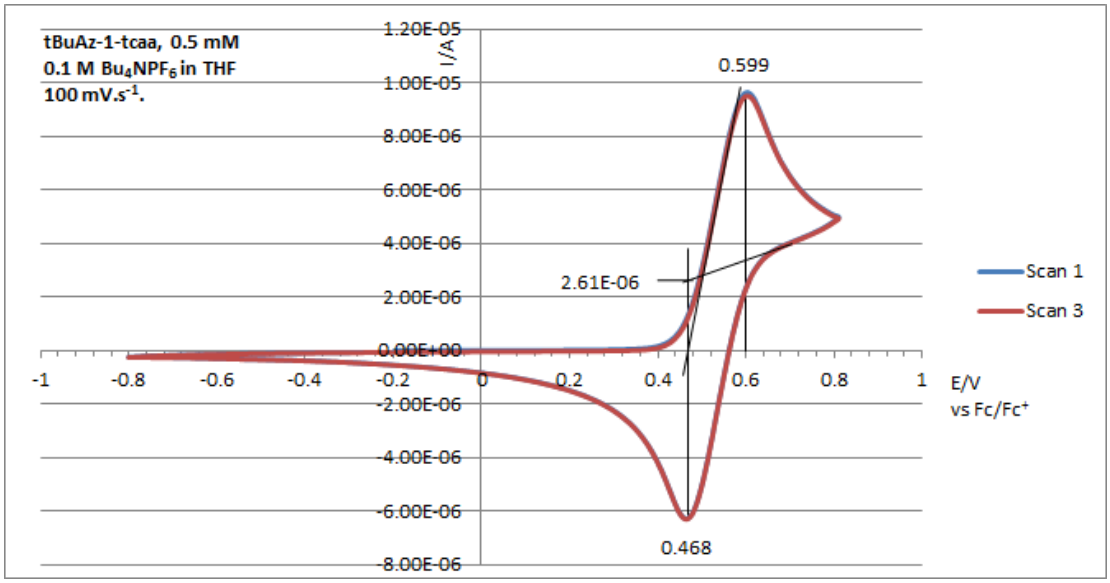

Voltammogram 11. CV of tBuAz-1-tcaa dye in THF

Both of the radical shielding groups therefore appear to do a good job of protecting the radical cation formed by abstracting an electron from the dye molecules. The CVs of the dyes containing a methylthio group (MeTAz-1-tcaa **203** and MeTTMAz-1-tcaa **204**) are very similar; the three methyl groups attached to the 7-membered ring increase the dye oxidation potential by approximately 40 mV. The difference between the methylthio and *tert*-butyl shielding groups is more striking; the shift in oxidation potential between MeTAz-1-tcaa (**203**) and tBuAz-1-tcaa (**205**) is over

250 mV, showing that the dye HOMO energy level can be 'tuned' to a certain extent by changing the shielding group.

Electrochemical data extracted from the cyclic voltammograms are presented in Table 13. In the ideal case of a reversible one electron redox couple, the difference between the peak cathodic and anodic potentials (E_{pc} and E_{pa}), ΔE_p is approximately 59 mV (at 25 °C) and the ratio of the peak anodic and cathodic currents (I_{pa} and I_{pc}) is unity.[162] The three dyes clearly depart somewhat from this ideal; ΔE_p = 131 mV for all three dyes and I_{pc}/I_{pa} varies from 0.92 to 0.94. The estimation of I_{pc} is quite subjective and relies on extrapolation of the "baseline" established during the reverse sweep just before the onset of the reduction wave to the point of intersection with a vertical line at E_{pc} and is therefore subject to some error. It is interesting to note that the values for ΔE_p are identical for each dye, suggesting that the slower than ideal electrode dynamics may be due to a different factor, eg solvent or electrolyte, which were constant for each experiment.

Dye	**E_{pa} mV**	**E_{pc} mV**	**ΔE_p mV**	**$E^0_{½}$ mV**	**I_{pa} µA**	**I_{pc} µA**	**$\frac{I_{pc}}{I_{pa}}$**	**E_{ox} mV**	**D* V vs NHE**
Az-1-caa (**154**)	837	-	-	-	18.04	-	-	670	1.30
TMAz-1-caa (**155**)	697	-	-	-	12.98	-	-	540	1.17
Az-1-tcaa (**84**)	455	-	-	-	15.79	-	-	310	0.94
TMAz-1-tcaa (**147**)	455	-	-	-	9.22	-	-	320	0.95
MeTAz-1-tcaa (**203**)	352	221	131	287	8.45	7.72	0.92	210	0.84
MeTTMAz-1-tcaa (**204**)	378	247	131	312	7.38	6.95	0.94	240	0.87

tBuAz-1-tcaa (**205**)	599	468	131	534	9.63	9.10	0.92	470	1.1

Table 13. First and second generation dyes electrochemical data in THF (E/V vs. Fc/Fc^+)

A cyclic voltammogram of tBuAz-1-tcaa (**205**) in DCM (Voltammogram 12) gave a I_{pc}/I_{pa} of 0.98 and ΔE_p value of 101 mV, ie closer to the ideal than the result obtained in THF (Voltammogram 11 and Table 13). The deviation from ideal behaviour is therefore assumed to be due to diffusion rates of the dyes and / or their oxidised species.

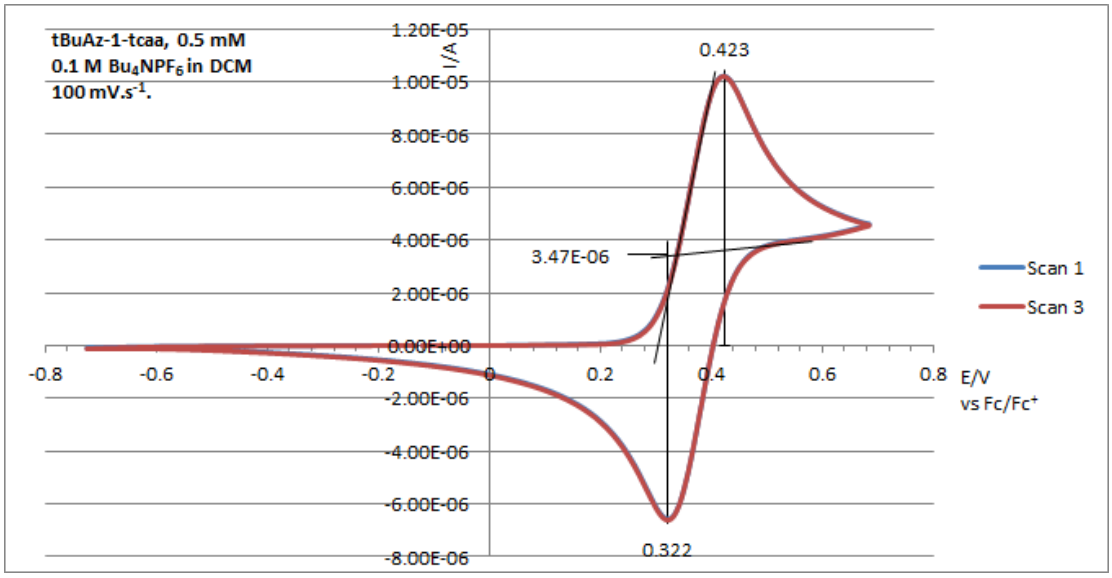

Voltammogram 12. CV of tBuAz-1-tcaa dye in DCM

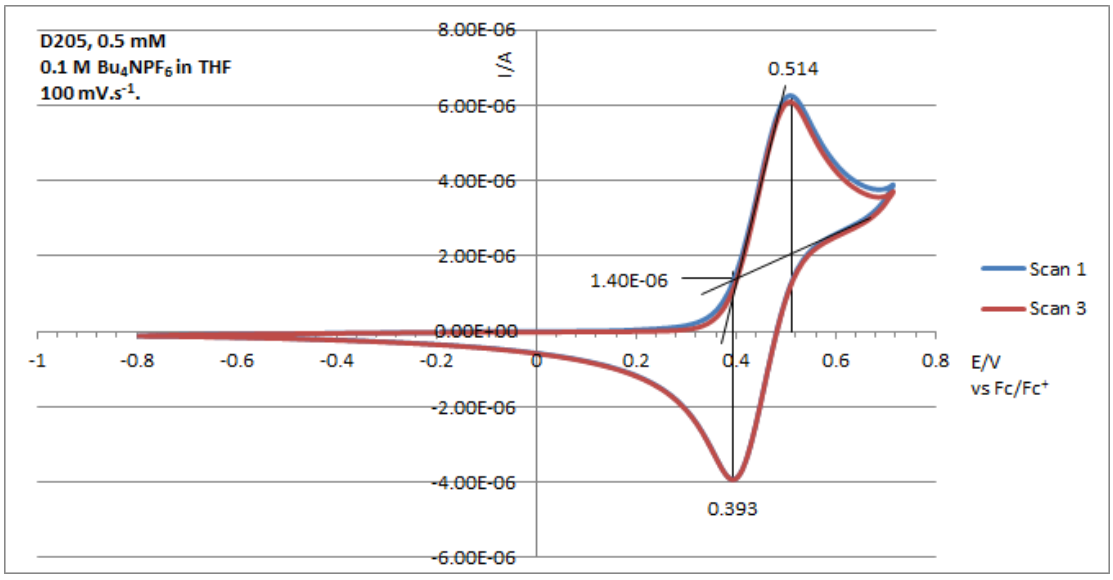

5.7.2 UV-Vis Spectroscopy

UV-Vis spectra were acquired for each of the three 2nd generation dyes (Figure 60) at 0.01, 0.03 and 0.05 mM concentrations. During the dye synthesis and purification steps, it was noted that the colour of the dyes in solution differed slightly depending on the solvent used (solvatochromism). When in dichloromethane solution, for instance, the dyes appeared to be somewhat bluer than when acetonitrile was used. Spectra were therefore acquired in three solvents: acetonitrile (MeCN), tetrahydrofuran (THF) and dichloromethane (DCM) (Spectrum 8 to Spectrum 19).

The UV-Vis data for the 2nd generation dyes is presented in Table 14. The extinction coefficients quoted are an average of coefficients calculated for the three dye concentrations.

The three 2nd generation dyes all have two principal absorption bands in the region of interest, one in the visible with λ_{max} ~430 - 520 nm (band A) and the other in the near UV with λ_{max} ~350 – 380 nm (band B). Dye MeTTMAz-1-tcaa (**204**) has an additional absorption band with λ_{max} ~320 nm.

With dyes MeTAz-1-tcaa (**203**) and tBuAz-1-tcaa (**205**) (ie without methyl groups in the azulene 7-membered ring), the absorption band A is the strongest of the two. However, with dye MeTTMAz-1-tcaa (**204**), the absorption band B is stronger than the absorption band A, with the magnitudes of the extinction coefficients for bands A and B reversed compared with MeTAz-1-tcaa.

The band A absorption is assumed to be due to charge transfer between the thiophene linker and the azulene moiety. The methyl group at the azulene C-8 position of MeTTMAz-1-tcaa (assuming that the thiophene linker is attached to the azulene C-1 position) sterically clashes with the thiophene linker group forcing it to be out-of-plane with the azulene 5-membered ring. This restricts π-orbital overlap and disrupts conjugation between the two rings, which in turn will limit the charge

transfer efficiency. This could explain the reduction in extinction coefficient for the band A absorption.

Dye	**Solvent**	**λ_{max} nm**	**ε (λ_{max}) L.mol^{-1}.cm^{-1}**	**λ_{onset} nm**	**E_g (opt) eV**
MeTAz-1-tcaa (**203**)	MeCN	A: 436 B: 357	1.99 x 10^4 1.57 x 10^4	515	2.41
	THF	A: 478 B: 357	2.57 x 10^4 1.52 x 10^4	563	2.20
	DCM	A: 497 B: 363	2.56 x 10^4 1.43 x 10^4	592	2.09
MeTTMAz-1-tcaa (**204**)	MeCN	A: 482 B: 367	1.15 x 10^4 2.47 x 10^4	597	2.08
	THF	A: 475 B: 362	1.15 x 10^4 2.63 x 10^4	585	2.12
	DCM	A: 506 B: 377	1.13 x 10^4 2.62 x 10^4	628	1.97
tBuAz-1-tcaa (**205**)	MeCN	A: 488 B: 351	4.12 x 10^4 2.06 x 10^4	567	2.19
	THF	A: 487 B: 353	3.57 x 10^4 1.57 x 10^4	556	2.23
	DCM	A: 512 B: 358	3.97 x 10^4 1.68 x 10^4	586	2.12

Table 14. UV/Vis data, 2nd generation dyes

The dye with the *tert*-butyl shielding group, tBuAz-1-tcaa (**205**) is more efficient at absorbing photons than the analogue with the methylthio shielding group, MeTAz-1-tcaa (**203**), having an average extinction coefficient for band A which is 64% greater.

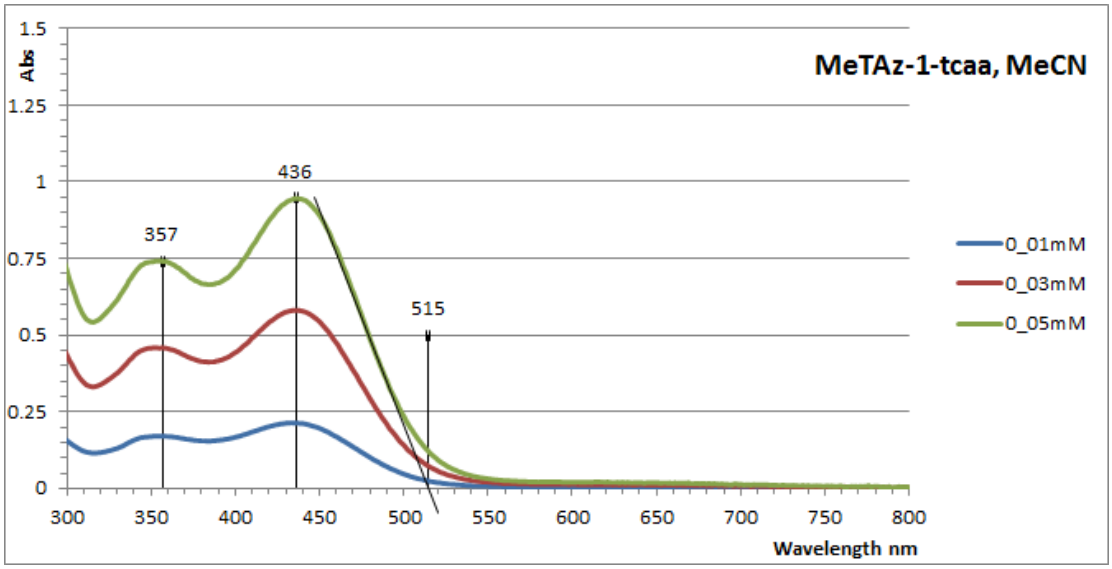

Spectrum 8. UV/Vis MeTAz-1-tcaa (203) in acetonitrile

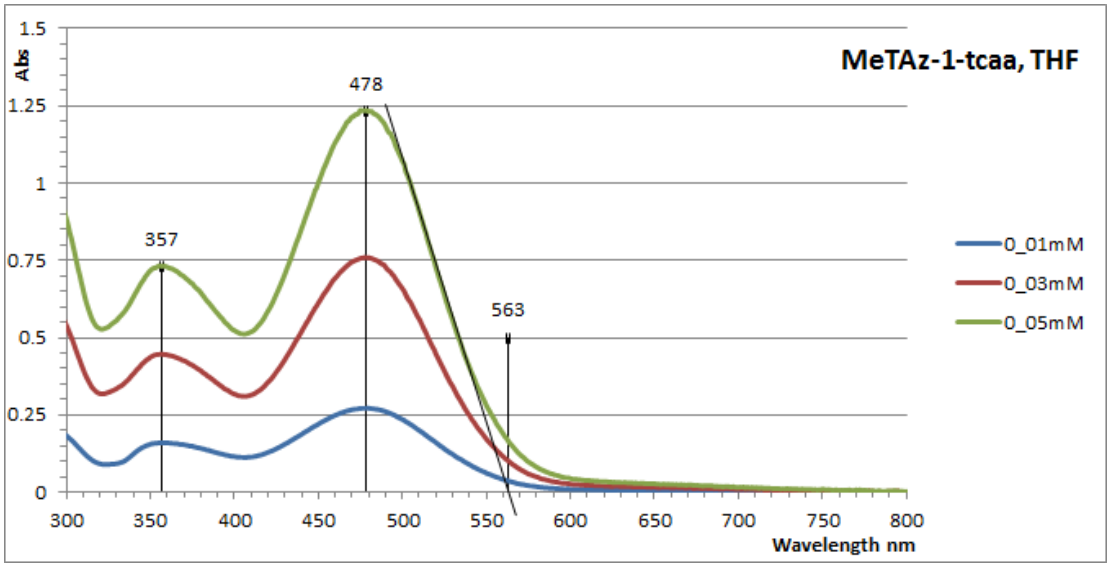

Spectrum 9. UV/Vis MeTAz-1-tcaa (203) in tetrahydrofuran

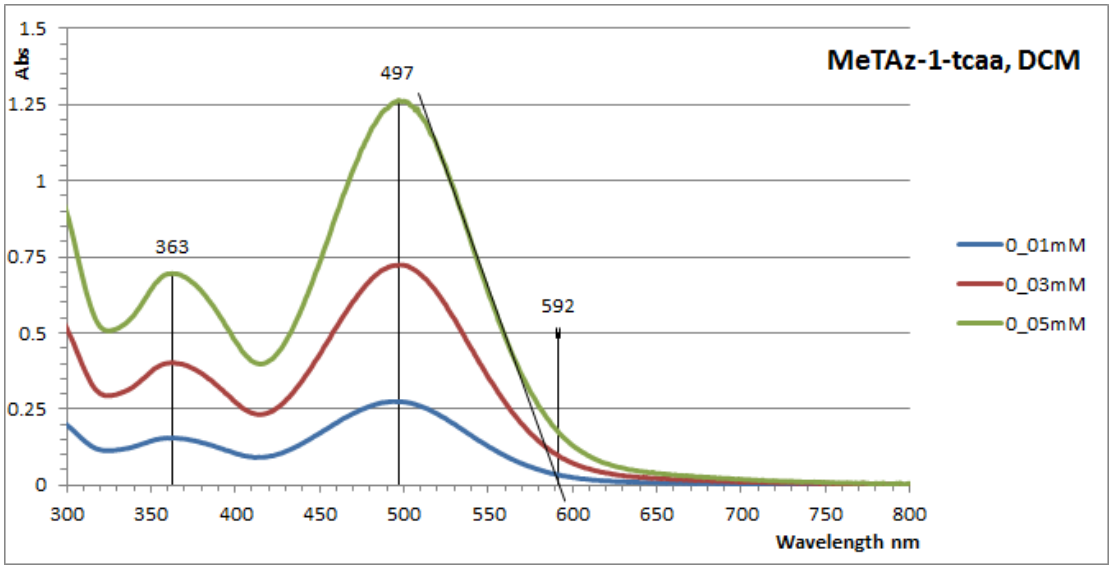

Spectrum 10. UV/Vis MeTAz-1-tcaa (203) in dichloromethane

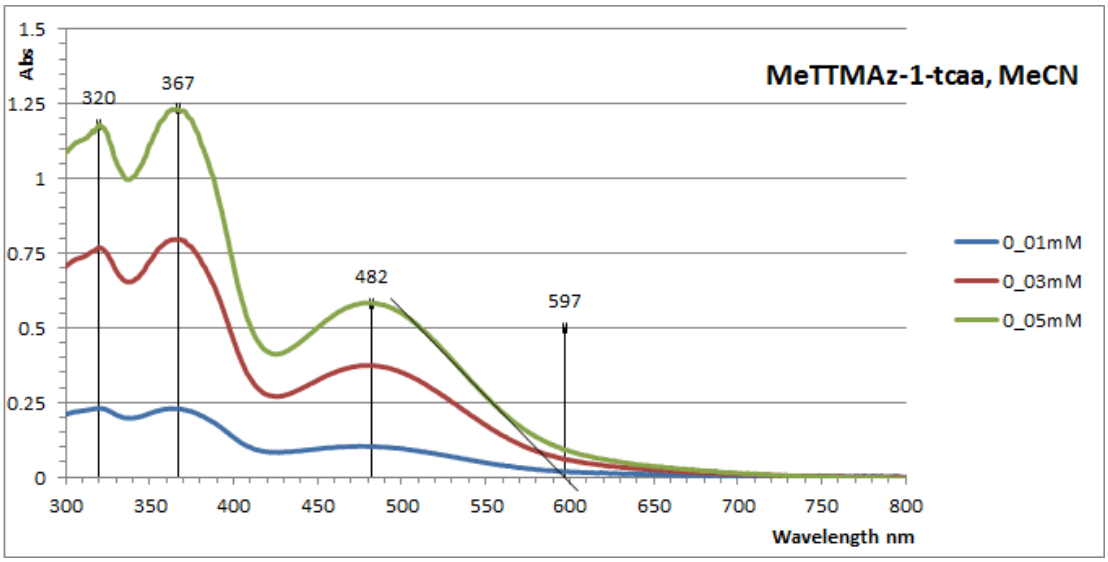

Spectrum 11. UV/Vis MeTTMAz-1-tcaa (204) in acetonitrile

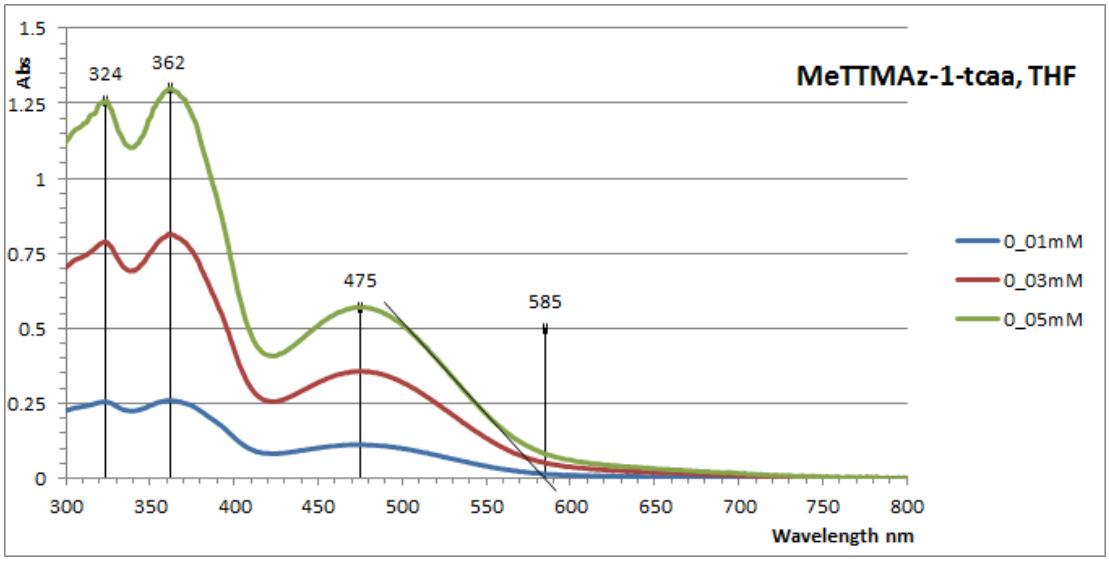

Spectrum 12. UV/Vis MeTTMAz-1-tcaa (204) in tetrahydrofuran

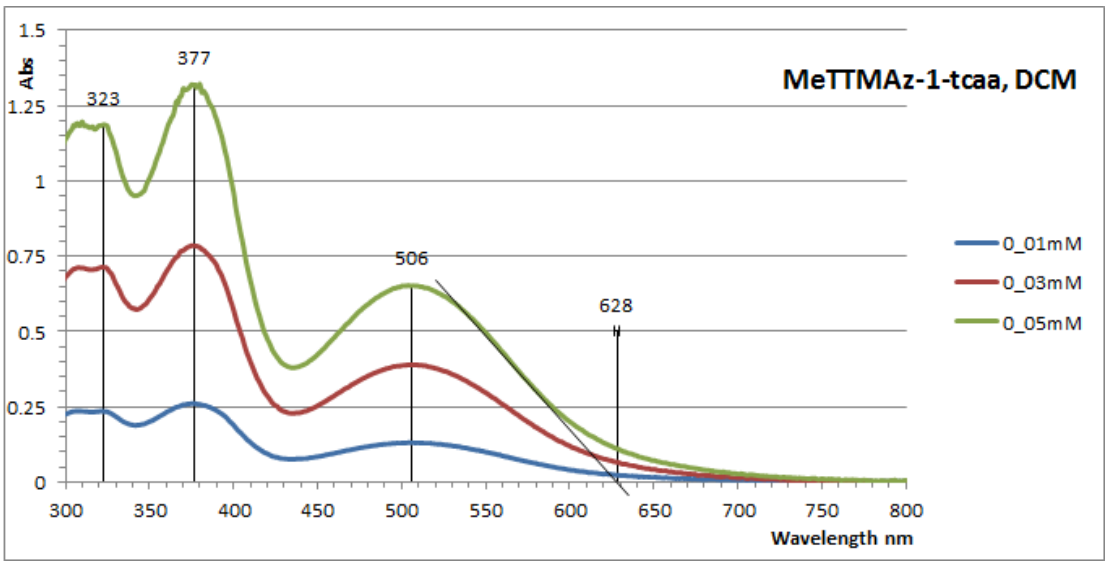

Spectrum 13. UV/Vis MeTTMAz-1-tcaa (204) in dichloromethane

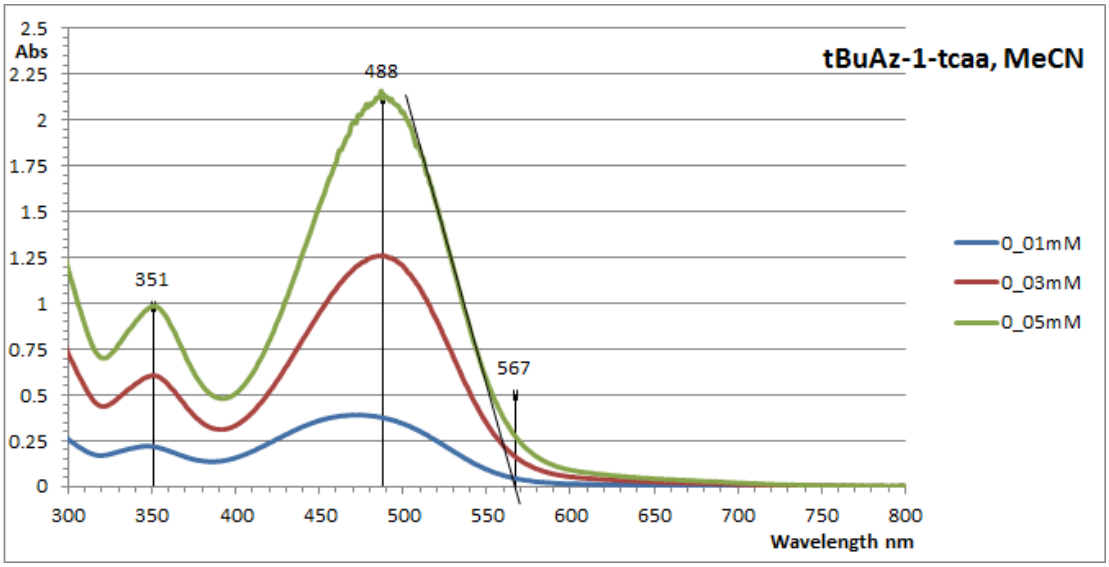

Spectrum 14. UV/Vis tBuAz-1-tcaa (205) in acetonitrile

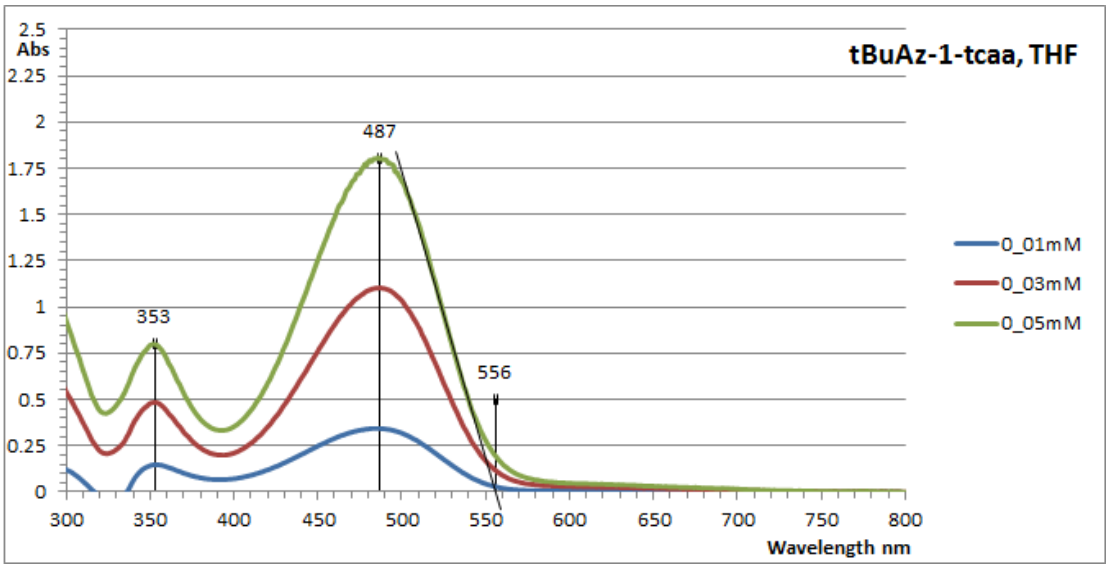

Spectrum 15. UV/Vis tBuAz-1-tcaa (205) in tetrahydrofuran

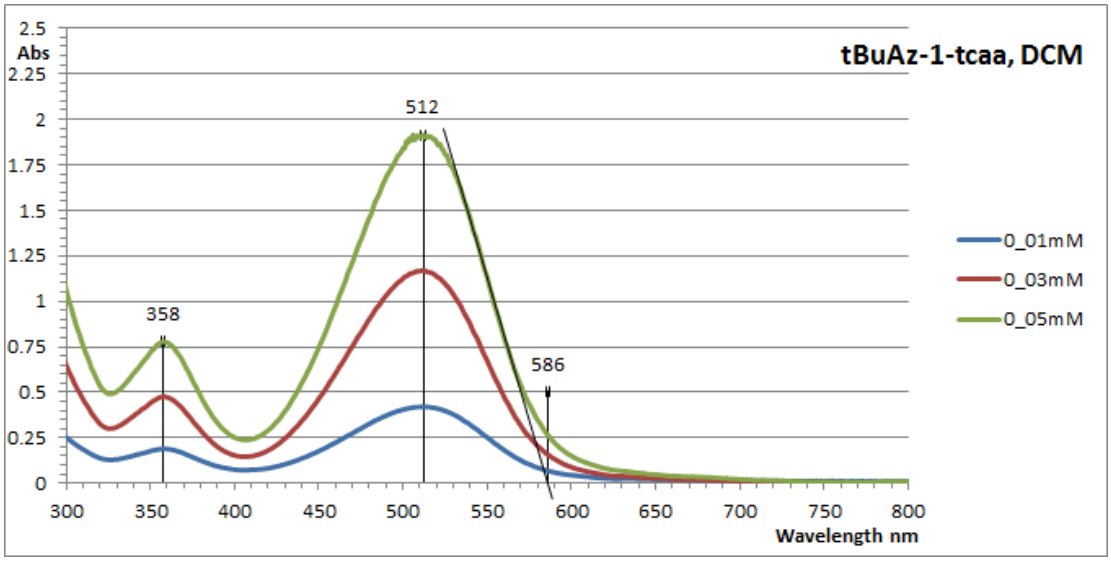

Spectrum 16. UV/Vis tBuAz-1-tcaa (205) in dichloromethane

All three 2nd generation dyes exhibited solvatochromism, although the effect of the three solvents tested was not completely consistent across the three dyes (Spectrum 17 to Spectrum 19). Light absorption was most bathochromic (red-shifted) in DCM. In THF, all three dyes exhibited a hypsochromic (blue shift) absorption compared to DCM. In MeCN, MeTAz-1-tcaa (**203**) exhibited a further hypsochromic shift but with lower extinction coefficient (Spectrum 17) but the spectra of the other two dyes were hardly different to those in THF, although tBuAz-1-tcaa had a higher extinction coefficient in MeCN (Spectrum 19).

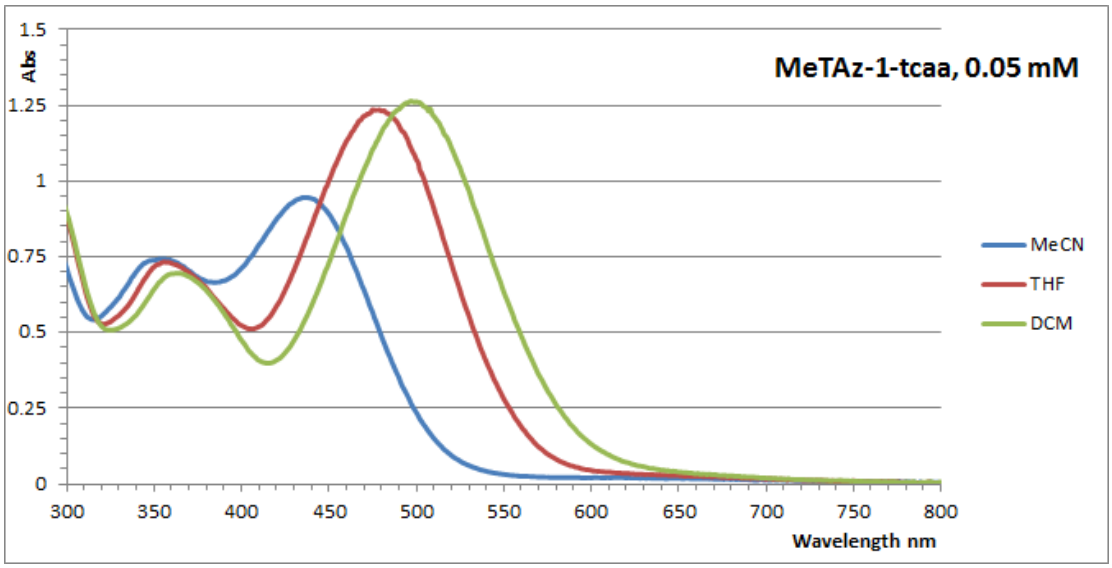

Spectrum 17. UV/Vis MeTAz-1-tcaa (203) solvent effect

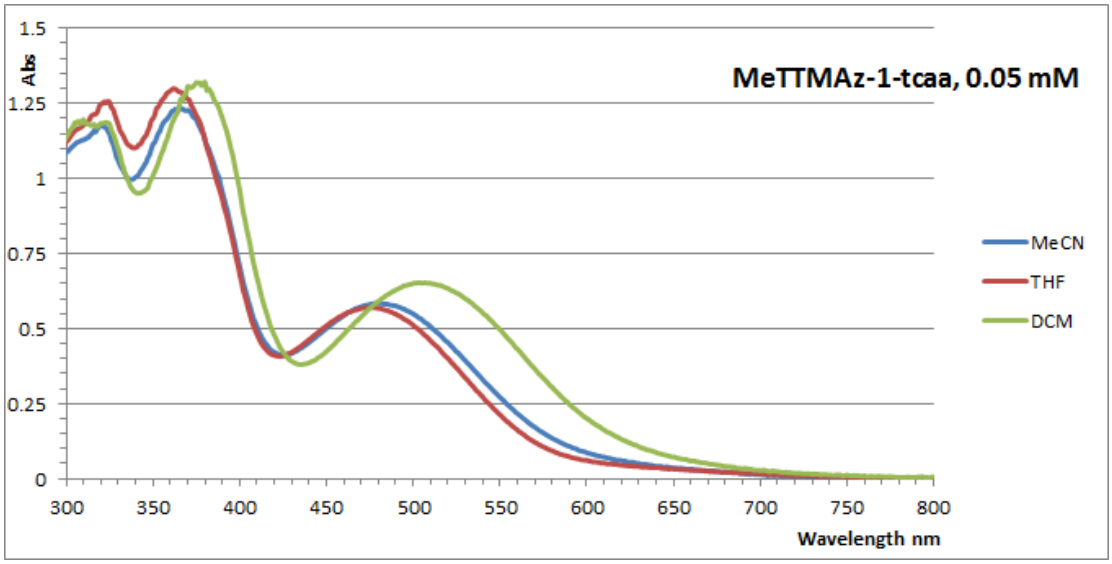

Spectrum 18. UV/Vis MeTTMAz-1-tcaa solvent effect

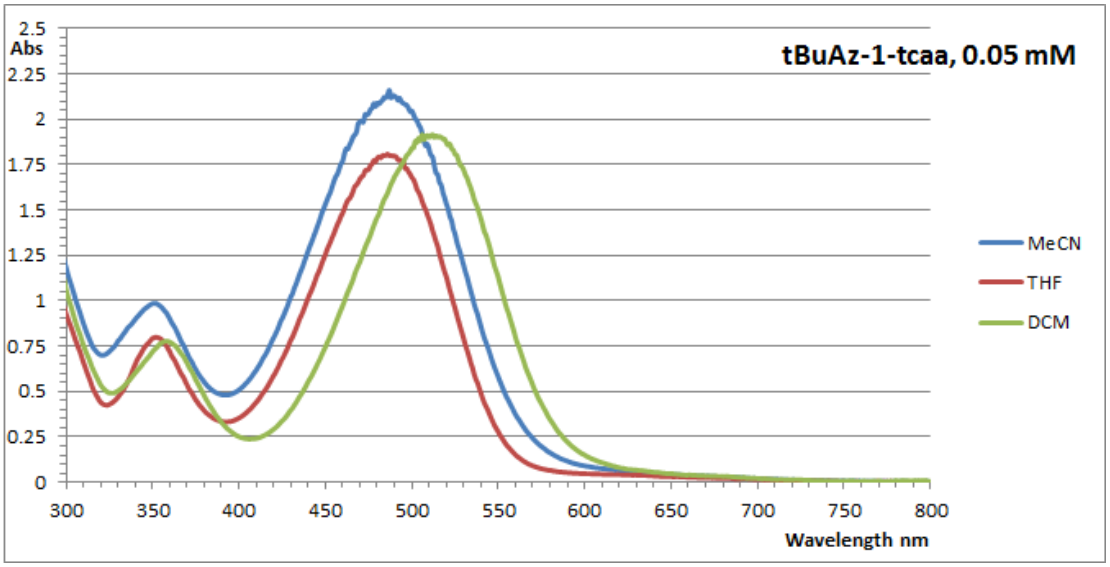

Spectrum 19. UV/Vis tBuAz-1-tcaa (205) solvent effect

The solvatochromic effect is due to polarity difference between the ground and excited states of a chromophore. A change in the solvent polarity leads to different stabilisation of the ground and excited states and therefore a change in the band gap between these states. If the chromophore excited state is more polar than the ground state, then a more polar solvent will stabilise the excited state and result in a narrower band gap. This translates to a bathochromic shift in the absorption and is termed positive solvatochromism. Conversely, if the excited state is less polar than the ground state, more polar solvents will destabilise the excited state producing a

wider band gap and a hypsochromic shift in the absorption. This is termed negative solvatochromism.[163]

Table 15 lists the polarity indices for the solvents tested, with DCM being the least polar and MeCN the most polar.

Solvent	**Polarity Index p**
DCM	3.1
THF	4.0
MeCN	5.8

Table 15. UV-Vis solvent polarity indices[164]

Increasing solvent polarity (DCM -> THF) produced a hypsochromic shift in the absorption or negative solvatochromism, which means the dye excited states must be less polar than their ground states. The change in polarity is evidence of a transfer of electrons within the molecule; however the direction of the electron transfer is uncertain.

5.7.3 Dye Sensitised Solar Cells

Energy level data for the second generation dyes are summarised in Table 9. The ground state (D^0/D^+) potentials and band gap (E_g) values are taken from the electrochemistry and UV/Vis spectrometry results (sections 5.7.1 and 5.7.2 above). Subtracting E_g from D^0/D^+ gives the excited state potential D* (Equation 18):

Dye	$\frac{D^0}{D^+}$ **V vs NHE**	**E_g (opt) eV**	**D* V vs NHE**
MeTAz-1-tcaa (**203**)	0.84	2.20	-1.36
MeTTMAz-1-tcaa (**204**)	0.87	2.12	-1.25
tBuAz-1-tcaa (**205**)	1.1	2.23	-1.13

Table 16. Second generation dyes energy levels.

All of the second generation dyes clearly satisfy the energy level requirements to function as DSSC sensitisers. The excited state potentials provide an electron injection driving force of 0.63 to 0.86 V. and the redox potential of the ground state is 0.44 to 0.70 V. below that of the I^-/I_3^- couple used in the electrolyte.

DSSCs were prepared, with my assistance, by Adam Pockett, a fellow student working in Petra Cameron's group on perovskite solar cells.

For comparison purposes, DSSCs were also prepared with the "industry standard" ruthenium (II) based dye N719[24] (Figure 6), an indoline dye D205[26] (Figure 14) and two of the first generation dyes Az-1-tcaa (**84**) and TMAz-1-tcaa (**147**).

Three batches of DSSCs were prepared. The first batch of cells, using N719, D205, TMAz-1-TCAA (first generation) and MeTTMAz-1-tcaa (second generation, with added methythio shielding group) dyes, was prepared using the 'standard' electrolyte formulation as used with the first generation DSSCs (Table 10, section 4.3.6 above):

The cell test results are presented in Table 17. The DSSCs based on the literature dyes N719 and D205 produced the best efficiencies. N719 gave a mean efficiency of 6.48% and D205 also performed well, giving an efficiency of 5.17%. These efficiencies are not as high as figures quoted in the literature, with 11.18% reported for N719[165] and 9.52% for D205.[26] However, the literature values were obtained with much smaller DSSC cell sizes and optimised DSSC structures and electrolyte formulations. The efficiencies obtained with N719 and D205 in this work provide context for evaluating the azulene based dyes.

The efficiencies obtained from the two azulene-dye based DSSCs were much lower than those obtained from the D719 and D205 cells, with TMAz-1-tcaa giving 0.16% and MeTTMAz-1-tcaa giving only 0.05% efficiency.

Dye	**V_{oc} (V)**	**J_{sc} (mA)**	**FF %**	**Eff %**
N719	0.741	13.42	66.9	6.65
	0.734	12.56	65.9	6.07
	0.743	13.71	64.6	6.58
	0.733	13.09	69.2	6.65
Mean	*0.738*	*13.20*	*66.7*	*6.48*
D205	0.774	9.62	69.4	5.17
TMAz-1-tcaa	0.560	0.39	75.0	0.17
(**147**)	0.550	0.36	74.9	0.15
	0.550	0.37	73.8	0.15

	0.553	0.37	72.8	0.15
Mean	*0.553*	*0.37*	*74.13*	*0.16*
MeTTMAz-1-tcaa	0.504	0.16	66.2	0.05
(**203**)	0.503	0.19	66.6	0.06
	0.496	0.17	64.5	0.05
	0.487	0.13	65.1	0.04
Mean	*0.498*	*0.16*	*65.6*	*0.05*

Table 17. DSSC batch 1, standard electrolyte

As a "quick and dirty" experiment, after DSSC testing the electrolyte was removed from the DSSCs sensitised with MeTTMAz-1-tcaa dye and they were re-filled with modified electrolytes containing 0.1 M lithium iodide or 0.1 M chenodeoxycholic acid (CA). After sealing, the cells were re-tested. The results are summarised in Table 18.

Dye	**Additive**	**V_{oc} (V)**	**J_{sc} (mA)**	**FF %**	**Eff %**
MeTTMAz-1-tcaa	CA	0.482	0.21	63.9	0.06
(**203**)		0.472	0.16	64.0	0.05
	Mean	*0.477*	*0.19*	*64.0*	*0.06*
	Li	0.458	0.25	68.6	0.08
		0.472	0.33	69.8	0.11
	Mean	*0.465*	*0.29*	*69.2*	*0.10*

Table 18. DSSC batch 1, refilled with electrolyte containing additive

Although the efficiencies of the refilled cells were still low, the lithium iodide additive did increase the mean efficiency from 0.05% to 0.10%. Lithium ions added to the cell electrolyte adsorb onto the surface of the TiO_2 and lower the conduction band energy level making it easier for electrons to be injected into the conduction band, increasing the short circuit current (J_{SC}) which has a beneficial effect on DSSC efficiency.[166] However, since the TiO_2 Fermi level is lowered by adding lithium ions, the cell V_{OC} and hence efficiency is adversely impacted. This was the case with the refilled cells; mean V_{OC} decreased by 6.1% but the mean J_{SC} increased by 81%.

Chenodeoxycholic acid has been shown to increase DSSC efficiency when used as a dyebath co-adsorbant *and* as an electrolyte additive.[167] In this experiment, the

effect was to lower the V_{OC} by 4.6% but increase the J_{SC} by 11.8%, producing a slight increase in efficiency.

These results led to the use of lithium iodide and chenodeoxycholic acid additives in the second batch of cells.

A second batch of cells was prepared with N719, two of the first generation dyes (Az-1-tcaa and TMAz-1-tcaa) and all three second generation dyes (MeTAz-1-tcaa, MeTTMAz-1-tcaa and tBuAz-1-tcaa). The electrolyte formulation for batch two is shown in Table 19.

Component	**Concentration**
Iodine	0.05 M
1-methyl-3-propyl-imidazonium iodide (ionic liquid)	0.60 M
Lithium Iodide	0.10 M
Chenodeoxycholic acid	0.10 M

Table 19. DSSC batch 2, electrolyte formulation in acetonitrile

The DSSC test results for the batch 2 cells are presented in Table 20 and graphically in Figure 61 (V_{OC}), Figure 62 (J_{SC}), Figure 63 (fill factor) and Figure 64 (efficiency).

The best result was again achieved with the reference dye N719, although the efficiency was lower than achieved with the batch 1 cells, despite the higher current (J_{SC}) generated, due to the much lower voltage (V_{OC}).

The V_{OC} values were also lowered with the azulene-based dyes compared to the batch 1 DSSCs, however the J_{SC} values were much improved leading to a highest mean efficiency of 1.20% for the first generation dye TMAz-1-tcaa (**147**). The next highest performing cells were based on the second generation dye MeTTMAz-1-tcaa (**203**). It is interesting to note that, contrary to expectation, the best performing dyes were the ones based on 4,6,8-trimethylazulene (**48**) and therefore had a methyl group in the seven-membered ring that causes a large torsional angle between the plane of the azulene rings and the thiophene ring of the linker group (section 7.2 below). This is thought to be why these dyes have a lower extinction coefficient than the other dyes and was expected to disrupt conjugation between the

azulene and thiophene rings and therefore restrict charge transfer between them too, limiting DSSC performance.

Another factor that detrimentally influences DSSC efficiency is re-combination of electrons injected into the TiO_2 with the oxidised dye species. The high torsional angle of the dyes based on 4,6,8-trimethylazulene may be beneficial in this respect, helping to block charge transfer from TiO_2 to the oxidised azulene moiety, resulting in improved efficiency.

Dye	**V_{oc} (V)**	**J_{sc} (mA)**	**FF %**	**Eff %**
N719	0.549	16.07	55.7	4.96
Az-1-tcaa	0.309	3.01	61.0	0.57
(**84**)	0.311	3.15	59.3	0.59
	0.305	2.98	54.8	0.50
Mean	*0.308*	*3.05*	*58.4*	*0.55*
TMAz-1-tcaa	0.387	5.38	60.3	1.27
(**147**)	0.378	5.17	61.0	1.21
	0.366	5.07	60.1	1.13
Mean	*0.377*	*5.21*	*60.5*	*1.20*
MeTAz-1-tcaa	0.256	1.71	52.0	0.23
(**203**)	0.254	1.78	51.1	0.23
	0.245	1.80	48.5	0.22
Mean	*0.252*	*1.76*	*50.5*	*0.23*
MeTTMAz-1-tcaa	0.350	3.38	62.3	0.75
(**204**)	0.342	3.61	60.8	0.76
	0.335	3.29	59.1	0.66
Mean	*0.342*	*3.43*	*60.7*	*0.72*
tBuAz-1-tcaa	0.303	3.06	61.0	0.57
(**205**)	0.310	2.54	60.7	0.48
	0.325	3.11	61.7	0.63
Mean	*0.313*	*2.90*	*61.1*	*0.56*

Table 20. DSSC batch 2, with lithium iodide

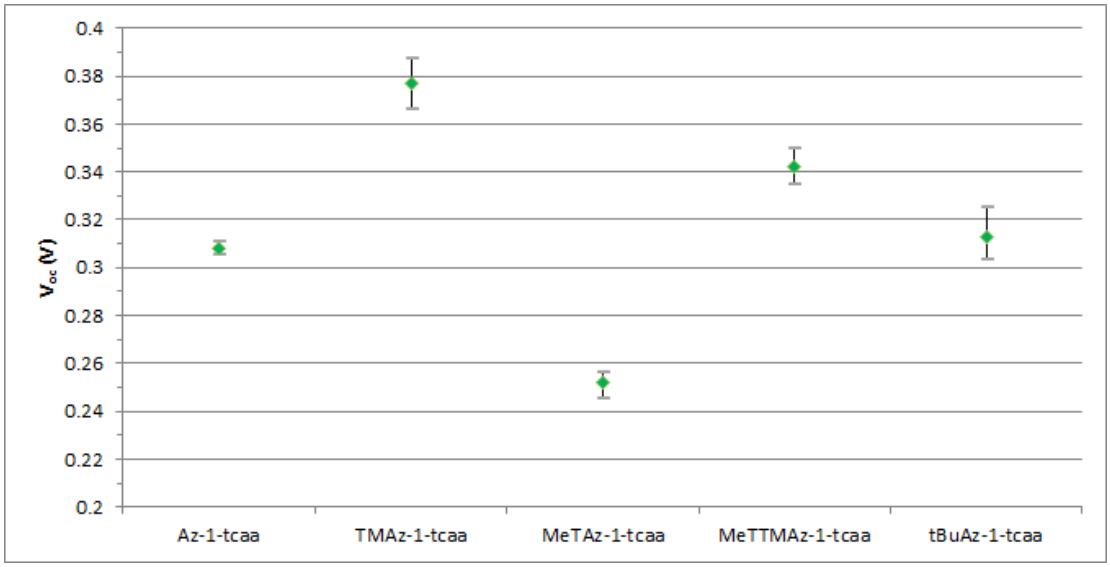

Figure 61. DSSC batch 2, open circuit voltage

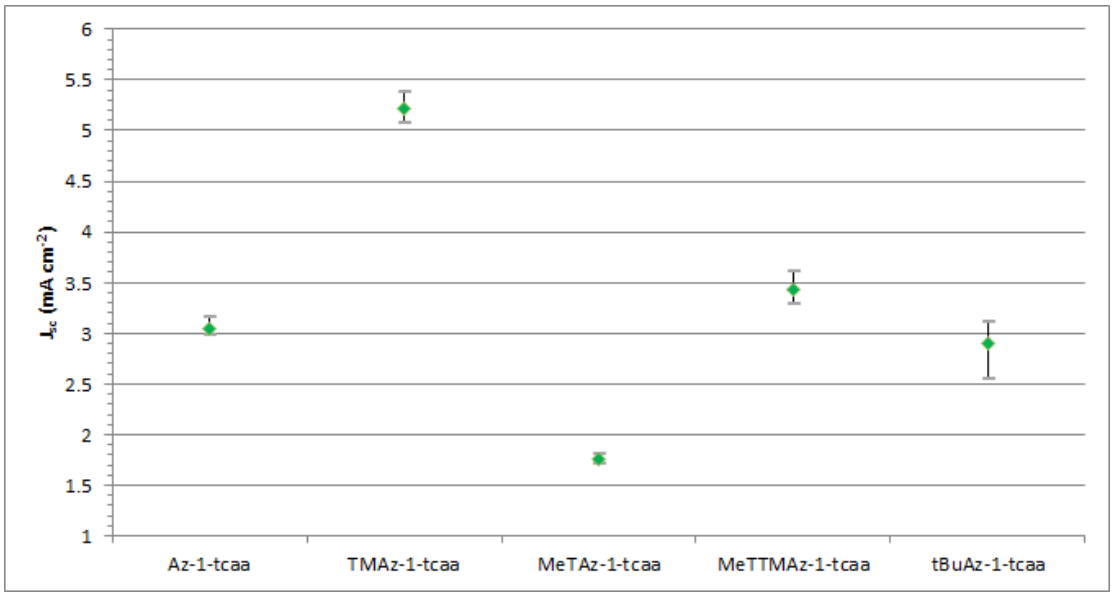

Figure 62. DSSC batch 2, short circuit current

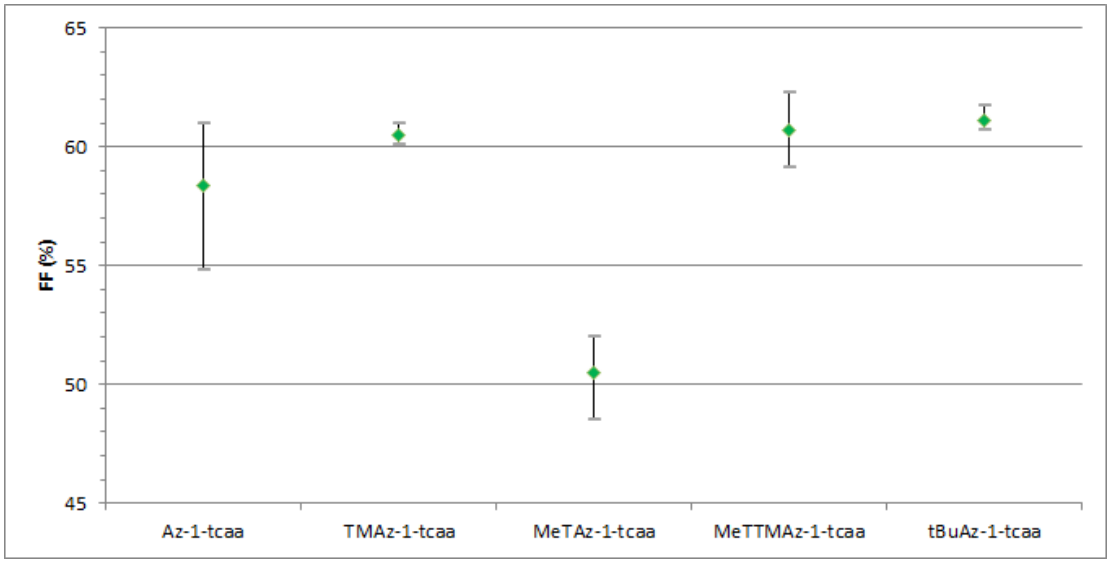

Figure 63. DSSC batch 2, fill factor

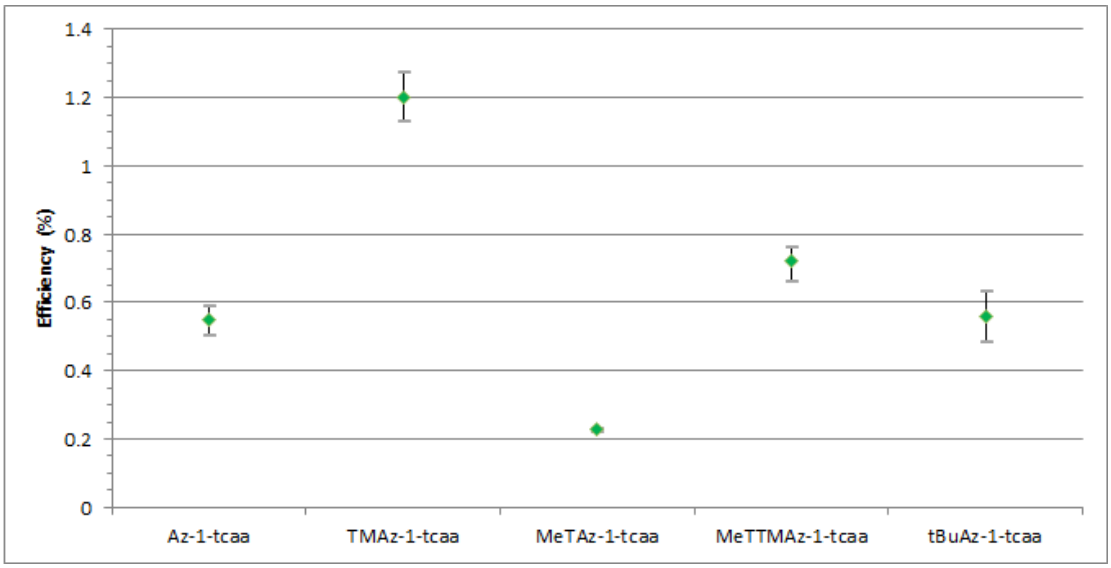

Figure 64. DSSC batch 2, efficiency

A third batch of cells was prepared to better evaluate the effect of electrolyte additives:

1. Lithium iodide (Li);
2. Chenodeoxycholic acid (CA); and
3. Guanidine thiocyanate (GT).

GT has also been shown to increase DSSC short circuit current density (J_{SC}) and therefore increase efficiency.[168]

Two dyes were selected for the electrolyte additive analysis: first generation dye TMAz-1-tcaa (**147**) and second generation dye tBuAz-1-tcaa (**205**). The DSSC test results for batch 3 are presented in Table 21 and graphically in Figure 65 (V_{OC}), Figure 66 (J_{SC}), Figure 67 (fill factor) and Figure 68 (efficiency).

Dye	**Additive**	**V_{oc} (V)**	**J_{sc} (mA)**	**FF %**	**Eff %**
TMAz-1-tcaa (**147**)	Li	0.498	1.55	71.8	0.56
		0.503	1.40	73.0	0.51
	Mean	*0.501*	*1.48*	*72.4*	*0.54*
	CA, Li	0.391	5.72	59.3	1.33
		0.390	5.73	58.6	1.32
	Mean	*0.391*	*5.73*	*59.0*	*1.33*
	CA, GT	0.544	1.22	75.7	0.50
		0.554	1.37	75.6	0.58
	Mean	*0.549*	*1.30*	*75.7*	*0.54*
	CA, Li, GT	0.482	2.97	69.1	0.99
		0.474	3.00	69.5	0.99
	Mean	*0.478*	*2.99*	*69.3*	*0.99*

tBuAz-1-tcaa (**205**)	Li	0.479	1.11	73.6	0.39
		0.494	1.31	73.4	0.47
	Mean	*0.487*	*1.21*	*73.5*	*0.43*
	CA, Li	0.370	4.14	58.1	0.89
		0.372	4.35	58.1	0.94
	Mean	*0.371*	*4.25*	*58.1*	*0.92*
	CA, GT	0.524	0.94	74.4	0.37
		0.495	0.88	68.1	0.30
	Mean	*0.510*	*0.91*	*71.3*	*0.34*
	CA, Li, GT	0.442	1.89	70.7	0.59
		0.447	2.05	69.1	0.63
	Mean	*0.445*	*1.97*	*69.9*	*0.61*

Table 21. DSSC batch 3, additive analysis

The best DSSC efficiencies for both dyes were obtained with the combination of of both lithium iodide and chenodeoxycholic acid. As before, the first generation dye TMAz-1-tcaa (**147**) produced the highest efficiency of 1.33% while the second generation dye tBuAz-1-tcaa (**205**) managed just 0.92%.

The addition of guanidine thiocyanate to the DSSC electrolyte actually had a detrimental effect, reducing DSSC efficiency by 25 – 33%. Rather than increase short circuit current density, the J_{SC} was severely reduced while open circuit voltage was increased.

The addition of lithium ions and/or chenodeoxycholic acid to the electrolyte both have a positive influence on cell efficiencies and seem to exhibit a synergistic effect when both are added together. The lithium ions and chenodeoxycholic acid both influence the DSSC efficiencies by increasing the closed circuit current density (J_{SC}). While both also reduce the open circuit voltage (V_{OC}), the effect on efficiencies is more than offset by the increased J_{SC}.

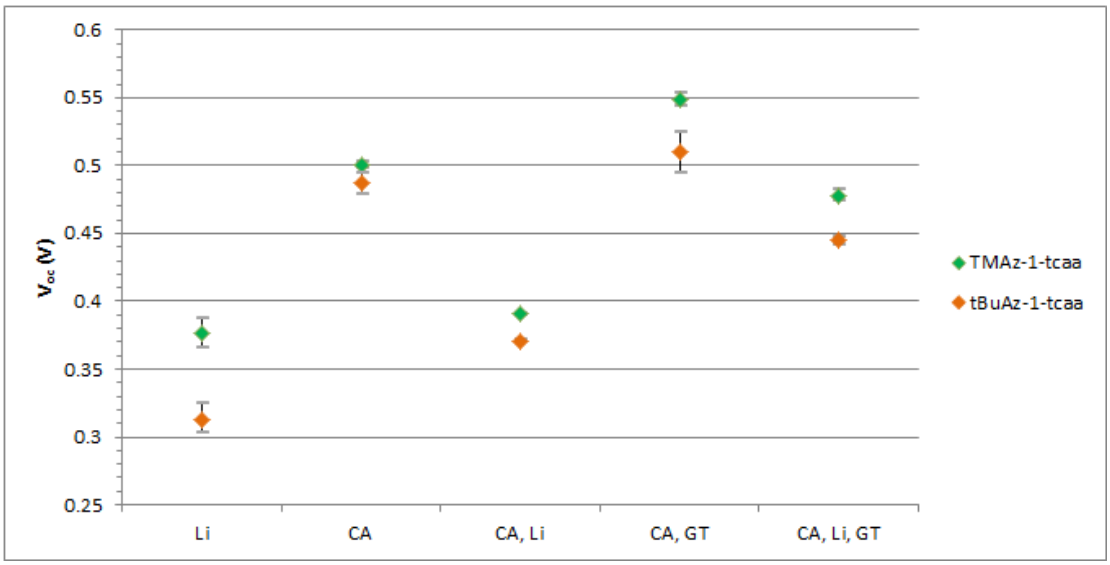

Figure 65. DSSC batch 3, open circuit voltage

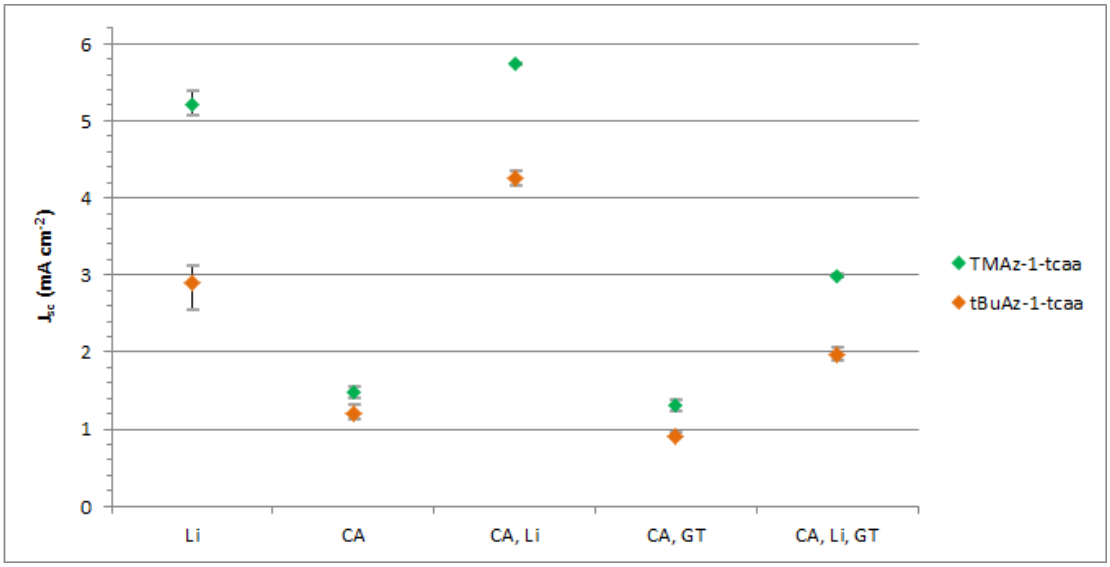

Figure 66. DSSC batch 3, short circuit current

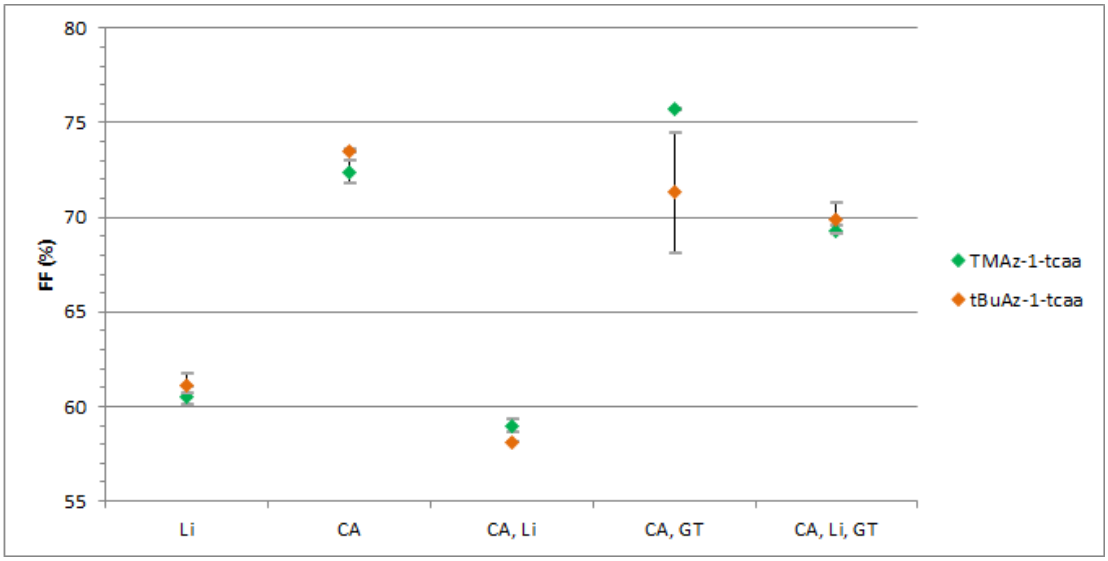

Figure 67. DSSC batch 3, fill factor

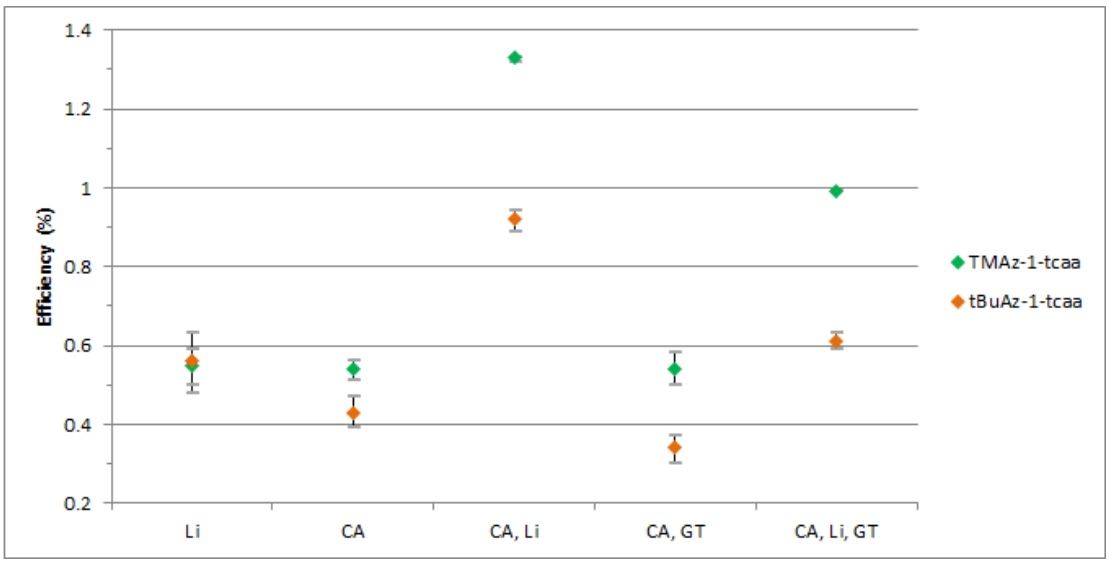

Figure 68. DSSC batch 3, efficiency

5.8 Conclusions

A range of azulene-based dyes for DSSCs has been successfully synthesised with "radical shielding" groups attached at the azulene C-3 position. These dyes exhibited chemically reversible redox behaviour in cyclic voltammetry studies, indicating that the radical cations formed by electron injection in a DSSC should be less labile than the analogues without radical shielding groups. This in turn is expected to lead to DSSCs with a much improved operational lifetime.

DSSCs were prepared with efficiencies up to 1.33%; however the best efficiencies were recorded with cells based on one of the first generation dyes without a radical shielding group. This suggests that while the shielding groups may lead to DSSCs with greater longevity, they don't necessarily result in cells with greater efficiencies, at least in the short term. The best efficiencies were achieved with dyes having the greatest torsional angle between the azulene rings and the thiophene linker, possibly as a result of reducing the rate of charge recombination with the oxidised dye species following electron injection.

A study to determine the effects of several DSSC electrolyte additives showed that marked improvement in efficiencies can be achieved with the azulene-based dyes by the addition of lithium ions and chenodeoxycholic acid to the electrolyte.

The discovery that easily prepared and purified azulene sulfonium salts participate in Suzuki-Miyaura cross-coupling reactions has made the preparation of mono-arylated azulene compounds much more convenient.

6 Azulene Dyes – Towards 3rd Generation

6.1 Introduction

The second generation dyes with radical shielding groups proved to exhibit excellent redox chemistry. This demonstrates that the radical cations formed by electron injection are much less susceptible to reactions that would result in destruction of the dyes and therefore lead to higher longevity DSSCs. However, the second generation dyes performed less well as DSSC sensitisers than the first generation dye TMAz-1-tcaa, at least for the short time of the DSSC testing.

For the last few months of experimental time for this project, rather than try to synthesise azulene based dyes with the linker/anchor group at other positions in the azulene framework as originally planned, a decision was made to leverage the chemistry already developed to synthesise analogues of the first and second generation dyes with extended π-linker conjugation. Extending the length of the conjugation should broaden the UV-Vis absorption, leading to more efficient light harvesting.

The linker unit chosen for the extended π-conjugated analogues of the first and second generation dyes was 2,2-bithiopnene (**211**).

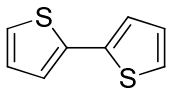

211

Figure 69. Extended π-linker chosen for third generation dyes: 2,2-bithiophene

It was hoped that this compound would have chemistry sufficiently similar to the thiophene linker used in the first and second generation dyes to allow use of the same protocols to synthesise the dyes with extended π-linker. The target molecules are listed in Table 22 and the structures are shown in Figure 70.

Dye compound	**Code**
3-(5'-(azulen-1-yl)-[2,2'-bithiophen]-5-yl)-2-cyanoacrylic acid (**212**)	Az-1-ttcaa

3-(5'-(4,6,8-trimethylazulen-1-yl)-[2,2'-bithiophen]-5-yl)-2-cyanoacrylic acid (**213**)	TMAz-1-ttcaa
3-(5'-(3-methylthioazulen-1-yl)-[2,2'-bithiophen]-5-yl)-2-cyanoacrylic acid (**214**)	MeTAz-1-ttcaa
3-(5'-(3-tert-butylazulen-1-yl)-[2,2'-bithiophen]-5-yl)2-cyanoacrylic acid (**215**)	tBuAz-1-ttcaa

Table 22. Third generation dyes target molecules

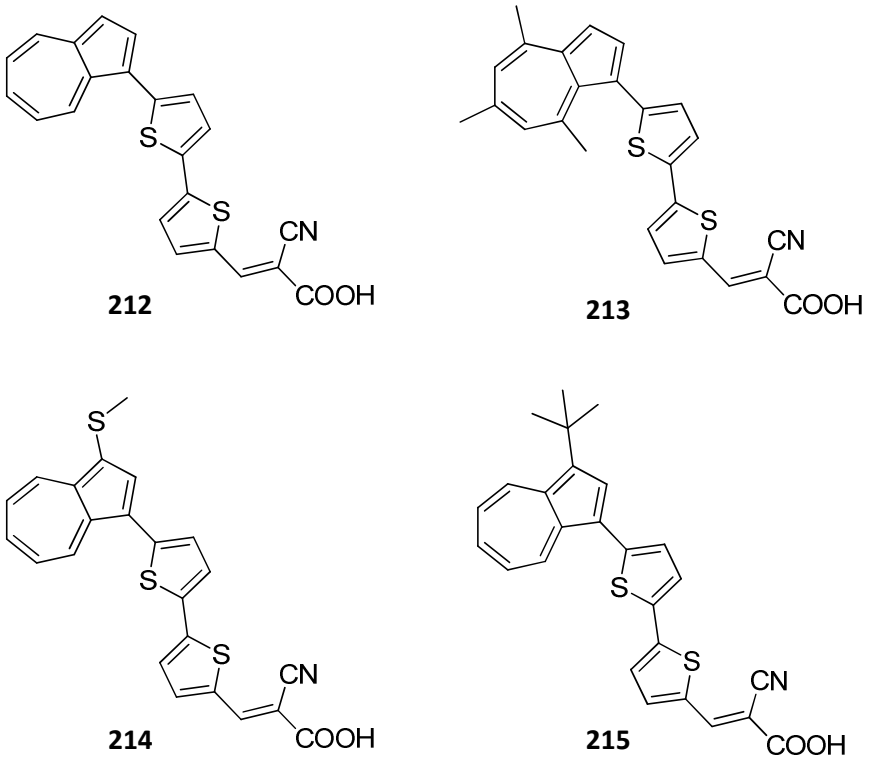

Figure 70. Third generation dyes target molecules

6.2 Dye Synthesis

The strategy adopted to synthesise the third generation dyes was the same as that used to synthesise the first and second generation dyes. This is the application of Suzuki-Miyaura cross-coupling to couple an azulenyl electrophilic partner bearing a halogen or sulfonium group with a boron functionalised nucleophilic partner bearing an aldehyde or masked aldehyde group. The aldehyde group of the coupled product is then condensed with cyanoacetic acid to create the acceptor/anchor group of the dye.

The electrophilic azulenyl coupling partners for the third generation dyes are the same as those used to synthesise the first and second generation dyes. The extended π-conjugated linker unit of the third generation dyes is implemented via the nucleophilic cross-coupling partner, so the synthesis of these dyes is focused on the synthesis of this compound, an ester of (5'-formyl-[2,2'-bithiophen]-5-yl)boronic acid (**216**) (Figure 71).

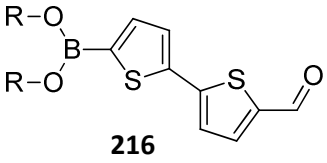

216

Figure 71. Nucleophilic coupling partner

6.2.1 2,2′-Bithiophene-5-carboxaldehyde

Unlike thiophene-2-carboxaldehyde (**133**), 2,2′-bithiophene-5-carboxaldehyde (**218**) is not cheaply available, so it was synthesised from the readily available 2,2′-bithiophene (**217**) via Vilsmeier-Haak formylation (Scheme 88).

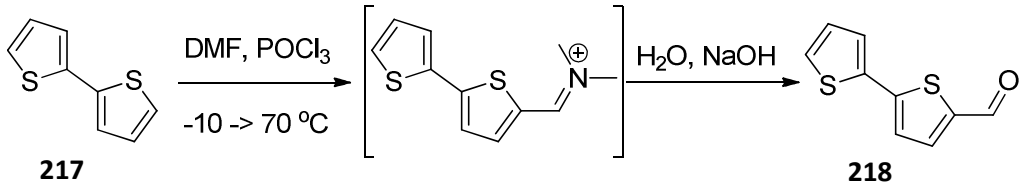

217 **218**

Scheme 88. Formylation of 2,2'-bisthiophene

6.2.2 2,2′-Bithiophene-5-carboxaldehyde protection

Prior to the borylation step, the aldehyde group must be protected to avoid reaction with the strong base used for deprotonation. The protection strategy adopted for the first generation dyes, ie with thiophene-2-carboxaldehyde (**133**), was formation of a cyclic acetal by acid catalysed reaction of **133** with ethylene glycol (Scheme 49). However, a brief literature search suggested that acid catalysed acetalisation with neopentyl glycol (**219**) to give 2-([2,2'-bithiophen]-5-yl)-5,5-dimethyl-1,3-dioxane (**220**) was the preferred method[169] (Scheme 89).

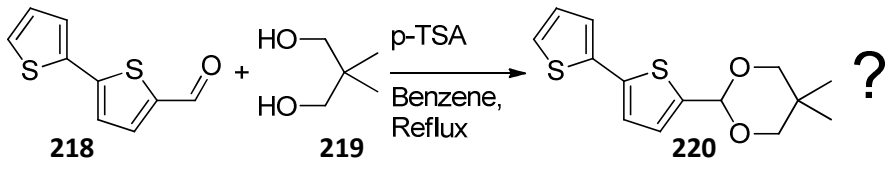

218 **219** **220**

Scheme 89. Acid catalysed acetalisation of 218 with neopentyl glycol

However, in my hands this reaction produced a green solid (in benzene) or green oil (in toluene) and not the white crystalline solid reported in the literature, even under strictly oxygen-free conditions.

Another literature search revealed two possible alternative acetalisation methods, one under basic conditions[170] the other under mildly acidic conditions,[171] both at room temperature or below.

6.2.2.1 Acetalisation Under Basic Conditions

Barbasiewicz and Makosza[170] reported that nonenolisable aldehydes and ketones react with 2-chloroethanol and 3-chloropropan-1-ol under basic conditions (potassium *tert*-butoxide in DMF/THF) to form 2-substituted 1,3-dioxolanes and 1,3-dioxanes respectively.

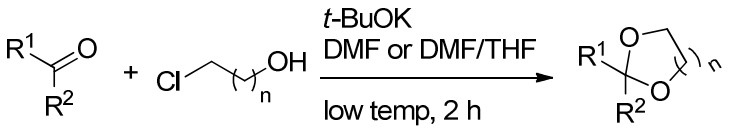

Scheme 90. Acetalisation under basic conditions. Reproduced from reference 170

2-Chloroethanol has a tendency to cyclise to ethylene epoxide in the presence of strong base so a temperature ~ -60 °C is necessary to minimise this. 3-Chloropropan-1-ol is less susceptible to cyclisation, however, because a four membered ring would be formed, so higher temperatures of -5 to 0 °C are used.

At the time, we happened to have some 3-bromopropan-1-ol (**221**) in the fridge which I expected to be a good substitute for 3-chloropropan-1-ol, so used it for the initial trials. A test experiment was carried out using thiophene-2-carboxaldehyde (**133**) as the substrate in DMF at -5 °C. A solution of potassium *tert*-butoxide in DMF was added dropwise to the cold vigorously stirred solution of **133** and **221**, then the reaction mixture was allowed to warm to RT after a further 90 minutes stirring at -5 °C (Scheme 91). Following aqueous workup, a ^{1}H NMR of the crude product indicated a single reaction product contaminated with a little starting material. Integrations of the aldehyde and acetal protons indicated a conversion of ~96%.

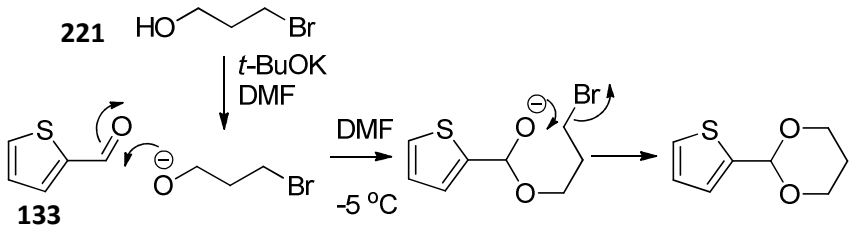

Scheme 91. Test reaction - acetalisation under basic conditions

Following the success of the trial reaction, the same protocol was applied with 2,2′-bithiophene-5-carboxaldehyde (**218**) as the substrate giving 2-([2,2'-bithiophen]-5-yl)-1,3-dioxane (**222**) in 70% isolated yield (Scheme 92). Unfortunately, the purified product contained ~10% of **218** which was not removed by re-purification by flash chromatography suggesting that the acetal of **222** may be liable to silica-gel catalysed hydrolysis. Purification by recrystallisation from ethanol and water successfully removed the starting material.

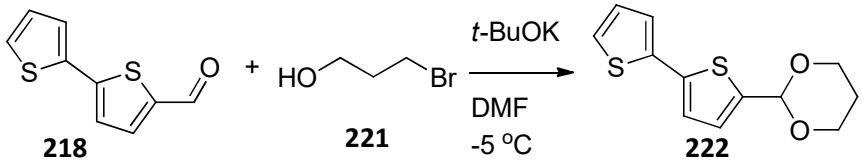

Scheme 92. Acetalisation of 2,2'-bithiophene-5-carboxaldehyde under basic conditions

6.2.2.2 Oxalic Acid Catalysed Acetalisation

Andersen and Uh[171] reported an interesting protocol whereby *"many aldehydes can be converted to acetals using only an alcohol, anhydrous oxalic acid and a co-solvent. The reaction proceeds to completion in less than an hour."*. The procedure is deceptively simple: the aldehyde is stirred in a solution of dry oxalic acid and glycol in dry acetonitrile for 20 minutes, then the product is isolated by adding water and extracting into a 1:1 mixture of pentane and diethyl ether.

As with the acetalisation under basic conditions, initial trials were conducted with thiophene-2-carboxaldehyde (**133**) as substrate, in this case reacted with neopentyl glycol for one hour to give 5,5-dimethyl-2-(thiophen-2-yl)-1,3-dioxane (**223**) (Scheme 93).

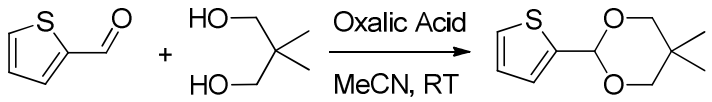

133 **219** **223**

Scheme 93. Test reaction – oxalic acid catalysed acetalisation

With four equivalents of **219** and two equivalents of oxalic acid, the yield of crude product was 82%. ^{1}H NMR showed a small amount of aldehyde starting material amounting to ~10% by integration of the aldehyde and acetal protons. Increasing the reaction time to two hours reduced the quantity of starting material in the crude to ~5%.

The same protocol was then applied to protect 2,2'-bithiophene-5-carboxaldehyde (**218**) to give 2-([2,2'-bithiophen]-5-yl)-5,5-dimethyl-1,3-dioxane (**224**) (Scheme 94). The ratio of glycol to aldehyde was increased to eight equivalents in an attempt to increase product yield with the reaction time maintained at two hours. Crude yield was 96% after aqueous workup, with 75% isolated yield following purification by recrystallisation from ethanol.

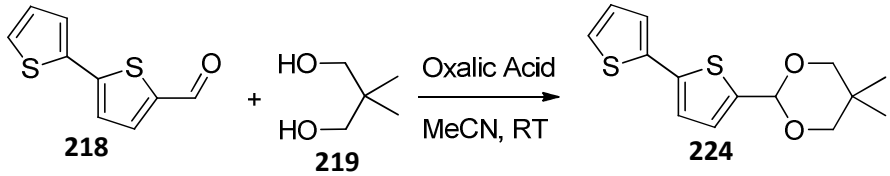

218 **219** **224**

Scheme 94. Oxalic acid catalysed acetalisation of 2,2'-bithiophene-5-carboxaldehyde

6.2.3 Borylation of 2,2'-Bithiophene-5-carboxaldehyde Acetals

Both of the acetals were successfully borylated using the protocol used to synthesise 2-(5-(1,3-dioxolan-2-yl)thiophen-2-yl)-4,4,5,5-tetramethyl-1,3,2-dioxaborolane (**142**) (Scheme 53). Lithiation of the protected aldehydes with n-BuLi followed by quenching with ITDB yielded the boronic acid pinacol esters 2-(5'-(1,3-dioxan-2-yl)-[2,2'-bithiophen]-5-yl)-4,4,5,5-tetramethyl-1,3,2-dioxaborolane (**225**) and 2-(5'-(5,5-dimethyl-1,3-dioxan-2-yl)-[2,2'-bithiophen]-5-yl)-4,4,5,5-tetramethyl-1,3,2-dioxaborolane (**226**) in 47% and 78% yield respectively following aqueous workup (Scheme 95). No further purification was necessary.

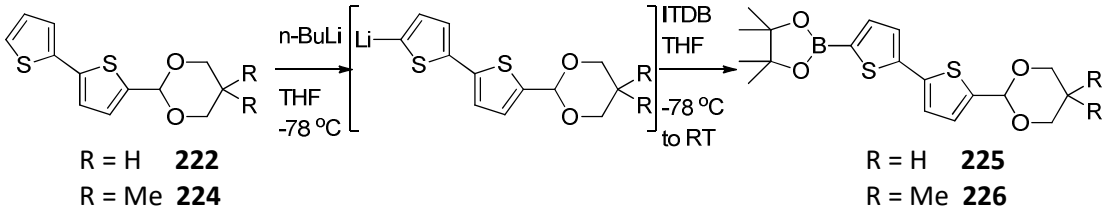

Scheme 95. Borylation of 2,2'-bithiophene-5-carboxaldehyde acetals

6.2.4 Suzuki-Miyaura Cross-Coupling and Aldehyde Deprotection

Cross-coupling reactions using the procedures established for the first and second generation dyes were performed with **225** and **226** using azulenyl-1-tetrahydrothiophenium PF_6 (**207**) as the electrophilic coupling partner The p-TSA catalysed aldehyde deprotection in wet acetone was carried out on the coupling reaction crude, without isolating **227**/**228** affording 5'-(azulen-1-yl)-[2,2'-bithiophene]-5-carboxaldehyde (**229**) (Scheme 96).

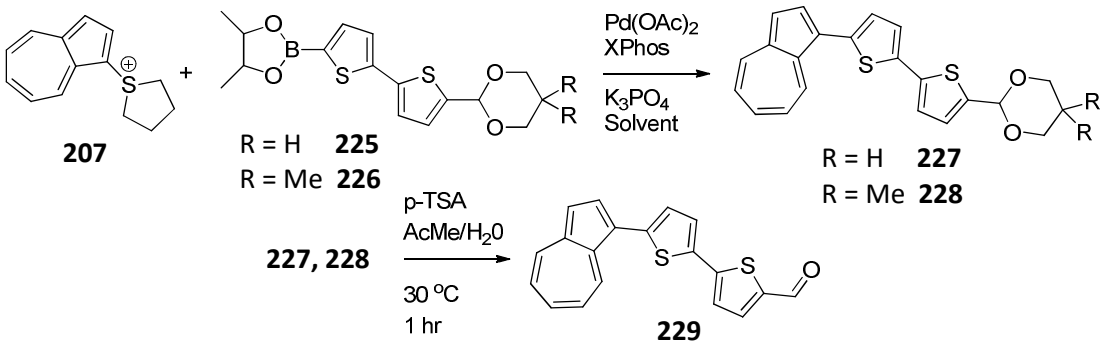

Scheme 96. Suzuki-Miyaura cross coupling and aldehyde deprotection

As with previous S-M cross-couplings, the reaction with **225** was carried out in degassed propan-2-ol and appeared to proceed smoothly with the starting material being consumed in less than two hours by TLC. Before the workup of **227**, however, it was noted that a significant quantity of a hard waxy material had formed / remained in the reaction mixture, which appeared to be **225**. The overall yield of **229** was only 29%.

A quick experiment showed that the solubility of **225** in propan-2-ol is poor, so the reaction was repeated in DMF which had been shown to be the optimum solvent in the azulene sulfonium salts investigation work.[161] There was no sign of the hard waxy material in the reaction mixture before workup, and the overall yield of **229** increased to 48%.

The solubility of **226** in propan-2-ol was much better than **225**, and the overall yield of **229** with the cross-coupling carried out in degassed propan-2-ol was 65%.

Since the oxalic acid catalysed acetalisation procedure was far simpler than the base catalysed one and propal-2-ol is much easier and more pleasant to work with than DMF, neopentyl glycol was chosen as the aldehyde protection agent and IPA the coupling reaction solvent for subsequent dye syntheses (Scheme 97).

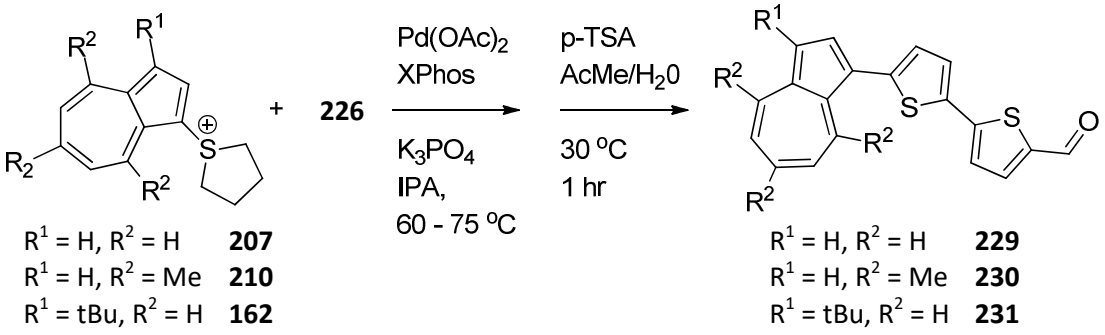

Scheme 97. S-M cross-coupling and aldehyde deprotection for third generation dyes

6.2.5 Dyes Bearing a Methylthio Radical Shielding Group

With the second generation dyes MeTAz-1-tcaa (**203**) and MeTTMAz-1-tcaa (**204**), the methylthio group was added following the cross-coupling and aldehyde deprotection step using the protocol of Shoji *et al.*.[177] This method proved to be successful for the third generation dyes too, using the same reaction conditions to afford 5'-(3-(methylthio)azulen-1-yl)-[2,2'-bithiophene]-5-carboxaldehyde (**232**) (Scheme 98).

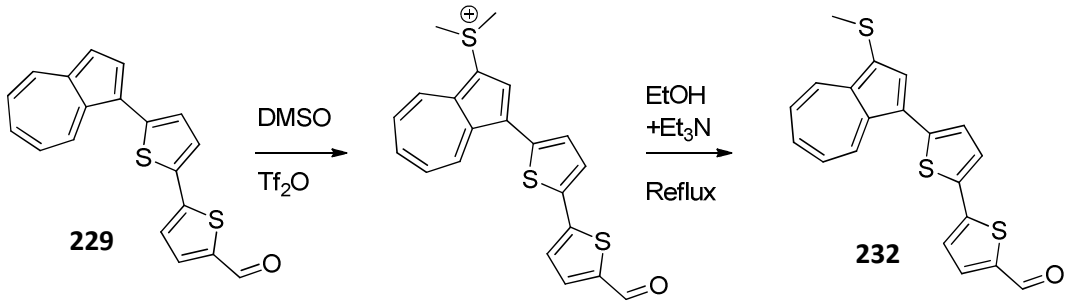

Scheme 98 - Dyes bearing a methylthio radical shielding group

6.2.6 Cyanoacrylic Acid Acceptor/Anchor Group

The final step in the synthesis is Knoevenagel condensation of the aldehyde intermediates with cyanoacetic acid. The amino acid catalysed reaction developed

for the second generation dyes proved to be successful with the third generation dyes also (Scheme 99).

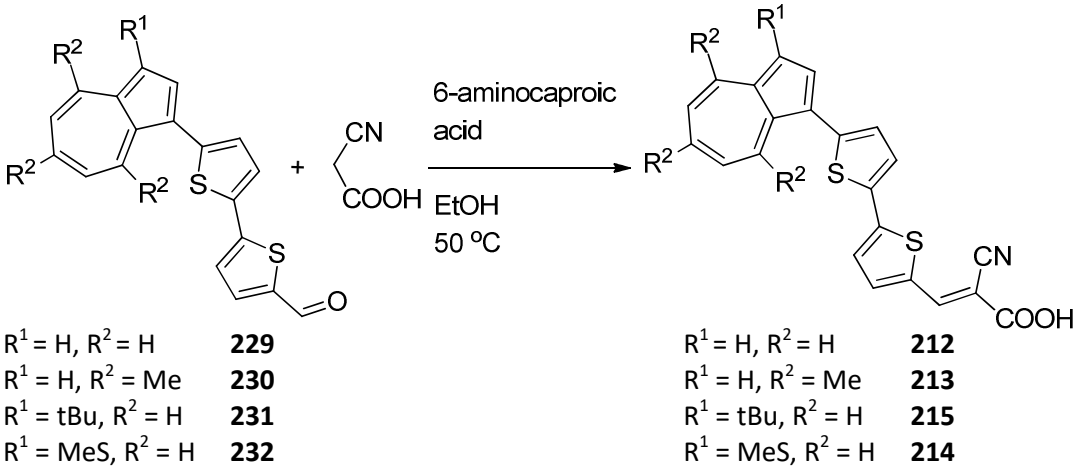

R^1 = H, R^2 = H	**229**	R^1 = H, R^2 = H	**212**
R^1 = H, R^2 = Me	**230**	R^1 = H, R^2 = Me	**213**
R^1 = tBu, R^2 = H	**231**	R^1 = tBu, R^2 = H	**215**
R^1 = MeS, R^2 = H	**232**	R^1 = MeS, R^2 = H	**214**

Scheme 99. Cyanoacrylic acid acceptor/anchor group installation

6.2.7 Solubility and Purification

During the synthesis of the third generation dyes it became clear that the solubility of azulene dyes containing the bithiophene linker group was much lower than that of the first and second generation dyes. For instance, in DCM it was possible to make a 0.4 mM solution of TMAz-1-ttcaa (**213**) but the solubility of tBuAz-1-ttcaa (**215**) was < 0.1 mM and MeTAz-1-ttcaa (**214**) was almost insoluble. Solubility in acetone was not good for any of the dyes. This became an issue with purification by recrystallisation (and cleaning of glassware!) since large volumes of solvent (eg ethanol or propan-2-ol) were required to completely dissolve small quantities of the dyes. In addition, it was difficult to tell when all of the compounds were dissolved because they are highly coloured making it impossible to see small amounts of undissolved material.

Eventually it was discovered, by trial and error while attempting to clean glassware contaminated with the dyes, that acetone mixed with a small quantity of aqueous sulfuric acid formed a good solvent system. This solvent system was eventually used to re-crystallise MeTAz-1-ttcaa (**214**) and to obtain ESI-MS spectra of all the third generation dyes.

6.3 Dye Characterisation

6.3.1 Electrochemistry

Cyclic voltammograms were acquired for each of the third generation dyes using the same conditions as were used for the first and second generation dyes. The two dyes without a radical shielding group, Az-1-ttcaa (**212**) and TMAz-1-ttcaa (**213**), exhibited similar, non-reversible redox chemistry as had been observed with the first generation dye analogues (Voltammogram 13 and Voltammogram 14).

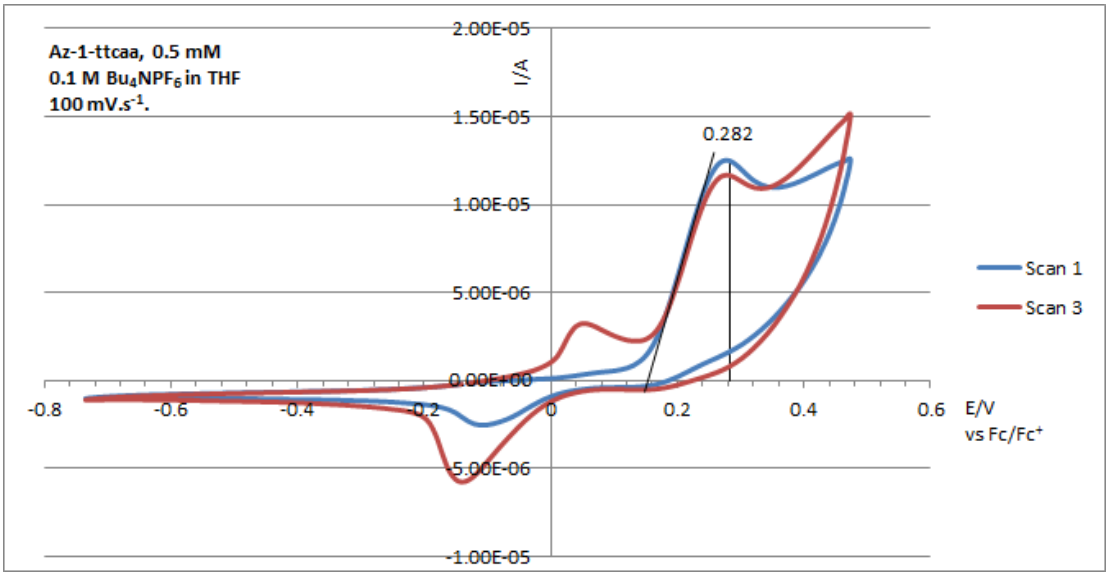

Voltammogram 13. CV of Az-1-ttcaa dye in THF

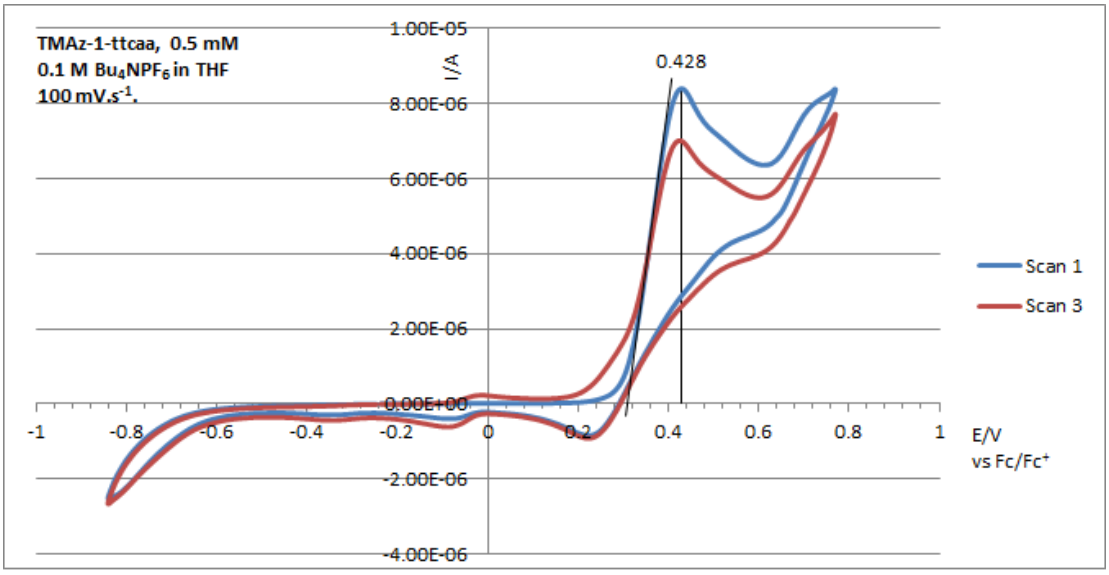

Voltammogram 14. CV of TMAz-1-ttcaa dye in THF

Both of these dyes exhibited a strong oxidation wave, but without a corresponding reduction wave indicating that the radical cations formed by oxidation were too labile to survive until the redox potential was reached on the reverse sweep (approximately four seconds). In addition, on the second and subsequent scans, additional peaks appeared which are presumed to be due to the products of reaction or decomposition of the oxidised dye.

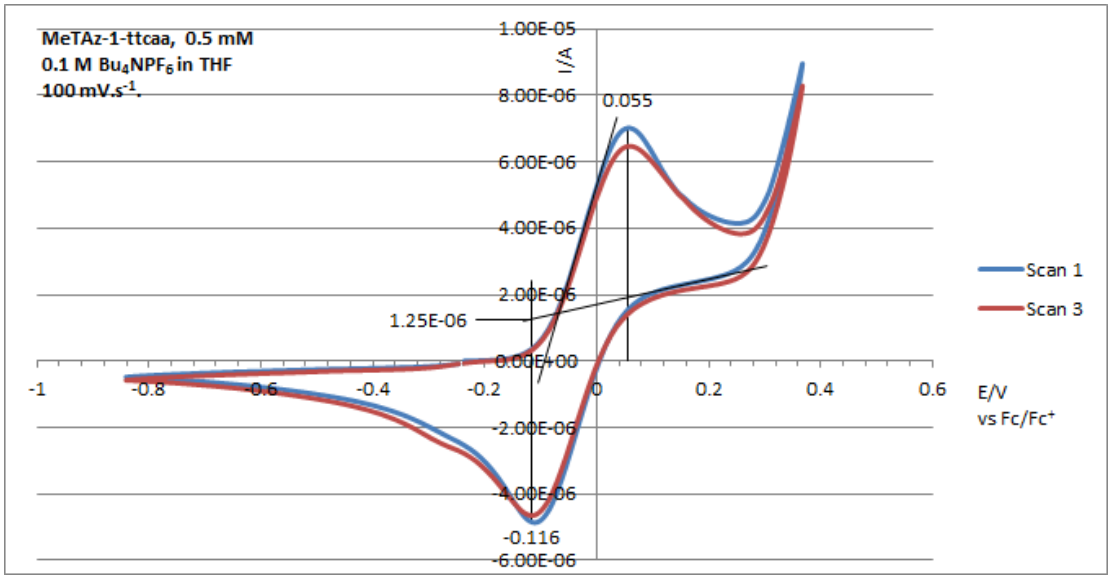

Voltammogram 15. CV of MeTAz-1-ttcaa dye in THF

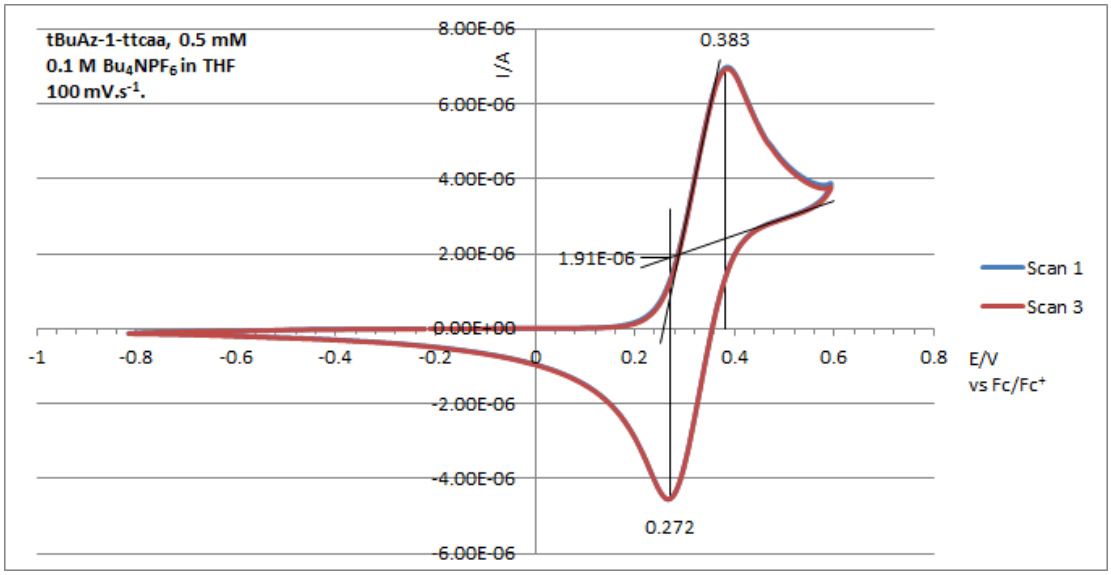

Voltammogram 16. CV of tBuAz-1-ttcaa dye in THF

The two dyes with a radical shielding group, MeTAz-1-ttcaa (**214**) and tBuAz-1-ttcaa (**215**), did exhibit quasi-reversible redox chemistry, both displaying oxidation and

corresponding reduction waves. The dye bearing the methylthio radical shielding group, MeTAz-1-ttcaa (**214**), did show some signs of poor reproducibility on the second and subsequent scans, with indication that some other species were appearing as a result of oxidation and reduced anodic currents. The CV of the dye bearing the *tert*-butyl radical shielding group, tBuAz-1-ttcaa (**215**), was much cleaner, with the first and subsequent scans almost exactly superimposed and no sign of reaction/decomposition products or reduction in anodic current apparent.

Electrochemical data extracted from the cyclic voltammograms are presented in Table 23.

Dye	**E_{pa} mV**	**E_{pc} mV**	**ΔE_p mV**	**$E^0_{½}$ mV**	**I_{pa} µA**	**I_{pc} µA**	**$\frac{I_{pc}}{I_{pa}}$**	**E_{ox} mV**	**HOMO V vs NHE**
Az-1-ttcaa (**212**)	282	-	-	-	12.6	-	-	155	0.79
TMAz-1-ttcaa (**213**)	428	-	-	-	8.4	-	-	310	0.94
MeTAz-1-ttcaa (**214**)	55	-116	171	-30.5	7.0	6.1	0.87	-10	0.62
tBuAz-1-ttcaa (**215**)	383	272	111	328	7.0	6.4	0.92	255	0.89

Table 23. Third generation dyes electrochemical data in THF (E/V vs. Fc/Fc^+)

Generally, the effect of adding the additional thiophene unit to the dye linker in the third generation dyes is to lower the redox potentials of the dyes to varying extents. The greatest change in E_{ox} was seen with the dyes bearing a radical shielding group, MeTAz-1-ttcaa (**214**) and tBuAz-1-ttcaa (**215**), where the change in E_{ox} compared to the second generation analogues MeTAz-1-tcaa (**203**) and tBuAz-1-tcaa (**205**) was -220 and -215 mV respectively. Az-1-ttca (**212**) has E_{ox} -155 mV compared with Az-1-tcaa (**84**) and TMAz-1-ttcaa (**213**) is almost unchanged over TMAz-1-tcaa (**147**) at -10 mV. The change in E_{ox} impacts the peak oxidation and reduction potentials (E_{pa} and E_{pc}) proportionally for each of the dyes.

The consequence of the negative changes in E_{ox} is corresponding increases in the HOMO energy levels of the dyes. In a DSSC, the HOMO level of the dye sensitiser

must be lower than that of the electrolyte redox couple, otherwise the oxidised dye will not be reduced back to the dye molecule and the DSSC will fail to work.

6.3.2 UV-Vis Spectroscopy

UV-Vis spectra were acquired for each of the three 2nd generation dyes at 0.01, 0.03 and 0.05 mM concentrations. Because of the limited solubility of the dyes in acetonitrile and dichloromethane, data and spectra in tetrahydrofuran (THF) only are presented in Table 24 and Spectrum 20 to Spectrum 23.

Dye	**Solvent**	**λ_{max} nm**	**ε (λ_{max}) L.mol^{-1}.cm^{-1}**	**λ_{onset} nm**	**E_g (opt) eV**
Az-1-ttcaa (**212**)	THF	488	3.58×10^4	580	2.14
TMAz-1-ttcaa (**213**)	THF	448	3.17×10^4	548	2.26
MeTAz-1-ttcaa (**214**)	THF	492	3.50×10^4	587	2.11
tBuAz-1-ttcaa (**215**)	THF	500	3.42×10^4	594	2.09

Table 24. UV/Vis data, third generation dyes

The generation three dyes exhibit a bathochromic shift in the absorption band λ_{max} of ~14 nm and λ_{onset} of 24-38 nm, showing that the optical bandgap is reduced over the first and second generation dyes and the absorption band is broadened, as expected.

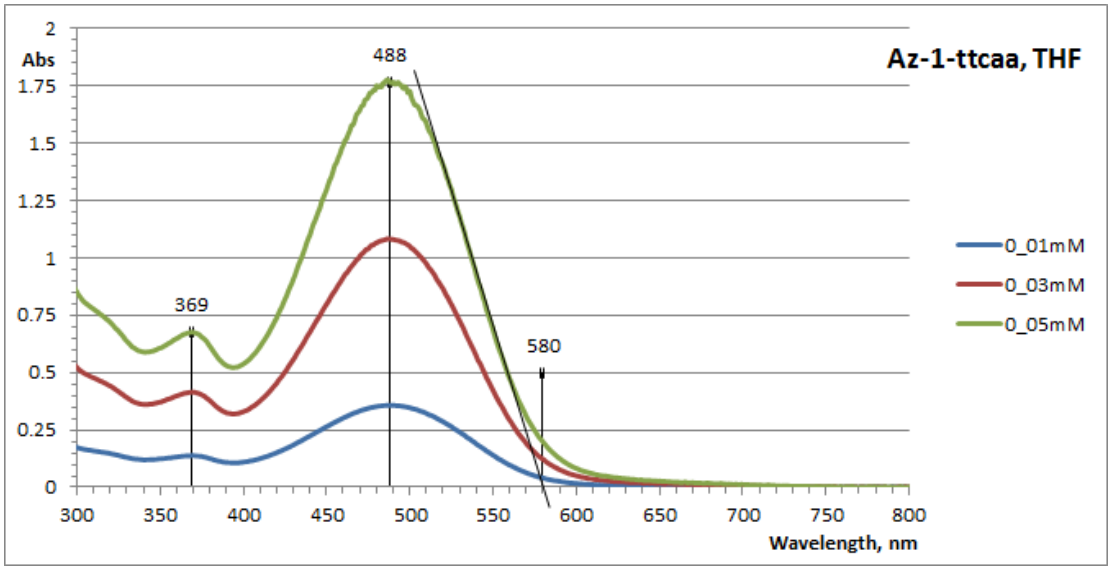

Spectrum 20. UV/Vis Az-1-ttcaa (212) in THF

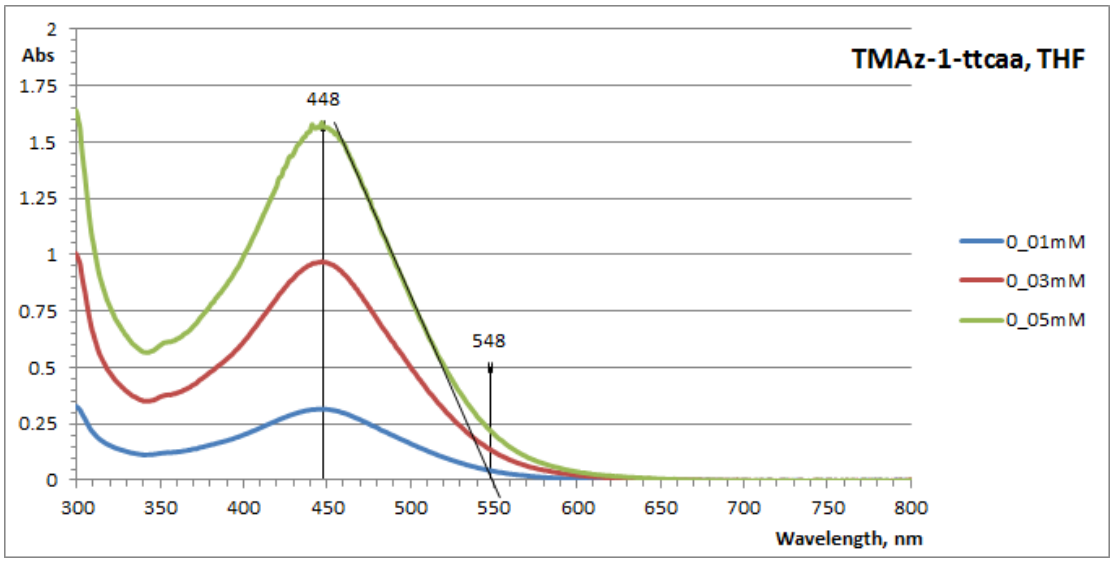

Spectrum 21. UV/Vis TMAz-1-ttcaa (213) in THF

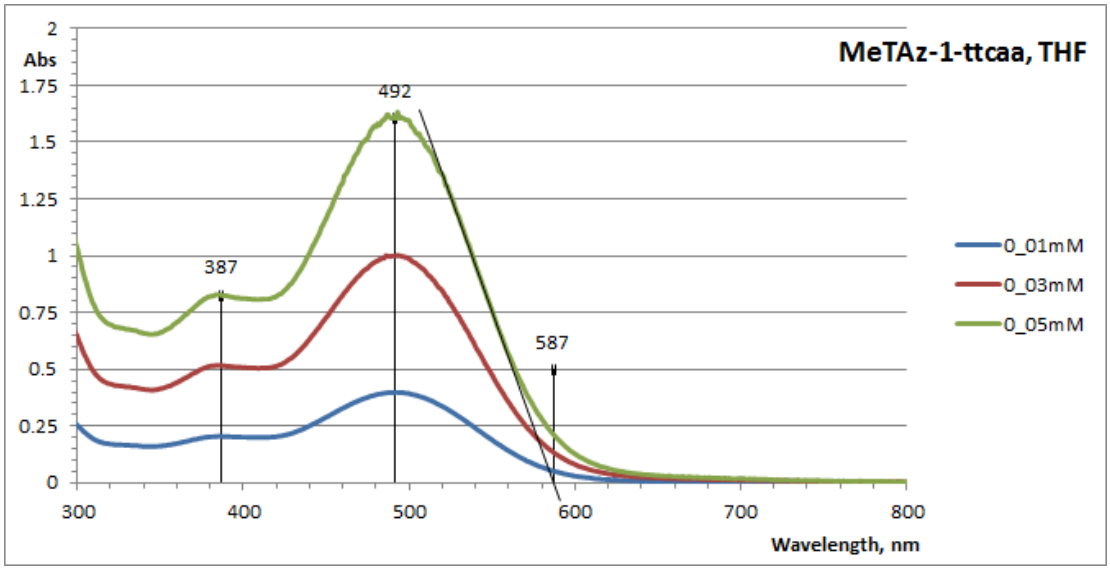

Spectrum 22. UV/Vis MeTAz-1-ttcaa (214) in THF

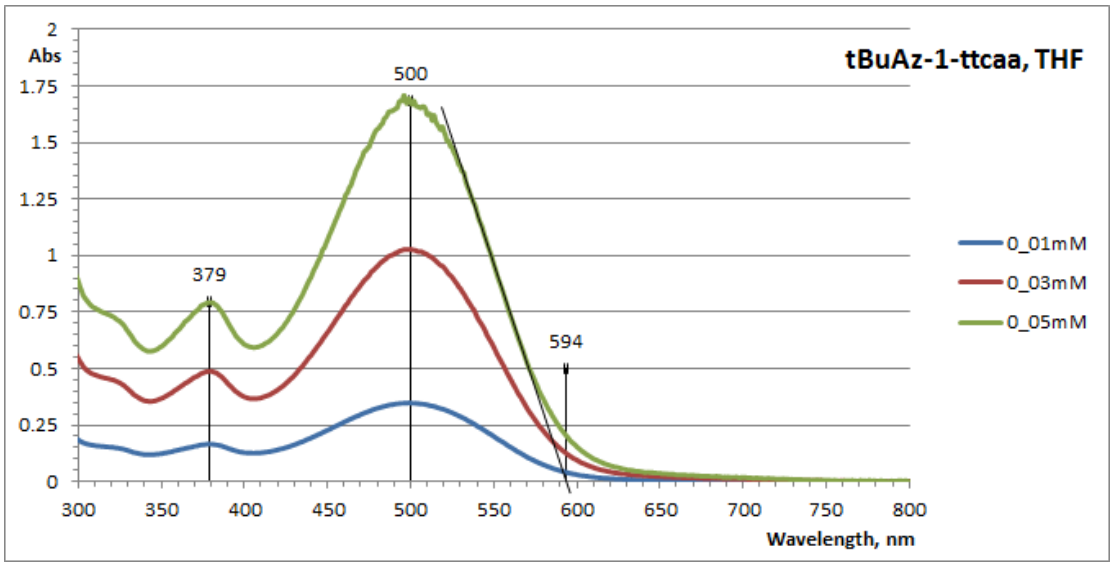

Spectrum 23. UV/Vis tBuAz-1-ttcaa (215) in THF

6.3.3 Dye Sensitised Solar Cells

Energy level data for the third generation dyes are summarised in Table 25. The ground state (D^0/D^+) potentials and band gap (E_g) values are taken from the electrochemistry and UV/Vis spectrometry results (sections 6.3.1 and 6.3.2 above). Subtracting E_g from D^0/D^+ gives the excited state potential D* (Equation 18):

Dye	$\frac{D^0}{D^+}$ **V vs NHE**	**E_g (opt) eV**	**D* V vs NHE**
Az-1-ttcaa (**212**)	0.79	2.14	-1.35
TMAz-1-ttcaa (**213**)	0.94	2.26	-1.32
MeTAz-1-ttcaa (**214**)	0.62	2.11	-1.49
tBuAz-1-ttcaa (**215**)	0.89	2.09	-1.20

Table 25. Third generation dyes energy levels

The ground and excited state energy levels fall within the ranges required for operation in DSSCs based on TiO_2 semiconductor and I^-/I_3^- electrolyte redox couple.

6.3.4 Conclusions

A range of azulene-based dyes for DSSCs with a bithiophene linker group have been successfully synthesised. Two of the third generation dyes, MeTAz-1-ttcaa (**214**) and tBuAz-1-ttcaa (**215**) were equipped with radical shielding groups similar to the second generation dyes while the other two dyes had no radical shielding group.

As with the first generation dyes, the third generation dyes without a radical shielding group exhibited non-reversible redox chemistry. The dyes with a radical shielding group had chemically reversible redox chemistry. The dye with the *tert*-butyl shielding group proved to have the least labile radical cation following oxidation, while the dye with the methylthio shielding group showed some signs of instability.

The bithiophene linker group had the desired effect of broadening and bathochromically shifting the absorption in the visible region of the spectrum. This should lead to more efficient light harvesting and in turn more efficient DSSCs.

Unfortunately, there was insufficient time at the end of the project to construct and test the third generation DSSCs, mainly due to the difficulties encountered with isolation and purification of the dyes because of their low solubilities.

7 Crystallography

Crystals of sufficiently high quality to obtain crystal structures by x-ray crystallography were obtained for some of the azulenesulfonium salts and azulene-based dyes synthesised during this project.

7.1 Sulfonium Salts

Azulene sulfonium salts were prepared as coupling partners for Suzuki-Miyaura cross coupling reactions. These reactions were used to attach the linker moiety to the azulene framework.

Crystal structures for three azulene sulfonium salts are presented below: azulyl-1-tetrahydrothiophenium hexafluorophosphate (Az-1-TMS, **207**) (Figure 72), 1-(3-*tert*-butylazulen-1-yl)tetrahydrothiophenium hexafluorophosphate (tBuAz-1-TMS, **162**) (Figure 73) and 1-(4,6,8-trimethylazulen-1-yl)tetrahydrothiophenium hexafluorophosphate (TMAz-1-TMS, **210**) (Figure 74). The crystal structures confirm the expected molecular structures for the three compounds.

The sp^3 hybridised sulfur atom of the sulfonium group gives the expected pyramidal geometry, with the tetramethylene ring oriented away from the azulene 7-membered ring. The plane of the tetramethylene ring is normal to the plane of the azulene rings.

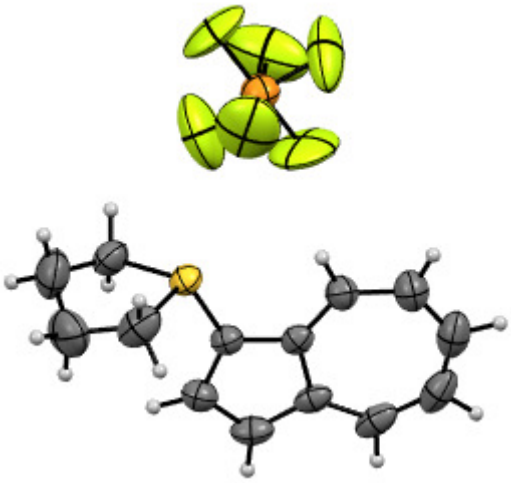

Figure 72. Crystal structure of azulene-1-tetramethylenesulfonium^{+} $^{-}PF_6$

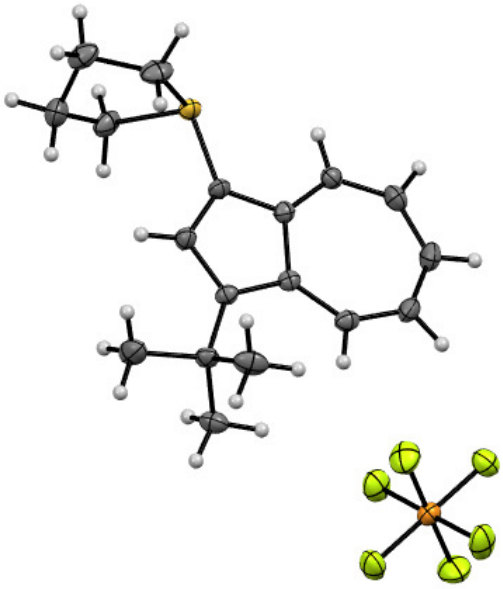

Figure 73. Crystal structure of 1-tert-butylazulene-3-tetramethylenesulfonium^{+} $^{-}PF_6$

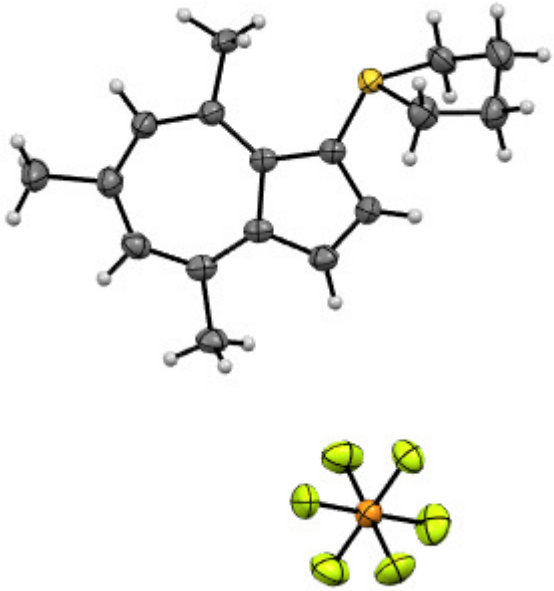

Figure 74. Crystal structure of 4,6,8-trimethylazulene-1-tetramethylenesulfonium^{+} $^{-}PF_6$

The methyl group at the azulene C-8 position influences the sulfur-azulene bond angle. The relevant bond angles are listed in Table 26, where C-1, C-2 and C-9 refer to the respective azulene carbon atoms.

Sulfonium Salt	Bond Angles (°)	
	S-(C-1)-(C-2)	S-(C-1)-(C-9)
Az-1-TMS (**207**)	128.75	121.80
tBuAz-1-TMS (**162**)	128.11	122.29
TMAz-1-TMS (**210**)	122.35	127.47

Table 26. Sulfonium salt S-Azulene bond angles

The presence of the methyl group therefore causes some additional strain on the sulfur-azulene bond, which may account for the colour of the trimethylazulene sulfonium salt (bright scarlet) compared with the other azulene sulfonium salts (dark purple).

7.2 Azulene-based Dyes

Crystal structures for six azulene-based dyes are presented below. The crystal structures all confirm the expected molecular structures of the dyes and in addition reveal some interesting information regarding the conformation and geometry of the thiophene ring linker group in relation to the azulene framework.

The geometry of the cyanoacrylic acid acceptor/anchor group relative to the attached thiophene ring is identical in all of the dyes. The cyanoacrylic acid group is always arranged with the cyano group cis- to the thiophene ring, with the sulfur atom nearest to the cyano group. This arrangement presumably is of the lowest energy.

Torsion and bond angles are presented in Table 27. There is a range if torsion angles between the azulene and attached thiophene rings from almost coplanar (2.53°, MeTAz-1-tcaa) to almost normal to each other (88.34°, TMAz-1-ttcaa). Conjugation between the azulene and thiophene rings will be more or less disrupted depending on the deviation from co-planarity, which in turn will influence the charge transfer properties and photophysics of the molecule. Figure 75 shows two views of

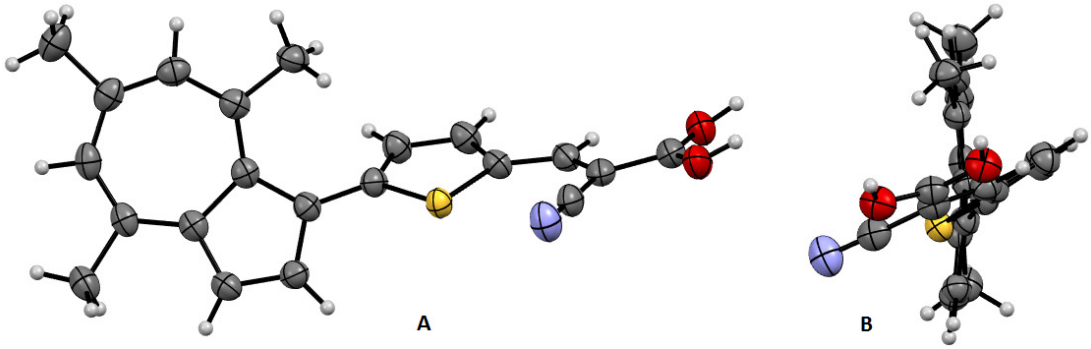

Figure 75. Crystal structure of TMAz-1-tcaa (A) and rotated through 90° in the horizontal plane to show the "end elevation" view (B)

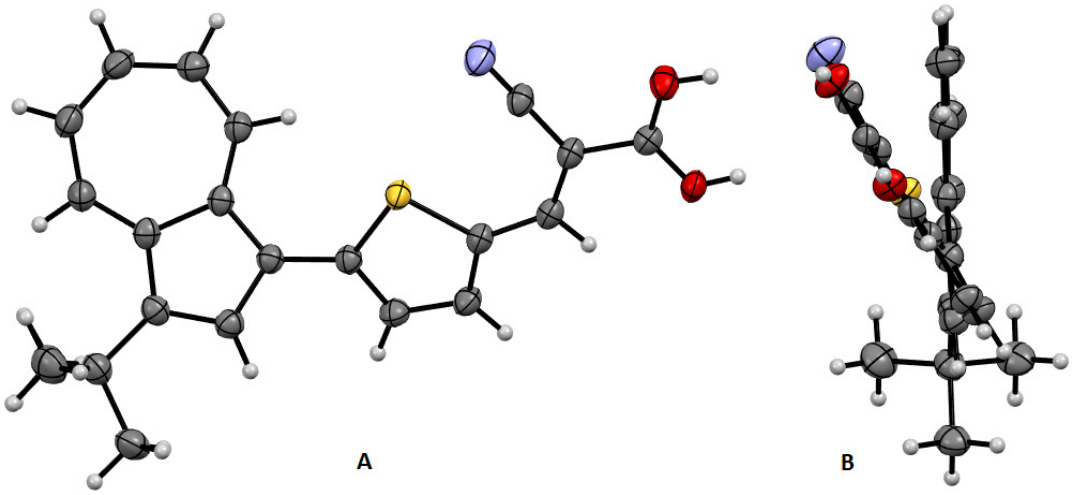

Figure 76. Crystal structure of tBuAz-1-tcaa (A) and rotated through 90° in the horizontal plane to show the "end elevation" view (B)

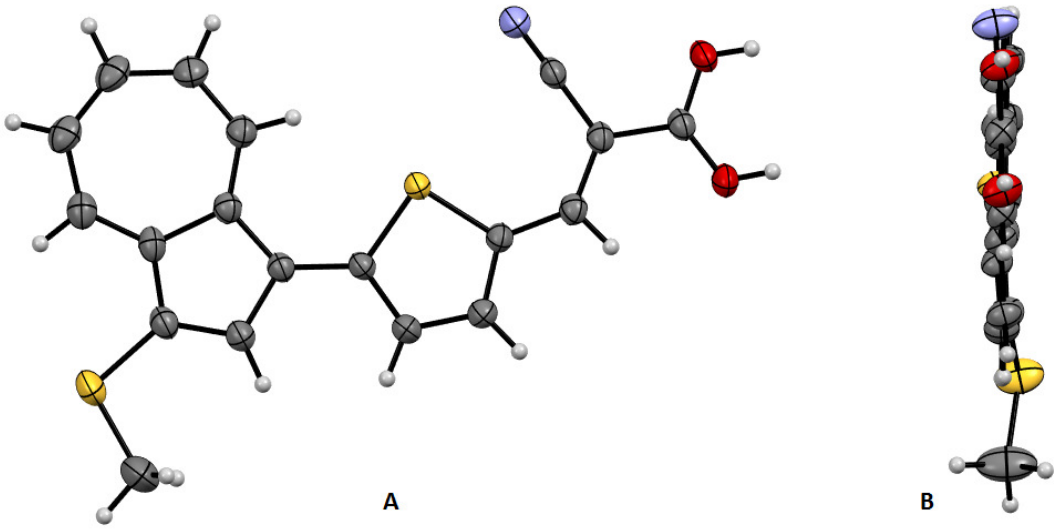

Figure 77. Crystal structure of MeTAz-1-tcaa (A) and rotated through 90° in the horizontal plane to show the "end elevation" view (B)

TMAz-1-tcaa (**147**). Figure 75 (A) shows the molecular structure and Figure 75 (B) the "end-on" view of the molecule rotated through 90°. In the end elevation, the high torsion angle can be seen between the thiophene ring and the azulene ring. In Figure 76 (B), the torsion angle in tBuAz-1-tcaa (**205**) is quite marked but less than TMAz-1-tcaa and in Figure 77 (B) the torsion angle in MeTAz-1-tcaa is minimal. Some of the torsional strain can be attributed to steric clash of the thiophene ring with the methyl group at azulene C-8 in TMAz-1-tcaa. The geometry of MeTAz-1-tcaa demonstrates that co-planarity can be achieved in the absence of the C-8 methyl group; however in tBuAz-1-tcaa the molecule crystallises with a reasonably large torsional angle despite the lack of a C-8 methyl group.

In some of the dyes the thiophene ring sulfur atom is oriented away from the azulene 7-membered ring ("forwards") and in others it is oriented towards the azulene 7-membered ring ("backwards"). The preference for forwards or backwards orientation of the thiophene ring seems to be as much to do with the fitting of the molecule into the crystal lattice as it is to do with minimising the molecular energy, however, as evidenced in the crystal structure of Az-1-ttcaa (Figure 80). This dye crystallised as a dimer with hydrogen bonding between the carboxylic acid groups. In one of the dimer molecules, the thiophene ring adopted a forwards orientation, and in the other a backwards orientation. Figure 78 shows the crystal structure of the symmetrical 1,3-dithienylazulene which has neither sterically hindering methyl groups in the azulene 7-membered ring nor any interference from cyanoacrylic acid anchor groups. The thiophene rings are in the forwards orientation and the torsional angle is 34.83°.

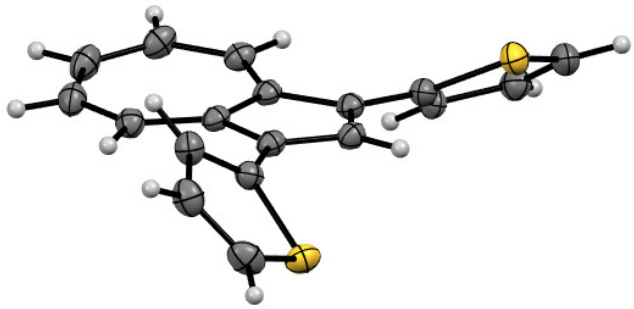

Figure 78. Crystal structure of 1,3-dithienylazulene showing "propeller like" arrangement of the thienyl substituents

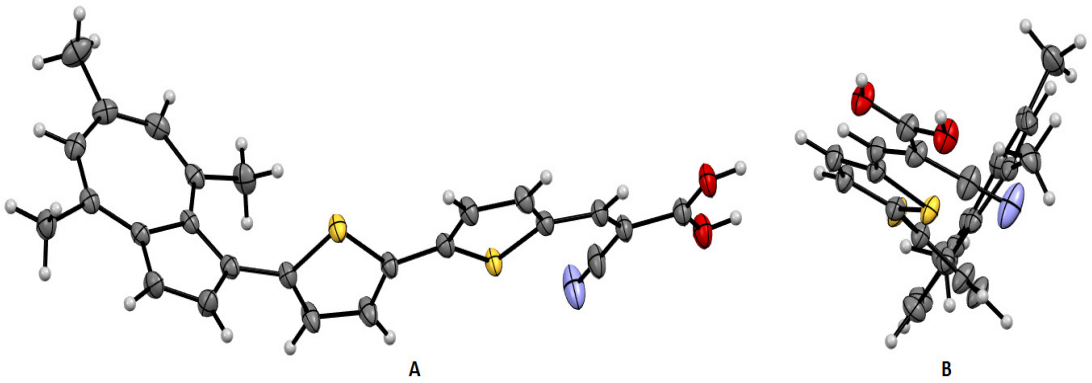

Figure 79. Crystal structure of TMAz-1-ttcaa (A) and rotated 90° in the horizontal plane to show the "end elevation" view (B)

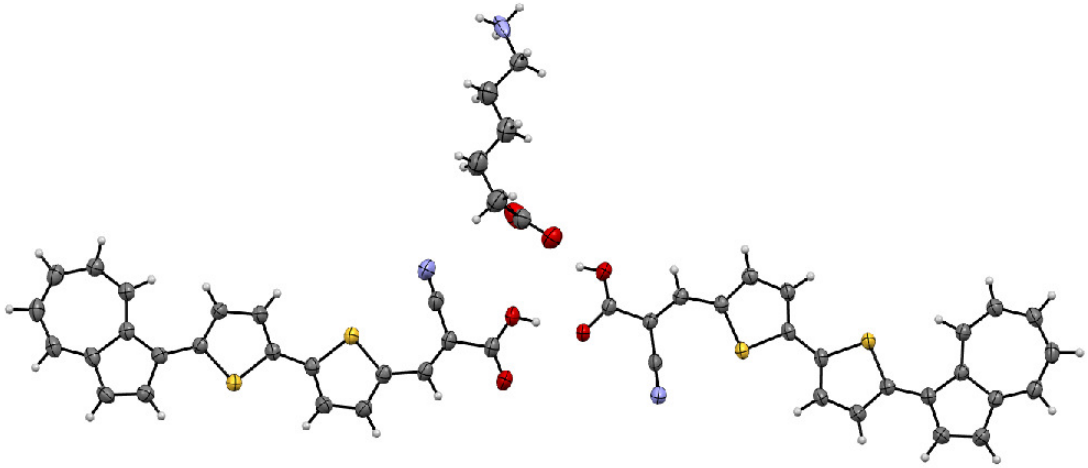

Figure 80. Crystal structure of Az-1-ttcaa co-crystallised with 6-aminocaproic acid in a 2:1 ratio

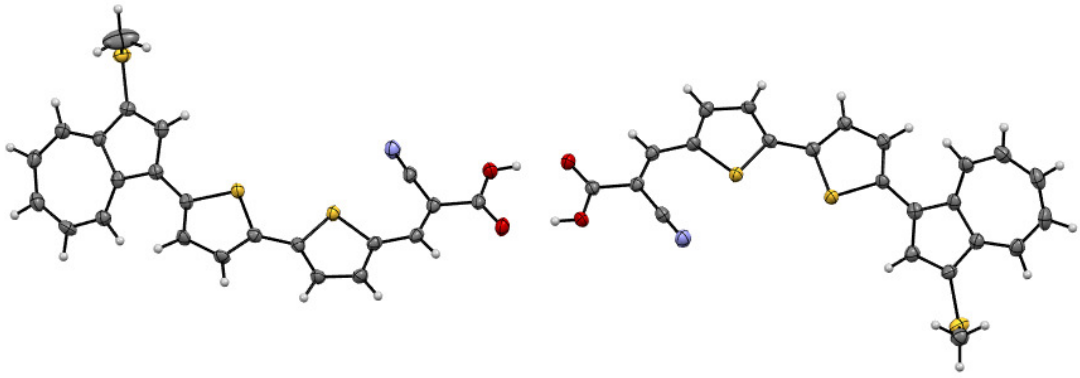

Figure 81. Crystal structure of MeTAz-1-ttcaa dimer

Dye	Torsion Angle (°)	Bond Angles (°)	
		S-(C-1)-(C-2)	S-(C-1)-(C-9)
TMAz-1-tcaa (**147**)	52.34	121.54	129.37
tBuAz-1-tcaa (**205**)	28.90	121.97	130.50
MeTAz-1-tcaa (**204**)	2.53	121.46	131.00
TMAz-1-ttcaa	88.34	121.33	129.99
Az-1-ttcaa	7.20	121.21	131.20
MeTAz-1-ttcaa	38.29	124.15	128.07

Table 27. Azulene dyes torsion and S-Azulene bond angles

In conclusion, the orientation of the thiophene ring and the torsional angle seem to be due at least in part to the geometry adopted by the molecules to enable them to fit most easily into the crystal lattice. The geometry adopted in solution or when adsorbed onto a TiO_2 nanoparticle (ie not in a crystalline state) may therefore be very different to that in the crystalline state. However, a methyl group at the azulene C-8 position is bound to cause torsional distortion between the azulene ring and the attached thiophene ring with consequential disruption to conjugation between the rings. The much lower molar extinction coefficient of TMAz-1-tcaa may be due to this effect.

8 Experimental

8.1 General

Reactions which required the use of anhydrous, inert atmosphere techniques were carried out under an atmosphere of argon. In most cases, solvents were obtained by passing through anhydrous alumina columns using an Innovative Technology Inc. PS-400-7 solvent purification system. Anhydrous and oxygen-free (dry) THF was obtained by distillation from sodium / benzophenone ketyl. All other solvents were purchased as "anhydrous" grade from Fisher Scientific. "Petrol" refers to petroleum spirit b.pt. 40-60 °C.

TLC was performed using aluminium backed plates precoated with Alugram®SIL G/UV 254 nm. Where necessary, visualization was accomplished by UV light and/or $KMnO_4$ dip followed by gentle warming. Organic layers were routinely dried with anhydrous $MgSO_4$ and evaporated using a Büchi rotary evaporator. When necessary, further drying was facilitated by high vacuum. Flash column chromatography was carried out using Davisil LC 60 Å silica gel (35-70 micron) purchased from Fisher Scientific.

IR spectra were recorded on a Perkin-Elmer 1600 FTIR spectrometer with only selected absorbances quoted as v in cm^{-1}. ^{1}H and ^{13}C NMR spectra were run in $CDCl_3$ (unless otherwise specified) on Agilent ProPulse 500 MHz or Bruker Avance 250, 300, 400 or 500 MHz instruments at 298 K. The following abbreviations are used: s, singlet; d, doublet; t, triplet; q, quartet; quin, quintet; sex, sextet; sep, septet; dd, doublet of doublets; dq, doublet of quartets; td, triplet of doublets; m, multiplet and br, broad.

A microTOF electrospray time-of-flight (ESI-TOF) mass spectrometer (Bruker Daltonik GmbH, Bremen, Germany) was used; this was coupled to an Agilent 1200 LC system (Agilent Technologies, Waldbronn, Germany). The LC system was used as an autosampler only. 10 µL of sample was injected into a 30:70 flow of water:acetonitrile at 0.6 mL/min to the mass spectrometer. For each acquisition 10 µL of calibrant of 5 mM sodium formate was injected after the sample. The observed mass and isotope pattern matched the corresponding theoretical values as calculated from the expected elemental formula.

X-Ray crystallography was recorded on a Nonius Kappa CCD diffractometer with Mo-Kα radiation (λ=0.71074 Å). All structures were solved by direct methods and refined on all F2 data using SHELX-97 suite of programs.

Extended Hückel Molecular orbital models were calculated using Cambridgesoft Chem3D Pro version 12 software. Chemical structures were drawn directly in Chem3D or in ChemDraw Ultra version 12 and then pasted into Chem3D. Molecular Mechanics 2 (MM2) energy minimisation was performed with a minimum RMS gradient of 0.01. When necessary, manual adjustments to the adopted molecular conformation were applied followed by repeating the MM2 energy minimisation until the lowest energy state was achieved. Extended Hückel Surfaces were then calculated followed by choosing the molecular orbital surface and setting the resolution to 100. The shapes of molecular orbitals can then be viewed by selecting the required molecular orbital.

All NMR spectra were processed using ACD/NMR Processor Academic Edition version 12.01.

8.2 Synthesis

Synthetic procedures for dyes and intermediate compounds are detailed in the following pages.

8.2.1 2,4,6-Trimethylpyryliumtetrafluoroborate (44)

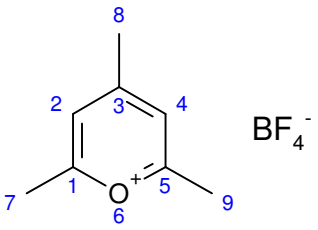

4-Hydroxy-4-methyl-2-pentanone (122 mL, 0.99 mol) was added to acetic anhydride (1.0 L, 9.71 mol) in a 3-necked 2 L round bottomed flask. The solution was stirred for 5 minutes at RT.

Fluoroboric acid (50% in H_2O) (174 mL, 0.99 mol) was added at a rate to maintain the reaction temperature below 100 °C (approx.. 1 hour). The solution changed from colourless to dark brown during the addition, with a final temperature of 95 °C.

After allowing the reaction mixture to cool to 80 °C naturally, it was cooled to 5 °C in an ice bath and then 200 mL of diethyl ether was added to complete product precipitation. The product was filtered from the mixture under vacuum and rinsed with diethyl ether. The product was slurried with diethyl ether, filtered under vacuum again and rinsed with diethyl ether.

Pale yellow crystalline solid (146.9 g, 0.7 mol, 70.7% yield). ^{1}H NMR (300 MHz, CHLOROFORM-*d*) δ_H/ppm 2.77(s, 3H, H^8), 2.95(s, 6H, H^7 and H^9), 7.67(s, 2H, H^2 and H^4), in agreement with literature data.[172]

8.2.2 4,6,8-Trimethylazulene (TMAz) (48)

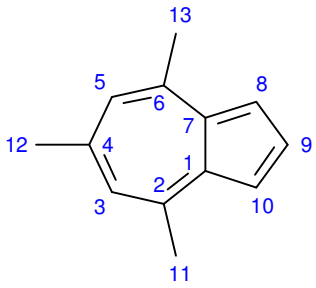

Cyclopentadiene was freshly prepared by cracking and distillation from dicyclopentadiene.

Cyclopentadiene (9.0 mL, 107.02 mmol) was added dropwise at 0 °C to a suspension of sodium hydride (1.125 g, 46.88 mmol) in anhydrous THF (200 mL). The reaction mixture became deep red in colour as the cyclopentadiene was added. After stirring at 0 °C for 1 hour, the temperature was allowed to rise to RT. This solution was then added to 2,4,6-trimethylpyrylium tetrafluoroborate (5.375 g, 25.6 mmol) via cannula transfer at RT and stirred for 30 minutes. The reaction mixture turned dark blue immediately on adding to the pyrylium salt.

After removing the solvent under reduced pressure, the product was dissolved in diethyl ether and washed repeatedly with water until the water remained clear, then with saturated brine. Purification of the crude using flash chromatography with petroleum ether (40/60) as eluent followed by recrystallization from ethanol yielded the title compound.

Blue-black platelets (1.4247 g, 8.38 mmol, 33% yield). ^{1}H NMR (300 MHz, CHLOROFORM-*d*) δ_H/ppm 2.67 (s, 3 H, H^{12}) 2.92 (s, 6 H, H^{11} & H^{13}) 7.10 (s, 2 H, H^{3} & H^{5}) 7.39 (d, *J*=3.8 Hz, 2 H, H^{8} & H^{10}) 7.70 (t, *J*=3.9 Hz, 1 H, H^{9}), in agreement with literature data.[173] ^{13}C NMR (75 MHz, CHLOROFORM-*d*) δ/ppm 25.04, 28.69, 115.96, 127.06, 132.33, 136.07, 145.58, 146.17. IR v_{max} (cm^{-1}) 2914, 1574, 1543, 1487, 1424, 1367, 1330. HRMS (+ve ESI-TOF) m/z calculated for $(C_{13}H_{14}+H)^{+}$ 171.1174, found 171.1173.

8.2.3 4,6,8-Trimethylazulene-1-carboxaldehyde (120)

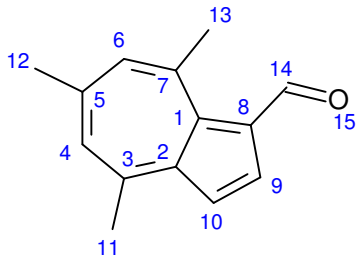

The Vilsmeier reagent was prepared by adding $POCl_3$ (1.7 mL, 18 mmol) to DMF (8.0 mL, 7.6 g, 104 mmol) at 0 °C.

4,6,8-Trimethylazulene (**48**) (1.02 g, 6 mmol) was dissolved in DMF (60 mL) and the solution was then cooled to 0 °C in a water ice bath. The pre-prepared Vilsmeier reagent was added during 10 minutes with stirring. There was an immediate colour change from deep purple to claret red.

The reaction flask was removed from the ice bath and stirring continued for a further 15 minutes. After quenching the reaction with ice, aq. NaOH (1.0 M, 18.0 mL) was added. The reaction mixture was transferred to a separating funnel and extracted with chloroform x 3. The combined extractions were concentrated under reduced pressure and the residue dissolved in diethyl ether. The solution was washed repeatedly with water, saturated LiCl solution, water and saturated NaCl solution, dried over magnesium sulphate and filtered. The solvent was removed under reduced pressure and the residue dried *in vacuo.*. No further purification was necessary.

Dark red solid (0.966 g, 4.88 mmol, 81% yield). ^{1}H NMR (300 MHz, CHLOROFORM-d) δ_H/ppm 2.65 (s, 3 H, H^{12}), 2.87 (s, 3 H, H^{13}), 3.11 (s, 3 H, H^{11}), 7.26 (d, J=4.5 Hz, 1 H, H^{10}), 7.33 (s, 1 H, H^4), 7.35 (s, 1 H, H^6), 8.25 (d, J=4.5 Hz, 1 H, H^9), 10.60 (s, 1 H, H^{14}) in agreement with literature data.[173]

8.2.4 1-Formylazulene (3)

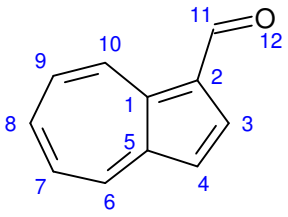

The method used to prepare 4,6,8-trimethylazulene-1-carboxaldehyde (**120**) was followed, save for the substitution of 4,6,8-trimethylazulene with azulene.

Red oil in 86% yield. ^{1}H NMR (300 MHz, CHLOROFORM-*d*) δ/ppm 7.29 (d, *J*=4.1 Hz, 1 H, H^{10}), 7.47 (t, *J*=9.8 Hz, 1 H, H^{7} or H^{9}), 7.52 - 7.60 (m, 1 H, H^{7} or H^{9}), 7.75 - 7.84 (m, 1 H, H^{8}), 8.23 (d, *J*=4.1 Hz, 1 H, H^{6}), 8.44 (dd, *J*=9.6, 0.57 Hz, 1 H, H^{4}), 9.52 (d, *J*=9.6 Hz, 1 H, H^{3}), 10.33 (s, 1 H, H^{11}); in agreement with literature data.[174] ^{13}C NMR (75 MHz, CHLOROFORM-*d*) δ/ppm 118.99, 125.84, 128.17, 129.37, 137.33, 138.92, 139.65, 140.26, 141.78, 145.98, 186.41.

8.2.5 1-Bromo-4,6,8-trimethylazulene (1-Br-TMAz) (108)

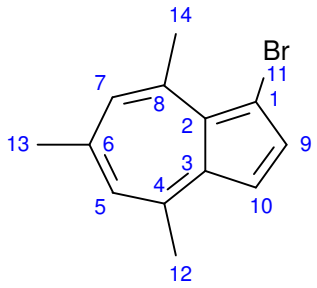

A 100 mL round bottom flask was wrapped in aluminium foil to exclude light to minimise radical reactions.

NBS (106.8 mg, 0.6 mmol) was added in portions with stirring during approximately 10 minutes to a solution of 4,6,8-trimethylazulene (TMAz) (102 mg, 0.6 mmol) in dry THF at room temperature. The mixture changed colour immediately, becoming dark blue from blue/violet. TLC showed three separate coloured compounds: lilac (unreacted TMAz), purple (1-bromo-TMAz) and dark blue (1,3-dibromo-TMAz).

The solvent was removed under reduced pressure. The dried solid changed colour overnight to green, indicating decomposition or polymerisation; with subsequent reactions isolation of the product was not attempted but used immediately in crude form, or after work-up to remove the succinimide by-product as follows:

After removing the reaction solvent (THF) under reduced pressure, the residue was partitioned between petroleum ether (40/60) and water. The organic layer was washed with water, aq. NaOH (1 M) and saturated brine, then dried over magnesium sulphate. The solvent was removed under reduced pressure, then the product was immediately dissolved in the appropriate solvent ready for the next synthetic step.

No characterisation data were acquired.

8.2.6 1-Chloroazulene (112)

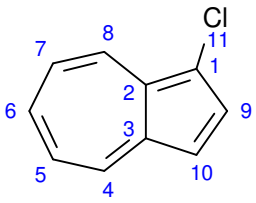

A 100 mL round bottom flask was wrapped in aluminium foil to exclude light to minimise radical reactions.

NCS (267 mg, 2 mmol) was added in portions with stirring during approximately 20 minutes to a solution of azulene (256 mg, 2 mmol) in dry THF (15 mL) at room temperature. The mixture changed colour immediately, becoming slightly greener than the indigo blue azulene. TLC showed three separate coloured compounds: indigo blue (unreacted azulene), greenish-blue (1-chloroazulene) and blue-green (1,3-dichloroazulene).

The solvent was removed under reduced pressure, and the residue purified by flash chromatography (silica gel) eluted with petroleum ether (40/60).

Greenish-blue oil (246 mg, 1.507 mmol, 75% yield). ^{1}H NMR (300 MHz, CHLOROFORM-d) δ_H/ppm 7.16 (t, J=10.2 Hz, 1 H, H^7), 7.21 (t, J=9.8 Hz, 1 H, H^5), 7.33 (d, J=4.1 Hz, 1 H, H^{10}), 7.63 (t, J=9.6 Hz, 1 H, H^6), 7.80 (d, J=4.1 Hz, 1 H, H^9), 8.25 (d, J=9.4 Hz, 1 H, H^4), 8.41 (d, J=9.8 Hz, 1 H, H^8).

8.2.7 1-Chloro-4,6,8-trimethylazulene (144)

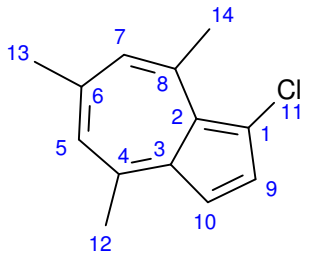

A 100 mL round bottom flask was wrapped in aluminium foil to exclude light to minimise radical reactions.

NCS (534 mg, 4.0 mmol) was added in portions with stirring during approximately 20 minutes to a solution of 4,6,8-trimethylazulene (TMAz) (**48**) (680 mg, 4.0 mmol) in dry THF (30.0 mL) at room temperature. The mixture changed colour immediately, becoming bluer than the purple TMAz. TLC showed three separate coloured compounds: purple (unreacted TMAz), indigo blue (1-chloro-4,6,8-trimethylazulene) and blue (1,3-dichloro-4,6,8-trimethylazulene).

The solvent was removed under reduced pressure, and the residue purified by flash chromatography (silica gel) eluted with petroleum ether (40/60).

Purple solid (528 mg, 2.58 mmol, 65% yield). ^{1}H NMR (300 MHz, *CHLOROFORM-d*) δ ppm 2.58 (s, 3 H, H^{13}), 2.81 (s, 3 H, H^{14}), 3.18 (s, 3 H, H^{12}), 6.93 (s, 1 H, H^{5} or H^{7}), 6.95 (s, 1 H, H^{5} or H^{7}), 7.25 (d, *J*=4.3 Hz, 1 H, H^{10}), 7.50 (d, *J*=4.5 Hz, 1 H, H^{9}); ^{13}C NMR (75 MHz, *CHLOROFORM-d*) δ ppm 25.10, 27.56, 28.61, 114.22, 116.58, 127.10, 128.87, 129.49, 133.57, 135.25, 146.59, 147.76, 147.84.

8.2.8 2-(Thiophene-2-yl)-1,3-dioxolane (135)

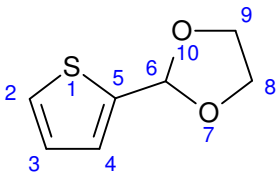

2-Thiophenecarboxaldehyde (1.0 eq., 12.9 mL, 15.5 g, 134 mmol), ethylene glycol (1.51 eq., 11.3 mL, 12.58 g, 203 mmol) and *p*-toluenesulphonic acid anhydride (38 mg, 0.2 mmol) catalyst were dissolved in toluene (50 mL) in a 250 mL round bottomed flask equipped with Dean-Stark apparatus and condenser. The Dean-Stark collector was filled with toluene (10 mL). The reaction mixture was refluxed for 2 hours (oil bath temperature 160 °C).

After cooling to RT, the reaction mixture was washed with saturated sodium bicarbonate solution, water and saturated brine, dried over magnesium sulphate and filtered. The solvent was removed under reduced pressure. Purification was by fractional distillation under vacuum (15 mbar, boiling range 97-99 °C).

Clear, colourless liquid (12.46 g, 80.4 mmol, 60% yield). ^{1}H NMR (300 MHz, CHLOROFORM-*d*) δ_H/ppm 3.92 - 4.05 (m, 2 H, $H^{8'}$ and $H^{9'}$), 4.05 - 4.17 (m, 2 H, $H^{8''}$ and $H^{9''}$), 6.11 (s, 1 H, H^{6}), 7.00 (dd, *J*=5.1, 3.6 Hz, 1 H, H^{3}), 7.16 - 7.21 (m, 1 H, H^{4}), 7.33 (dd, *J*=5.1, 1.3 Hz, 1 H, H^{2}). In agreement with literature data.[175]

Density of product = 1.245 g.cm^{-3}.

8.2.9 5-Formyl-2-thiopheneboronic acid (138)

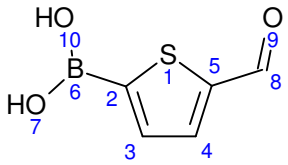

2-(Thiophen-2-yl)-1,3-dioxolane (**135**) (1.0 eq., 1.25 mL, 1.56 g, 10.0 mmol) was dissolved in dry THF (15.0 mL) under N_2 atmosphere cooled to 0 °C in a water ice/brine bath. *n*–BuLi (2.24 M in hexanes) (1.2 eq., 5.36 mL, 12.0 mmol) was added dropwise during 20 minutes with stirring at 0 °C. The colour of the reaction mixture changed from colourless to dark green.

The reaction was allowed to stir for a further 1 hour at 0 °C before transferring to a dry ice/acetone bath and cooling to -78 °C. Trimethylborate (2.0 eq., 2.3 mL, 20.0 mmol) was added dropwise with stirring at -78 °C. The colour changed from dark green to dark brown during the addition. After removing from the cold bath, the reaction was allowed to stir for a further 1 hour while warming to RT.

The reaction mixture was partitioned between diethyl ether and saturated sodium bicarbonate solution. The aqueous phase was removed and the organic phase was washed with saturated sodium bicarbonate solution x 3.

The organic phase was washed with saturated brine, dried over magnesium sulphate and filtered. The solvent was removed under reduced pressure, leaving a brown oil, 849 mg.

The combined alkaline aqueous washings were returned to the separating funnel and extracted with diethyl ether x 2. A small amount of brown, insoluble material was removed from the separating funnel, then the aqueous phase was acidified with 2M Aq. HCl. CO_2 gas was evolved and the solution became cloudy. The solution was extracted with diethyl ether (20 mL) x 4. The ethereal extracts were pale yellow and the aqueous phase became colourless.

The combined ethereal extracts were dried over magnesium sulphate, filtered and concentrated under reduced pressure yielding a pinkish solid (712 mg, 5.02 mmol, 50% yield). ^{1}H NMR (300 MHz, Acetone) δ_H/ppm 7.75 - 7.83 (broad s, 2 H, H^7 and H^{10}), 7.77 (d, J=3.8 Hz, 1 H, H^3), 7.96 (d, J=3.8 Hz, 1 H, H^4), 10.01 (s, 1 H, H^8); ^{13}C

NMR (75 MHz, Acetone) δ/ppm 137.04, 137.90, 149.18, 184.28; in agreement with literature data.[176]

Recrystallisation of the product from boiling water gave yellow crystals containing 1:1 product:water of crystallisation. The water was removed by dissolving the crystals in diethyl ether, drying over magnesium sulphate, filtering then removing the solvent under reduced pressure and drying *in vacuo*..

8.2.10 2-(5-(1,3-Dioxolan-2-yl)thiophen-2-yl)-4,4,5,5-tetramethyl-1,3,2-dioxaborolane (142)

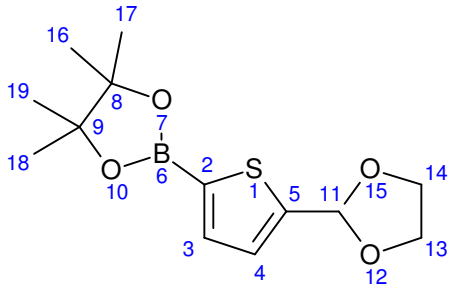

A 250 mL round bottomed flask fitted with a rubber septum was evacuated and back-filled with argon. Dry THF (30.0 mL) was added and cooled to -78 °C in a dry ice/acetone bath. 2-(Thiophene-2-yl)-1,3-dioxolane (**135**) (1.0 eq., 2.51 mL, 3.125 g, 20.0 mmol) was added. *n*–BuLi (2.2 M in hexanes) (1.2 eq., 10.91 mL, 24.0 mmol) was added dropwise with stirring at -78 °C. The reaction was allowed to stir for a further 15 minutes at -78 °C before removing from the cold bath, then for 20 minutes until the colour changed from yellow to green. Once the colour had changed, the flask was replaced into the cold bath and cooled to -78 °C.

2-Isopropoxy-4,4,5,5-tetramethyl-1,3,2-dioxaborolane (ITDB) (1.225 eq., 5.0 mL, 24.5 mmol) was added dropwise with stirring at -78 °C. The reaction was removed from the cold bath and stirred for a further 2 hours.

The reaction mixture was partitioned between saturated sodium bicarbonate solution and diethyl ether. The ethereal layer was removed and the aqueous layer extracted with diethyl ether. The combined ethereal extracts were concentrated under reduced pressure then dried *in vacuo.*. No further purification was done.

Waxy orange solid (4.07 g, 14.4 mmol, 72% yield). ^{1}H NMR (300 MHz, CHLOROFORM-*d*) δ_H/ppm 1.32 (s, 12 H, H^{16} H^{17} H^{18} and H^{19}), 3.95 - 4.15 (complex m, 4 H, H^{13} and H^{14}), 6.16 (s, 1 H, H^{11}), 7.20 (d, *J*=3.6 Hz, 1 H, H^{4}), 7.50 (d, *J*=3.6 Hz, 1 H, H^{3}); in agreement with literature data.[175]

8.2.11 5-(Azulen-1-yl)thiophene-2-carboxaldehyde (87)

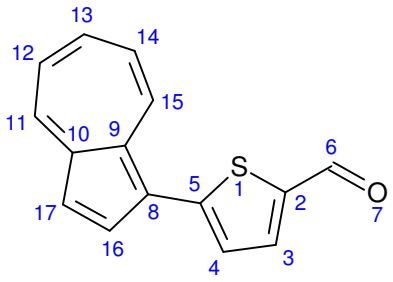

1-Chloroazulene (**112**) (1.0 eq., 463 mg, 2.85 mmol), 2-(5-(1,3-dioxolan-2-yl)thiophen-2-yl)-4,4,5,5-tetramethyl-1,3,2-dioxaborolane (**142**) (1.5 eq., 1211 mg, 4.28 mmol), palladium acetate (4 mol%, 25.6 mg, 0.114 mmol), XPhos ligand (10 mol%, 136 mg, 0.285 mmol) and potassium phosphate (2 eq., 1208 mg, 5.7 mmol) were placed in a dry 25 mL round bottomed flask. The flask was evacuated and back-filled with argon twice and then degassed 2-propanol (9.25 mL) was added. The flask was placed in an oil bath pre-heated to 70 °C and stirred under argon.

TLC showed no starting material remaining after 3.5 hours. The flask was removed from the oil bath and allowed to cool. The solvent was removed under reduced pressure, and the residue extracted with diethyl ether.

The combined ethereal extracts were concentrated under reduced pressure and the residue was dissolved in acetone (20 mL) and water (2 mL). A catalytic quantity of *p*-toluenesulphonic acid anhydride (40 mg) was added and the solution was stirred at 30 °C until TLC showed complete conversion of the dioxolane to the aldehyde product (approx. 2 hours).

After removing the acetone under reduced pressure, the residue was partitioned between diethyl ether and water. The ethereal layer was removed, dried over magnesium sulphate, filtered and solvent removed under reduced pressure.

The product was purified by flash chromatography. Silica gel, eluted with ethyl acetate/petroleum ether (1:9). Green oil (411 mg, 1.73 mmol, 54% yield). ^{1}H NMR (300 MHz, CHLOROFORM-*d*) δ/ppm 7.28 (t, *J*=9.6 Hz, 2 H), 7.3 (t, *J*=1.00 Hz, 1 H), 7.42 (d, *J*=3.8 Hz, 2 H), 7.70 (t, *J*=1.0 Hz, 1 H), 7.81 (d, *J*=3.8 Hz, 1 H), 8.13 (d, *J*=4.1 Hz, 1 H), 8.37 (d, *J*=9.4 Hz, 1 H), 8.86 (d, *J*=9.8 Hz, 1 H), 9.91 (s, 1 H); ^{13}C

NMR (75 MHz, CHLOROFORM-*d*) δ/ppm 118.75, 122.15, 125.06, 125.19, 125.25, 135.62, 135.72, 137.37, 137.67, 138.04, 139.23, 141.30, 143.68, 150.32, 182.61; IR v_{max} (cm^{-1}) 1643 (s), 1460 (s), 1391 (s), 1228 (s); HRMS (+ve ESI-TOF) m/z calculated for $(C_{15}H_{10}OS + H)^+$ 239.0531, found 239.0548. R_f (EtOAc 3:7 Petrol) 0.35.

8.2.12 5-(4,6,8-Trimethylazulen-1-yl)thiophene-2-carboxaldehyde (146)

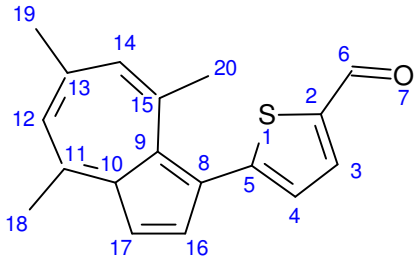

1-Chloro-4,6,8-trimethylazulene (**144**) (1.0 eq., 409 mg, 2.0 mmol), 2-(5-(1,3-dioxolan-2-yl)thiophen-2-yl)-4,4,5,5-tetramethyl-1,3,2-dioxaborolane (**142**) (1.5 eq., 849 mg, 3.0 mmol), palladium acetate (4 mol%, 18 mg, 0.08 mmol), XPhos ligand (10 mol%, 95 mg, 0.2 mmol) and potassium phosphate (2.0 eq., 848 mg, 4.0 mmol) were placed in a dry 25 mL round bottomed flask. The flask was evacuated and back-filled with argon twice, then degassed 2-propanol (6.5 mL) was added. The flask was placed in an oil bath pre-heated to 60 °C and stirred under argon.

TLC showed no starting material remaining after 1 hour. The TLC also indicated the presence of some 4,6,8-trimethylazulene (**48**), ie some of the starting material had become de-chlorinated. The flask was removed from the oil bath and allowed to cool. The solvent was removed under reduced pressure, and the residue extracted with diethyl ether.

The combined ethereal extracts were concentrated under reduced pressure and the residue was dissolved in acetone (20 mL) and water (2 mL). A catalytic quantity of *p*-toluenesulphonic acid anhydride (40 mg) was added and the solution was stirred at 30 °C until TLC showed complete conversion of the dioxolane to the aldehyde product (approx. 1 hour).

After removing the acetone under reduced pressure, the residue was partitioned between diethyl ether and water. The ethereal layer was removed, dried over magnesium sulphate, filtered and solvent removed under reduced pressure.

The product was purified by flash chromatography. Silica gel, eluted with ethyl acetate/petroleum ether (1:9).

Dark maroon oil (328 mg, 1.17 mmol, 59% yield). ^{1}H NMR (300 MHz, CHLOROFORM-*d*) δ/ppm 2.64 (s, 3 H, H^{19}), 2.65 (s, 3 H, H^{20}), 2.91 (s, 3 H, H^{18}), 7.02 (d, *J*=3.8 Hz, 1 H, H^{4}), 7.10 (s, 1 H, H^{14}), 7.16 (s, 1 H, H^{12}), 7.36 (d, *J*=4.1 Hz, 1 H, H^{17}), 7.65 (d, *J*=4.1 Hz, 1 H, H^{16}), 7.72 (d, *J*=4.0 Hz, 1 H, H^{3}), 9.90 (s, 1 H, H^{6}); ^{13}C NMR (75 MHz, CHLOROFORM-*d*) δ/ppm 25.57, 28.14, 28.43, 115.33, 121.71, 128.50, 129.15, 130.26, 132.60, 136.36, 137.16, 138.53, 142.58, 146.63, 147.24, 147.61, 154.66, 182.81. IR v_{max} (cm^{-1}) 1655, 1577, 1462, 1412, 1227; HRMS (ESI+) m/z calcd. For $(C_{18}H_{16}OS+H^{+})^{+}$ 281.0995, found 281.0949 R_f (EtOAc 3:7 Petrol) 0.53.

8.2.13 Az-1-tcaa, 3-(5-(Azulen-1-yl)thiophen-2-yl)-2-cyanoacrylic acid (84)

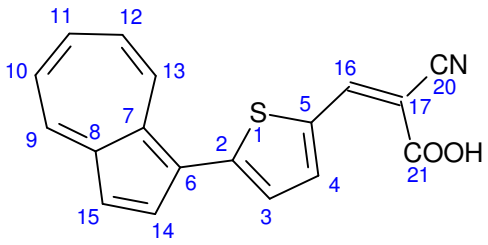

5-(Azulen-1-yl)thiophene-2-carboxaldehyde (**87**) (1.0 eq, 295 mg, 1.24 mmol) and cyanoacetic acid (**88**) (3.5 eq, 369 mg, 3.72 mmol) were dissolved in acetonitrile (12.5 mL). A catalytic quantity (6 drops) of piperidine was added and the solution was refluxed for 6 hours. TLC showed that the starting material had been consumed.

The solvent was removed under reduced pressure. The residue was triturated in dichloromethane, filtered and the insoluble residue recrystallised from hot ethanol.

Black crystalline solid (225 mg, 0.73 mmol, 60% yield). Melting point 230 – 231 °C. ^{1}H NMR (300 MHz, Acetone) δ/ppm 7.26 - 7.34 (m, 1 H, H^{12}), 7.34 - 7.43 (m, 1 H, H^{10}), 7.40 (d, J=4.1 Hz, 1 H, H^{3}), 7.57 (d, J=4.1 Hz, 1 H, H^{15}), 7.73 (t, J=9.8 Hz, 1 H, H^{11}), 7.94 (d, J=4 Hz, 1 H, H^{14}), 8.15 (d, J=4.1 Hz, 1 H, H^{4}), 8.34 (s, 1 H, H^{16}), 8.41 (d, J=9.6 Hz, 1 H, H^{13}), 8.83 (d, J=10.0 Hz, 1 H, H^{9}); ^{13}C NMR (75 MHz, Acetone) δ/ppm 97.71, 117.62, 120.57, 123.04, 126.81, 127.06, 127.12, 135.19, 136.79, 137.06, 138.6, 139.69, 141.05, 141.93, 145.5, 147.8, 151.63, 164.62. IR v_{max} (cm^{-1}) 212, 1677, 1558, 1503, 1415, 1378. HRMS (-ve ESI-TOF) m/z calculated for $(C_{18}H_{11}NO_2S\text{-}H^{+})^{-}$ 304.0432, found 304.0430. R_f (EtOAc 3:7 Petrol) 0.12.

8.2.14 TMAz-1-tcaa, 3-(5-(4,6,8-Trimethylazulen-1-yl)thiophen-2-yl)-2-cyanoacrylic acid (147)

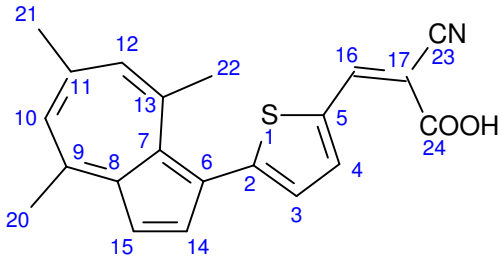

5-(4,6,8-Trimethylazulen-1-yl)thiophene-2-carboxaldehyde (**146**) (1.0 eq, 398 mg, 1.42 mmol) and cyanoacetic acid (**88**) (4.0 eq, 483 mg, 5.68 mmol) were dissolved in acetonitrile (14.25 mL). A catalytic quantity (7 drops) of piperidine was added and the solution was refluxed for 6 hours. TLC showed that the starting material had been consumed.

The solvent was removed under reduced pressure. The residue was triturated in dichloromethane, filtered and the insoluble residue recrystallised from hot ethanol.

Dark grey/green crystalline solid (307 mg, 0.88 mmol, 62% yield). Melting point 241 – 243 °C. ^{1}H NMR (500 MHz, Acetone) δ/ppm 2.65 (s, 3 H, H^{21}), 2.69 (s, 3 H, H^{22}), 2.91 (s, 3 H, H^{20}), 7.18 (d, J=3.8 Hz, 1 H, H^{3}), 7.23 (s, 1 H, H^{12}), 7.29 (s, 1 H, H^{10}), 7.41 (d, J=4.4 Hz, 1 H, H^{15}), 7.69 (d, J=4.1 Hz, 1 H, H^{14}), 7.96 (d, J=3.8 Hz, 1 H, H^{4}), 8.46 (s, 1 H, H^{16}). ^{13}C NMR (75 MHz, Acetone) δ/ppm 25.64, 28.44 (2 C), 98.11, 116.68, 117.10, 122.49, 129.65, 130.65, 131.33, 133.77, 136.10, 138.08, 140.00, 140.38, 147.73, 147.99, 148.56, 148.70, 155.47, 164.18. IR ν_{max} (cm^{-1}) 2216, 1669, 1570, 1606, 1454, 1405. HRMS (-ve ESI-TOF) m/z calculated for $(C_{21}H_{17}NO_2S\text{-}H^{+})^{-}$ 346.0902, found 346.0901. R_f (EtOAc 3:7 Petrol) 0.14.

8.2.15 1,3-di-*tert*-Butylazulene (160)

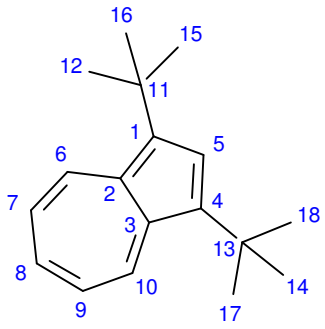

Azulene (**1**) (1.0 eq., 512 mg, 4.0 mmol), *tert*-butanol (23.0 eq., 6.8 g, 92.0 mmol) were dissolved in diethyl ether (15.0 mL) and 4 Å molecular sieves were added. The flask was evacuated and back-filled with argon. Tetrafluoroboronic acid etherate (54%) (11.0 eq., 6.0 mL, 7.14 g, 44.0 mmol) was added dropwise with stirring.

After stirring for 1 hour at RT, TLC showed that all the starting material had been consumed; however there were two product spots with higher R_f than the azulene starting material. These were assumed to be the mono- and di-substituted products. After stirring for 2 hours at RT, TLC showed only a single product spot, the lower Rf spot could no longer be seen.

The reaction mixture was partitioned between water and diethyl ether and neutralised with 1 M NaOH solution. The ethereal layer was washed with water and saturated brine then dried over magnesium sulfate and filtered.

The solvent was removed under reduced pressure. The residue was purified by flash chromatography: Silica gel, eluted with ethyl acetate/petroleum ether (1:39).

Sapphire blue solid (595 mg, 2.48 mmol, 62% yield). Melting point 96-97 °C. ^{1}H NMR (300 MHz, *CHLOROFORM-d*) δ ppm 8.59 (d, *J*=9.8 Hz, 2 H, H^{6} & H^{10}), 7.78 (s, 1 H, H^{5}), 7.47 (t, *J*=9.8 Hz, 1 H, H^{8}), 6.96 (t, *J*=10.1 Hz, 2 H, H^{7} & H^{9}), 1.59 (s, 18 H, H^{12}, H^{14}, H^{15}, H^{16}, H^{17}, & H^{18}); ^{13}C NMR (75 MHz, *CHLOROFORM-d*) δ ppm 136.81, 136.76, 135.51, 135.04, 135.02, 119.83, 33.26, 32.19. In agreement with literature data.[140]

8.2.16 1,3-Bis(methylthio)azulene (170)

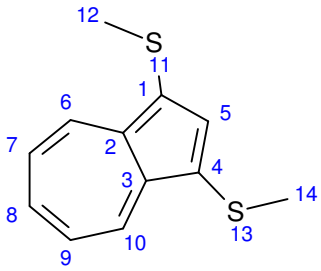

Azulene (**1**) (1.0 eq, 128 mg, 1.0 mmol) was placed into a dry 50 mL round bottom flask. The flask was evacuated and back-filled with argon. DCM (20 mL) was added followed by DMSO (5.0 eq, 390 mg, 0.354 mL, 5.0 mmol) and the solution was stirred.

Triflic anhydride (2.4 eq, 676 mg, 0.405 mL, 2.4 mmol) was added dropwise with stirring. The solution became slightly warmer and its colour changed from blue to dark orange. Stirring was continued for a further 30 minutes at RT, then the solvent was removed under reduced pressure.

A 1:1 mixture of ethanol (20.0 mL) and triethylamine (20.0 mL) was added. A condenser was fitted to the flask and the solution was refluxed for 30 minutes. After cooling to RT, the ethanol and triethylamine were removed under reduced pressure.

The residue was purified by flash chromatography: Silica gel, eluted with ethyl acetate/petroleum ether (1:19).

Green oil (187 mg, 0.85 mmol, 85% yield). ^{1}H NMR (300 MHz, *CHLOROFORM-d*) δ ppm 8.52 (d, *J*=9.4 Hz, 2 H, H^{6} & H^{10}), 7.99 (s, 1 H, H^{5}), 7.60 (t, *J*=9.8 Hz, 1 H, H^{8}), 7.19 (t, *J*=9.8 Hz, 2 H, H^{7} & H^{9}), 2.49 (s, 6 H, H^{12} & H^{14}). ^{13}C NMR (75 MHz, *CHLOROFORM-d*) δ ppm 141.60, 139.88, 139.17, 135.45, 123.65, 121.29, 20.21 in agreement with literature data.[177]

8.2.17 Ethyl 5-*iso*propyl-3,8-dimethylazulene-1-carboxylate (172)

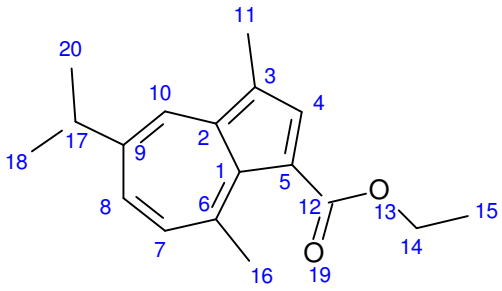

Guaiazulene (**2**) (1.0 eq., 198 mg, 1.0 mmol) was placed into a 25 mL round bottom flask. The flask was evacuated and back-filled with argon. Dry diethyl ether (5.0 mL) was added and stirred to dissolve **2**.

Oxalyl bromide (1.0 eq., 0.094 mL, 216 mg, 1.0 mmol) was added dropwise with stirring. There was an immediate colour change from blue to brick red. The solution was stirred for a further two hours at RT.

Ethanol (3.0 eq., 0.175 mL, 3.0 mmol) was added dropwise with stirring. The reaction mixture became warmer to the touch and there was an immediate colour change from brick red to violet. The solution was stirred for a further one hour.

The reaction mixture was partitioned between diethyl ether and water. The aqueous phase was coloured blue. The ethereal phase was washed with water and saturated brine, dried over magnesium sulfate and filtered. The solvent was removed under reduced pressure.

The residue was purified by flash chromatography: Silica gel eluted with ethyl acetate/petoleum ether (1:9).

Violet-blue oil (139 mg, 0.51 mmol, 51% yield). ^{1}H NMR (300 MHz, *CHLOROFORM-d*) δ ppm 8.27 (d, *J*=2.3 Hz, 1 H, H^{10}), 7.99 (s, 1 H, H^{4}), 7.52 (dd, *J*=10.9, 2.1 Hz, 1 H, H^{8}), 7.26 (d, *J*=10.9 Hz, 1 H, H^{7}), 4.42 (q, *J*=7.2 Hz, 2 H, H^{14}), 3.12 (sep, *J*=6.9 Hz, 1 H, H^{17}), 3.01 (s, 3 H, H^{16}), 2.62 (s, 3 H, H^{11}), 1.45 (t, *J*=7.1 Hz, 3 H, H^{15}), 1.39 (d, *J*=6.8 Hz, 6 H, H^{18} & H^{20}); ^{13}C NMR (75 MHz, *CHLOROFORM-d*) δ ppm 167.12, 147.10, 143.31, 140.16, 140.14, 135.90, 135.69, 134.26, 130.35, 123.83, 117.02, 60.27, 37.85, 27.70, 24.49, 14.43, 12.72. In agreement with literature data.[139]

8.2.18 Ethyl 3-formyl-5-*iso*propyl-8-methylazulene-1-carboxylate (173)

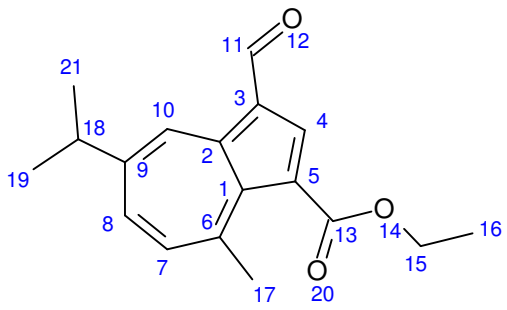

Ethyl 5-*iso*propyl-3,8-dimethylazulene-1-carboxylate (**172**) (1.0 eq., 265 mg, 0.98 mmol) was dissolved in aqueous acetone (10% water, 25 mL). DDQ (2.2 eq., 490 mg, 2.16 mmol) was added and the solution was stirred for 10 minutes at RT. There was a colour change from blue to red. TLC showed that all starting material had been consumed; there were two product spots. There was no change after stirring for a further 50 minutes.

The solvent was removed under reduced pressure and the residue was partitioned between diethyl ether and water. The ethereal phase was washed several times with water then saturated brine. After drying over magnesium sulfate and filtering, the solvent was removed under reduced pressure.

The residue was purified by flash chromatography: Silica gel eluted with ethyl acetate/petroleum ether (1:9).

Red oil (100 mg, 0.35 mmol, 36% yield). ^{1}H NMR (300 MHz, *CHLOROFORM-d*) δ ppm 10.22 (s, 1 H, H^{11}), 9.89 (d, *J*=2.1 Hz, 1 H, H^{10}), 8.45 (s, 1 H, H^{4}), 7.77 (dd, *J*=10.7, 2.1 Hz, 1 H, H^{8}), 7.63 (d, *J*=10.9 Hz, 1 H, H^{7}), 4.39 (q, *J*=7.2 Hz, 2 H, H^{15}), 3.21 (spt, *J*=6.9 Hz, 1 H, H^{18}), 2.99 (s, 3 H, H^{17}), 1.42 (t, J=7.2 Hz, 3 H, H^{16}), 1.38 (d, J=7 Hz, 6 H, H^{19} & H^{21}); ^{13}C NMR (75 MHz, *CHLOROFORM-d*) δ ppm 186.83, 166.43, 152.35, 150.80, 146.42, 141.82, 141.48, 138.65, 138.56, 135.23, 123.45, 120.28, 60.84, 38.16, 28.02, 24.32, 14.33. In agreement with literature data.[139]

8.2.19 N-*tert*-Butyl-α-(7-*iso*propyl-4-methyl-3-ethoxycarbonyl-azulen-1-yl)nitrone (175)

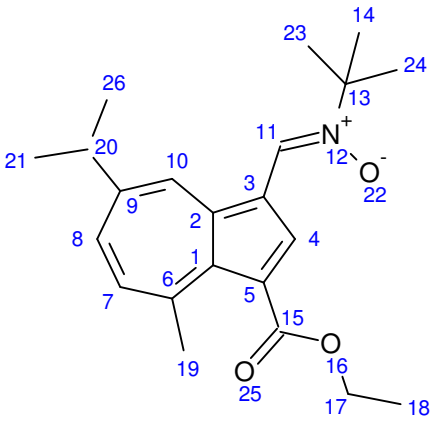

Ethyl 3-formyl-5-*iso*propyl-8-methylazulene-1-carboxylate (**173**) (1.0 eq., 100 mg, 0.35 mmol) was added to a 50 mL round borrom flask. N-*tert*-Butylhydroxylamine hydrochloride (1.5 eq., 66 mg, 0.525 mmol) and pyridine (3.5 mL) were added. A condenser was fitted to the flask and the reaction was heated to 95 °C in an oil bath and stirred at 95 °C for seven hours. TLC showed a small amount of starting material remained, which had not changed over the previous hour.

The solvent was removed under reduced pressure. The residue was partitioned between ethyl acetate and water. The organic phase was washed with water and saturated brine, dried over magnesium sulfate and filtered. The solvent was removed under reduced pressure.

The residue was purified by flash chromatography: Silica gel eluted with ethyl acetate/petroleum ether (3:1).

Green waxy solid (118 mg, 0.33 mmol, yield=95%). ^{1}H NMR (500 MHz, *CHLOROFORM-d*) δ ppm 9.72 (s, 1 H, H^{11}), 8.33 (d, *J*=1.9 Hz, 1 H, H^{10}), 8.14 (s, 1 H, H^{4}), 7.59 (dd, *J*=10.9, 1.7 Hz, 1 H, H^{8}), 7.38 (d, *J*=11.0 Hz, 1 H, H^{7}), 4.34 (q, *J*=7.3 Hz, 2 H, H^{17}), 3.12 (spt, *J*=6.9 Hz, 1 H, H^{20}), 2.94 (s, 3 H, H^{19}), 1.67 (s, 9 H, H^{14}, H^{23}, & H^{24}), 1.37 (t, *J*=7.3 Hz, 3 H, H^{18}), 1.35 (d, *J*=6.9 Hz, 6 H, H^{21} & H^{26}); ^{13}C NMR (126 MHz, *CHLOROFORM-d*) δ ppm 167.13, 148.52, 145.71, 141.24, 140.83, 137.57, 136.64, 132.58, 132.43, 122.70, 120.66, 117.16, 69.50, 60.66, 38.17, 28.31, 27.80, 24.33, 14.30. In agreement with literature data.[139]

8.2.20 1-*tert*-Butylazulene (159)

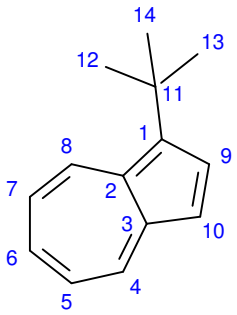

1-*tert*-Butyl-3-formyazulene (**185**) (1.0 eq., 583 mg, 2.75 mmol) was dissolved in glacial acetic acid (13.75 mL). Pyrrole (XS ~14.5 eq., 2.75 mL, 2.67 g, 39.7 mmol) was added and the solution stirred at RT for 16 hours. TLC showed that all the starting material had been consumed.

1 M aq. NaOH was added to neutralise the reaction mixture which was then partitioned with diethyl ether. The ethereal layer was washed repeatedly with water until the washings were clear and colourless, then with saturated brine. After drying over magnesium sulfate and filtering, the solvent was removed under reduced pressure.

The residue was purified by flash chromatography: Silica gel eluted with ethyl acetate/petroleum ether (1:99 – 15:85).

Blue oil (382 mg, 2.09 mmol, yield=76%). ^{1}H NMR (500 MHz, *CHLOROFORM-d*) δ ppm 8.73 (d, *J*=9.8 Hz, 1 H, H^{4}), 8.31 (dd, *J*=9.3, 1.0 Hz, 1 H, H^{8}), 7.92 (d, *J*=2.9 Hz, 1 H, H^{9}), 7.57 (t, *J*=9.8 Hz, 1 H, H^{6}), 7.35 (d, *J*=3.4 Hz, 1 H, H^{10}), 7.13 (t, *J*=10.0 Hz, 1 H, H^{5} or H^{7}), 7.10 (t, *J*=9.5 Hz, 1 H, H^{5} or H^{7}), 1.67 (s, 9 H, H^{12}, H^{13} & H^{14}); ^{13}C NMR (126 MHz, *CHLOROFORM-d*) δ ppm 141.59, 139.54, 137.14, 136.63, 135.63, 134.63, 122.00, 120.81, 116.33, 33.48, 32.25. In agreement with literature values.[178]

8.2.21 1-*tert*-Butyl-3-formylazulene (185)

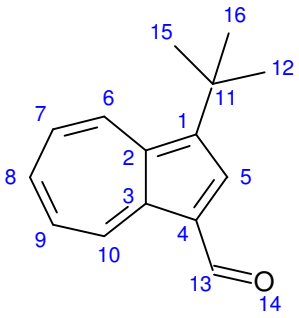

1,3-di-*tert*-Butylazulene (**160**) (1.0 eq., 1113 mg, 4.64 mmol) was dissolved in dimethylformamide (50 mL). Phosphoryl chloride (6.0 eq., 3.0 mL, 4265 mg, 27.8 mmol) was added dropwise with stirring. The flask was placed in an oil bath and the temperature raised to 100 °C. Stirring was continued for a further 90 minutes at 100 °C. TLC showed that all of the starting material had been consumed.

The flask was removed from the oil bath and allowed to cool to RT. The reaction mixture was transferred to a separating funnel and water (50 mL added). The mixture was neutralised with 2.5 M aq. NaOH (50 mL), then extracted into diethyl ether. The combined ethereal extracts were washed with water, 5% lithium chloride solution and saturated brine, dried over magnesium sulfate and filtered. The solvent was removed under reduced pressure.

The residue was purified by flash chromatography: Silica gel eluted with ethyl acetate / petroleum ether (ramped 1:39 – 1:19 – 1:9).

Purple solid, 669 mg, 3.15 mmol, yield=68%). Melting point 70-72 °C. ^{1}H NMR (300 MHz, *CHLOROFORM-d*) δ ppm 10.35 (s, 1 H, H^{13}), 9.51 (d, *J*=9.8 Hz, 1 H, H^{6}), 8.84 (d, *J*=10.2 Hz, 1 H, H^{10}), 8.21 (s, 1 H, H^{5}), 7.80 (t, *J*=9.8 Hz, 1 H, H^{8}), 7.53 (t, *J*=9.8 Hz, 1 H, H^{7} or H^{9}), 7.48 (dd, *J*=10.2, 9.8 Hz, 1 H, H^{7} or H^{9}), 1.58 (s, 9 H, H^{12}, H^{15} & H^{16}); ^{13}C NMR (75 MHz, *CHLOROFORM-d*) δ ppm 186.13, 142.45, 141.61, 140.61, 139.86, 139.57, 138.02, 136.63, 129.05, 126.71, 123.59, 33.11, 31.67. In agreement with literature values.[143]

8.2.22 1-(3-*tert*-Butylazulen-1-yl)tetrahydrothiophenium hexafluorophosphate (162)

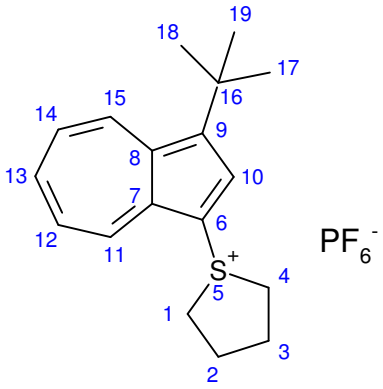

1-*tert*-Butylazulene (**159**) (1.0 eq., 437 mg, 2.375 mmol) was placed into a 50 mL round bottom flask. The flask was evacuated and back-filled with argon. DCM (16 mL) was added followed by tetrahydrothiophene-1-oxide (7.5 eq., 1.65 mL, 1.85 g, 17.8 mmol).

A 0.5 M solution of trifluoroacetic anhydride (TFAA) in DCM was prepared. The TFAA solution was added dropwise with stirring at RT to the reaction solution until TLC indicated that all starting material was consumed (8.0 mL, 4.0 mmol TFAA added).

The reaction mixture was diluted with diethyl ether, then extracted into water. The combined aqueous extracts were washed with diethyl ether and potassium hexafluorophosphate (excess) was added. The aqueous solution was extracted into DCM. The combined DCM extracts were dried over magnesium sulfate, and filtered. The solvent was removed under reduced pressure. The product was purified by recrystalisation from DCM/petroleum ether.

Purple crystalline solid (939 mg, 2.26 mmol, yield = 95%). Melting point 239-240 °C (dec). ^{1}H NMR (300 MHz, *acetone-d*^{6}) δ (ppm) 9.22 (d, *J* = 10.0 Hz, 1H, H^{11} or H^{15}), 8.93 (d, *J* = 9.8 Hz, 1H, H^{11} or H^{15}), 8.32 (s, 1H, H^{10}), 8.16 (t, *J* = 9.8 Hz, 1H, H^{13}), 7.81 (t, *J* = 9.8 Hz, 1H, H^{12} or H^{14}), 7.79 (t, *J* = 9.8 Hz, 1H, H^{12} or H^{14}), 4.29-4.20 (m, 2H, H$^{1'}$ & H$^{4'}$), 3.91-3.83 (m, 2H, H$^{1''}$ & H$^{4''}$), 2.94-2.81 (m, 2H, H$^{2'}$ & H$^{3'}$), 2.61-2.50 (m, 2H, H$^{2''}$ & H$^{3''}$), 1.62 (s, 9H, H^{17}, H^{18} & H^{19}); ^{13}C NMR (75 MHz, *acetone-d*^{6}) δ (ppm) 144.6, 143.3, 142.3, 140.6, 140.5, 136.0, 134.4, 129.0, 128.2, 103.4, 51.0, 34.4, 32.0, 30.0; IR $_{vmax}$ (cm^{-1}) (neat) 2956, 2873, 1578, 1381, 1218, 1205, 1133,

879, 821, 752. HRMS (ESI+) m/z calcd. for (C18H23S) [M]+ 271.1515, found 271.1519.

8.2.23 5-(3-*tert*-Butylazulen-1-yl)thiophene-2-carboxaldehyde (164)

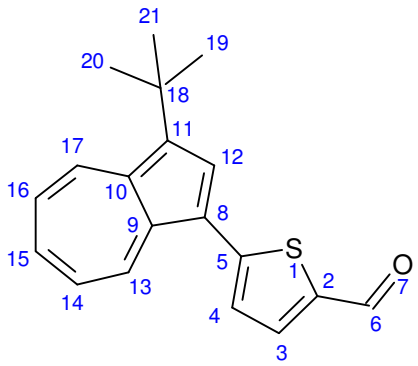

1-(3-*tert*-Butylazulen-1-yl)tetrahydrothiophenium hexafluorophosphate (**162**) (1.0 eq., 939 mg, 2.26 mmol), 2-(5-(1,3-dioxolan-2-yl)thiophen-2-yl)-4,4,5,5-tetramethyl-1,3,2-dioxaborolane (**142**) (1.5 eq., 956 mg, 3.39 mmol), palladium acetate (4 mol%, 20.25 mg, 0.09 mmol), X-Phos (10 mol%, 108 mg, 0.226 mmol) and potassium phosphate (2.0 eq., 958 mg, 4.52 mmol) were placed into a 50 mL round bottom flask. The flask was evacuated and back-filled with argon. Degassed 2-propanol (13.6 mL) was added. The flask was placed in an oil bath and the temperature raised to 80 °C. Stirring was continued for 50 minutes at 80 °C when TLC indicated that the starting material had been consumed.

After cooling to RT, the solvent was removed under reduced pressure. The residue was extracted with diethyl ether. The combined ethereal extracts were washed with water and saturated brine, dried over magnesium sulfate and filtered. The solvent was removed under reduced pressure.

The residue was dissolved in acetone 9:1 water (25 mL) and catalytic *p*TSA was added. The solution was stirred at RT for 30 minutes, when TLC indicated that the reaction was complete. The acetone was removed under reduced pressure.

The residue was purified by flash chromatography; silica gel eluted with ethyl acetate / petroleum ether (1 : 9).

Dark green/grey solid (485 mg, 1.65 mmol, yield = 73%). Melting point = 150 – 151 °C. ^{1}H NMR (500 MHz, *CHLOROFORM-d*) δ ppm 9.90 (s, 1 H, H^{6}), 8.77 (dd, *J*=10.3, 1.0 Hz, 1 H, H^{17}), 8.69 (d, *J*=9.3 Hz, 1 H, H^{13}), 8.02 (s, 1 H, H^{12}), 7.80 (d, *J*=3.9 Hz, 1 H, H^{3}), 7.63 (t, *J*=9.5 Hz, 1 H, H^{15}), 7.39 (d, *J*=3.9 Hz, 1 H, H^{4}), 7.21 (t,

J=9.3 Hz, 1 H, H^{14} or H^{16}), 7.20 (t, *J*=9.8 Hz, 1 H), 1.62 (s, 9 H, H^{19}, H^{20} & H^{21}); ^{13}C NMR (126 MHz, *CHLOROFORM-d*) δ ppm 182.46, 150.41, 141.14, 139.86, 138.95, 138.66, 137.53, 136.78, 136.75, 136.02, 135.31, 124.99, 124.57, 123.31, 119.95, 33.22, 31.90. IR $_{vmax}$ (cm^{-1}) 2948, 2786, 2726, 1639, 1565, 1456, 1441, 1358, 1285, 1231, 1084, 873, 833, 789, 746, 660. HRMS (+ve ESI-TOF) m/z calculated for $(C_{19}H_{18}OS+H^{+})^{+}$ 295.11566, found 295.1085. R_f (EtOAc 3:7 Petroleum Ether) 0.52.

8.2.24 1-(Methylthio)azulene (198)

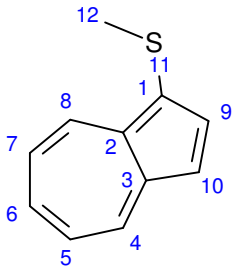

Azulene (1.0 eq., 128 mg, 1.0 mmol) was placed into a 50 mL round bottom flask. The flask was evacuated and back-filled with argon. DCM (10 mL) was added followed by DMSO (excess, 1.1 g, 1.0 mL, 14.0 mmol). TFAA (1.2 eq., 252 mg, 1.2 mmol) dissolved in DCM (10 mL) was added dropwise with stirring at RT. Stirring was continued for a further hour at RT. TLC showed that all starting material had been consumed. The solvent was removed under reduced pressure.

Ethanol (10.0 mL) and triethylamine (10.0 mL) were added and a reflux condenser was fitted to the flask. The solution was stirred under reflux for 30 minutes.

The solvent was removed under reduced pressure. The residue was purified by flash chromatography, silica gel eluted with ethyl acetate / petroleum ether (5:195).

Dark blue oil (160 mg, 0.96 mmol, yield=96%). ^{1}H NMR (300 MHz, *CHLOROFORM-d*) δ ppm 8.65 (d, *J*=9.6 Hz, 1 H, H^{4} or H^{8}), 8.28 (d, *J*=9.4 Hz, 1 H, H^{4} or H^{8}), 7.99 (d, *J*=4.0 Hz, 1 H, H^{9}), 7.62 (t, *J*=9.8 Hz, 1 H, H^{6}), 7.40 (d, *J*=4.0 Hz, 1 H, H^{10}), 7.24 (t, *J*=10.3 Hz, 1 H, H^{5} or H^{7}), 7.16 (t, *J*=9.9 Hz, 1 H, H^{5} or H^{7}), 2.50 (s, 3 H, H^{12}); ^{13}C NMR (75 MHz, *CHLOROFORM-d*) δ ppm 141.59, 139.90, 138.83, 138.40, 137.03, 135.38, 123.66, 123.16, 121.75, 117.36, 20.59. In agreement with literature data.[177]

8.2.25 5-(3-(Methylthio)azulen-1-yl)thiophene-2-carbaldehyde (200)

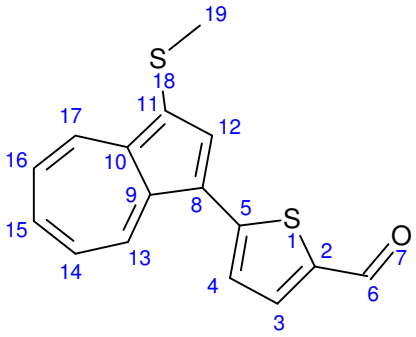

5-(Azulen-1-yl)thiophene-2-carboxaldehyde (**87**) (1.0 eq., 107 mg, 0.45 mmol) was placed into a 50 mL round bottom flask. The flask was evacuated and back-filled with argon. DCM (5 mL) followed by DMSO (excess, 550 mg, 0.5 mL, 7.0 mmol) was added and the solution stirred. Triflic anhydride (1.2 eq., 0.09 mL, 151 mg, 0.535 mmol) in DCM (5 mL) was added dropwise with stirring at RT. There was a colour change from green to dark grey-green. After stirring at RT for a further 15 minutes, TLC showed that the starting material had been consumed. The solvent was removed under reduced pressure.

Ethanol (5.0 mL) and triethylamine (5.0 mL) were added and a reflux condenser was fitted to the flask. The solution was stirred under reflux for 60 minutes. After allowing to cool to RT, the solvent was removed under reduced pressure.

The residue was purified by flash chromatography: silica gel eluted with ethyl acetate / petroleum ether (1:4).

Brown solid (green in solution) (83 mg, 0.29 mmol, yield=65%). Melting point 108 – 110 °C. ^{1}H NMR (300 MHz, *CHLOROFORM-d*) δ ppm 9.91 (s, 1 H, H^{6}), 8.76 (d, *J*=9.8 Hz, 1 H, H^{13} or H^{17}), 8.61 (d, *J*=9.6 Hz, 1 H, H^{13} or H^{17}), 8.13 (s, 1 H, H^{12}), 7.82 (d, *J*=4.0 Hz, 1 H, H^{3}), 7.70 (t, *J*=9.9 Hz, 1 H, H^{15}), 7.40 (d, *J*=4.0 Hz, 1 H, H^{4}), 7.32 (t, *J*=9.6 Hz, 1 H, H^{14} or H^{16}), 7.29 (t, *J*=9.6 Hz, 1 H, H^{14} or H^{16}), 2.53 (s, 3 H, H^{19}); ^{13}C NMR (75 MHz, *CHLOROFORM-d*) δ ppm 182.58, 149.25, 141.60, 141.50, 140.13, 139.11, 137.53, 136.82, 136.56, 135.95, 125.71, 125.31, 125.15, 123.33, 121.39, 19.92. IR $_{vmax}$ (cm^{-1}) 3073, 2920, 2814, 1626, 1571, 1461, 1237, 800. HRMS (+ve ESI-TOF) m/z calculated for $(C_{16}H_{13}OS_2+H^+)^+$ 285.04078, found 285.0416. R_f (EtOAc 3:7 Petroleum Ether) 0.49.

8.2.26 5-(4,6,8-Trimethyl-3-(methylthio)azulen-1-yl)thiophene-2-carboxaldehyde (202)

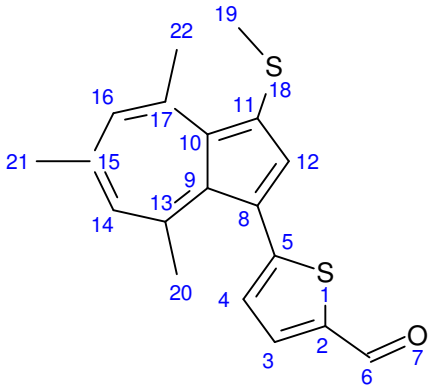

5-(4,6,8-Trimethylazulen-1-yl)thiophene-2-carboxaldehyde (**146**) (1.0 eq., 365 mg, 1.3 mmol) was placed into a 50 mL round bottom flask. The flask was evacuated and back-filled with argon. DCM (20 mL) followed by DMSO (excess, 1560 mg, 1.42 mL, 20.0 mmol) was added and the solution stirred. The flask was placed into an ice/water bath. A 0.25 M solution of triflic anhydride (0.42 mL, 2.5 mmol) in DCM (9.58 mL, 10 mL total volume) was prepared and added dropwise with stirring at 0 °C until TLC showed all starting material was consumed (1.1 eq., 1.43 mmol Tf2O added). The solvent was removed under reduced pressure.

Ethanol (10.0 mL) and triethylamine (10.0 mL) were added and a reflux condenser was fitted to the flask. The solution was stirred under reflux for 30 minutes. After allowing to cool to RT, the solvent was removed under reduced pressure.

The residue was extracted into diethyl ether. The ethereal solution was washed with water and saturated brine, dried over magnesium sulfate and filtered. The solvent was removed under reduced pressure. The residue was purified by flash chromatography: silica gel, eluted with ethyl acetate and petroleum ether (1:9).

Dark green solid (363 mg, 1.11 mmol, yield = 86%). Melting point 104 – 105 °C. ^{1}H NMR (500 MHz, *CHLOROFORM-d*) δ ppm 9.89 (s, 1 H, H^{6}), 7.71 (d, *J*=3.9 Hz, 1 H, H^{3}), 7.47 (s, 1 H, H^{12}), 6.98 (d, *J*=3.4 Hz, 1 H, H^{4}), 6.90 (s, 1 H, H^{14} or H^{16}), 6.84 (s, 1 H, H^{14} or H^{16}), 3.21 (s, 3 H, H^{20}), 2.54 (s, 3 H, H^{22}), 2.52 (s, 3 H, H^{19}), 2.51 (s, 3 H, H^{21}); ^{13}C NMR (126 MHz, *CHLOROFORM-d*) δ ppm 182.84, 149.49, 147.90, 147.62, 142.72, 136.42, 136.35, 135.34, 133.64, 130.01, 129.54, 129.11, 123.56, 121.50, 109.71, 28.72, 28.58, 28.10, 19.20. IR $_{vmax}$ (cm^{-1}) 2922, 2803, 1655, 1571,

1491, 1464, 1435, 1224. HRMS (+ve ESI-TOF) m/z calculated for $(C_{19}H_{18}OS_2+H^+)^+$ 327.08773, found 327.0829. R_f (EtOAc 3:7 Petroleum Ether) 0.51.

8.2.27 3-(5-(3-(Methylthio)azulen-1-yl)thiophen-2-yl)cyanoacrylic acid (203)

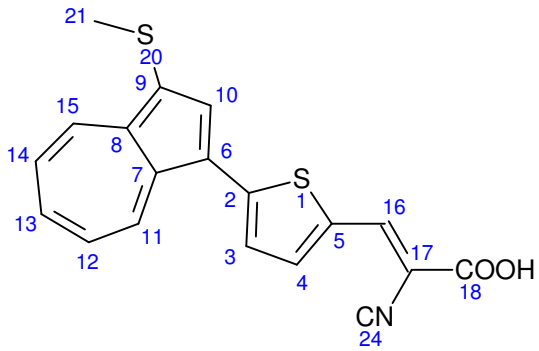

5-(3-(Methylthio)azulen-1-yl)thiophene-2-carboxaldehyde (**200**) (1.0 eq., 425 mg, 1.5 mmol), 6-aminocaproic acid (100 mol%, 198 mg, 1.5 mmol), cyanoacetic acid (1.5 eq., 191 mg, 2.25 mmol) were mixed with ethanol (9 mL). The flask was placed into an oil bath at 50 °C, and stirred for 3.5 hours. TLC indicated that the starting material was consumed.

After cooling to RT, aqueous 1M sulfuric acid (15.0 mL) was added to precipitate the product which was removed by vacuum filtration, washed with water and ice-cold ethanol and dried. The product was purified by re-crystallisation from hot 2-propanol and water.

Black crystalline solid (356 mg, 1.01 mmol, yield=67%). Melting point 223-224 °C (dec). ^{1}H NMR (300 MHz, *Acetone*) δ ppm 8.88 (d, *J*=9.8 Hz, 1 H, H^{11}), 8.61 (d, *J*=9.6 Hz, 1 H, H^{15}), 8.48 (s, 1 H, H^{16}), 8.34 (s, 1 H, H^{10}), 8.07 (d, *J*=4.1 Hz, 1 H, H^{4}), 7.87 (t, *J*=9.8 Hz, 1 H, H^{13}), 7.71 (d, *J*=4.1 Hz, 1 H, H^{3}), 7.48 (t, *J*=9.7 Hz, 1 H, H^{12} or H^{14}), 7.46 (t, *J*=9.5 Hz, 1 H, H^{12} or H^{14}), 2.59 (s, 3 H, H^{21}); ^{13}C NMR (75 MHz, *Acetone*) δ ppm 199.03, 164.21, 150.21, 147.47, 142.30, 141.72, 141.45, 139.52, 137.66, 137.43, 137.15, 135.26, 127.25, 126.95, 126.58, 125.19, 122.18, 67.12, 19.31. IR $_{vmax}$ (cm^{-1}) 3100, 2219, 1661, 1559, 1498, 1412, 1400, 1369, 1304, 1232, 1208, 1081, 929, 803, 728. HRMS (+ve ESI-TOF) m/z calculated for $(C_{19}H_{13}NO_2S_2+H^+)^+$ 352.0466, found 352.0398. R_f (EtOAc 3:7 Petroleum Ether) 0.0.

8.2.28 3-(5-(4,6,8-Trimethyl-3-(methylthio)azulen-1-yl)thiophen-2-yl)cyanoacrylic acid (204)

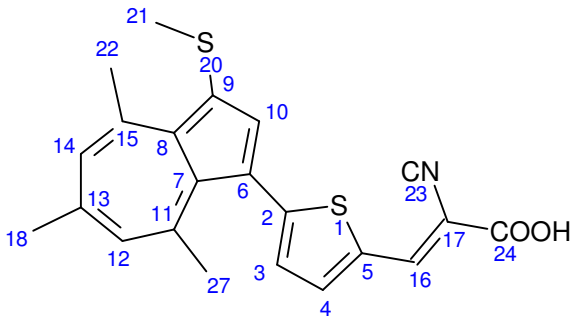

5-(4,6,8-Trimethyl-3-(methylthio)azulen-1-yl)thiophene-2-carboxaldehyde (**202**) (1.0 eq., 281 mg, 0.86 mmol), 6-aminicaproic acid (100 mol%, 114 mg, 0.86 mmol), cyanoacetic acid (1.5 eq., 110 mg, 1.29 mmol) were mixed with ethanol (5.2 mL). The flask was placed into an oil bath at 50 °C, and stirred for 3.5 hours. TLC indicated that the starting material was consumed.

After cooling to RT, aqueous 1M sulfuric acid (10 mL) was added to precipitate the product which was removed by vacuum filtration, washed with water and ice-cold ethanol and dried. The product was purified by re-crystallisation from hot 2-propanol and water.

Black crystalline solid (213 mg, 0.54 mmol, yield=63%). Melting point 234-235 °C (dec). ^{1}H NMR (500 MHz, *acetone*) δ ppm 8.47 (s, 1 H, H^{16}), 7.96 (d, *J*=4.4 Hz, 1 H, H^{4}), 7.60 (s, 1 H, H^{10}), 7.17 (d, *J*=3.9 Hz, 1 H, H^{3}), 7.03 (s, 1 H, H^{12} or H^{14}), 6.98 (s, 1 H, H^{12} or H^{14}), 3.19 (s, 3 H, H^{21}), 2.58 (s, 3 H, H^{18}, H^{22} or H^{27}), 2.56 (s, 3 H, H^{18}, H^{22} or H^{27}), 2.54 (s, 3 H, H^{18}, H^{22} or H^{27}); ^{13}C NMR (126 MHz, *acetone*) δ ppm 205.36, 163.13, 153.62, 149.21, 148.33, 147.56, 146.92, 139.27, 136.37, 135.34, 129.99, 129.62, 129.60, 121.39, 116.06, 97.33, 27.96, 27.66, 27.05, 18.16. IR $_{vmax}$ (cm^{-1}) 2953, 2222, 1668, 1653, 1571, 1501, 1402, 1365, 1293, 1236, 1203. HRMS (+ve ESI-TOF) m/z calculated for $(C_{22}H_{19}NO_2S_2+H^+)^+$ 394.09355, found 394.0955. R_f (EtOAc 3:7 Petroleum Ether) 0.0.

8.2.29 3-(5-(3-(*tert*-Butyl)azulen-1-yl)thiophen-2-yl)cyanoacrylic acid (205)

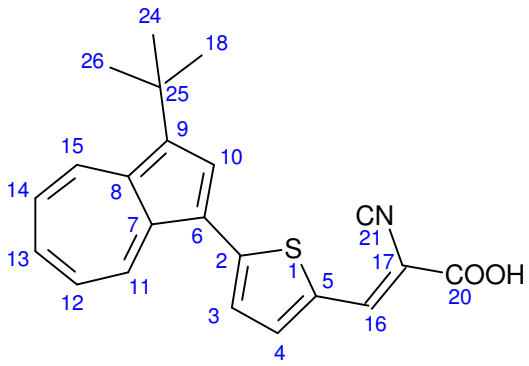

5-(3-(*tert*-Butyl)azulen-1-yl)thiophene-2-carboxaldehyde (**164**) (1.0 eq., 273 mg, 0.93 mmol), cyanoacetic acid (1.5 eq., 118 mg, 1.4 mmol) and 6-aminocaproic acid (100 mol%, 123 mg, 0.93 mmol) were mixed with ethanol (5.6 mL). The flask was placed into an oil bath at 50 °C and stirred for 3.5 hours when TLC indicated that the starting material had been consumed.

After cooling to RT, aqueous sulfuric acid (1M, 10 mL) was added to the stirred solution to precipitate the product. The product precipitated into a tar which could not be filtered. The tar was dissolved in DCM. The DCM solution was washed with water and then the solvent was removed under reduced pressure. The product was purified by recrystallisation from DCM/petroleum ether.

Dark green needles (165 mg, 0.46 mmol, yield=49%). Melting point 236-237 °C. ^{1}H NMR (300 MHz, *Acetone*) δ ppm 8.89 (d, *J*=4.0 Hz, 1 H, H^{15}); 8.86 (d, *J*=4.1 Hz, 1 H, H^{11}); 8.46 (d, *J*=0.6 Hz, 1 H, H^{16}); 8.17 (s, 1 H, H^{10}); 8.05 (dd, *J*=4.1, 0.4 Hz, 1 H, H^{4}); 7.79 (t, *J*=9.8 Hz, 1 H, H^{13}); 7.68 (d, *J*=4.1 Hz, 1 H, H^{3}); 7.33 - 7.44 (m, 2 H, H^{12} and H^{14}); 1.63 (s, 9 H, H^{18}, H^{24} and H^{26}); ^{13}C NMR (75 MHz, *Acetone*) δ ppm 164.67, 151.81, 147.81, 141.99, 141.38, 140.85, 140.46, 138.59, 138.14, 137.13, 136.69, 135.06, 126.88, 126.55, 125.51, 120.94, 117.67, 97.36, 34.26, 32.51. IR $_{vmax}$ (cm^{-1}) 2960, 2214, 1678, 1567, 1403, 1207, 1156, 1056. HRMS (+ve ESI-TOF) m/z calculated for $(C_{22}H_{19}NO_2S+H^+)^+$ 362.12147, found 362.1229. R_f (EtOAc 3:7 Petroleum Ether) 0.0.

8.2.30 1-(Azulen-1-yl)tetrahydrothiophenium hexafluorophosphate (207)

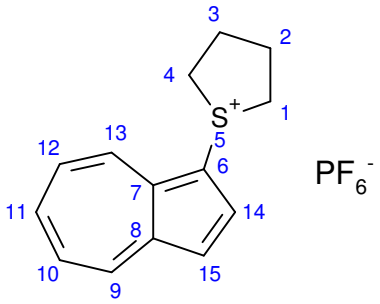

Azulene (**1**) (1.0 eq., 1.28 g, 10 mmol) was placed into a 500 mL round bottom flask. The flask was evacuated and back-filled with nitrogen. DCM (50 mL) and tetrahydrothiophene-1-oxide (7.5 eq., 5.0 mL, 5.6 g, 75.0 mmol) were added and the solution was stirred.

A 0.5 M solution of trifluoroacetic anhydride (TFAA) in DCM was prepared. The TFAA solution was added dropwise with stirring until the starting material was consumed by TLC (30.0 mL of solution added, 15.0 mmol, 1.5 eq.).

The reaction mixture was extracted into water. The extracted DCM organic phase was discarded, and the combined aqueous extracts placed into a separating funnel. KPF_6 (4.0 eq., 7.2 g) was added and once it had fully dissolved the solution was extracted into DCM (approx.. 300 mL in total). The combined DCM extracts were dried over magnesium sulfate, filtered and the solvent removed under reduced pressure. The residue was washed with diethyl ether, providing material of sufficient purity for further reactions. Further purification was achieved by recrystallisation from DCM/Petroleum ether.

Dull red crystalline solid (3.11 g, 8.64 mmol, yield = 86%). Melting point 182-183 °C. ^{1}H NMR (300 MHz, *CHLOROFORM-d*) δ ppm 9.01 (d, *J*=10.0 Hz, 1 H, H^{13}), 8.87 (dd, *J*=9.6, 0.6 Hz, 1 H, H^{9}), 8.46 (d, *J*=4.5 Hz, 1 H, H^{14}), 8.22 (dd, J=10.0, 9.6 Hz, 1 H, H^{11}), 7.90 (t, *J*=9.7 Hz, 1 H, H^{9}), 7.85 (t, *J*=9.8 Hz, 1 H, H^{13}), 7.76 (d, *J*=4.5 Hz, 1 H, H^{15}), 4.22 - 4.34 (m, 2 H, $H^{1'}$, $H^{4'}$), 3.80 - 3.92 (m, 2 H, $H^{1''}$, $H^{4''}$), 2.79 - 2.96 (m, 2 H, $H^{2'}$, $H^{3'}$), 2.50 - 2.68 (m, 2 H, $H^{2''}$, $H^{3''}$); ^{13}C NMR (75 MHz, *Acetone*) δ ppm 145.08, 142.94, 142.66, 141.83, 136.94, 136.52, 129.87, 129.51,

121.79, 105.67, 51.32, 29.99. IR $_{vmax}$ (cm^{-1}) (neat) 2956, 1587, 1406, 820. HRMS (ESI+) m/z calcd. for ($C_{14}H_{15}S$) [M]+ 215.0889; found 215.0886.

8.2.31 1-(4,6,8-Trimethylazulen-1-yl)tetrahydrothiophenium hexafluorophosphate (210)

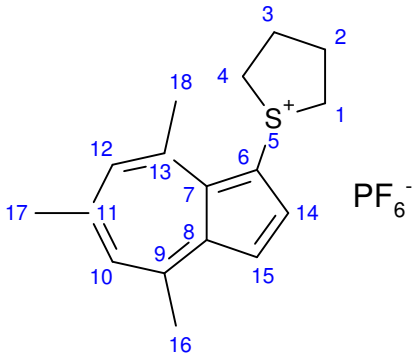

4,6,8-Trimethylazulene (**48**) (1.0 eq, 1084 mg, 6.34 mmol) was placed into a 250 mL round bottom flask. The flask was evacuated and back-filled with nitrogen. DCM (43 mL) and tetrahydrothiophene-1-oxide (7.5 eq., 3.2 mL, 3.6 g, 48 mmol) were added and the solution was stirred.

A 0.5 M solution of trifluoroacetic anhydride (TFAA) in DCM was prepared. The TFAA solution was added dropwise with stirring until the starting material was consumed by TLC (19.0 mL of solution added, 9.5 mmol, 1.5 eq.).

The reaction mixture was diluted with hexane and extracted into water. The extracted DCM organic phase was discarded, and the combined aqueous extracts placed into a separating funnel. After extracting with diethyl ether, KPF_6 (4 eq., 4.6 g) was added and once it had fully dissolved the solution was extracted into DCM. The combined DCM extracts were dried over magnesium sulfate, filtered and the solvent removed under reduced pressure. The residue was washed with diethyl ether, providing material of sufficient purity for further reactions.

Bright red crystalline solid (2.45 g, 6.09 mmol, yield = 96%). Melting point 186-187 °C. ^{1}H NMR (500 MHz, *acetone*) δ ppm 8.16 (d, *J*=4.9 Hz, 1 H, H^{14}), 7.69 (s, 1 H, H^{10} or H^{12}), 7.67 (s, 1 H, H^{10} or H^{12}), 7.66 (d, *J*=4.9 Hz, 1 H, H^{15}), 4.26 - 4.34 (m, 2 H, $H^{1'}$, $H^{4'}$), 3.79 - 3.86 (m, 2 H, , $H^{1''}$, $H^{4''}$), 3.35 (s, 3 H, H^{18}), 3.00 (s, 3 H, H^{16}), 2.79 - 2.90 (m, 2 H, $H^{2'}$, $H^{3'}$), 2.76 (s, 3 H, H^{17}), 2.47 - 2.58 (m, 2 H, $H^{2''}$, $H^{3''}$); ^{13}C NMR (126 MHz, *acetone*) δ ppm 152.76, 151.72, 149.34, 142.11, 138.41, 135.93, 134.98, 133.80, 119.98, 111.12, 105.58, 52.90, 30.56, 30.02, 28.83; IR $_{vmax}$ (cm^{-1})

(neat) 2987, 1586, 1417, 1325, 1257, 1220, 1173, 1084, 823, 713; HRMS (ESI+) m/z calcd. for ($C_{17}H_{21}S$) [M]+ 257.1358, found 257.1378.

8.2.32 2,2'-Bithiophene-5-carboxaldehyde (218)

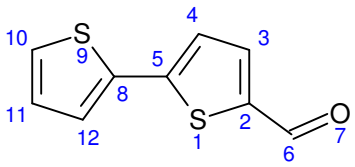

2,2'-Bithiophene (1.0 eq., 6.98 g, 42.0 mmol) was dissolved in dry DMF (40 mL). The solution was cooled to -10 °C (water ice / brine). Separately, $POCl_3$ (2.0 eq., 7.8 mL, 84.0 mmol) was diluted with dry DMF (20 mL) and the solution cooled to -10 °C (Vilsmeier reagent). The Vilsmeier reagent was added with stirring to the 2,2'-bithiophene solution at -10 °C. Once all of the Vilsmeier reagent had been added, the reaction flask was removed from the cold bath and allowed to warm to RT (30 minutes) before placing it into an oil bath and raising the temperature to 70 °C. Stirring was continued for a further two hours, at which point TLC indicated that the starting material was consumed. The flask was removed from the oil bath and allowed to cool to RT.

The reaction mixture was transferred to a separating funnel and ice added. The mixture was neutralised with 1M aqueous NaOH (~300 mL added), then extracted into diethyl ether. The combined ethereal extracts were washed with water, 5% LiCl solution and saturated brine, dried over $MgSO_4$, filtered and the solvent removed under reduced pressure. Purification was by flash chromatography, Si-gel eluted with ethyl acetate/petroleum ether (1:9 – 15:85).

Pale yellow crystalline solid (5.72 g, 29.5 mmol, yield=70%). ^{1}H NMR (500 MHz, *CHLOROFORM-d*) δ ppm 9.85 (s, 1 H), 7.66 (d, *J*=3.9 Hz, 1 H), 7.35 - 7.37 (m, 1 H), 7.35 (s, 1 H), 7.24 (d, *J*=3.9 Hz, 1 H), 7.07 (dd, *J*=4.9, 3.9 Hz, 1 H); ^{13}C NMR (126 MHz, *CHLOROFORM-d*) δ ppm 182.48, 147.11, 141.66, 137.25, 135.99, 128.31, 127.05, 126.11, 124.20; in agreement with literature data.[179]

8.2.33 2-([2,2'-Bithiophen]-5-yl)-5,5-dimethyl-1,3-dioxane (224)

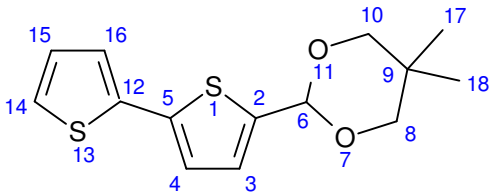

2,2'-Bithiophene-5-carboxaldehyde (**218**) (1.0 eq., 2.33 g, 12.0 mmol), neopentyl glycol (8.0 eq., 10.0 g, 96.0 mmol) and anhydrous oxalic acid (2.0 eq., 2.16 g, 24.0 mmol) were dissolved in dry acetonitrile (150 mL). The solution was stirred at RT for two hours. During stirring, there was a colour change from pale green to golden yellow.

The reaction mixture was neutralised with 1 M aq. NaOH (24.0 mL), diluted with water and extracted into diethyl ether/pentane (1:1). The combined extracts were washed with water and saturated brine, dried over $MgSO_4$, filtered and the solvent removed *in vacuo*. Purification was by recrystallisation from ethanol.

White crystalline solid (2.53 g, 9.0 mmol, yield=75%). Melting point 61-62 °C. ^{1}H NMR (500 MHz, *CHLOROFORM-d*) δ ppm 7.20 (dd, *J*=5.1, 1.2 Hz, 1 H), 7.16 (dd, *J*=3.7, 1.2 Hz, 1 H), 7.05 (d, *J*=3.4 Hz, 1 H), 7.03 (d, *J*=3.4 Hz, 1 H), 7.00 (dd, *J*=5.1, 3.7 Hz, 1 H), 5.61 (s, 1 H), 3.76 (dd, *J*=11.3, 1.5 Hz, 2 H),3.64 (d, *J*=10.8 Hz, 2 H), 1.29 (s, 3 H), 0.80 (s, 3 H); ^{13}C NMR (126 MHz, *CHLOROFORM-d*) δ ppm 140.17, 137.70, 137.32, 127.75, 125.67, 124.50, 123.84, 123.09, 98.15, 77.52, 30.19, 22.96, 21.81; IR $_{vmax}$ (cm^{-1}) (neat) 3120, 2951, 2853, 1469, 1380, 1308, 1216, 1201, 1186, 1089, 1013, 967, 801, 703; HRMS (ESI+) m/z calcd. for $(C_{14}H_{18}O_2S_{2+}H^+)^+$ 281.067, found 281.0667.

8.2.34 2-(5'-(5,5-Dimethyl-1,3-dioxan-2-yl)-[2,2'-bithiophen]-5-yl)-4,4,5,5-tetramethyl-1,3,2-dioxaborolane (226)

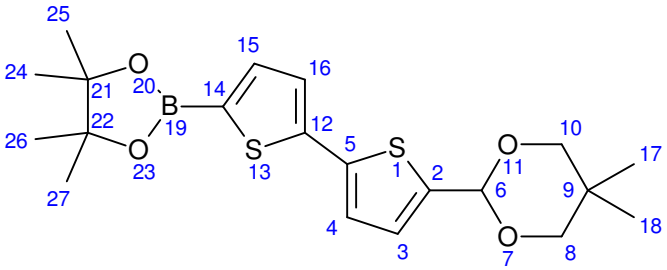

2-([2,2'-Bithiophen]-5-yl)-5,5-dimethyl-1,3-dioxane (**224**) (1.0 eq., 1.68 g, 6.0 mmol) was placed into a 100 mL round bottom flask. The flask was evacuated and back-filled with argon. Dry THF (18 mL) was added and stirred to dissolve **224**. The solution was cooled to -78 °C. n-BuLi (1.2 eq., 3.13 mL of 2.3 M soln., 7.2 mmol) was added dropwise with stirring at -78 °C, then stirred for a further 15 minutes at -78 °C. The flask was removed from the cold bath and allowed to warm to 0 °C. Stirring was continued for a further 30 minutes at 0 °C with a colour change to emerald green. The flask was cooled to -78 °C and 2-Isopropoxy-4,4,5,5-tetramethyl-1,3,2-dioxaborolane (ITDB) (1.2 eq., 1.34 g, 1.47 mL, 7.2 mmol) added dropwise with stirring at -78 °C. Stirring was continued for a further 10 minutes at -78 °C before removing the flask from the cold bath and allowing it to warm to RT.

The reaction mixture was diluted with water and then extracted into chloroform. The combined organic extracts were washed with water and saturated brine, filtered, dried over $MgSO_4$ and the solvent removed *in vacuo*.

Greyish green solid (1.903 g, 4.69 mmol, yield=78%). Melting point 164-166 °C. ^{1}H NMR (500 MHz, *CHLOROFORM-d*) δ ppm 7.51 (d, *J*=3.4 Hz), 7.22 (d, *J*=3.9 Hz), 7.10 (d, *J*=3.9 Hz), 7.03 (d, *J*=3.5 Hz), 5.61 (s), 3.76 (d, *J*=11.2 Hz), 3.64 (d, *J*=10.3 Hz), 1.34 (s), 1.28 (s), 0.80 (s); ^{13}C NMR (126 MHz, *CHLOROFORM-d*) δ ppm 144.03, 140.83, 137.89, 137.53, 125.79, 125.06, 123.78, 98.09, 84.15, 77.51, 30.20, 24.75, 22.95, 21.82; IR $_{vmax}$ (cm^{-1}) (neat) 2956, 1527, 1444, 1354, 1270, 1140, 1095, 1017, 852, 801, 666; HRMS (ESI+) m/z calcd. for $(C_{20}H_{27}BO_4S_{2+}H^+)^+$ 407.1522, found 407.1536.

8.2.35 5'-(Azulen-1-yl)-[2,2'-bithiophene]-5-carboxaldehyde (229)

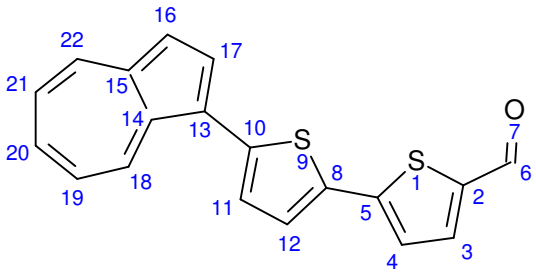

1-(Azulen-1-yl)tetrahydrothiophenium hexafluorophosphate (**207**) (1.0 eq., 1.08 g, 3.0 mmol), 2-(5'-(5,5-dimethyl-1,3-dioxan-2-yl)-[2,2'-bithiophen]-5-yl)-4,4,5,5-tetramethyl-1,3,2-dioxaborolane (**226**) (1.33 equ., 1.624 g, 4.0 mmol), palladium acetate (4 mol%, 27 mg, 0.12 mmol), SPhos (10 mol%, 123 mg, 0.3 mmol) and potassium phosphate (2 eq., 1.272 g, 6.0 mmol) were placed into a 50 mL round bottom flask. The flask was evacuated and back-filled with argon. Degassed propan-2-ol (18 mL) was added and the mixture stirred. The flask was placed into an oil bath and the temperature raised to 75 °C. After stirring at 75 °C for 75 minutes the starting material had been consumed by TLC. The flask was removed from the oil bath and allowed to cool to RT.

The solvent was removed under reduced pressure. The residue was extracted into diethyl ether. After filtering the combined ethereal extract was washed with water and saturated brine, then the solvent was removed under reduced pressure.

The residue was dissolved in a mixture of acetone and water (9:1, 30 mL) and catalytic p-TSA was added (~20 mg). The flask was placed into an oil bath at 40 °C and stirred for 7 hours when TLC indicated that the starting material had been consumed. The flask was removed from the oil bath and allowed to cool to RT.

After neutralising the reaction mixture with saturated sodium bicarbonate, the acetone was removed under reduced pressure. The remaining aqueous suspension was partitioned between chloroform and water (the product had poor solubility in diethyl ether). The organic layer was washed with water and saturated brine, dried over $MgSO_4$ then filtered. The solvent was removed under reduced pressure. Purification was by flash chromatography, Si-gel eluted with petroleum ether/DCM (3:1 – 1:3).

Dark green gum (green in ethyl acetate/petroleum ether solution but red in DCM) (625 mg, 1.95 mmol, yield=65%). ^{1}H NMR (500 MHz, *CHLOROFORM-d*) δ ppm 9.87 (s, 1 H), 8.77 (d, *J*=9.8 Hz, 1 H), 8.33 (d, *J*=9.3 Hz, 1 H), 8.07 (d, *J*=3.9 Hz, 1 H), 7.68 (d, *J*=3.9 Hz, 1 H), 7.64 (t, *J*=9.8 Hz, 1 H), 7.43 (d, *J*=3.9 Hz, 1 H), 7.41 (d, *J*=4.4 Hz, 1 H), 7.28 (d, *J*=3.9 Hz, 1 H), 7.26 (d, *J*=3.9 Hz, 1 H), 7.21 (t, *J*=9.5 Hz, 1 H); ^{13}C NMR (126 MHz, *CHLOROFORM-d*) δ ppm 182.36, 142.90, 142.04, 141.11, 138.90, 137.68, 137.50, 136.98, 135.64, 134.28, 127.03, 125.40, 124.32, 124.29, 123.54, 122.52, 118.28; IR $_{vmax}$ (cm^{-1}) (neat) 2785, 1647, 1570, 1472, 1393, 1223, 1045, 785, 735, 666; HRMS (ESI+) m/z calcd. for $(C_{19}H_{12}OS_2+Na^+)^+$ 343.02273, found 343.0216; R_f (EtOAc/Petrol 3:7) 0.38.

8.2.36 5'-(4,6,8-Trimethylazulen-1-yl)-[2,2'-bithiophene]-5-carboxaldehyde (230)

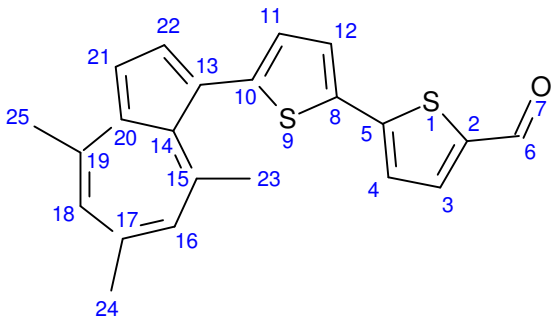

1-(4,6,8-Trimethylazulen-1-yl)tetrahydrothiophenium hexafluorophosphate (**210**) (1.0 eq., 402 mg, 1.0 mmol), 2-(5'-(5,5-dimethyl-1,3-dioxan-2-yl)-[2,2'-bithiophen]-5-yl)-4,4,5,5-tetramethyl-1,3,2-dioxaborolane (**226**) (1.25 eq., 508 mg, 1.25 mmol), palladium acetate (4 mol%, 9.0 mg, 0.04 mmol), SPhos (10 mol%, 41.0 mg, 0.1 mmol) and potassium phosphate (2.0 eq., 424 mg, 2.0 mmol) were placed into a 25 mL round bottom flask. The flask was evacuated and back-filled with argon. Degassed propan-2-ol (6 mL) was added and the mixture stirred. The flask was placed into an oil bath and the temperature raised to 75 °C. After stirring at 75 °C for 55 minutes the starting material had been consumed by TLC. The flask was removed from the oil bath and allowed to cool to RT.

The solvent was removed under reduced pressure. The residue was extracted into diethyl ether. After filtering the combined ethereal extract was washed with water and saturated brine, then the solvent was removed under reduced pressure.

The residue was dissolved in a mixture of acetone and water (9:1, 10 mL) and catalytic p-TSA was added (~10 mg). The flask was placed into an oil bath at 35 °C and stirred for two hours when TLC indicated that the starting material had been consumed. The flask was removed from the oil bath and allowed to cool to RT.

After neutralising the reaction mixture with saturated sodium bicarbonate, the acetone was removed under reduced pressure. The remaining aqueous suspension was partitioned between diethyl ether and water. The ethereal layer was washed with water and saturated brine, dried over $MgSO_4$ then filtered. The solvent was removed under reduced pressure. Purification was by flash chromatography, Si-gel eluted with ethyl acetate/petroleum ether (1:19 – 15:85).

Grey/black solid (rust-red colour in solution) (215 mg, 0.59 mmol. Yield=59%). Melting point 147-150 °C. ^{1}H NMR (500 MHz, *CHLOROFORM-d*) δ ppm 9.86 (s, 1 H), 7.67 (1H, d, *J*=4.4 Hz), 7.66 (1H, d, *J*=4.3 Hz), 7.36 (d, *J*=3.9 Hz, 1 H), 7.34 (d, *J*=3.4 Hz, 1 H), 7.25 (d, *J*=4.4 Hz, 1 H), 7.12 (s, 1 H), 7.07 (s, 1 H), 6.88 (d, *J*=3.4 Hz, 1 H), 2.91 (s, 3 H), 2.71 (s, 3 H), 2.63 (s, 3 H); ^{13}C NMR (126 MHz, *CHLOROFORM-d*) δ ppm 182.42, 147.85, 147.78, 146.99, 146.41, 145.96, 141.06, 138.15, 137.48, 137.35, 135.16, 132.69, 130.00, 129.18, 128.10, 125.87, 123.57, 121.86, 115.16, 28.49, 27.94, 25.58; IR $_{vmax}$ (cm^{-1}) (neat) 3095, 2806, 1650, 1577, 1442, 1224, 1049, 842, 797, 662; HRMS (ESI+) m/z calcd. for $(C_{22}H_{18}OS_2+H^+)^+$ 363.08773, found 363.084; R_f 0.44 (EtOAc/Petrol 3:7).

8.2.37 5'-(3-(*tert*-Butyl)azulen-1-yl)-[2,2'-bithiophene]-5-carboxaldehyde (231)

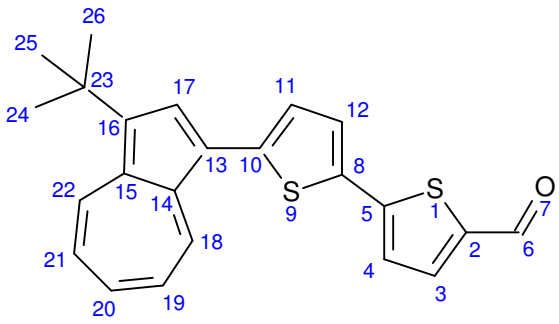

1-(3-*tert*-Butylazulen-1-yl)tetrahydrothiophenium hexafluorophosphate (**162**) (1.0 eq., 998 mg, 2.4 mmol), 2-(5'-(5,5-dimethyl-1,3-dioxan-2-yl)-[2,2'-bithiophen]-5-yl)-4,4,5,5-tetramethyl-1,3,2-dioxaborolane (**226**) (1.25 equ., 1.218 g, 3.0 mmol), palladium acetate (4 mol%, 22.0 mg, 0.096 mmol), SPhos (10 mol%, 99.0 mg, 0.24 mmol) and potassium phosphate (2.0 eq., 1.018 g, 4.8 mmol) were placed into a 50 mL round bottom flask. The flask was evacuated and back-filled with argon. Degassed propan-2-ol (22 mL) was added and the mixture stirred. The flask was placed into an oil bath and the temperature raised to 75 °C. After stirring at 75 °C for 35 minutes the starting material had been consumed by TLC. The flask was removed from the oil bath and allowed to cool to RT.

The solvent was removed under reduced pressure. The residue was extracted into diethyl ether. After filtering the combined ethereal extract was washed with water and saturated brine, then the solvent was removed under reduced pressure.

The residue was dissolved in a mixture of acetone and water (9:1, 10 mL) and catalytic p-TSA was added (~20 mg). The flask was placed into an oil bath at 35 °C and stirred for two hours when TLC indicated that the starting material had been consumed. The flask was removed from the oil bath and allowed to cool to RT.

After neutralising the reaction mixture with saturated sodium bicarbonate, the acetone was removed under reduced pressure. The remaining aqueous suspension was partitioned between diethyl ether and water. The ethereal layer was washed with water and saturated brine, dried over $MgSO_4$ then filtered. The solvent was removed under reduced pressure. Purification was by flash chromatography, Si-gel eluted with ethyl acetate/petroleum ether (1:19 – 15:85).

Red solid (green in solution) (736 mg, 1.96 mmol, yield=82%). Melting point 95-97 °C. ^{1}H NMR (500 MHz, *CHLOROFORM-d*) δ ppm 9.87 (s, 1 H), 8.69 (d, *J*=9.8 Hz, 1 H), 8.65 (d, *J*=9.8 Hz, 1 H), 7.97 (s, 1 H), 7.69 (d, *J*=3.9 Hz, 1 H), 7.57 (t, *J*=9.8 Hz, 1 H), 7.43 (d, *J*=3.9 Hz, 1 H), 7.28 (d, *J*=3.9 Hz, 1 H), 7.24 (d, *J*=3.9 Hz, 1 H), 7.14 (t, *J*=9.5 Hz, 1 H), 7.12 (t, *J*=9.8 Hz, 1 H), 1.62 (s, 9 H); ^{13}C NMR (126 MHz, *CHLOROFORM-d*) δ ppm 182.35, 147.76, 142.21, 141.03, 139.50, 138.69, 137.81, 137.53, 136.49, 136.24, 135.79, 135.33, 134.17, 127.01, 125.42, 123.63, 123.47, 122.49, 120.33, 33.27, 32.01; IR $_{vmax}$ (cm^{-1}) (neat) 2949, 1675, 1666, 1569, 1459, 1441, 1363, 1225, 1050, 869, 801, 789, 727, 668; HRMS (ESI+) m/z calcd. for $(C_{23}H_{20}OS_2+H^+)^+$ 377.10338, found 377.1015; Rf 0.59 (EtOAc/Petrol 3:7).

8.2.38 5'-(3-(Methylthio)azulen-1-yl)-[2,2'-bithiophene]-5-carboxaldehyde (232)

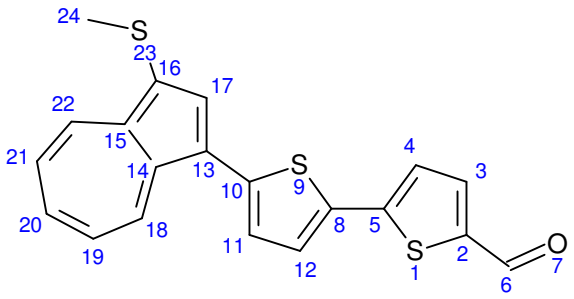

5'-(Azulen-1-yl)-[2,2'-bithiophene]-5-carboxaldehyde (**229**) (1.0 eq., 272 mg, 0.85 mmol) was placed into a 50 mL round bottom flask. The flask was evacuated and back-filled with argon. Dry DCM (3.5 mL) was added followed by dry DMSO (XS, 0.93 mL, 13.0 mmol). The flask was placed into a water ice/ brine bath and cooled to 0 °C.

Separately, a 0.25 M solution of triflic anhydride (0.42 mL, 2.5 mmol) in dry DCM (9.58 mL) was prepared.

The triflic anhydride solution was added dropwise to the reaction solution with stirring at 0 °C until TLC indicated that the starting material had been consumed (4.0 mL of solution added, 1.0 mmol=1.18 eq.). The solvent was removed under reduced pressure.

A mixture of ethanol/triethylamine (1:1, 20 mL) was added. The flask was fitted with a reflux condenser and placed into an oil bath. The reaction was refluxed with stirring for 30 minutes, then removed from the oil bath and allowed to cool to RT. The solvent was removed under reduced pressure.

The residue was dissolved in diethyl ether and partitioned with water. The ethereal layer was washed with water and saturated brine, dried over $MgSO_4$, filtered and the solvent removed under reduced pressure. Purification was by flash chromatography, silica gel eluted with ethyl acetate/petroleum ether (1:9).

Dark red/brown solid (91 mg, 0.249 mmol, yield=29%). Melting point 122-123 °C. ^{1}H NMR (500 MHz, *CHLOROFORM-d*) δ ppm 9.87 (s, 1 H), 8.68 (d, *J*=9.3 Hz, 1 H), 8.58 (d, *J*=9.3 Hz, 1 H), 8.08 (s, 1 H), 7.69 (d, *J*=3.9 Hz, 1 H), 7.64 (t, *J*=10.0 Hz, 1

H), 7.43 (d, *J*=3.9 Hz, 1 H), 7.28 (d, *J*=4.4 Hz, 1 H), 7.20 - 7.27 (m, 3 H, overlapping peaks), 2.53 (s, 3 H); ^{13}C NMR (126 MHz, *CHLOROFORM-d*) δ ppm 182.38, 147.44, 141.25, 141.05, 140.83, 139.85, 138.92, 137.47, 136.48, 136.28, 135.93, 127.00, 125.71, 124.87, 124.39, 123.67, 122.81, 121.83, 110.01, 20.03; IR_{vmax} (cm^{-1}) (neat) 3073, 2920, 2814, 1626, 1571, 1461, 1237, 800. HRMS (ESI+) m/z calcd. for $(C_{20}H_{14}OS_3+H^+)^+$ 389.01045, found 389.0095; R_f 0.53 (EtOAc/Petrol 3:7).

8.2.39 3-(5'-(Azulen-1-yl)-[2,2'-bithiophen]-5-yl)-2-cyanoacrylic acid – Az-1-ttcaa (212)

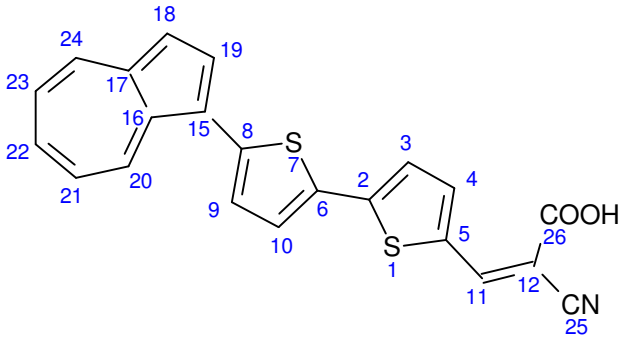

5'-(Azulen-1-yl)-[2,2'-bithiophene]-5-carboxaldehyde (**229**) (1.0 eq., 248 mg, 0.775 mmol), cyanoacetic acid (1.5 eq., 99.0 mg, 1.625 mmol) and 6-aminocaproic acid (1.0 eq., 102 mg, 0.775 mmol) were dissolved in ethanol (4.7 mL). The flask was placed in an oil bath and the temperature raised to 50 °C. Stirring was continued at 50 °C for five hours, when TLC indicated no further reaction. The flask was removed from the oil bath and allowed to cool to RT. Aq. sulfuric acid (1 M, 8.0 mL) was added to precipitate the product which was removed by filtration and washed with water and ice cold ethanol. Purification was by recrystallisation from propan-2-ol/water.

Dark green-grey solid (150 mg, 0.39 mmol, yield=50%). Melting point 244-245 °C. ^{1}H NMR (500 MHz, *DMSO-d*$_6$) δ ppm 8.78 (d, *J*=10.3 Hz, 1 H), 8.45 (s, 1 H), 8.43 (d, *J*=9.3 Hz, 1 H), 8.18 (d, *J*=3.9 Hz, 1 H), 7.95 (d, *J*=4.4 Hz, 1 H), 7.75 (t, *J*=9.8 Hz, 1 H), 7.67 (d, *J*=3.4 Hz, 1 H), 7.58 (d, *J*=3.9 Hz, 1 H), 7.51 (d, *J*=3.9 Hz, 1 H), 7.46 (d, *J*=4.4 Hz, 1 H), 7.37 (t, *J*=9.8 Hz, 1 H), 7.30 (t, *J*=9.5 Hz, 1 H); ^{13}C NMR (126 MHz, *DMSO-d*$_6$) δ ppm 163.73, 146.40, 146.19, 142.84, 141.76, 141.52, 139.64, 138.15, 136.82, 135.58, 133.97, 133.40, 132.92, 128.23, 126.04, 125.03, 124.96, 124.49, 121.54, 118.71, 116.68, 97.30; IR_{vmax} (cm^{-1}) (neat) 2209, 1674, 1562, 1494, 1412, 1257, 1202, 1148, 1058, 806, 784, 730; HRMS (ESI+) m/z calcd. for $(C_{22}H_{13}NO_2S_2+H^+)^+$ 388.0466, found 388.0455; R_f 0.21 (EtOAc/Petrol 3:7).

8.2.40 3-(5'-(4,6,8-Trimethylazulen-1-yl)-[2,2'-bithiophen]-5-yl)-2-cyanoacrylic acid - TMAz-1-ttcaa (213)

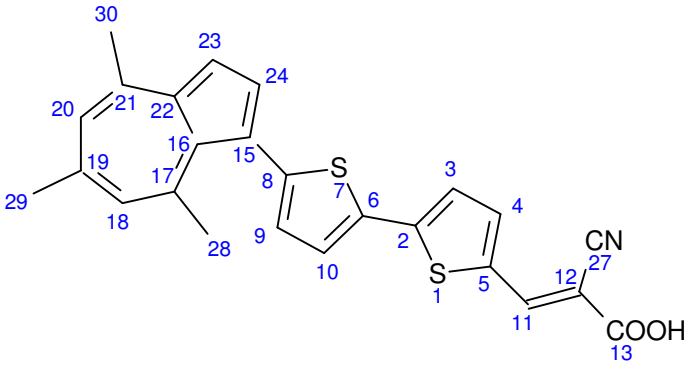

5'-(4,6,8-Trimethylazulen-1-yl)-[2,2'-bithiophene]-5-carboxaldehyde (**230**) (1.0 eq., 217 mg, 0.6 mmol), cyanoacetic acid (1.5 eq., 77.0 mg, 0.9 mmol) and 6-amonocaproic acid (1.0 eq., 79.0 mg, 0.6 mmol) were dissolved in ethanol (3.6 mL). The flask was placed into an oil bath and the temperature raised to 50 °C. Stirring was continued at 50 °C for five hours, when TCL indicated that the starting material had been consumed. Aq. sulfuric acid (1 M, 7 mL) was added to precipitate the product which was removed by filtration then washed with water and ice cold ethanol. Purification was by recrystallisation from hot ethanol.

Dark grey powder (72 mg, 0.17 mmol, yield=28%). Melting point 264-265 °C. ^{1}H NMR (500 MHz, *DMSO-d*$_6$) δ ppm 8.48 (s, 1 H), 7.98 (d, *J*=4.4 Hz, 1 H), 7.62 (d, *J*=3.9 Hz, 1 H), 7.59 (d, *J*=3.4 Hz, 1 H), 7.57 (d, *J*=3.9 Hz, 1 H), 7.36 (d, *J*=3.9 Hz, 1 H), 7.23 (s, 1 H), 7.15 (s, 1 H), 7.01 (d, *J*=3.9 Hz, 1 H), 2.86 (s, 3 H), 2.65 (s, 3 H), 2.61 (s, 3 H); ^{13}C NMR (126 MHz, *DMSO-d*$_6$) δ ppm 164.10, 147.81, 147.72, 146.87, 146.59, 145.70, 142.03, 138.31, 137.43, 134.54, 133.95, 132.52, 130.37, 130.31, 128.57, 127.42, 125.02, 121.66, 117.03, 115.90, 98.06, 28.30, 27.82; IR_{vmax} (cm^{-1}) (neat) 2219, 1671, 1567, 1509, 1410, 1288, 1252, 1216, 1193, 1057, 852, 795, 778, 717; HRMS (ESI+) m/z calcd. for $(C_{25}H_{19}NO_2S_2+H^+)^+$ 430.09355, found 430.1031; R_f 0.23 (EtOAc/Petrol 3:7).

8.2.41 3-(5'-(3-Methylthioazulen-1-yl)-[2,2'-bithiophen]-5-yl)-2-cyanoacrylic acid - MeTAz-1-ttcaa (214)

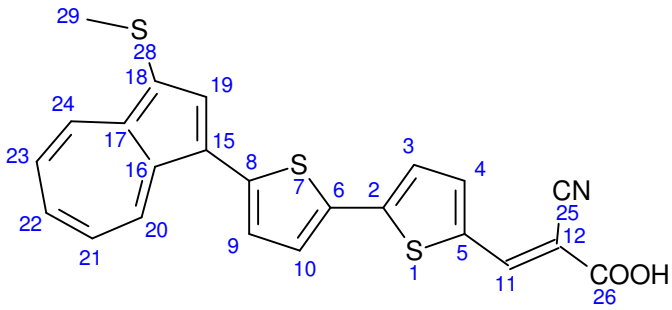

5'-(3-(Methylthio)azulen-1-yl)-[2,2'-bithiophene]-5-carboxaldehyde (**232**) (1.0 eq., 299 mg, 0.82 mmol), cyanoacetic acid (1.5 eq., 162 mg, 1.23 mmol) and 6-aminocaproic acid (1.0 eq., 108 mg, 0.82 mmol) were dissolved in ethanol (5 mL). The flask was placed into an oil bath and the temperature raised to 70 °C.

It became apparent that 5 mL of solvent wasn't sufficient to dissolve the starting materials, so additional ethanol (2 x 5 mL) was added.

In an attempt to drive the reaction to completion, additional cyanoacetic acid (156 mg, 1.84 mmol) and 6-aminocaproic acid (54 mg, 0.41 mmol) were added after stirring for two hours at 70 °C. After stirring for a total of 5.5 hours at 70 °C TCL indicated that most of the starting material had been consumed. The flask was removed from the oil bath and allowed to cool to RT. Aq. sulfuric acid (1M, 10 mL) was added to precipitate the product which was removed by filtration then washed with water and ice cold ethanol. Purification was by recrystallisation from acidified acetone (with 1M sulfuric acid).

Green/black crystalline solid (216 mg, 0.5 mmol, yield=61%). Melting point 236-237 °C with decomposition. ^{1}H NMR (500 MHz, *DMSO-d*$_6$) δ ppm 8.73 (d, *J*=9.8 Hz, 1 H), 8.49 (s, 1 H), 8.43 (d, *J*=9.3 Hz, 1 H), 8.29 (s, 1 H), 8.00 (d, *J*=3.9 Hz, 1 H), 7.77 (t, *J*=10.0 Hz, 1 H), 7.73 (d, *J*=3.9 Hz, 1 H), 7.63 (d, *J*=4.4 Hz, 1 H), 7.58 (d, *J*=3.9 Hz, 1 H), 7.36 (t, *J*=9.8 Hz, 1 H), 7.33 (t, *J*=9.8 Hz, 1 H), 2.57 (s, 3 H); ^{13}C NMR (126 MHz, *DMSO-d*$_6$) δ ppm 163.66, 146.37, 145.99, 141.73, 140.63, 140.41, 139.55, 137.43, 135.98, 135.83, 135.08, 133.47, 133.26, 128.16, 126.50, 125.41, 124.72, 124.56, 122.94, 121.03, 116.59, 97.37, 18.34; IR_{vmax} (cm^{-1}) (neat) 2915, 2218, 1656, 1563, 1496, 1397, 1370, 1271, 1253, 1206, 1149, 932, 808, 745;

HRMS (ESI+) m/z calcd. for $(C_{23}H_{15}NO_2S_3+H^+)^+$ 434.03432, found 434.0351; R_f 0.12 (EtOAc/Petrol 3:7).

8.2.42 3-(5'-(3-*tert*-Butylazulen-1-yl)-[2,2'-bithiophen]-5-yl)2-cyanoacrylic acid - tBuAz-1-ttcaa (215)

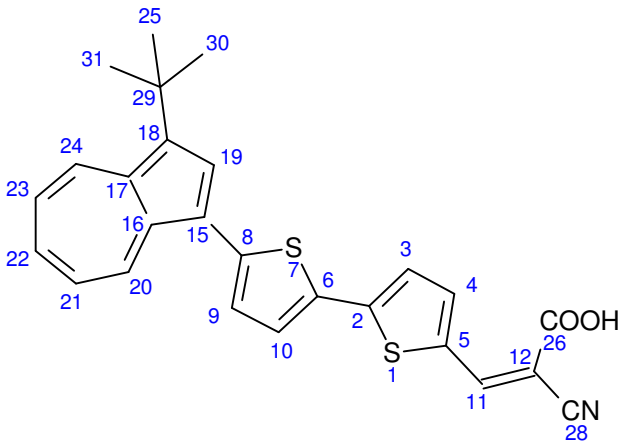

5'-(3-(*tert*-Butyl)azulen-1-yl)-[2,2'-bithiophene]-5-carboxaldehyde (**231**) (1.0 eq., 512 mg, 1.373 mmol), cyanoacetic acid (1.5 eq., 175 mg, 2.06 mmol) and 6-aminocaproic acid (1.0 eq., 181 mg, 1.373 mmol) were dissolved in ethanol (8.25 mL). The flask was placed into an oil bath and the temperature raised to 50 °C. Stirring was continued at 50 °C for three hours, when TCL indicated that the starting material had been consumed. Aq. sulfuric acid (1 M, 13 mL) was added to precipitate the product which was removed by filtration then washed with water and ice cold ethanol. Purification was by recrystallisation from hot propan-2-ol/water.

Green/black crystalline solid (328 mg, 0.74 mmol, yield=54%). Melting point 246-247 °C. ^{1}H NMR (500 MHz, *DMSO-d*$_6$) δ ppm 8.72 (t, *J*=9.5 Hz, 2 H), 8.48 (s, 1 H), 8.05 (s, 1 H), 7.99 (d, *J*=4.4 Hz, 1 H), 7.67 - 7.74 (m, 2 H), 7.62 (d, *J*=3.9 Hz, 1 H), 7.52 (d, *J*=3.9 Hz, 1 H), 7.22 - 7.31 (m, 2 H), 1.57 (s, 9 H); ^{13}C NMR (126 MHz, *DMSO-d*$_6$) δ ppm 163.69, 146.34, 146.20, 141.76, 141.52, 139.35, 139.06, 137.62, 136.83, 135.29, 135.17, 135.10, 133.32, 132.79, 128.17, 126.06, 124.39, 124.30, 123.44, 119.28, 116.64, 97.25, 32.85, 31.68; IR_{vmax} (cm^{-1}) (neat) 2960, 2214, 1678, 1567, 1403, 1363, 1315, 1277, 1255, 1207, 1156, 1085, 1056, 930, 869, 802, 728; HRMS (ESI+) m/z calcd. for $(C_{26}H_{21}NO_2S_2+H^+)^+$ 444.1092, found 444.1094; R_f 0.15 (EtOAc/Petrol 3:7).

8.3 Electrochemistry – Cyclic Voltammetry General Method

Cyclic voltammagrams (CVs) were taken using a Metrohm Autolab Potentiostat/Galvanostat connected to a three-electrode cell. Boron doped diamond working-, platinum foil counter- and platinum wire pseudo reference electrodes were used. All CVs were referenced to the ferrocene/ferrocenium (Fc/Fc^+) redox couple as an internal reference.

All CVs were taken in dry THF which was degassed by sparging with argon for one hour to remove dissolved oxygen prior to making up solutions. The supporting electrolyte was 0.1 M tetrabutylammonium hexafluorophosphate (Bu_4NPF_6) which was used as received from the vendor (Sigma-Aldrich) without further purification.

A typical procedure was as follows:

A four-necked heart-shaped glass flask ("electrochemical cell" or "cell") was sequentially cleaned with THF and acetone then dried using a heat gun. The working electrode was cleaned in THF and acetone then polished with fine alumina paste, rinsed with deionised water and acetone and air dried. The platinum counter- and reference electrodes were cleaned with THF and acetone, dried and then heated to glowing in a Bunsen burner flame to remove any residual organic material. The working and counter electrodes were inserted through holes drilled into rubber septa which in turn were inserted into the cell with one electrode/septum in each of two necks. The platinum wire reference electrode was inserted into a third neck and held in place with a stopper. The fourth neck was stoppered after purging the cell with argon, and used to add/remove solutions to/from the cell with a syringe.

A 0.1 M solution of Bu_4NPF_6 in dry, degassed THF was prepared ("stock solution"). Some of the stock solution was then used to prepare a 1 mM solution of the dye to be analysed ("dye solution"). A 25 mM solution of ferrocene in dry THF was prepared for the internal reference ("reference solution").

The cell was charged with 24 mL of stock solution which was enough to ensure that the electrodes were sufficiently covered. The solution in the cell was sparged briefly with argon. Background CVs were taken at a scan rate of 100 $mV.s^{-1}$ and a variety of potential ranges. 12 mL of solution was then removed from the cell and replaced with 12 mL of dye solution, resulting in 24 mL of 0.5 mM dye in stock solution. After

sparging briefly with argon, CVs were taken at a variety of potential ranges. Finally, 0.5 mL of reference solution was added to the cell, resulting in 0.5 mM ferrocene solution, and a CV taken for the internal reference.

8.4 Dye Sensitised Solar Cell Construction, General Method

Fluorinated Tin Oxide (FTO) coated glass was cleaned in a sonicator using a sequential multi-step process of washing in Decon 90 solution, rinsing in deionised water and cleaning in 2-propanol then ethanol. This procedure ensured that the FTO glass surface was free from dirt, grease and ionic contamination.

During solar cell construction it is important to keep the FTO glass and all equipment as clean as possible to prevent contamination, particularly with grease and iron salts, which could interfere with film fabrication or dyeing and impact on cell performance.

8.4.1 Working Electrode (Anode)

FTO glass was cut into strips 7.5 cm x 2.5 cm and cleaned with Decon 90 solution, deionised water, 2-propanol and ethanol in a sonicator.

A blocking layer was applied by spray pyrolysis using a hand-held atomiser. A solution of 0.2 M titanium di-isopropoxide bis(acetylacetonate) in 2-propanol was sprayed in short bursts onto the FTO glass strips on a hotplate at 450 ^{o}C. Part of the FTO glass strips were masked with a microscope slide so that the FTO under the mask was left unblocked. The unblocked areas enable external electrical connections to be made to the finished cells.

A film of mesoporous titanium dioxide was deposited in a 1 cm wide strip on top of the blocking layer. A single thickness (approximately 60 µm) of Scotch Magic tape was used as a mask and the titanium dioxide paste (Dyesol) was applied by doctoring with a glass rod. The freshly coated FTO glass was placed in ethanol vapour for 30 seconds; a small quantity of ethanol is absorbed and causes the films to flow slightly, smoothing the surface. The films were then dried on a hotplate at approximately 100 ^{o}C before sintering in air at 500 ^{o}C for 30 minutes.

After cooling, the FTO glass strips were cut into 1½ x 2½ cm tiles. The mesoporous titanium dioxide films were then dyed at room temperature in a 0.3 mM solution of

the dye in an appropriate solvent. After dying, the films were rinsed in the same solvent and then allowed to dry. The dyed mesoporous films were then trimmed by scraping away excess film to leave a 1 cm^2 square of dyed film in the centre of the electrode.

8.4.2 Counter Electrode (Cathode)

FTO glass was cut into 1½ x 2½ cm tiles. Two cell filling holes were drilled in each tile so as to be positioned within the 1 cm^2 active cell area and the tiles were cleaned using the procedure described above.

A thin, transparent platinum coating was deposited on to the FTO by applying two drops of platinum solution, drying and then baking in air at 390 ^oC for 15 minutes. The platinum coating on the counter electrode catalyses the reduction of tri-iodide (I_3^-) to iodide (I^-) in the solar cell.

8.4.3 Cell Assembly

A 1½ x 1½ cm gasket of Suryln film with a 1 x 1 cm hole was placed on a working electrode so that the gasket surrounded the 1 x 1 cm dyed mesoporous film. The electrode with gasket was placed on a hotplate to soften the Surlyn and a counter electrode was placed on top, ensuring that the platinum coated side was face down and that the drilled filling holes were correctly positioned. Pressure was then applied to seal the cell with the softened Surlyn gasket, ensuring that a good seal was made (ie no air gaps) around the entire cell perimeter. The cell was then removed from the hotplate.

After cooling, the cells were filled with I^-/I_3^- electrolyte by placing a drop of electrolyte on each of the filling holes. The electrolyte can be seen to fill the cell by capillary action. After wiping away any excess electrolyte the cells were sealed by placing a 1 x 1 cm square of Surlyn (created as a by-product when making the Surlyn sealing gasket) over the counter electrode so that the filling holes were covered, then placing a square of slide cover glass over it and applying light pressure with a hot press to soften the Surlyn square. Care must be taken not to overheat the electrolyte while ensuring that the cell is properly sealed.

To make electrical contacts to the sealed cell, conductive sticky-backed copper tape was applied to the exposed FTO areas of the two electrodes or the exposed FTO was painted with silver-loaded (conductive) paint.

9 References

[1] REN21, Renewables 2011: Global Status Report, **2011**, p17,18

[2] European Photovoltaic Industry Association, *Market Report 2011*, **2012**

[3] Smil, V., *General Energetics Energy in the Biosphere and Civilization*. John Wiley, New York, **1991**, 240

[4] Morton O,. *Nature*, **2006**, 443, 19-22

[5] Streetman B.G., *Solid State Electronic Devices*, Prentice-Hall Inc., **1980**, ch. 3

[6] Dilly Z., **2009,** *Intrinsic and Extrinsic Semiconductors, Fermi-Dirac Distribution Function, the Fermi level and carrier concentrations*, [ONLINE] Available at: www.eng.umd.edu/~dilli/courses/enee313_spr09/files/supplement1_carrierconc.pdf, [Accessd 4 July 2016]

[7] Hagfeldt A., Boschloo G., Sun L., Kloo L., Pettersson H., *Chem. Rev.*, **2010**, 110, 6595-6663

[8] Repins I., Contreras M., Romero M., Yan Y., Metzger W., Li J., Johnston S., Egass B., DeHart C., Scharf J., McCandless B.E., Noufi R., *Characterization of 19.9%-Efficient CIGS Absorbers*, National Renewable Energy Laboratory, **2008**

[9] Shockley W., Queisser H.J., *J. Appl. Phys.*, **1961**, 32, 510

[10] Peter L.M., *Phys. Chem. Chem. Phys.*, **2007**, 9, 2630-2642

[11] Gurney R.W., Mott N.F, *Proc. R. Soc. Lond. A*, **1938**, 164, 151-167

[12] Zollinger H., *Color Chemistry*, Verlag Helvetica Chimica Acta AG & Wiley-VCH GmbH & Co., **2003**, 505

[13] Kuhn H. in Berg F.W., Mazzucato U., Meier G., Semerano G. (Eds), *Dye Sensitization*, Focal, London, **1970**, 199

[14] Tsubomura H., Matsamura M., Noyamura Y., Amamyiaya T., *Nature*, **1976**, 261, 402

[15] O'Regan B., Grätzel M., *Nature*, **1991**, 353, 737–740

[16] Grätzel M., *C. R. Chim.*, **2006**, 9, 578–583

[17] Chiba Y., Islam A., Watanabe Y., Komiya R., Koide N., Han L., *Jpn. J. Appl. Phys.*, **2006**, 45, L638

[18] Gao F., Wang Y., Shi D., Zhang J., Wang M., Jing X., Humphrey-Baker R., Wang P., Zakeeruddin S.M., Grätzel M., *J. Am. Chem. Soc.*, **2008**, 130, 10720

[19] Chen C.Y., Wang M., Li J.Y., Pootrakulchote N., Alibabaei L., Ngoc-le C.H., Decoppet J.D., Tsai J.H., Grätzel C., Wu C.G., Zakeeruddin S.M., Grätzel M., *ACS Nano*, **2009**, 3, 3103

[20] Bessho T., Yonada E., Yum J.H., Guglielmi M., Tavernelli I., Imai H., Rothlisburger U., Nazeeruddin M.K., Grätzel M., *J. Am. Chem. Soc.*, **2009**, 131, 5930

[21] Chou C.C., Wu K.L., Chi Y., Hu W.P., Yu S.J., Lee G.H., Lin C.L., Chou P.T., *Angew. Chem. Int. Ed.*, **2011**, 50, 2054

[22] Nazeeruddin M.K., Kay A., Rodicio I., Humphry-Baker R., Mueller E., Liska P., lachopoulos N., Grätzel M., *J. Am. Chem. Soc.,* **1993**, 115, 6382

[23] Grätzel M., *J. Photochem. Photobiol. A.,* **2004**, 164, 3-14

[24] Nazeeruddin M.K., Zakeeruddin S.M., Humphrey-Baker R., Jirousek M., Liska P., Vlachopoulos N., Shklover V., Fischer C.H., Grätzel M., *Inorg. Chem.*, **1999**, 38, 6298

[25] Zakeeruddin S.M., Pechy P., Renouard T., Humphry-Baker R., Comte P., Liska P., Cevey L., Costa E., Shklover V., Spiccia L., Deacon G.B., Bignozzi C. A., Grätzel M., *J. Am. Chem. Soc.*, **2001**, 123, 1613

[26] Ito S., Miura H., Uchida S., Takata M., Sumioka K., Liska P., Comte P., Pechy P., Grätzel M., *Chem. Commun.*, **2008**, 5194-5196

[27] Zeng W., Cao Y., Bai Y., Wang Y., Shi Y., Zhang M., Wang F., Pan C., Wang P., *Chem. Mater.*, **2010**, 22, 1915

[28] Bessho T., Zakeeruddin S.M., Yeh C.Y., Diau E. W.-G., Grätzel M., *Angew. Chem., Int. Ed.*, **2010**, 49, 6646

[29] Yella A., Lee H.W., Tsao H.N., Yi C., Chandiran A.K., Nazeeruddin M.K., Diau E.W.G., Yeh C.Y., Zakeeruddin S.M., Grätzel M., *Science*, **2011**, 334, 629

[30] Xu M., Zhou D., Cai N., Liu J., Li R., Wang P., *Energy Environ. Sci.*, **2011**, 4, 4735

[31] Yella A., Lee H.W., Tsao H.N., Yi C., Chandiran A.K., Nazeeruddin M.K., Diau E.W.G., Yeh C.Y., Zakeeruddin S.M., Grätzel M., *Science*, **2011**, 334, 629

[32] Daeneke T., Kwon T.H., Holmes A.B., Duffy N.W., Bach U., Spiccia L., *Nat. Chem.*, **2011**, 3, 211

[33] Cherian S., Wamser C.C., *J. Phys. Chem. B*, **2000**, 104, 3624

[34] Wang Q., Campbell W.M., Bonfantani E.E., Jolley K.W., Officer D.L., Walsh P.J., Gordon K., Humphry-Baker R., Nazeeruddin M.K., Grätzel M., *J. Phys. Chem. B*, **2005**, 109, 15397

[35] Imahori H., Hayashi S., Umeyama T., Eu S., Oguro A., Kang S., Matano Y., Shishido T., Ngamsinlapasathian S., Yoshikawa S., *Langmuir*, **2006**, 22, 11405

[36] Wang X.F., Kitao O., Zhou H., Tamiaki H., Sasaki S.I., *J. Phys. Chem. C*, **2009**, 113, 7954

[37] Wang X.F., Tamiaki H., Wang L., Tamai N., Kitao O., Zhou H., Sasaki S.I., *Langmuir*, **2010**, 26, 6320

[38] Nazeeruddin M.K., Humphry-Baker R., Grätzel M., Wöhrle D., Schnurpfeil G., Schneider G., Hirth A., Trombach N., *J. Porphyrins Phthalocyanines*, **1999**, 3, 230

[39] He J., Benko G., Korodi F., Polívka T., Lomoth R., Akermark B., Sun L., Hagfeldt A., Sundstrom V., *J. Am. Chem. Soc.*, **2002**, 124, 4922

[40] Reddy P.Y., Giribabu L., Lyness C., Snaith H.J., Vijaykumar C., Chandrasekharam M., Lakshmikantam M., Yum J.H., Kalyanasundaram K., Grätzel M., Nazeeruddin M. K., *Angew. Chem., Int. Ed.*, **2007**, 46, 373

[41] Cid J.J., Yum J.H., Jang S.R., Nazeeruddin M.K., Martínez-Ferrero E., Palomares E., Ko J., Grätzel M., Torres T., *Angew. Chem., Int. Ed.*, **2007**, 46, 8358

[42] Mori S., Nagata M., Nakahata Y., Yasuta K., Goto R., Kimura M., Taya M., *J. Am. Chem. Soc.*, **2010**, 132, 4054

[43] Kimura M., Nomoto H., Masaki N., Mori S., *Angew. Chem., Int. Ed.*, **2012**, 51, 4371

[44] Ragoussi M.E., Cid J.J., Yum J.H., de la Torre G., Di Censo D., Grätzel M., Nazeeruddin M. K., Torres T., *Angew. Chem., Int. Ed.*, **2012**, 51, 4375

[45] Hara K., Kurashige M., Dan-oh Y., Kasada C., Shinpo A., Suga S., Sayama K., Arakawa H., *New J. Chem.*, **2003**, 27, 783

[46] Wang Z.S., Cui Y., Dan-oh Y., Kasada C., Shinpo A., Hara K., *J. Phys. Chem. C*, **2007**, 111, 7224

[47] Li C., Yum J.H., Moon S.J., Herrmann A., Eickemeyer F., Pschirer N.G., Erk P., Schöneboom J., Müllen K., Grätzel M., Nazeeruddin M.K., *ChemSusChem*, **2008**, 1, 615

[48] Shi Y., Hill R.B.M., Yum J.H., Dualeh A., Barlow S., Grätzel M., Marder S. R., Nazeeruddin M.K., *Angew. Chem., Int. Ed.*, **2011**, 50, 6619

[49] Clifford J.N., Planells M., Palomares E., *J. Mater. Chem.*, **2012**, 22, 24195

[50] Mishra A., Fischer M. K. R., Bäuerle P., *Angew. Chem. Int. Ed.*, **2009**, 48, 2474

[51] Zhang X-H., Li C., Wang W-B., Cheng X-X., Wang X-S., Zhang B-W., *J. Mater. Chem.*, **2007**, 17, 642

[52] (a) Kurotobi K., Kim K.S., Noh S.B., Kim D., Osuka A., *Angew.Chem. Int. Ed.* **2006**, 45, 3944

(b) Puodziukynaite E., Wang H.-W., Lawrence J., Wise A.J., Russell T.P., Barnes M.D., Emrick T.J., *J. Am. Chem. Soc.,* **2014**, 136, 11043

(c) Muranaka A., Yonehara M., Uchiyama M.J., *Am. Chem. Soc.,* **2010**, 132, 7844

(d) Oda M., Thanh N.C., Ikai M., Fujikawa H., Nakajima K., Kuroda S., *Tetrahedron*, **2007**, 63, 10608

(e) Thanh N.C., Ikai M., Kajioka T., Fujikawa H., Taga Y., Zhang Y., Ogawa S., Shimada H., Miyahara Y., Kuroda S., Oda M., *Tetrahedron*, **2006**, 62, 11227

(f) Koch M., Blacque O., Venkatesan K., *Org. Lett.*, **2012**, 14, 1580

(g) Koch M., Blacque O., Venkatesan K.J., *Mater. Chem. C*, **2013**, 1, 7400

[53] Ito S., Morita N., *Eur. J. Org. Chem.*, **2009**, 4567

[54] (a) Yamaguchi Y., Ogawa K., Nakayama K.-I., Ohba, Y., Katagiri H.J., *Am. Chem. Soc.*, **2013**, 135, 19095.

(b) Wang F., Lai Y.-H., Kocherginsky N.M., Kosteski Y.Y., *Org. Lett.*, **2003**, 5, 995

[55] (a) Lacroix P.G., Malfant I., Iftime G., Razus A.C., Nakatani K., Delaire J.A., *Chem. Eur. J.*, **2000**, 6, 2599

(b) Cristian L., Sasaki I., Lacroix P.G., Donnadieu B., Asselberghs I., Clays K., Razus A.C., *Chem. Mater.*, **2004**, 16, 3543

[56] (a) Ramadan M., Goeters S., Watzer B., Krause E., Lohmann K., Bauer R., Hempel B., Imming P.J., *Nat. Prod.*, **2006**, 69, 1041

(b) Rekka E., Chrysselis M., Siskou I., Kourounakis A., *Chem. Pharm. Bull.*, **2002**, 50, 904

[57] (a) Zhang L-Y., Yang F., Shi W.-Q., Zhang P., Li Y., Yin S.-F., *Bioorg. Med. Chem. Lett.*, **2011**, 21, 5722

(b) Yanagisawa T., Kosakai K., Tomiyama T., Yasunami M., Takase K., *Chem. Pharm. Bull.*, **1990**, 38, 3355

(c) Yanagisawa T., Wakabayashi S., Tomiyama T., Yasunami M., Takase K., *Chem. Pharm. Bull.*, **1988**, 36, 641

[58] (a) Sekine T., Takahashi J., Nishishiro M., Arai A., Wakabayashi H., Kurihara T., Kobayashi M., Hashimoto K., Kikuchi H., Katayama T., Kanda Y., Kunii S., Motohashi N., Sakagami H., *Anticancer Res.*, **2007**, 27, 133

(b) Wakabayashi H., Hashiba K., Yokoyama K., Hashimoto K., Kikuchi H., Nishikawa H., Kurihara T., Satoh K., Shioda S., Sato S., Kusano S., Nakashima H., Motohashi N., Sakagami H., *Anticancer Res.*, **2003**, 23, 4747

(c) Asato A.E., Peng A., Hossain M.Z., Mirzadegan T., Bertram J.S., *J. Med. Chem.*, **1993**, 36, 3137

(d) Ishihara M., Wakabayashi H., Motohashi N., Sakagami H., *Anticancer Res.*, **2011**, 31, 515

[59] Gordon M., *Chem. Rev.*, **1951**, 50, 127-200

[60] Piesse, *Compt. rend.*, **1864**, 57, 1016

[61] Sherndal A.E., *J. Am. Chem. Soc.*, **1915**, 37, 167, 1537

[62] Pfau P., Plattner P.I., *Helv. Chim. Acta.*, **1936**, 19, 858

[63] Liu R.S.H., *J. Chem. Ed*. **2002**, 183

[64] Wheland G.W., Mann D.E., *J. Chem. Phys.*, **1949**, 17, 264

[65] Franke H., Muhlstadt M.J., *Prakt. Chem.*, **1967**, 249

[66] Treibs W., *Tetrahedron Letters*, **1967**, 4707-4709

[67] Anderson A.G., Replogle L.L., *J. Org. Chem.*, **1960**, 25, 1275

[68] Hafner K., Patzelt H., Kaiser H., *Liebigs Ann. Chem.*, **1962**, 24, 656

[69] Anderson A.G., Steckler B.M., *J. Am. Chem. Soc.*, **1959**, 81, 4941

[70] Treibs W., Schroth W., *Liebigs Ann. Chem.*, **1954**, 586, 202

[71] Reid D.H., Stafford W.H., Ward J.P., *J. Chem. Soc.*, **1958**, 1100-1109

[72] Treibs W., Jost K., Kurpjun C., Grunduez-Schroth G., *Chem.Ber.*, **1961**, 94, 1728

[73] Kirby E.C., Reid D.H., *J. Chem. Soc.*, **1960**, 494-501

[74] Anderson A.G., Scotoni R., Cowles E.J., Fritz C.G., *J.Org.Chem.*, **1957**, 22, 1193

[75] Anderson A.G., Nelson J. A., Tazuma J. J., *J. Am. Chem. Soc.*, **1953**, 75, 4980

[76] Treibs W., *Angew. Chem.*, **1955**, 67, 76

[77] Hafner K., Moritz K.-L., *Liebigs Ann. Chem.*, **1962**, 656, 40

[78] Hafner K., Stephan A., Bernhard C., *Liebigs Ann. Chem.*, **1961**, 650, 42

[79] Anderson A.G., McDonald R.N., *J. Am. Chem. Soc.*, **1959**, 81, 5669

[80] Anderson A.G., Gale D.J., McDonald R.N., Anderson R.G., Rhodes R. C., *J. Org. Chem.*, **1964**, 29, 1373

[81] Nefedov V.A., *Zhur.Obshch.Khim. (Russian Journal of General Chemistry)*, **1968**, 38, 2185 in Mochalin V.B., Porshnev Yu.N., *Uspekhi Khimii (Russian Chemical Reviews)*, **1977**, 46, 530

[82] Anderson A.G., Cowles E.J., Tazuma J.J., Nelson J. A., *J. Am. Chem. Soc.*, **1955**, 77, 6321

[83] (a) Hafner K., Bernard C., Müller R., *Liebigs Ann. Chem.*, **1961**, 650, 35
(b) Hafner K., Weldes H., *Liebigs Ann. Chem.*, **1957**, 606, 90

[84] Abe N., Morita T., Takase K., *Tetrahedron Letters*, **1973**, 3883

[85] Plattner P.A., Pfau A.S., *Helv. Chim. Acta.,* **1937**, 20, 224 – 232

[86] (a) Buchner E., Curtius T., *Ber. Dtsch. Chem. Ges.*, **1885**, 18, 2377–2379
(b) Buchner E., Curtius T., *Ber. Dtsch. Chem. Ges.*, **1885**, 18, 2371–2377

[87] Rao A.S., Muthana M.S., *J. Ind. Inst. Sci.*, **1955**, 37, 79-83

[88] Zeigler K., Hafner K., *Angew. Chem.*, **1955**, 67, 301

[89] Nozoe T., Matsumura S., Murase Y., Seto S., *Chem. Ind. (London)*, **1955**, 1257

[90] Machiguchi T., Hasegawa T., Yamabe S., Minato T., Yamazaki S., Nozoe T., *J. Org. Chem.*, **2012**, 77, 5318-5330

[91] (a) Hafner K., *Liebigs Ann. Chem.*, **1957**, 606, 79–89
(b) Hafner K., Kaiser H., *Org. Synth.*, **1964**, 44, 94

[92] Scott L.T., Minton M.A., Kirms M.A., *J. Am. Chem. Soc.*, **1980**, 102, 6311-6314

[93] Kane J.L. Jr., Shea K.M., Crombie A.L., Danheiser R.L., *Org. Lett.*, **2001**, 3, 7, 1081-1084

[94] Moiseev A.M., Balenkova E.S., Nenajdenko V.G., *Russ.Chem.Bull., Int.Ed.*, **2006**, 55, 1, 141-146

[95] Dunn L.C., Houk K.N., *Tetrahedron Letters*, **1978**, 37, 3411-3414

[96] Gupta Y.N., Mani S.R., Houk K.N., *Tetrahedron Letters*, **1982**, 23, S, 495-498

[97] Mukherjee D., Dun L.C., Houk K.Y., *J. Am. Chem. Soc.*, **1979**, 101, 1, 251-252

[98] (a) Ghosez L., Montaigne R., Mollet P., *Tetrahedron Letters*, **1966**, 1, 135-139;
(b) Ghosez L., Montaigne R., Roussel A., Vanlierde H., Mollet P., *Tetrahedron*, **1971**, 27, 615-633;
(c) Brady, W.T., *Tetrahedron*, **1981**, 37, 17, 2949-2966 and references therein

[99] Greene A.E., Deprés J-P., *J. Am. Chem. Soc.*, **1979**, 101, 14, 4003-4005

[100] Coquerel Y., Blanc A., Deprés J-P., Greene A.E., Averbuch-Pouchot M-T., Philouzea C., Durifa A., *Acta Cryst. C.*, **2000**, 56, 1480-1481

[101] Deprés J-P., Greene A.E., *J. Org. Chem.*, **1980**, 45, 2037-2039

[102] Carret S., Blanc A., Coquerel Y., Berthod M., Greene A.E., Deprés J.-P., *Angew. Chem. Int. Ed.*, **2005**, 44, 5130

[103] Yokoyama R., Ito S., Watanabe M., Harada N., Kabuto C., Morita N., *J. Chem. Soc., Perkin Trans. 1*, **2001**, 2257–2261

[104] Ito S., Nomura A., Morita N., Kabuto C., Kobayashi H., Maejima S., Fujimori K., Yasunami M., *J. Org. Chem.*, **2002**, 67, 7295-7302

[105] Nazeeruddin M.K., Gratzel M., *Comprehensive Coordination Chemistry II*, Elsevier, **2004**, Ch 9.16, p719

[106] Grätzel M., *Inorg. Chem.*, **2005**, 44, 6841-6851

[107] Fisher A.C., *Electrode Dynamics*, Oxford University Press, **1996**, 1

[108] Gritzner G., Kuta J., *Pure & Appi. Chem.*, **1984**, 56, 4, 461-466

[109] Fisher A.C., *Electrode Dynamics*, Oxford University Press, **1996**, 13-16

[110] Fisher A.C., *Electrode Dynamics*, Oxford University Press, **1996**, 10

[111] Wardle B., *Principles and Applications of Photochemistry*, John Wiley and Sons Ltd., **2009**, 30-39

[112] Byron C.M., Werner T.C., *J. Chem. Educ.*, **1991**, 68, 433

[113] Kalyanasundaram K.; Grätzel M., *Coord. Chem. Rev.*, **1998**, 177, 347−414

[114] (a) Yan S.J., Hupp J.T., *J. Phys. Chem.*, **1996**, 100, 17, 6867-6870
(b) Merrins A., Kleverlaan C., Will G., Rao S.N., Scandola F., Fitzmaurice D., *J. Phys. Chem. B*, **2001**, 105, 2998-3004

[115] Polo A.S., Itokazu M.K., Iha N.Y.M., *Coord. Chem. Rev.*, **2004**, 248, 1343-1361

[116] Galoppini G., *Coord. Chem. Rev.*, **2004**, 1283-1297

[117] Takahashi K., Yui H., *J. Phys. Chem. C*, **2009**, 113, 20322-20327

[118] Kungwan N., Khongpracha P., Namuangruk S., Meeprasert J., Chitpakdee C., Jungsuttiwong S., Promarak V., *Theor. Chem. Acc.* **2014,** 133, 1523

[119] Albero J., Atienzar P., Corma A., Hermenegildo Garcia H., *Chem. Rec.,* **2015**, 15, 803–828

[120] Bearpark M.J., Bernardi F., Clifford S., Olivucci M., Robb M.A., Smith B.R., Vreven T., *J. Am. Chem. Soc.*, **1996**, 118, 169

[121] Liu, R.S.H., Asato E.A., *Journal of Photochemistry and Photobiology C: Photochemistry*, **2003**, 4, 179

[122] Lamberto M., Pagba C., Piotrowiak P., Galoppini E., *Tetrahedron Letters*, **2005**, 46, 4895-4899

[123] Okujima T., Ito S., Morita N., *Tetrahedron Letters*, **2002**, 1261-1364

[124] Ito S., Terazono T., Kubo T., Okujima T., Morita N., Murafuji T., Sugihara Y., Fujimori K., Kawakamia J., Tajiria A., *Tetrahedron*, **2004**, 60, 5357-5366

[125] Walker S.D., Barder T.E., Martinelli J.R., Buchwald S.L., *Angew. Chem. Int. Ed.*, **2004**, 43, 1871

[126] Stetter H., *Angew. Chem. Int. Ed.*, **1976**, 15, 639

[127] Breslow R., J. Am. Chem. Soc., **1958**, 80, 3719

[128] Kaptein B., Barf G., Kellogg R.M., Van Bolhuis F., *J. Org. Chem.*, **1990**, 55, 1890

[129] Crombie A.L., Kane J.L., Shea K.M., Danheiser R.L., *J. Org. Chem.*, **2004**, 69, 8652

[130] Kropp P.J., Daus K.A., Tubergen M.W., Kepler K.D., Wilson V.P., Craig S.L., Baillargeon M.M., Breton G.W., *J. Am. Chem. Soc.*, **1993**, 115, 3071

[131] ORTEP diagrams produced with Mercury CSD 3:
Macrae C.F., Edgington P.R., McCabe P., Pidcock E., Shields G.P., Taylor R., Towler M., van de Streek J., *J. Appl. Cryst.*, **2006**, 39, 453-457

[132] Hall D.G., "Structure, Properties, and Preparation Of Boronic Acid Derivatives. Overview of Their Reactions and Applications." in Hall D.G., *Boronic Acids*, WILEY-VCH Verlag GmbH & Co. KGaA, Weinheim, **2005**, 62

[133] Reilly M.K., *Masking Boronic Acids for Suzuki Coupling*, **2011**, available at: http://www.youtube.com/watch?v=jnw-bEjKcOU, accessed 03 May 2013

[134] Reilly M.K., Rychnovsky S.D., *SYNLETT*, **2011**, 16, 2392

[135] Bonin H., Leuma-Yona R., Marchiori B., Demonchaux P., Gras E., *Tetrahedron Letters*, **2011**, 1132

[136] Billingsley K., Buchwald S.L., *J. Am. Chem. Soc.*, **2007**, 129, 3358

[137] Gerson F., Scholz M., Hansen H-J., Uebelhartb P., *J. Chem. Soc. Perkin Trans. 2*, **1995**, 215

[138] Shoji T., Ito S., Toyota K., Iwamoto T., Yasunami M., Morita N., *Eur. J. Org. Chem.*, **2009**, 4307–4315

[139] Becker D.A., Natero R., Echegoyen L, Lawson R.C., *J. Chem. Soc., Perkin Trans. 2*, **1998**, 1289

[140] Hafner K., Stephan A., Bernhardt C., *Liebigs Ann. Chem.*, **1961**, 650, 57

[141] Treibs W., Orttmann H., Schlimper R., Lindig C. Chem., *Chem. Ber.*, **1959**, 92, 2152

[142] Amemiya T., Yasunami M., Takase K., *Chem. Lett.,* **1977**, 587

[143] Hafner K., Moritz K.L., *Justus Liebigs Ann. Chem.*, **1962**, 656, 40

[144] Shoji T., Ito S., Okujima T., Higashi J., Yokoyama R., Toyota K., Yasunami M., Morita N., *Eur. J. Org. Chem.*, **2009**, 1554-1563

[145] Nenajdenko V.G., Popov V.I., Balenkova E.S., Sulfur Lett. 1996, 20, 75–83

[146] Yadav J.S., Reddy B.S.S., Basak A.K., Visali B., Narsaiah A.V., Nagaiah K., *Eur. J. Org. Chem.*, **2004**, 546-551

[147] Ebitani K., Motokura K., Mori K., Mizugaki T., Kaneda K., *J. Org. Chem.*, **2006**, 71, 5440-5447

[148] Ogiwara Y., Takahashi K., Kitazawa T., Sakai N., *J. Org. Chem.*, **2015**, 80, 3101-3110

[149] Mase N., Horibe T., *Org. Lett.*, **2013**, 15, 1854-1857

[150] Mohite A.R., Bhat R.G., *Org. Lett.*, **2013**, 15, 4564-4567

[151] Shanthan Rao P., Venkataratnam R.V., *Tetrahedron Letters,* **1991**, 41, 5821-5822

[152] (a) Ranu B.C., Jana R., *Eur. J. Org. Chem.*, **2006**, 3767-3770

(b) Su C., Chen Z.-C., Zhen Q.-G., *Synthesis*, **2003**, 555-559

[153] (a) Cardillo, G., Fabbroni S., Gentilucci L., Gianotti M., Tolomelli A., *Synthetic Communications*, **2006**, 1587-1594

(b) Srikrishna D., Tasqeeruddin S., Dubey P.K., *Letters in Organic Chemistry*, **2014**, 11, 556-563

[154] (a) Prout F.S., *J. Org. Chem.*, **1953**, 18, 928–933

(b) Prout F.S., Abel-Latif A.A., Kamal M.R., *J. Chem. Eng. Data*, **1963**, 8, 597-599

[155] Zhu L., Lei N., Miao Z., Sheng C., Zhuang C., Yao J., Zhang W., *Chin. J. Chem.*, **2012**, 30, 139—143

[156] (a) Leino T.O., Baumann M., Yli-Kauhaluoma J., Baxendale I.R., Wallén E.A.A., *J. Org. Chem.*, **2015**, 80, 11513-11520

(b) Dragu E.A., Ion A.E., Shova S., Bala D., Mihailciuc C., Voicescu M., Ionescu S., Nica S., *RSC Adv.*, **2015**, 5, 63282–63286

(c) Dubovik J., Bredihhin A., *Synthesis,* **2015**, 2663–2669

(d) Dubovik J., Bredihhin A., *Synthesis*, **2015**, 538–548

(e) Iyoda M., Sato K., Oda M., *Tetrahedron Lett.*, **1985**, 26, 3829–3832

(f) Grovenstein E. Jr., Schmalstieg F. C., *J. Am. Chem. Soc.*, **1967**, 89, 5084–5085

(g) Hafner K., Patzelt H., Kaiser H., *Justus Liebigs Ann. Chem.*, **1962**, 656, 24– 33

(h) Ukita T., Miyazaki M., Watanabe H., *Pharm. Bull.*, **1955**, 3, 199–203

(i) Anderson A.G. Jr., Nelson J.A., Tazuma J.J., *J. Am. Chem. Soc.*, **1953**, 75, 4980–4989

[157] Srogl J., Allred G.D., Liebeskind L.S., *J.Am. Chem. Soc.*, **1997**, 119, 12376–12377

[158] Zhang S., Marshall D., Liebeskind L.S., *J. Org. Chem.*, **1999**, 64, 2796-2804

[159] Divald S., Chun M.C., Joullie M.M., *J. Org. Chem.*, **1976**, 41, 2835

[160] Asao T., Ito S., Morita N., *Tetrahedron Lett.*, **1989**, 30, 6345–6348

[161] Cowper P., Jin Y., Turton M.D., Kociok-Köhn G., Lewis S.E., *Angew. Chem. Int. Ed.*, **2016**, 55, 2564–2568

[162] Fisher A.C., *Electrode Dynamics*, Oxford University Press, **1996**, 31-32

[163] Reichard C., *Chem. Rev.,* 1994, 94, 2319-2358

[164] Solvent Misciblility Table – Phenomenex, available at: https://research.cbc.osu.edu/turro.1/wp-content/uploads/2017/02/solvent.miscibility.pdf, accessed 15th May, 2017

[165] Nazeeruddin M.K., De Angelis F., Fantacci S., Selloni A., Viscardi G., Liska P., Ito S., Takeru B., Grätzel M., *J. Am. Chem. Soc.*, **2005**, 127, 16835-16847

[166] (a) Taya S., Kuwahara S., Shen Q., Toyoda T., Katayama K., *RSC Adv.*, **2014**, 4, 21517–21520

(b) Bai Y., Zhang J., Wang Y., Zhang M., Wang P., *Langmuir*, **2011**, 27, 4749–4755

[167] (a) Daeneke T., Kwon T-H., Holmes A.B., Duffy N.W., Bach U., Spiccia L., *Nature Chemistry*, **2011**, 3, 211-215

(b) Salvatori P., Marotta G., Cinti A., Anselmi C., Mosconi E., De Angelis F., *J. Phys. Chem. C*, **2013**, 117, 3874-3887

[168] Zhang C., Huang Y., Huo Z., Chen S., Dai S., *J. Phys. Chem. C*, **2009**, 113, 21779–21783

[169] (a) Luponosov Y.N., Min J., Solodukhin A.N., Bakirov A.V., Dmitryakov P.V., Shcherbina M.A., Peregudova S.M., Cherkaev G.V., Chvalun S.N., Brabec C.J., Ponomarenko S.A., *J. Mater. Chem. C*, **2016**, 4, 7061

(b) Heo D.U., Kim S.J., Yoo B.J., Kim B., Ko M.J., Cho M.J., Choi D.H., Bull, Korean Chem. Soc., 2013, 34, 1081-1088

[170] Barbasiewicz M., Makosza M., *Org. Lett.*, **2006**, 8, 17, 3745-3748

[171] Anderson N.H., Uh H-S., *Synth. Commun.*, **1973**, 3, 2, 125-128

[172] Tsai Y-C., Stephens F.H., Meyer K., Mendiratta A., Gheorghiu M.D., Christopher C. Cummins C.C., *Organometallics*, **2003**, 22, 2902

[173] Matsubara Y., Takekuma S-I., Yokoi K., Yamamoto H., Nozoe T., *Bull. Chem. Soc. Jpn.*, **1987**, 60, 1415

[174] Takekuma S-i., Matsubara Y., Yamamoto H., Nozoe T., *Bull. Chem. Soc. Jpn.*, **1987**, 60, 3621

[175] Steinberger S., Mishra A., Reinold E., Mena-Osteritz E., Muller H., Uhrich C., Pfeiffer M., Bauerle P., *J. Mater. Chem.*, **2012**, 22, 2701

[176] Molander G.A., Cavalcanti L.N., Canturk B., Pan P-S., Kennedy L.E., *J. Org. Chem.*, **2009**, 74, 7364–7369

[177] Shoji T., Higashi J., Ito S., Toyota K., Asao T., Yasunami M., Fujimori K., Morita N., *Eur. J. Org. Chem.*, **2008**, 1242–1252

[178] Ito S., Morita N., Asao T., *Bull. Chem. Soc. Jpn.*, **1995**, 68, 5, 1409-1436

[179] Lu T-J., Lin P-H., Lee K-M., Liu C-Y., *Eur. J. Org. Chem.*, **2017**, 111–123

10 Appendix 1. X-Ray Crystallographic Data

Crystallographic data are presented in the following pages.

Table 28. Crystal data and structure refinement for 1-(azulen-1-yl)tetrahydrothiophenium hexafluorophosphate (**207**)

Identification code	s14sel1	
Empirical formula	C14 H15 F6 P S	
Formula weight	360.29	
Temperature	150(2) K	
Wavelength	1.54184 Å	
Crystal system	Monoclinic	
Space group	P21/n	
Unit cell dimensions	a = 6.9015(2) Å	a= 90°.
	b = 8.1374(3) Å	b= 91.477(3)°.
	c = 26.9719(9) Å	g = 90°.
Volume	1514.25(9) $Å^3$	
Z	4	
Density (calculated)	1.580 Mg/m^3	
Absorption coefficient	3.462 mm^{-1}	
F(000)	736	
Crystal size	0.190 x 0.074 x 0.033 mm^3	
Theta range for data collection	5.679 to 72.148°.	
Index ranges	-5<=h<=8, -10<=k<=10, -33<=l<=33	
Reflections collected	14711	
Independent reflections	2975 [R(int) = 0.0680]	
Completeness to theta = 67.684°	99.90%	
Absorption correction	Semi-empirical from equivalents	
Max. and min. transmission	1.00000 and 0.70011	
Refinement method	Full-matrix least-squares on F2	
Data / restraints / parameters	2975 / 0 / 254	
Goodness-of-fit on F2	1.025	
Final R indices [I>2sigma(I)]	R1 = 0.0626, wR2 = 0.1732	
R indices (all data)	R1 = 0.0755, wR2 = 0.1869	
Extinction coefficient	n/a	
Largest diff. peak and hole	0.453 and -0.343 $e.Å^{-3}$	

Table 29. Atomic coordinates (x 10^4) and equivalent isotropic displacement parameters (Å^2 x 10^3) for 1-(azulen-1-yl)tetrahydrothiophenium hexafluorophosphate (**207**). U(eq) is defined as one third of the trace of the orthogonalized U^{ij} tensor.

	x	y	z	U(eq)
S	2523(1)	4804(1)	3411(1)	46(1)
C(1)	4459(5)	3704(5)	3104(1)	60(1)
C(2)	3475(8)	2683(7)	2710(2)	89(1)
C(3)	1615(9)	2114(7)	2891(2)	95(2)
C(4)	605(5)	3535(6)	3132(1)	70(1)
C(5)	2694(4)	4227(4)	4028(1)	42(1)
C(6)	2464(3)	5369(3)	4415(1)	39(1)
C(7)	2119(4)	7038(4)	4361(1)	49(1)
C(8)	1877(5)	8199(5)	4733(2)	63(1)
C(9)	1929(5)	7985(6)	5244(2)	70(1)
C(10)	2202(5)	6585(6)	5519(1)	66(1)
C(11)	2509(4)	4985(5)	5359(1)	56(1)
C(12)	2640(3)	4408(4)	4875(1)	44(1)
C(13)	2989(4)	2777(4)	4741(1)	53(1)
C(14)	3021(5)	2647(4)	4231(1)	52(1)
P	7211(2)	8776(1)	3424(1)	63(1)
F(1)	9430(30)	9230(30)	3558(11)	175(9)
F(2)	6810(30)	10603(17)	3542(5)	159(8)
F(3)	5220(20)	8270(30)	3275(9)	162(8)
F(4)	8050(30)	6918(18)	3420(7)	167(7)
F(5)	7490(14)	9190(20)	2839(4)	119(4)
F(6)	6930(30)	8380(20)	3976(5)	178(8)
F(1A)	9309(19)	8510(30)	3447(9)	160(7)
F(2A)	7370(20)	10651(14)	3424(7)	161(7)
F(3A)	4980(20)	9120(30)	3388(10)	168(7)
F(4A)	6710(30)	6952(13)	3418(7)	180(7)
F(6A)	7090(40)	8823(19)	3986(4)	199(9)
F(5A)	7400(30)	8750(40)	2927(6)	251(12)

Table 30. Bond lengths [Å] for 1-(azulen-1-yl)tetrahydrothiophenium hexafluorophosphate (**207**)

Bond	Length	Bond	Length
S-C(5)	1.730(3)	C(9)-C(10)	1.370(7)
S-C(1)	1.824(3)	C(9)-H(9)	0.95
S-C(4)	1.826(4)	C(10)-C(11)	1.389(6)
C(1)-C(2)	1.498(6)	C(10)-H(10)	0.95
C(1)-H(1A)	0.99	C(11)-C(12)	1.394(4)
C(1)-H(1B)	0.99	C(11)-H(11)	0.95
C(2)-C(3)	1.460(7)	C(12)-C(13)	1.397(5)
C(2)-H(2A)	0.99	C(13)-C(14)	1.382(5)
C(2)-H(2B)	0.99	C(13)-H(13)	0.95
C(3)-C(4)	1.506(7)	C(14)-H(14)	0.95
C(3)-H(3A)	0.99	P-F(5A)	1.351(17)
C(3)-H(3B)	0.99	P-F(1A)	1.464(12)
C(4)-H(4A)	0.99	P-F(3)	1.483(14)
C(4)-H(4B)	0.99	P-F(6A)	1.520(10)
C(5)-C(6)	1.409(4)	P-F(4A)	1.524(9)
C(5)-C(14)	1.414(4)	P-F(2A)	1.530(11)
C(6)-C(7)	1.386(4)	P-F(6)	1.540(12)
C(6)-C(12)	1.469(4)	P-F(2)	1.547(11)
C(7)-C(8)	1.392(5)	P-F(3A)	1.563(15)
C(7)-H(7)	0.95	P-F(1)	1.610(18)
C(8)-C(9)	1.387(6)	P-F(4)	1.618(12)
C(8)-H(8)	0.95	P-F(5)	1.629(11)

Table 31. Bond angles for 1-(azulen-1-yl)tetrahydrothiophenium hexafluorophosphate (**207**).

Bond	Angle (°)	Bond	Angle (°)
C(5)-S-C(1)	105.70(16)	C(11)-C(10)-H(10)	115.4
C(5)-S-C(4)	105.86(16)	C(10)-C(11)-C(12)	128.4(3)
C(1)-S-C(4)	93.85(18)	C(10)-C(11)-H(11)	115.8
C(2)-C(1)-S	105.7(3)	C(12)-C(11)-H(11)	115.8
C(2)-C(1)-H(1A)	110.6	C(11)-C(12)-C(13)	125.3(3)
S-C(1)-H(1A)	110.6	C(11)-C(12)-C(6)	127.3(3)
C(2)-C(1)-H(1B)	110.6	C(13)-C(12)-C(6)	107.4(3)
S-C(1)-H(1B)	110.6	C(14)-C(13)-C(12)	109.6(3)
H(1A)-C(1)-H(1B)	108.7	C(14)-C(13)-H(13)	125.2
C(3)-C(2)-C(1)	109.0(4)	C(12)-C(13)-H(13)	125.2
C(3)-C(2)-H(2A)	109.9	C(13)-C(14)-C(5)	108.1(3)
C(1)-C(2)-H(2A)	109.9	C(13)-C(14)-H(14)	126
C(3)-C(2)-H(2B)	109.9	C(5)-C(14)-H(14)	126
C(1)-C(2)-H(2B)	109.9	F(5A)-P-F(1A)	85.4(13)
H(2A)-C(2)-H(2B)	108.3	F(5A)-P-F(6A)	177.5(14)
C(2)-C(3)-C(4)	108.7(4)	F(1A)-P-F(6A)	92.2(14)
C(2)-C(3)-H(3A)	109.9	F(5A)-P-F(4A)	90.2(15)
C(4)-C(3)-H(3A)	109.9	F(1A)-P-F(4A)	94.7(9)
C(2)-C(3)-H(3B)	109.9	F(6A)-P-F(4A)	91.0(8)
C(4)-C(3)-H(3B)	109.9	F(5A)-P-F(2A)	90.2(14)
H(3A)-C(3)-H(3B)	108.3	F(1A)-P-F(2A)	94.4(10)
C(3)-C(4)-S	105.9(3)	F(6A)-P-F(2A)	88.9(8)
C(3)-C(4)-H(4A)	110.6	F(4A)-P-F(2A)	170.9(10)
S-C(4)-H(4A)	110.6	F(3)-P-F(6)	93.6(13)
C(3)-C(4)-H(4B)	110.6	F(3)-P-F(2)	98.9(10)
S-C(4)-H(4B)	110.6	F(6)-P-F(2)	88.5(8)
H(4A)-C(4)-H(4B)	108.7	F(5A)-P-F(3A)	93.4(13)
C(6)-C(5)-C(14)	109.4(3)	F(1A)-P-F(3A)	177.8(12)
C(6)-C(5)-S	121.8(2)	F(6A)-P-F(3A)	88.9(14)
C(14)-C(5)-S	128.7(2)	F(4A)-P-F(3A)	87.3(8)
C(7)-C(6)-C(5)	126.2(3)	F(2A)-P-F(3A)	83.7(10)
C(7)-C(6)-C(12)	128.3(3)	F(3)-P-F(1)	175.8(12)

Table 31 continued

Bond	Angle (°)	Bond	Angle (°)
C(5)-C(6)-C(12)	105.4(3)	F(6)-P-F(1)	88.5(13)
C(6)-C(7)-C(8)	127.9(3)	F(2)-P-F(1)	84.7(11)
C(6)-C(7)-H(7)	116.1	F(3)-P-F(4)	93.8(9)
C(8)-C(7)-H(7)	116.1	F(6)-P-F(4)	82.3(10)
C(9)-C(8)-C(7)	129.0(4)	F(2)-P-F(4)	164.7(9)
C(9)-C(8)-H(8)	115.5	F(1)-P-F(4)	82.9(9)
C(7)-C(8)-H(8)	115.5	F(3)-P-F(5)	85.9(10)
C(10)-C(9)-C(8)	130.0(4)	F(6)-P-F(5)	179.5(10)
C(10)-C(9)-H(9)	115	F(2)-P-F(5)	91.6(9)
C(8)-C(9)-H(9)	115	F(1)-P-F(5)	92.0(11)
C(9)-C(10)-C(11)	129.1(3)	F(4)-P-F(5)	97.8(10)
C(9)-C(10)-H(10)	115.4		

Table 32. Anisotropic displacement parameters ($Å^2$ x 10^3) for 1-(azulen-1-yl)tetrahydrothiophenium hexafluorophosphate (**207**). The anisotropic displacement factor exponent takes the form: $-2\pi^2[h^2 a^{*2}U^{11} + ... + 2 h k a^* b^* U^{12}]$.

	U11	U22	U33	U23	U13	U12
S	54(1)	49(1)	35(1)	3(1)	2(1)	1(1)
C(1)	60(2)	67(2)	54(2)	2(2)	16(1)	1(2)
C(2)	103(3)	95(3)	69(3)	-30(2)	13(2)	4(3)
C(3)	120(4)	83(3)	82(3)	-23(3)	-9(3)	-29(3)
C(4)	53(2)	105(3)	50(2)	-1(2)	-5(1)	-15(2)
C(5)	44(1)	44(1)	39(1)	3(1)	2(1)	-1(1)
C(6)	32(1)	48(2)	39(1)	0(1)	1(1)	-3(1)
C(7)	51(1)	49(2)	47(2)	-3(1)	0(1)	-2(1)
C(8)	68(2)	58(2)	64(2)	-11(2)	1(2)	1(2)
C(9)	58(2)	88(3)	64(2)	-28(2)	6(2)	1(2)
C(10)	46(2)	108(3)	42(2)	-18(2)	4(1)	-9(2)
C(11)	39(1)	91(2)	38(1)	7(2)	0(1)	-14(1)
C(12)	32(1)	60(2)	39(1)	10(1)	0(1)	-9(1)
C(13)	50(2)	59(2)	51(2)	21(1)	-4(1)	-6(1)
C(14)	58(2)	45(2)	54(2)	6(1)	4(1)	-3(1)
P	76(1)	58(1)	56(1)	6(1)	2(1)	-3(1)
F(1)	147(10)	164(15)	209(19)	63(13)	-93(11)	-56(10)
F(2)	272(19)	110(9)	93(6)	-34(6)	-34(8)	101(11)
F(3)	93(9)	200(20)	195(13)	-42(14)	0(9)	-69(11)
F(4)	185(14)	97(8)	219(14)	-60(8)	-20(12)	47(10)
F(5)	93(5)	234(12)	31(4)	32(5)	6(3)	2(5)
F(6)	267(17)	150(11)	120(10)	100(10)	64(10)	24(10)
F(1A)	85(6)	194(19)	197(13)	21(13)	-48(7)	34(9)
F(2A)	174(9)	77(6)	233(16)	58(8)	37(9)	-29(7)
F(3A)	85(5)	182(15)	240(20)	21(13)	48(8)	6(9)
F(4A)	223(16)	55(4)	257(15)	-14(6)	-73(14)	-18(8)
F(6A)	400(20)	134(9)	66(6)	-49(7)	24(9)	-78(12)
F(5A)	300(20)	400(30)	57(6)	70(10)	37(7)	44(18)

Table 33. Crystal data and structure refinement for 1-(3-*tert*-butylazulen-1-yl)tetrahydrothiophenium hexafluorophosphate (**162**)

Identification code	e15sel3	
Empirical formula	C18 H23 F6 P S	
Formula weight	416.39	
Temperature	150(2) K	
Wavelength	0.71073 Å	
Crystal system	Monoclinic	
Space group	$P2_1$	
Unit cell dimensions	a = 10.3988(5) Å	a= 90°.
	b = 8.4387(3) Å	b= 99.950(4)°.
	c = 10.9923(4) Å	g = 90°.
Volume	950.09(7) $Å^3$	
Z	2	
Density (calculated)	1.456 Mg/m^3	
Absorption coefficient	0.310 mm^{-1}	
F(000)	432	
Crystal size	0.350 x 0.200 x 0.150 mm^3	
Theta range for data collection	3.469 to 30.078°.	
Index ranges	-13<=h<=14, -11<=k<=11, -13<=l<=15	
Reflections collected	8526	
Independent reflections	4570 [R(int) = 0.0244]	
Completeness to theta = 25.242°	99.70%	
Absorption correction	Semi-empirical from equivalents	
Max. and min. transmission	1.00000 and 0.95173	
Refinement method	Full-matrix least-squares on F2	
Data / restraints / parameters	4570 / 1 / 238	
Goodness-of-fit on F2	1.031	
Final R indices [I>2sigma(I)]	R1 = 0.0385, wR2 = 0.0740	
R indices (all data)	R1 = 0.0461, wR2 = 0.0771	
Absolute structure parameter	0.45(4)	
Extinction coefficient	n/a	
Largest diff. peak and hole	0.249 and -0.262 $e.Å^{-3}$	

Table 34. Atomic coordinates (x 10^4) and equivalent isotropic displacement parameters ($Å^2$ x 10^3) for 1-(3-*tert*-butylazulen-1-yl)tetrahydrothiophenium hexafluorophosphate (**162**). U(eq) is defined as one third of the trace of the orthogonalized U^{ij} tensor.

	x	y	z	U(eq)
S	7093(1)	1643(1)	7889(1)	23(1)
C(1)	8718(3)	1180(4)	8721(3)	30(1)
C(2)	8951(3)	2262(5)	9833(3)	39(1)
C(3)	7660(3)	2453(4)	10270(2)	32(1)
C(4)	6652(3)	2834(4)	9146(3)	33(1)
C(5)	7323(3)	3013(3)	6760(2)	20(1)
C(6)	8074(3)	4404(3)	6903(2)	22(1)
C(7)	7992(3)	5180(3)	5776(2)	19(1)
C(8)	8659(3)	6752(4)	5596(2)	22(1)
C(9)	9534(3)	6620(4)	4604(2)	28(1)
C(10)	9539(4)	7241(4)	6809(3)	37(1)
C(11)	7631(3)	8041(4)	5244(3)	34(1)
C(12)	7157(3)	4257(3)	4881(2)	18(1)
C(13)	6735(3)	4627(3)	3642(2)	22(1)
C(14)	5924(3)	3782(4)	2724(2)	27(1)
C(15)	5334(3)	2329(4)	2786(2)	30(1)
C(16)	5356(3)	1338(4)	3802(2)	28(1)
C(17)	5953(3)	1586(4)	5012(2)	21(1)
C(18)	6735(3)	2839(3)	5512(2)	19(1)
P	7293(1)	7490(1)	635(1)	24(1)
F(1)	7873(2)	7014(2)	-569(2)	47(1)
F(2)	8147(2)	6128(2)	1398(2)	38(1)
F(3)	6695(2)	7939(2)	1832(2)	41(1)
F(4)	6427(2)	8845(2)	-131(2)	44(1)
F(5)	8465(2)	8715(2)	1029(2)	38(1)
F(6)	6124(2)	6249(2)	238(2)	33(1)

Table 35. Bond lengths [Å] for 1-(3-*tert*-butylazulen-1-yl)tetrahydrothiophenium hexafluorophosphate (**162**).

Bond	Length (Å)	Bond	Length (Å)
S-C(5)	1.742(3)	C(9)-H(9C)	0.98
S-C(1)	1.819(3)	C(10)-H(10A)	0.98
S-C(4)	1.829(3)	C(10)-H(10B)	0.98
C(1)-C(2)	1.511(4)	C(10)-H(10C)	0.98
C(1)-H(1A)	0.99	C(11)-H(11A)	0.98
C(1)-H(1B)	0.99	C(11)-H(11B)	0.98
C(2)-C(3)	1.511(5)	C(11)-H(11C)	0.98
C(2)-H(2A)	0.99	C(12)-C(13)	1.392(3)
C(2)-H(2B)	0.99	C(12)-C(18)	1.488(4)
C(3)-C(4)	1.511(4)	C(13)-C(14)	1.394(4)
C(3)-H(3A)	0.99	C(13)-H(13)	0.95
C(3)-H(3B)	0.99	C(14)-C(15)	1.379(4)
C(4)-H(4A)	0.99	C(14)-H(14)	0.95
C(4)-H(4B)	0.99	C(15)-C(16)	1.392(4)
C(5)-C(6)	1.404(4)	C(15)-H(15)	0.95
C(5)-C(18)	1.410(3)	C(16)-C(17)	1.383(4)
C(6)-C(7)	1.391(4)	C(16)-H(16)	0.95
C(6)-H(6)	0.95	C(17)-C(18)	1.388(4)
C(7)-C(12)	1.426(4)	C(17)-H(17)	0.95
C(7)-C(8)	1.526(4)	P-F(3)	1.5952(18)
C(8)-C(11)	1.528(4)	P-F(1)	1.5973(18)
C(8)-C(10)	1.538(4)	P-F(2)	1.599(2)
C(8)-C(9)	1.540(4)	P-F(5)	1.600(2)
C(9)-H(9A)	0.98	P-F(4)	1.601(2)
C(9)-H(9B)	0.98	P-F(6)	1.6062(19)

Table 36. Bond angles [°] for 1-(3-*tert*-butylazulen-1-yl)tetrahydrothiophenium hexafluorophosphate (**162**).

Bond	Angle (°)	Bond	Angle (°)
C(5)-S-C(1)	105.66(14)	C(8)-C(10)-H(10A)	109.5
C(5)-S-C(4)	104.87(14)	C(8)-C(10)-H(10B)	109.5
C(1)-S-C(4)	94.06(15)	H(10A)-C(10)-H(10B)	109.5
C(2)-C(1)-S	106.4(2)	C(8)-C(10)-H(10C)	109.5
C(2)-C(1)-H(1A)	110.5	H(10A)-C(10)-H(10C)	109.5
S-C(1)-H(1A)	110.5	H(10B)-C(10)-H(10C)	109.5
C(2)-C(1)-H(1B)	110.5	C(8)-C(11)-H(11A)	109.5
S-C(1)-H(1B)	110.5	C(8)-C(11)-H(11B)	109.5
H(1A)-C(1)-H(1B)	108.6	H(11A)-C(11)-H(11B)	109.5
C(3)-C(2)-C(1)	107.1(3)	C(8)-C(11)-H(11C)	109.5
C(3)-C(2)-H(2A)	110.3	H(11A)-C(11)-H(11C)	109.5
C(1)-C(2)-H(2A)	110.3	H(11B)-C(11)-H(11C)	109.5
C(3)-C(2)-H(2B)	110.3	C(13)-C(12)-C(7)	127.2(2)
C(1)-C(2)-H(2B)	110.3	C(13)-C(12)-C(18)	124.6(3)
H(2A)-C(2)-H(2B)	108.5	C(7)-C(12)-C(18)	108.1(2)
C(4)-C(3)-C(2)	107.0(2)	C(12)-C(13)-C(14)	130.0(3)
C(4)-C(3)-H(3A)	110.3	C(12)-C(13)-H(13)	115
C(2)-C(3)-H(3A)	110.3	C(14)-C(13)-H(13)	115
C(4)-C(3)-H(3B)	110.3	C(15)-C(14)-C(13)	129.6(3)
C(2)-C(3)-H(3B)	110.3	C(15)-C(14)-H(14)	115.2
H(3A)-C(3)-H(3B)	108.6	C(13)-C(14)-H(14)	115.2
C(3)-C(4)-S	105.8(2)	C(14)-C(15)-C(16)	128.9(3)
C(3)-C(4)-H(4A)	110.6	C(14)-C(15)-H(15)	115.5
S-C(4)-H(4A)	110.6	C(16)-C(15)-H(15)	115.5
C(3)-C(4)-H(4B)	110.6	C(17)-C(16)-C(15)	128.5(3)
S-C(4)-H(4B)	110.6	C(17)-C(16)-H(16)	115.7
H(4A)-C(4)-H(4B)	108.7	C(15)-C(16)-H(16)	115.7
C(6)-C(5)-C(18)	109.6(2)	C(16)-C(17)-C(18)	129.1(3)
C(6)-C(5)-S	128.1(2)	C(16)-C(17)-H(17)	115.4
C(18)-C(5)-S	122.3(2)	C(18)-C(17)-H(17)	115.4
C(7)-C(6)-C(5)	110.3(2)	C(17)-C(18)-C(5)	126.2(2)
C(7)-C(6)-H(6)	124.9	C(17)-C(18)-C(12)	128.9(2)

Table 36 continued

Bond	Angle (°)	Bond	Angle (°)
C(5)-C(6)-H(6)	124.9	C(5)-C(18)-C(12)	104.9(2)
C(6)-C(7)-C(12)	107.1(2)	F(3)-P-F(1)	178.95(13)
C(6)-C(7)-C(8)	124.4(2)	F(3)-P-F(2)	89.91(10)
C(12)-C(7)-C(8)	128.4(2)	F(1)-P-F(2)	89.92(11)
C(7)-C(8)-C(11)	109.8(2)	F(3)-P-F(5)	90.59(11)
C(7)-C(8)-C(10)	109.7(2)	F(1)-P-F(5)	90.45(11)
C(11)-C(8)-C(10)	108.3(3)	F(2)-P-F(5)	89.67(10)
C(7)-C(8)-C(9)	111.5(2)	F(3)-P-F(4)	90.02(11)
C(11)-C(8)-C(9)	110.2(2)	F(1)-P-F(4)	90.14(11)
C(10)-C(8)-C(9)	107.3(2)	F(2)-P-F(4)	179.54(13)
C(8)-C(9)-H(9A)	109.5	F(5)-P-F(4)	90.79(11)
C(8)-C(9)-H(9B)	109.5	F(3)-P-F(6)	89.69(10)
H(9A)-C(9)-H(9B)	109.5	F(1)-P-F(6)	89.27(10)
C(8)-C(9)-H(9C)	109.5	F(2)-P-F(6)	89.96(11)
H(9A)-C(9)-H(9C)	109.5	F(5)-P-F(6)	179.53(12)
H(9B)-C(9)-H(9C)	109.5	F(4)-P-F(6)	89.59(10)

Table 37. Anisotropic displacement parameters ($Å^2$ x 10^3) for 1-(3-*tert*-butylazulen-1-yl)tetrahydrothiophenium hexafluorophosphate (**162**). The anisotropic displacement factor exponent takes the form: $-2\pi^2[h^2 a^{*2}U^{11} + ... + 2 h k a^* b^* U^{12}]$.

	U11	U22	U33	U23	U13	U12
S	27(1)	21(1)	19(1)	5(1)	1(1)	-6(1)
C(1)	28(2)	36(2)	27(1)	11(1)	6(1)	12(1)
C(2)	33(2)	53(2)	27(1)	9(2)	-5(1)	-6(2)
C(3)	49(2)	26(2)	22(1)	-2(1)	9(1)	-1(2)
C(4)	34(2)	36(2)	33(2)	4(1)	18(1)	7(2)
C(5)	23(2)	19(1)	18(1)	4(1)	2(1)	-2(1)
C(6)	27(2)	21(1)	18(1)	1(1)	0(1)	-4(1)
C(7)	22(2)	16(1)	19(1)	1(1)	5(1)	1(1)
C(8)	27(2)	17(1)	23(1)	2(1)	6(1)	-6(1)
C(9)	28(2)	26(1)	33(1)	0(1)	11(1)	-6(1)
C(10)	49(2)	31(2)	28(1)	-1(1)	3(2)	-19(2)
C(11)	38(2)	18(2)	47(2)	4(1)	16(2)	-1(1)
C(12)	19(2)	18(1)	19(1)	0(1)	5(1)	2(1)
C(13)	23(2)	21(1)	23(1)	4(1)	6(1)	2(1)
C(14)	27(2)	36(2)	17(1)	3(1)	2(1)	1(1)
C(15)	30(2)	37(2)	21(1)	-4(1)	-2(1)	-4(2)
C(16)	26(2)	28(2)	29(1)	-3(1)	1(1)	-8(1)
C(17)	20(1)	20(1)	24(1)	3(1)	2(1)	0(1)
C(18)	18(2)	19(1)	20(1)	1(1)	4(1)	2(1)
P	25(1)	25(1)	22(1)	4(1)	3(1)	0(1)
F(1)	46(1)	68(2)	30(1)	-7(1)	18(1)	-10(1)
F(2)	34(1)	31(1)	44(1)	9(1)	-3(1)	6(1)
F(3)	41(1)	53(1)	32(1)	-8(1)	10(1)	4(1)
F(4)	45(1)	34(1)	46(1)	15(1)	-14(1)	1(1)
F(5)	34(1)	32(1)	43(1)	5(1)	-5(1)	-10(1)
F(6)	29(1)	32(1)	38(1)	-1(1)	5(1)	-5(1)

Table 38. Crystal data and structure refinement for 1-(4,6,8-trimethyllazulen-1-yl)tetrahydrothiophenium hexafluorophosphate (**162**)

Identification code	s15sel5	
Empirical formula	C17 H21 F6 P S	
Formula weight	402.37	
Temperature	150(2) K	
Wavelength	1.54184 Å	
Crystal system	Monoclinic	
Space group	$P2_1$	
Unit cell dimensions	a = 7.45260(10) Å	a= 90°.
	b = 13.57000(10) Å	b= 92.2460(10)°.
	c = 17.7705(2) Å	g = 90°.
Volume	1795.78(3) $Å^3$	
Z	4	
Density (calculated)	1.488 Mg/m^3	
Absorption coefficient	2.980 mm^{-1}	
F(000)	832	
Crystal size	0.25 x 0.18 x 0.05 mm^3	
Theta range for data collection	4.100 to 72.576°.	
Index ranges	-5<=h<=9, -16<=k<=16, -21<=l<=21	
Reflections collected	20432	
Independent reflections	6860 [R(int) = 0.0219]	
Completeness to theta = 67.684°	99.60%	
Absorption correction	Semi-empirical from equivalents	
Max. and min. transmission	1.00000 and 0.70200	
Refinement method	Full-matrix least-squares on F2	
Data / restraints / parameters	6860 / 7 / 512	
Goodness-of-fit on F2	1.073	
Final R indices [I>2sigma(I)]	R1 = 0.0376, wR2 = 0.0998	
R indices (all data)	R1 = 0.0380, wR2 = 0.1001	
Absolute structure parameter	0.011(6)	
Extinction coefficient	n/a	
Largest diff. peak and hole	0.517 and -0.328 $e.Å^{-3}$	

Table 39. Atomic coordinates (x 10^4) and equivalent isotropic displacement parameters ($Å^2$ x 10^3) for 1-(4,6,8-trimethyllazulen-1-yl)tetrahydrothiophenium hexafluorophosphate (**162**). U(eq) is defined as one third of the trace of the orthogonalized U^{ij} tensor.

	x	y	z	U(eq)
S(1)	9998(1)	2710(1)	5566(1)	32(1)
C(1)	8309(6)	3329(4)	4957(2)	43(1)
C(2)	9334(7)	3957(4)	4407(2)	46(1)
C(3)	11045(7)	3414(4)	4264(2)	50(1)
C(4)	11884(6)	3163(4)	5034(2)	41(1)
C(5)	10062(5)	3365(3)	6415(2)	29(1)
C(6)	10063(6)	4397(3)	6440(2)	35(1)
C(7)	9964(5)	4688(3)	7179(2)	33(1)
C(8)	9907(5)	3850(3)	7648(2)	27(1)
C(9)	9742(5)	3905(3)	8435(2)	30(1)
C(10)	9623(6)	4923(3)	8780(2)	38(1)
C(11)	9658(5)	3126(3)	8934(2)	35(1)
C(12)	9761(6)	2116(3)	8803(2)	38(1)
C(13)	9667(9)	1467(4)	9496(3)	55(1)
C(14)	9961(6)	1638(3)	8122(2)	37(1)
C(15)	10073(5)	1980(3)	7387(2)	32(1)
C(16)	10273(9)	1168(3)	6814(3)	59(2)
C(17)	10003(4)	2973(3)	7159(2)	26(1)
S(2)	5164(1)	5826(1)	7137(1)	32(1)
C(21)	3271(6)	6680(3)	7001(2)	37(1)
C(22)	4128(5)	7695(3)	6897(2)	38(1)
C(23)	5708(6)	7752(3)	7457(2)	40(1)
C(24)	6789(5)	6808(3)	7358(3)	42(1)
C(25)	4832(5)	5212(3)	7985(2)	30(1)
C(26)	4590(6)	5720(3)	8666(2)	37(1)
C(27)	4489(6)	5037(3)	9236(2)	40(1)
C(28)	4649(5)	4081(3)	8935(2)	34(1)
C(29)	4567(6)	3231(4)	9384(3)	43(1)
C(30)	4290(8)	3375(5)	10216(3)	61(1)
C(31)	4732(7)	2259(4)	9136(3)	51(1)

Table 39 continued

	x	y	z	U(eq)
C(32)	4982(6)	1879(3)	8427(3)	50(1)
C(33)	5117(9)	770(4)	8356(4)	70(2)
C(34)	5083(6)	2408(3)	7757(3)	40(1)
C(35)	5034(5)	3409(3)	7590(2)	32(1)
C(36)	5147(7)	3657(3)	6767(3)	43(1)
C(37)	4869(5)	4185(3)	8115(2)	28(1)
P(1)	4722(2)	5734(1)	4753(1)	40(1)
F(1)	2677(8)	5648(5)	4962(5)	72(2)
F(2)	6783(9)	5817(5)	4604(5)	99(3)
F(3)	5028(7)	6485(4)	5452(2)	61(1)
F(4)	5121(7)	4839(4)	5319(3)	74(2)
F(5)	4400(14)	5000(6)	4103(4)	109(3)
F(6)	4236(10)	6658(4)	4254(3)	85(2)
F(1A)	3170(30)	5480(19)	5272(11)	76(7)
F(2A)	6260(30)	6070(20)	4198(10)	89(8)
F(3A)	6210(20)	5690(20)	5358(8)	109(9)
F(4A)	4880(20)	4607(13)	4516(19)	98(10)
F(5A)	3270(20)	5880(30)	4073(13)	140(12)
F(6A)	4510(30)	6846(13)	4910(20)	116(9)
P(2)	10450(1)	8422(1)	8463(1)	35(1)
F(7)	9071(4)	7651(2)	8793(2)	56(1)
F(8)	10135(3)	7929(2)	7646(1)	44(1)
F(9)	11821(4)	9184(2)	8122(2)	58(1)
F(10)	10783(4)	8909(3)	9276(2)	60(1)
F(11)	12064(4)	7668(2)	8638(2)	58(1)
F(12)	8832(4)	9168(2)	8286(2)	56(1)

Table 40. Bond lengths for 1-(4,6,8-trimethyllazulen-1-yl)tetrahydrothiophenium hexafluorophosphate (**162**).

Bond	Length (Å)	Bond	Length (Å)
S(1)-C(5)	1.749(4)	C(23)-C(24)	1.527(6)
S(1)-C(4)	1.830(4)	C(23)-H(23A)	0.99
S(1)-C(1)	1.832(4)	C(23)-H(23B)	0.99
C(1)-C(2)	1.523(7)	C(24)-H(24A)	0.99
C(1)-H(1A)	0.99	C(24)-H(24B)	0.99
C(1)-H(1B)	0.99	C(25)-C(26)	1.411(5)
C(2)-C(3)	1.503(7)	C(25)-C(37)	1.413(5)
C(2)-H(2A)	0.99	C(26)-C(27)	1.377(6)
C(2)-H(2B)	0.99	C(26)-H(26)	0.95
C(3)-C(4)	1.521(6)	C(27)-C(28)	1.410(6)
C(3)-H(3A)	0.99	C(27)-H(27)	0.95
C(3)-H(3B)	0.99	C(28)-C(29)	1.406(6)
C(4)-H(4A)	0.99	C(28)-C(37)	1.480(6)
C(4)-H(4B)	0.99	C(29)-C(31)	1.397(7)
C(5)-C(6)	1.401(6)	C(29)-C(30)	1.513(7)
C(5)-C(17)	1.429(5)	C(30)-H(30A)	0.98
C(6)-C(7)	1.376(6)	C(30)-H(30B)	0.98
C(6)-H(6)	0.95	C(30)-H(30C)	0.98
C(7)-C(8)	1.412(6)	C(31)-C(32)	1.381(8)
C(7)-H(7)	0.95	C(31)-H(31)	0.95
C(8)-C(9)	1.411(5)	C(32)-C(34)	1.395(7)
C(8)-C(17)	1.476(5)	C(32)-C(33)	1.514(7)
C(9)-C(11)	1.383(6)	C(33)-H(33A)	0.98
C(9)-C(10)	1.516(5)	C(33)-H(33B)	0.98
C(10)-H(10A)	0.98	C(33)-H(33C)	0.98
C(10)-H(10B)	0.98	C(34)-C(35)	1.390(6)
C(10)-H(10C)	0.98	C(34)-H(34)	0.95
C(11)-C(12)	1.393(6)	C(35)-C(37)	1.416(6)
C(11)-H(11)	0.95	C(35)-C(36)	1.506(6)
C(12)-C(14)	1.388(6)	C(36)-H(36A)	0.98
C(12)-C(13)	1.517(6)	C(36)-H(36B)	0.98

Table 40 continued

Bond	Length (Å)	Bond	Length (Å)
C(13)-H(13A)	0.98	C(36)-H(36C)	0.98
C(13)-H(13B)	0.98	P(1)-F(3A)	1.517(14)
C(13)-H(13C)	0.98	P(1)-F(5)	1.536(6)
C(14)-C(15)	1.392(6)	P(1)-F(6A)	1.545(16)
C(14)-H(14)	0.95	P(1)-F(1A)	1.545(16)
C(15)-C(17)	1.406(5)	P(1)-F(6)	1.569(4)
C(15)-C(16)	1.512(6)	P(1)-F(2)	1.572(6)
C(16)-H(16A)	0.98	P(1)-F(1)	1.588(7)
C(16)-H(16B)	0.98	P(1)-F(4A)	1.592(16)
C(16)-H(16C)	0.98	P(1)-F(4)	1.598(4)
S(2)-C(25)	1.748(4)	P(1)-F(5A)	1.601(16)
S(2)-C(24)	1.833(4)	P(1)-F(2A)	1.605(19)
S(2)-C(21)	1.834(4)	P(1)-F(3)	1.616(4)
C(21)-C(22)	1.533(6)	P(2)-F(9)	1.590(3)
C(21)-H(21A)	0.99	P(2)-F(7)	1.595(3)
C(21)-H(21B)	0.99	P(2)-F(12)	1.596(3)
C(22)-C(23)	1.514(6)	P(2)-F(10)	1.598(3)
C(22)-H(22A)	0.99	P(2)-F(11)	1.601(3)
C(22)-H(22B)	0.99	P(2)-F(8)	1.609(3)

Table 41. Bond angles for 1-(4,6,8-trimethyllazulen-1-yl)tetrahydrothiophenium hexafluorophosphate (**162**).

Bond	Angle (°)	Bond	Angle (°)
C(5)-S(1)-C(4)	106.2(2)	S(2)-C(24)-H(24A)	110.4
C(5)-S(1)-C(1)	105.8(2)	C(23)-C(24)-H(24B)	110.4
C(4)-S(1)-C(1)	93.7(2)	S(2)-C(24)-H(24B)	110.4
C(2)-C(1)-S(1)	106.6(3)	H(24A)-C(24)-H(24B)	108.6
C(2)-C(1)-H(1A)	110.4	C(26)-C(25)-C(37)	110.1(3)
S(1)-C(1)-H(1A)	110.4	C(26)-C(25)-S(2)	122.3(3)
C(2)-C(1)-H(1B)	110.4	C(37)-C(25)-S(2)	127.5(3)
S(1)-C(1)-H(1B)	110.4	C(27)-C(26)-C(25)	108.4(4)
H(1A)-C(1)-H(1B)	108.6	C(27)-C(26)-H(26)	125.8
C(3)-C(2)-C(1)	106.5(4)	C(25)-C(26)-H(26)	125.8
C(3)-C(2)-H(2A)	110.4	C(26)-C(27)-C(28)	109.4(4)
C(1)-C(2)-H(2A)	110.4	C(26)-C(27)-H(27)	125.3
C(3)-C(2)-H(2B)	110.4	C(28)-C(27)-H(27)	125.3
C(1)-C(2)-H(2B)	110.4	C(29)-C(28)-C(27)	122.2(4)
H(2A)-C(2)-H(2B)	108.6	C(29)-C(28)-C(37)	130.3(4)
C(2)-C(3)-C(4)	106.2(4)	C(27)-C(28)-C(37)	107.5(4)
C(2)-C(3)-H(3A)	110.5	C(31)-C(29)-C(28)	126.1(4)
C(4)-C(3)-H(3A)	110.5	C(31)-C(29)-C(30)	116.6(4)
C(2)-C(3)-H(3B)	110.5	C(28)-C(29)-C(30)	117.3(5)
C(4)-C(3)-H(3B)	110.5	C(29)-C(30)-H(30A)	109.5
H(3A)-C(3)-H(3B)	108.7	C(29)-C(30)-H(30B)	109.5
C(3)-C(4)-S(1)	104.1(3)	H(30A)-C(30)-H(30B)	109.5
C(3)-C(4)-H(4A)	110.9	C(29)-C(30)-H(30C)	109.5
S(1)-C(4)-H(4A)	110.9	H(30A)-C(30)-H(30C)	109.5
C(3)-C(4)-H(4B)	110.9	H(30B)-C(30)-H(30C)	109.5
S(1)-C(4)-H(4B)	110.9	C(32)-C(31)-C(29)	131.1(4)
H(4A)-C(4)-H(4B)	109	C(32)-C(31)-H(31)	114.5
C(6)-C(5)-C(17)	110.0(3)	C(29)-C(31)-H(31)	114.5
C(6)-C(5)-S(1)	122.4(3)	C(31)-C(32)-C(34)	126.9(4)
C(17)-C(5)-S(1)	127.5(3)	C(31)-C(32)-C(33)	117.3(5)
C(7)-C(6)-C(5)	108.5(4)	C(34)-C(32)-C(33)	115.8(5)
C(7)-C(6)-H(6)	125.7	C(32)-C(33)-H(33A)	109.5

Table 41 continued

Bond	Angle (°)	Bond	Angle (°)
C(5)-C(6)-H(6)	125.7	C(32)-C(33)-H(33B)	109.5
C(6)-C(7)-C(8)	109.6(4)	H(33A)-C(33)-H(33B)	109.5
C(6)-C(7)-H(7)	125.2	C(32)-C(33)-H(33C)	109.5
C(8)-C(7)-H(7)	125.2	H(33A)-C(33)-H(33C)	109.5
C(9)-C(8)-C(7)	123.2(3)	H(33B)-C(33)-H(33C)	109.5
C(9)-C(8)-C(17)	129.3(3)	C(35)-C(34)-C(32)	133.1(5)
C(7)-C(8)-C(17)	107.5(3)	C(35)-C(34)-H(34)	113.5
C(11)-C(9)-C(8)	127.1(4)	C(32)-C(34)-H(34)	113.5
C(11)-C(9)-C(10)	115.6(4)	C(34)-C(35)-C(37)	126.0(4)
C(8)-C(9)-C(10)	117.3(4)	C(34)-C(35)-C(36)	115.0(4)
C(9)-C(10)-H(10A)	109.5	C(37)-C(35)-C(36)	118.9(4)
C(9)-C(10)-H(10B)	109.5	C(35)-C(36)-H(36A)	109.5
H(10A)-C(10)-H(10B)	109.5	C(35)-C(36)-H(36B)	109.5
C(9)-C(10)-H(10C)	109.5	H(36A)-C(36)-H(36B)	109.5
H(10A)-C(10)-H(10C)	109.5	C(35)-C(36)-H(36C)	109.5
H(10B)-C(10)-H(10C)	109.5	H(36A)-C(36)-H(36C)	109.5
C(9)-C(11)-C(12)	129.9(4)	H(36B)-C(36)-H(36C)	109.5
C(9)-C(11)-H(11)	115.1	C(25)-C(37)-C(35)	128.9(4)
C(12)-C(11)-H(11)	115.1	C(25)-C(37)-C(28)	104.6(3)
C(14)-C(12)-C(11)	127.9(4)	C(35)-C(37)-C(28)	126.5(4)
C(14)-C(12)-C(13)	116.6(4)	F(3A)-P(1)-F(6A)	89.4(17)
C(11)-C(12)-C(13)	115.5(4)	F(3A)-P(1)-F(1A)	96.4(11)
C(12)-C(13)-H(13A)	109.5	F(6A)-P(1)-F(1A)	91.3(12)
C(12)-C(13)-H(13B)	109.5	F(5)-P(1)-F(6)	93.9(4)
H(13A)-C(13)-H(13B)	109.5	F(5)-P(1)-F(2)	92.6(5)
C(12)-C(13)-H(13C)	109.5	F(6)-P(1)-F(2)	93.1(4)
H(13A)-C(13)-H(13C)	109.5	F(5)-P(1)-F(1)	90.3(5)
H(13B)-C(13)-H(13C)	109.5	F(6)-P(1)-F(1)	89.3(3)
C(12)-C(14)-C(15)	132.5(4)	F(2)-P(1)-F(1)	176.1(4)
C(12)-C(14)-H(14)	113.8	F(3A)-P(1)-F(4A)	94.9(16)
C(15)-C(14)-H(14)	113.8	F(6A)-P(1)-F(4A)	175.1(19)
C(14)-C(15)-C(17)	125.9(4)	F(1A)-P(1)-F(4A)	90.5(13)
C(14)-C(15)-C(16)	113.5(4)	F(5)-P(1)-F(4)	90.0(4)

Table 41 continued

Bond	Angle (°)	Bond	Angle (°)
C(17)-C(15)-C(16)	120.6(3)	F(6)-P(1)-F(4)	174.9(3)
C(15)-C(16)-H(16A)	109.5	F(2)-P(1)-F(4)	90.1(4)
C(15)-C(16)-H(16B)	109.5	F(1)-P(1)-F(4)	87.3(3)
H(16A)-C(16)-H(16B)	109.5	F(3A)-P(1)-F(5A)	173.7(15)
C(15)-C(16)-H(16C)	109.5	F(6A)-P(1)-F(5A)	87.0(19)
H(16A)-C(16)-H(16C)	109.5	F(1A)-P(1)-F(5A)	88.9(12)
H(16B)-C(16)-H(16C)	109.5	F(4A)-P(1)-F(5A)	88.5(17)
C(15)-C(17)-C(5)	128.4(3)	F(3A)-P(1)-F(2A)	85.8(10)
C(15)-C(17)-C(8)	127.2(3)	F(6A)-P(1)-F(2A)	85.4(13)
C(5)-C(17)-C(8)	104.4(3)	F(1A)-P(1)-F(2A)	176.0(14)
C(25)-S(2)-C(24)	106.0(2)	F(4A)-P(1)-F(2A)	92.6(14)
C(25)-S(2)-C(21)	106.33(19)	F(5A)-P(1)-F(2A)	88.7(12)
C(24)-S(2)-C(21)	93.87(19)	F(5)-P(1)-F(3)	178.3(3)
C(22)-C(21)-S(2)	105.2(3)	F(6)-P(1)-F(3)	87.3(3)
C(22)-C(21)-H(21A)	110.7	F(2)-P(1)-F(3)	88.6(3)
S(2)-C(21)-H(21A)	110.7	F(1)-P(1)-F(3)	88.5(3)
C(22)-C(21)-H(21B)	110.7	F(4)-P(1)-F(3)	88.7(3)
S(2)-C(21)-H(21B)	110.7	F(9)-P(2)-F(7)	179.10(17)
H(21A)-C(21)-H(21B)	108.8	F(9)-P(2)-F(12)	90.25(18)
C(23)-C(22)-C(21)	106.4(3)	F(7)-P(2)-F(12)	89.75(17)
C(23)-C(22)-H(22A)	110.4	F(9)-P(2)-F(10)	89.82(18)
C(21)-C(22)-H(22A)	110.4	F(7)-P(2)-F(10)	91.08(18)
C(23)-C(22)-H(22B)	110.4	F(12)-P(2)-F(10)	90.39(17)
C(21)-C(22)-H(22B)	110.4	F(9)-P(2)-F(11)	90.06(18)
H(22A)-C(22)-H(22B)	108.6	F(7)-P(2)-F(11)	89.93(18)
C(22)-C(23)-C(24)	106.4(4)	F(12)-P(2)-F(11)	179.48(18)
C(22)-C(23)-H(23A)	110.4	F(10)-P(2)-F(11)	90.03(16)
C(24)-C(23)-H(23A)	110.4	F(9)-P(2)-F(8)	89.95(15)
C(22)-C(23)-H(23B)	110.4	F(7)-P(2)-F(8)	89.15(15)
C(24)-C(23)-H(23B)	110.4	F(12)-P(2)-F(8)	90.14(16)
H(23A)-C(23)-H(23B)	108.6	F(10)-P(2)-F(8)	179.43(17)
C(23)-C(24)-S(2)	106.7(3)	F(11)-P(2)-F(8)	89.45(15)
C(23)-C(24)-H(24A)	110.4		

Table 42. Anisotropic displacement parameters ($Å^2$ x 10^3) for 1-(4,6,8-trimethyllazulen-1-yl)tetrahydrothiophenium hexafluorophosphate (**162**). The anisotropic displacement factor exponent takes the form: $-2\pi^2[h^2 a^{*2}U^{11} + ... + 2 h k a^* b^* U^{12}]$.

	U11	U22	U33	U23	U13	U12
S(1)	45(1)	25(1)	27(1)	0(1)	2(1)	0(1)
C(1)	41(2)	49(3)	38(2)	2(2)	-6(2)	3(2)
C(2)	63(3)	42(2)	33(2)	8(2)	-6(2)	3(2)
C(3)	66(3)	54(3)	29(2)	-1(2)	9(2)	-6(2)
C(4)	44(2)	48(2)	32(2)	-1(2)	9(2)	10(2)
C(5)	32(2)	27(2)	29(2)	-1(2)	3(1)	1(2)
C(6)	45(2)	28(2)	33(2)	2(2)	8(2)	-2(2)
C(7)	35(2)	28(2)	37(2)	-4(2)	3(2)	-2(2)
C(8)	22(2)	27(2)	32(2)	-5(2)	-1(1)	1(1)
C(9)	26(2)	30(2)	33(2)	-5(2)	-6(1)	3(2)
C(10)	46(2)	34(2)	35(2)	-10(2)	-1(2)	2(2)
C(11)	38(2)	40(2)	27(2)	-5(2)	-2(2)	5(2)
C(12)	48(2)	37(2)	28(2)	4(2)	-3(2)	0(2)
C(13)	97(4)	39(2)	30(2)	4(2)	2(2)	1(3)
C(14)	52(2)	28(2)	30(2)	2(2)	-1(2)	3(2)
C(15)	38(2)	26(2)	30(2)	-1(2)	0(2)	3(2)
C(16)	120(5)	27(2)	31(2)	1(2)	10(3)	21(3)
C(17)	23(2)	25(2)	29(2)	-3(1)	-1(1)	0(1)
S(2)	43(1)	25(1)	29(1)	1(1)	4(1)	1(1)
C(21)	38(2)	32(2)	40(2)	7(2)	-7(2)	0(2)
C(22)	42(2)	28(2)	45(2)	7(2)	-1(2)	1(2)
C(23)	46(2)	30(2)	44(2)	0(2)	0(2)	-3(2)
C(24)	31(2)	34(2)	59(3)	9(2)	4(2)	-1(2)
C(25)	35(2)	27(2)	29(2)	2(2)	-1(1)	0(2)
C(26)	45(2)	33(2)	34(2)	0(2)	0(2)	10(2)
C(27)	43(2)	45(2)	31(2)	3(2)	4(2)	13(2)
C(28)	25(2)	41(2)	38(2)	6(2)	0(1)	8(2)
C(29)	31(2)	47(3)	50(2)	18(2)	6(2)	2(2)
C(30)	71(3)	63(3)	50(3)	28(3)	17(2)	18(3)
C(31)	52(3)	41(3)	58(3)	21(2)	4(2)	3(2)

Table 43. Crystal data and structure refinement for 3-(5-(4,6,8-trimethylazulen-1-yl)thiophen-2-yl)-2-cyanoacrylic acid (**147**).

Identification code	s15sel2	
Empirical formula	C21 H17 N O2 S	
Formula weight	347.42	
Temperature	150(2) K	
Wavelength	1.54184 Å	
Crystal system	Monoclinic	
Space group	I2/a	
Unit cell dimensions	a = 9.6555(3) Å	a= 90°.
	b = 16.0617(5) Å	b= 94.454(3)°.
	c = 21.8419(9) Å	g = 90°.
Volume	3377.1(2) $Å^3$	
Z	8	
Density (calculated)	1.367 Mg/m^3	
Absorption coefficient	1.812 mm^{-1}	
F(000)	1456	
Crystal size	0.230 x 0.180 x 0.010 mm^3	
Theta range for data collection	5.357 to 72.050°.	
Index ranges	-7<=h<=11, -15<=k<=19, -26<=l<=26	
Reflections collected	10138	
Independent reflections	3262 [R(int) = 0.0402]	
Completeness to theta = 67.684°	99.60%	
Absorption correction	Semi-empirical from equivalents	
Max. and min. transmission	1.00000 and 0.74452	
Refinement method	Full-matrix least-squares on F2	
Data / restraints / parameters	3262 / 2 / 238	
Goodness-of-fit on F2	0.983	
Final R indices [I>2sigma(I)]	R1 = 0.0540, wR2 = 0.1341	
R indices (all data)	R1 = 0.0674, wR2 = 0.1427	
Extinction coefficient	n/a	
Largest diff. peak and hole	0.336 and -0.303 $e.Å^{-3}$	

Table 44. Atomic coordinates (x 10^4) and equivalent isotropic displacement parameters ($Å^2$ x 10^3) for 3-(5-(4,6,8-trimethylazulen-1-yl)thiophen-2-yl)-2-cyanoacrylic acid (**147**). U(eq) is defined as one third of the trace of the orthogonalized U^{ij} tensor.

	x	y	z	U(eq)
S	4056(1)	1839(1)	1192(1)	34(1)
N	1882(2)	3338(2)	731(1)	54(1)
O(1)	-1138(2)	1152(1)	111(1)	49(1)
O(2)	-1184(2)	2550(1)	150(1)	48(1)
C(1)	-576(3)	1853(2)	232(1)	40(1)
C(2)	871(2)	1872(2)	497(1)	38(1)
C(3)	1436(3)	2687(2)	621(1)	42(1)
C(4)	1546(2)	1160(2)	671(1)	38(1)
C(5)	2863(2)	1048(1)	993(1)	36(1)
C(6)	3358(3)	300(2)	1229(1)	42(1)
C(7)	4637(3)	360(2)	1567(1)	40(1)
C(8)	5177(2)	1153(1)	1589(1)	35(1)
C(9)	6529(2)	1440(1)	1848(1)	34(1)
C(10)	7449(3)	1863(1)	1489(1)	37(1)
C(11)	8750(2)	1904(2)	1803(1)	38(1)
C(12)	8696(2)	1529(1)	2378(1)	35(1)
C(13)	9851(2)	1419(1)	2802(1)	37(1)
C(14)	11261(3)	1648(2)	2595(1)	47(1)
C(15)	9854(3)	1105(1)	3392(1)	41(1)
C(16)	8750(3)	847(2)	3728(1)	41(1)
C(17)	9128(3)	559(2)	4379(1)	53(1)
C(18)	7346(3)	836(2)	3529(1)	42(1)
C(19)	6637(2)	1012(1)	2963(1)	37(1)
C(20)	5072(3)	967(2)	2964(1)	42(1)
C(21)	7237(2)	1256(1)	2427(1)	33(1)

Table 45. Bond lengths (Å) for 3-(5-(4,6,8-trimethylazulen-1-yl)thiophen-2-yl)-2-cyanoacrylic acid (**147**).

Bond	Length (Å)	Bond	Length (Å)
S-C(8)	1.730(2)	C(11)-H(11)	0.95
S-C(5)	1.747(2)	C(12)-C(13)	1.405(3)
N-C(3)	1.149(4)	C(12)-C(21)	1.488(3)
O(1)-C(1)	1.268(3)	C(13)-C(15)	1.383(4)
O(1)-H(1)	0.871(19)	C(13)-C(14)	1.513(3)
O(2)-C(1)	1.271(3)	C(14)-H(14A)	0.98
O(2)-H(2)	0.88(2)	C(14)-H(14B)	0.98
C(1)-C(2)	1.470(3)	C(14)-H(14C)	0.98
C(2)-C(4)	1.355(4)	C(15)-C(16)	1.402(4)
C(2)-C(3)	1.436(4)	C(15)-H(15)	0.95
C(4)-C(5)	1.416(3)	C(16)-C(18)	1.391(4)
C(4)-H(4)	0.95	C(16)-C(17)	1.513(4)
C(5)-C(6)	1.378(3)	C(17)-H(17A)	0.98
C(6)-C(7)	1.392(4)	C(17)-H(17B)	0.98
C(6)-H(6)	0.95	C(17)-H(17C)	0.98
C(7)-C(8)	1.376(3)	C(18)-C(19)	1.396(3)
C(7)-H(7)	0.95	C(18)-H(18)	0.95
C(8)-C(9)	1.458(3)	C(19)-C(21)	1.402(3)
C(9)-C(10)	1.404(3)	C(19)-C(20)	1.513(3)
C(9)-C(21)	1.420(3)	C(20)-H(20A)	0.98
C(10)-C(11)	1.384(3)	C(20)-H(20B)	0.98
C(10)-H(10)	0.95	C(20)-H(20C)	0.98
C(11)-C(12)	1.398(3)		

Table 46. Bond angles (°) for 3-(5-(4,6,8-trimethylazulen-1-yl)thiophen-2-yl)-2-cyanoacrylic acid (**147**).

Bond	Angle(°)	Bond	Angle (°)
C(8)-S-C(5)	92.04(12)	C(15)-C(13)-C(12)	127.1(2)
C(1)-O(1)-H(1)	122(3)	C(15)-C(13)-C(14)	115.5(2)
C(1)-O(2)-H(2)	120(4)	C(12)-C(13)-C(14)	117.3(2)
O(1)-C(1)-O(2)	124.6(2)	C(13)-C(14)-H(14A)	109.5
O(1)-C(1)-C(2)	118.6(2)	C(13)-C(14)-H(14B)	109.5
O(2)-C(1)-C(2)	116.8(2)	H(14A)-C(14)-H(14B)	109.5
C(4)-C(2)-C(3)	123.3(2)	C(13)-C(14)-H(14C)	109.5
C(4)-C(2)-C(1)	121.0(2)	H(14A)-C(14)-H(14C)	109.5
C(3)-C(2)-C(1)	115.4(2)	H(14B)-C(14)-H(14C)	109.5
N-C(3)-C(2)	178.7(3)	C(13)-C(15)-C(16)	130.4(2)
C(2)-C(4)-C(5)	129.9(2)	C(13)-C(15)-H(15)	114.8
C(2)-C(4)-H(4)	115.1	C(16)-C(15)-H(15)	114.8
C(5)-C(4)-H(4)	115.1	C(18)-C(16)-C(15)	127.0(2)
C(6)-C(5)-C(4)	124.7(2)	C(18)-C(16)-C(17)	116.6(2)
C(6)-C(5)-S	109.82(18)	C(15)-C(16)-C(17)	116.4(2)
C(4)-C(5)-S	125.41(18)	C(16)-C(17)-H(17A)	109.5
C(5)-C(6)-C(7)	113.9(2)	C(16)-C(17)-H(17B)	109.5
C(5)-C(6)-H(6)	123	H(17A)-C(17)-H(17B)	109.5
C(7)-C(6)-H(6)	123	C(16)-C(17)-H(17C)	109.5
C(8)-C(7)-C(6)	113.6(2)	H(17A)-C(17)-H(17C)	109.5
C(8)-C(7)-H(7)	123.2	H(17B)-C(17)-H(17C)	109.5
C(6)-C(7)-H(7)	123.2	C(16)-C(18)-C(19)	132.3(2)
C(7)-C(8)-C(9)	129.2(2)	C(16)-C(18)-H(18)	113.8
C(7)-C(8)-S	110.59(18)	C(19)-C(18)-H(18)	113.8
C(9)-C(8)-S	119.98(17)	C(18)-C(19)-C(21)	126.2(2)
C(10)-C(9)-C(21)	108.4(2)	C(18)-C(19)-C(20)	114.2(2)
C(10)-C(9)-C(8)	121.5(2)	C(21)-C(19)-C(20)	119.5(2)
C(21)-C(9)-C(8)	129.4(2)	C(19)-C(20)-H(20A)	109.5
C(11)-C(10)-C(9)	109.6(2)	C(19)-C(20)-H(20B)	109.5
C(11)-C(10)-H(10)	125.2	H(20A)-C(20)-H(20B)	109.5
C(9)-C(10)-H(10)	125.2	C(19)-C(20)-H(20C)	109.5
C(10)-C(11)-C(12)	109.2(2)	H(20A)-C(20)-H(20C)	109.5

Table 46 continued

Bond	Angle(°)	Bond	Angle (°)
C(10)-C(11)-H(11)	125.4	H(20B)-C(20)-H(20C)	109.5
C(12)-C(11)-H(11)	125.4	C(19)-C(21)-C(9)	126.9(2)
C(11)-C(12)-C(13)	124.3(2)	C(19)-C(21)-C(12)	126.7(2)
C(11)-C(12)-C(21)	107.0(2)	C(9)-C(21)-C(12)	105.5(2)
C(13)-C(12)-C(21)	128.6(2)		

Table 47. Anisotropic displacement parameters ($Å^2$ x 10^3) for 3-(5-(4,6,8-trimethylazulen-1-yl)thiophen-2-yl)-2-cyanoacrylic acid (**147**). The anisotropic displacement factor exponent takes the form: $-2\pi^2[h^2 a^{*2}U^{11} + ... + 2 h k a^* b^* U^{12}]$.

	U11	U22	U33	U23	U13	U12
S	30(1)	33(1)	39(1)	2(1)	-2(1)	1(1)
N	45(1)	46(1)	70(2)	1(1)	-7(1)	1(1)
O(1)	36(1)	56(1)	53(1)	0(1)	-3(1)	-4(1)
O(2)	35(1)	55(1)	53(1)	7(1)	-1(1)	4(1)
C(1)	35(1)	46(1)	38(1)	3(1)	2(1)	-1(1)
C(2)	35(1)	46(1)	33(1)	1(1)	4(1)	-1(1)
C(3)	31(1)	50(2)	43(1)	4(1)	-2(1)	6(1)
C(4)	34(1)	43(1)	37(1)	-3(1)	4(1)	-4(1)
C(5)	32(1)	36(1)	42(1)	-2(1)	4(1)	-4(1)
C(6)	36(1)	38(1)	52(2)	-1(1)	4(1)	-3(1)
C(7)	34(1)	37(1)	49(1)	4(1)	1(1)	3(1)
C(8)	31(1)	36(1)	37(1)	4(1)	2(1)	6(1)
C(9)	31(1)	32(1)	38(1)	-1(1)	3(1)	4(1)
C(10)	39(1)	37(1)	34(1)	0(1)	3(1)	-2(1)
C(11)	34(1)	38(1)	42(1)	-3(1)	7(1)	-4(1)
C(12)	34(1)	30(1)	40(1)	-5(1)	3(1)	0(1)
C(13)	31(1)	33(1)	47(1)	-7(1)	0(1)	1(1)
C(14)	34(1)	51(1)	55(2)	-7(1)	1(1)	-4(1)
C(15)	35(1)	36(1)	50(1)	-4(1)	-8(1)	5(1)
C(16)	50(1)	35(1)	38(1)	0(1)	-3(1)	4(1)
C(17)	64(2)	51(2)	43(2)	6(1)	-7(1)	5(1)
C(18)	48(1)	36(1)	41(1)	3(1)	7(1)	1(1)
C(19)	37(1)	31(1)	43(1)	2(1)	6(1)	3(1)
C(20)	37(1)	47(1)	44(1)	5(1)	10(1)	2(1)
C(21)	32(1)	27(1)	40(1)	-1(1)	1(1)	3(1)

Table 48. Crystal data and structure refinement for 3-(5-(3-(tert-butyl)azulen-1-yl)thiophen-2-yl)-2-cyanoacrylic acid (**205**).

Identification code	k15sel2	
Empirical formula	C22 H19 N O2 S	
Formula weight	361.44	
Temperature	150(2) K	
Wavelength	0.71073 Å	
Crystal system	Monoclinic	
Space group	C2/c	
Unit cell dimensions	a = 23.9276(5) Å	a= 90°.
	b = 8.0666(2) Å	b= 97.7080(8)°.
	c = 20.6336(4) Å	g = 90°.
Volume	3946.60(15) $Å^3$	
Z	8	
Density (calculated)	1.217 Mg/m^3	
Absorption coefficient	0.179 mm^{-1}	
F(000)	1520	
Crystal size	0.250 x 0.250 x 0.100 mm^3	
Theta range for data collection	3.260 to 27.463°.	
Index ranges	-30<=h<=30, -10<=k<=10, -26<=l<=26	
Reflections collected	40919	
Independent reflections	4519 [R(int) = 0.0850]	
Completeness to theta = 25.242°	99.80%	
Absorption correction	Semi-empirical from equivalents	
Max. and min. transmission	0.986 and 0.873	
Refinement method	Full-matrix least-squares on F2	
Data / restraints / parameters	4519 / 2 / 247	
Goodness-of-fit on F2	1.05	
Final R indices [I>2sigma(I)]	R1 = 0.0478, wR2 = 0.1015	
R indices (all data)	R1 = 0.0813, wR2 = 0.1154	
Extinction coefficient	n/a	
Largest diff. peak and hole	0.250 and -0.290 $e.Å^{-3}$	

Table 49. Atomic coordinates (x 10^4) and equivalent isotropic displacement parameters ($Å^2$ x 10^3) for 3-(5-(3-(tert-butyl)azulen-1-yl)thiophen-2-yl)-2-cyanoacrylic acid (**205**). U(eq) is defined as one third of the trace of the orthogonalized U^{ij} tensor.

	x	y	z	U(eq)
S	4040(1)	5771(1)	4296(1)	30(1)
O(1)	4829(1)	4600(2)	6873(1)	34(1)
O(2)	4824(1)	7383(2)	6884(1)	39(1)
N	4358(1)	8879(2)	5351(1)	46(1)
C(1)	4744(1)	5993(2)	6594(1)	28(1)
C(2)	4537(1)	6008(2)	5889(1)	29(1)
C(3)	4441(1)	7602(2)	5590(1)	32(1)
C(4)	4437(1)	4564(2)	5556(1)	29(1)
C(5)	4232(1)	4262(2)	4887(1)	28(1)
C(6)	4171(1)	2696(2)	4610(1)	33(1)
C(7)	3983(1)	2717(2)	3943(1)	33(1)
C(8)	3893(1)	4299(2)	3686(1)	28(1)
C(9)	3677(1)	4699(2)	3013(1)	28(1)
C(10)	3747(1)	6133(2)	2641(1)	28(1)
C(11)	4076(1)	7503(2)	2845(1)	31(1)
C(12)	4184(1)	8929(2)	2504(1)	38(1)
C(13)	3993(1)	9329(3)	1856(1)	41(1)
C(14)	3640(1)	8455(3)	1393(1)	40(1)
C(15)	3380(1)	6932(2)	1455(1)	35(1)
C(16)	3414(1)	5851(2)	1983(1)	29(1)
C(17)	3151(1)	4270(2)	1997(1)	31(1)
C(18)	2740(1)	3440(3)	1466(1)	36(1)
C(19)	2205(1)	4502(3)	1304(1)	50(1)
C(20)	3016(1)	3112(3)	849(1)	45(1)
C(21)	2555(1)	1755(3)	1710(1)	43(1)
C(22)	3322(1)	3601(2)	2612(1)	32(1)

Table 50. Bond lengths for 3-(5-(3-(tert-butyl)azulen-1-yl)thiophen-2-yl)-2-cyanoacrylic acid (**205**).

Bond	Length (Å)	Bond	Length (Å)
S-C(8)	1.7324(18)	C(12)-C(13)	1.390(3)
S-C(5)	1.7418(18)	C(12)-H(12)	0.95
O(1)-C(1)	1.266(2)	C(13)-C(14)	1.381(3)
O(1)-H(1)	0.849(18)	C(13)-H(13)	0.95
O(2)-C(1)	1.273(2)	C(14)-C(15)	1.391(3)
O(2)-H(2)	0.886(19)	C(14)-H(14)	0.95
N-C(3)	1.148(2)	C(15)-C(16)	1.390(3)
C(1)-C(2)	1.473(3)	C(15)-H(15)	0.95
C(2)-C(4)	1.358(3)	C(16)-C(17)	1.424(3)
C(2)-C(3)	1.432(3)	C(17)-C(22)	1.389(3)
C(4)-C(5)	1.421(2)	C(17)-C(18)	1.526(3)
C(4)-H(4)	0.95	C(18)-C(21)	1.535(3)
C(5)-C(6)	1.386(3)	C(18)-C(20)	1.537(3)
C(6)-C(7)	1.390(3)	C(18)-C(19)	1.539(3)
C(6)-H(6)	0.95	C(19)-H(19A)	0.98
C(7)-C(8)	1.388(3)	C(19)-H(19B)	0.98
C(7)-H(7)	0.95	C(19)-H(19C)	0.98
C(8)-C(9)	1.450(2)	C(20)-H(20A)	0.98
C(9)-C(10)	1.411(2)	C(20)-H(20B)	0.98
C(9)-C(22)	1.415(3)	C(20)-H(20C)	0.98
C(10)-C(11)	1.389(3)	C(21)-H(21A)	0.98
C(10)-C(16)	1.497(2)	C(21)-H(21B)	0.98
C(11)-C(12)	1.391(3)	C(21)-H(21C)	0.98
C(11)-H(11)	0.95	C(22)-H(22)	0.95

Table 51. Bond Angles for 3-(5-(3-(tert-butyl)azulen-1-yl)thiophen-2-yl)-2-cyanoacrylic acid (**205**).

Bond	Angle (°)	Bond	Angle (°)
C(8)-S-C(5)	92.22(9)	C(13)-C(14)-C(15)	128.88(19)
C(1)-O(1)-H(1)	116(2)	C(13)-C(14)-H(14)	115.6
C(1)-O(2)-H(2)	118(3)	C(15)-C(14)-H(14)	115.6
O(1)-C(1)-O(2)	124.37(17)	C(16)-C(15)-C(14)	130.21(19)
O(1)-C(1)-C(2)	117.89(16)	C(16)-C(15)-H(15)	114.9
O(2)-C(1)-C(2)	117.74(16)	C(14)-C(15)-H(15)	114.9
C(4)-C(2)-C(3)	122.97(17)	C(15)-C(16)-C(17)	126.70(17)
C(4)-C(2)-C(1)	120.47(16)	C(15)-C(16)-C(10)	125.80(17)
C(3)-C(2)-C(1)	116.55(16)	C(17)-C(16)-C(10)	107.50(15)
N-C(3)-C(2)	179.2(2)	C(22)-C(17)-C(16)	106.85(16)
C(2)-C(4)-C(5)	130.80(17)	C(22)-C(17)-C(18)	124.55(17)
C(2)-C(4)-H(4)	114.6	C(16)-C(17)-C(18)	128.56(17)
C(5)-C(4)-H(4)	114.6	C(17)-C(18)-C(21)	109.88(16)
C(6)-C(5)-C(4)	124.02(16)	C(17)-C(18)-C(20)	111.23(16)
C(6)-C(5)-S	110.18(13)	C(21)-C(18)-C(20)	107.13(17)
C(4)-C(5)-S	125.78(14)	C(17)-C(18)-C(19)	110.45(17)
C(5)-C(6)-C(7)	113.51(17)	C(21)-C(18)-C(19)	107.30(17)
C(5)-C(6)-H(6)	123.2	C(20)-C(18)-C(19)	110.71(18)
C(7)-C(6)-H(6)	123.2	C(18)-C(19)-H(19A)	109.5
C(8)-C(7)-C(6)	113.82(17)	C(18)-C(19)-H(19B)	109.5
C(8)-C(7)-H(7)	123.1	H(19A)-C(19)-H(19B)	109.5
C(6)-C(7)-H(7)	123.1	C(18)-C(19)-H(19C)	109.5
C(7)-C(8)-C(9)	126.02(17)	H(19A)-C(19)-H(19C)	109.5
C(7)-C(8)-S	110.25(13)	H(19B)-C(19)-H(19C)	109.5
C(9)-C(8)-S	123.64(14)	C(18)-C(20)-H(20A)	109.5
C(10)-C(9)-C(22)	107.50(16)	C(18)-C(20)-H(20B)	109.5
C(10)-C(9)-C(8)	130.50(17)	H(20A)-C(20)-H(20B)	109.5
C(22)-C(9)-C(8)	121.98(17)	C(18)-C(20)-H(20C)	109.5
C(11)-C(10)-C(9)	126.32(17)	H(20A)-C(20)-H(20C)	109.5
C(11)-C(10)-C(16)	127.33(16)	H(20B)-C(20)-H(20C)	109.5
C(9)-C(10)-C(16)	106.33(15)	C(18)-C(21)-H(21A)	109.5
C(10)-C(11)-C(12)	129.84(18)	C(18)-C(21)-H(21B)	109.5

Table 51 continued

Bond	Angle (°)	Bond	Angle (°)
C(10)-C(11)-H(11)	115.1	H(21A)-C(21)-H(21B)	109.5
C(12)-C(11)-H(11)	115.1	C(18)-C(21)-H(21C)	109.5
C(13)-C(12)-C(11)	128.30(19)	H(21A)-C(21)-H(21C)	109.5
C(13)-C(12)-H(12)	115.8	H(21B)-C(21)-H(21C)	109.5
C(11)-C(12)-H(12)	115.8	C(17)-C(22)-C(9)	111.80(17)
C(14)-C(13)-C(12)	129.60(19)	C(17)-C(22)-H(22)	124.1
C(14)-C(13)-H(13)	115.2	C(9)-C(22)-H(22)	124.1
C(12)-C(13)-H(13)	115.2		

Table 52. Anisotropic displacement parameters ($Å^2$ x 10^3) for 3-(5-(3-(tert-butyl)azulen-1-yl)thiophen-2-yl)-2-cyanoacrylic acid (**205**). The anisotropic displacement factor exponent takes the form: $-2\pi^2[h^2 a^{*2}U^{11} + ... + 2 h k a^* b^* U^{12}]$.

	U11	U22	U33	U23	U13	U12
S	38(1)	26(1)	24(1)	2(1)	2(1)	3(1)
O(1)	41(1)	34(1)	27(1)	7(1)	1(1)	2(1)
O(2)	55(1)	32(1)	29(1)	-2(1)	1(1)	7(1)
N	68(1)	35(1)	36(1)	4(1)	6(1)	6(1)
C(1)	29(1)	28(1)	29(1)	2(1)	7(1)	3(1)
C(2)	33(1)	29(1)	26(1)	4(1)	6(1)	4(1)
C(3)	39(1)	33(1)	26(1)	0(1)	6(1)	5(1)
C(4)	30(1)	30(1)	28(1)	5(1)	6(1)	4(1)
C(5)	31(1)	29(1)	26(1)	4(1)	4(1)	3(1)
C(6)	40(1)	27(1)	31(1)	5(1)	6(1)	2(1)
C(7)	41(1)	26(1)	32(1)	0(1)	4(1)	-1(1)
C(8)	30(1)	30(1)	25(1)	0(1)	3(1)	0(1)
C(9)	29(1)	29(1)	27(1)	0(1)	4(1)	1(1)
C(10)	28(1)	30(1)	26(1)	1(1)	4(1)	4(1)
C(11)	34(1)	32(1)	27(1)	0(1)	4(1)	3(1)
C(12)	44(1)	34(1)	37(1)	-1(1)	6(1)	-5(1)
C(13)	50(1)	32(1)	41(1)	9(1)	9(1)	-3(1)
C(14)	51(1)	37(1)	32(1)	9(1)	5(1)	1(1)
C(15)	39(1)	38(1)	28(1)	2(1)	1(1)	1(1)
C(16)	29(1)	34(1)	26(1)	0(1)	5(1)	3(1)
C(17)	29(1)	34(1)	29(1)	-3(1)	5(1)	0(1)
C(18)	33(1)	41(1)	33(1)	-2(1)	3(1)	-3(1)
C(19)	37(1)	56(1)	55(1)	-2(1)	-6(1)	-1(1)
C(20)	50(1)	52(1)	33(1)	-9(1)	2(1)	-9(1)
C(21)	40(1)	45(1)	42(1)	-7(1)	4(1)	-10(1)
C(22)	34(1)	31(1)	30(1)	1(1)	6(1)	-2(1)

Table 53. Crystal data and structure refinement for 3-(5-(3-(methylthio)azulen-1-yl)thiophen-2-yl)cyanoacrylic acid (**203**).

Identification code	k15sel1	
Empirical formula	C19 H13 N O2 S2	
Formula weight	351.42	
Temperature	150(2) K	
Wavelength	0.71073 Å	
Crystal system	Monoclinic	
Space group	$P2_1/c$	
Unit cell dimensions	a = 10.2894(3) Å	a= 90°.
	b = 15.1789(4) Å	b= 105.9551(11)°.
	c = 10.7696(4) Å	g = 90°.
Volume	1617.22(9) $Å^3$	
Z	4	
Density (calculated)	1.443 Mg/m^3	
Absorption coefficient	0.340 mm^{-1}	
F(000)	728	
Crystal size	0.600 x 0.250 x 0.020 mm^3	
Theta range for data collection	3.618 to 27.487°.	
Index ranges	-13<=h<=13, -18<=k<=19, -13<=l<=13	
Reflections collected	24449	
Independent reflections	3682 [R(int) = 0.0878]	
Completeness to theta = 25.242°	99.40%	
Absorption correction	Semi-empirical from equivalents	
Max. and min. transmission	0.999 and 0.827	
Refinement method	Full-matrix least-squares on F2	
Data / restraints / parameters	3682 / 2 / 226	
Goodness-of-fit on F2	1.039	
Final R indices [I>2sigma(I)]	R1 = 0.0516, wR2 = 0.1219	
R indices (all data)	R1 = 0.0774, wR2 = 0.1359	
Extinction coefficient	n/a	
Largest diff. peak and hole	0.869 and -0.506 e.$Å^{-3}$	

Table 54. Atomic coordinates (x 10^4) and equivalent isotropic displacement parameters (Å^2 x 10^3) for 3-(5-(3-(methylthio)azulen-1-yl)thiophen-2-yl)cyanoacrylic acid (**203**). U(eq) is defined as one third of the trace of the orthogonalized U^{ij} tensor.

	x	y	z	U(eq)
S(1)	-3351(1)	3777(1)	874(1)	51(1)
S(2)	3230(1)	5160(1)	2740(1)	29(1)
N	5705(2)	6641(2)	2765(3)	45(1)
O(1)	8829(2)	5748(1)	4174(2)	37(1)
O(2)	8610(2)	4354(1)	4787(2)	38(1)
C(1)	-2941(4)	2781(2)	1755(5)	72(1)
C(2)	-1796(2)	4331(2)	1317(3)	35(1)
C(3)	-1636(2)	5211(2)	961(3)	33(1)
C(4)	-2688(3)	5756(2)	310(3)	37(1)
C(5)	-2617(3)	6610(2)	-132(3)	41(1)
C(6)	-1494(3)	7122(2)	-55(3)	42(1)
C(7)	-141(3)	6948(2)	546(3)	41(1)
C(8)	447(3)	6194(2)	1211(3)	36(1)
C(9)	-162(2)	5417(2)	1420(2)	30(1)
C(10)	477(2)	4647(2)	2061(2)	29(1)
C(11)	-543(2)	4006(2)	1980(3)	34(1)
C(12)	1890(2)	4446(2)	2637(2)	28(1)
C(13)	2373(2)	3630(2)	3135(3)	32(1)
C(14)	3766(3)	3582(2)	3577(3)	33(1)
C(15)	4420(2)	4359(2)	3443(2)	29(1)
C(16)	5838(2)	4458(2)	3833(2)	31(1)
C(17)	6646(2)	5155(2)	3755(2)	30(1)
C(18)	6131(2)	5982(2)	3200(3)	33(1)
C(19)	8120(2)	5074(2)	4275(3)	31(1)

Table 55. Bond lengths (Å) for 3-(5-(3-(methylthio)azulen-1-yl)thiophen-2-yl)cyanoacrylic acid (**203**).

Bond	**Length (Å)**	**Bond**	**Length (Å)**
S(1)-C(2)	1.754(3)	C(6)-C(7)	1.389(4)
S(1)-C(1)	1.772(4)	C(6)-H(6)	0.95
S(2)-C(12)	1.734(2)	C(7)-C(8)	1.397(4)
S(2)-C(15)	1.745(2)	C(7)-H(7)	0.95
N-C(18)	1.140(3)	C(8)-C(9)	1.382(4)
O(1)-C(19)	1.278(3)	C(8)-H(8)	0.95
O(1)-H(1)	0.86(2)	C(9)-C(10)	1.424(3)
O(2)-C(19)	1.265(3)	C(10)-C(11)	1.417(3)
O(2)-H(2)	0.86(2)	C(10)-C(12)	1.447(3)
C(1)-H(1A)	0.98	C(11)-H(11)	0.95
C(1)-H(1B)	0.98	C(12)-C(13)	1.386(3)
C(1)-H(1C)	0.98	C(13)-C(14)	1.383(3)
C(2)-C(11)	1.381(4)	C(13)-H(13)	0.95
C(2)-C(3)	1.412(4)	C(14)-C(15)	1.384(3)
C(3)-C(4)	1.390(4)	C(14)-H(14)	0.95
C(3)-C(9)	1.493(3)	C(15)-C(16)	1.411(3)
C(4)-C(5)	1.390(4)	C(16)-C(17)	1.363(3)
C(4)-H(4)	0.95	C(16)-H(16)	0.95
C(5)-C(6)	1.377(4)	C(17)-C(18)	1.427(4)
C(5)-H(5)	0.95	C(17)-C(19)	1.471(3)

Table 56. Bond angles (°) for 3-(5-(3-(methylthio)azulen-1-yl)thiophen-2-yl)cyanoacrylic acid (**203**).

Bond	Angle(°)	Bond	Angle(°)
C(2)-S(1)-C(1)	101.41(15)	C(8)-C(9)-C(10)	127.6(2)
C(12)-S(2)-C(15)	92.47(11)	C(8)-C(9)-C(3)	126.1(2)
C(19)-O(1)-H(1)	117(4)	C(10)-C(9)-C(3)	106.2(2)
C(19)-O(2)-H(2)	118(5)	C(11)-C(10)-C(9)	107.4(2)
S(1)-C(1)-H(1A)	109.5	C(11)-C(10)-C(12)	121.5(2)
S(1)-C(1)-H(1B)	109.5	C(9)-C(10)-C(12)	131.0(2)
H(1A)-C(1)-H(1B)	109.5	C(2)-C(11)-C(10)	110.9(2)
S(1)-C(1)-H(1C)	109.5	C(2)-C(11)-H(11)	124.5
H(1A)-C(1)-H(1C)	109.5	C(10)-C(11)-H(11)	124.5
H(1B)-C(1)-H(1C)	109.5	C(13)-C(12)-C(10)	124.4(2)
C(11)-C(2)-C(3)	108.5(2)	C(13)-C(12)-S(2)	109.83(17)
C(11)-C(2)-S(1)	128.4(2)	C(10)-C(12)-S(2)	125.68(19)
C(3)-C(2)-S(1)	123.1(2)	C(14)-C(13)-C(12)	114.1(2)
C(4)-C(3)-C(2)	124.5(2)	C(14)-C(13)-H(13)	123
C(4)-C(3)-C(9)	128.5(2)	C(12)-C(13)-H(13)	123
C(2)-C(3)-C(9)	107.0(2)	C(13)-C(14)-C(15)	114.0(2)
C(3)-C(4)-C(5)	128.4(3)	C(13)-C(14)-H(14)	123
C(3)-C(4)-H(4)	115.8	C(15)-C(14)-H(14)	123
C(5)-C(4)-H(4)	115.8	C(14)-C(15)-C(16)	123.5(2)
C(6)-C(5)-C(4)	128.9(3)	C(14)-C(15)-S(2)	109.60(18)
C(6)-C(5)-H(5)	115.5	C(16)-C(15)-S(2)	126.87(19)
C(4)-C(5)-H(5)	115.5	C(17)-C(16)-C(15)	131.5(2)
C(5)-C(6)-C(7)	129.7(3)	C(17)-C(16)-H(16)	114.3
C(5)-C(6)-H(6)	115.2	C(15)-C(16)-H(16)	114.3
C(7)-C(6)-H(6)	115.2	C(16)-C(17)-C(18)	123.1(2)
C(6)-C(7)-C(8)	129.1(3)	C(16)-C(17)-C(19)	119.6(2)
C(6)-C(7)-H(7)	115.4	C(18)-C(17)-C(19)	117.3(2)
C(8)-C(7)-H(7)	115.4	N-C(18)-C(17)	179.0(3)
C(9)-C(8)-C(7)	129.1(3)	O(2)-C(19)-O(1)	124.1(2)
C(9)-C(8)-H(8)	115.4	O(2)-C(19)-C(17)	119.0(2)
C(7)-C(8)-H(8)	115.4	O(1)-C(19)-C(17)	116.9(2)

Table 57. Anisotropic displacement parameters ($Å^2$ x 10^3) for 3-(5-(3-(methylthio)azulen-1-yl)thiophen-2-yl)cyanoacrylic acid (**203**). The anisotropic displacement factor exponent takes the form: $-2\pi^2[h^2 a^{*2}U^{11} + ... + 2 h k a^* b^* U^{12}]$.

	U11	**U22**	**U33**	**U23**	**U13**	**U12**
S(1)	26(1)	46(1)	73(1)	2(1)	2(1)	-7(1)
S(2)	22(1)	26(1)	39(1)	1(1)	6(1)	-1(1)
N	31(1)	35(1)	66(2)	5(1)	7(1)	-2(1)
O(1)	23(1)	32(1)	55(1)	-3(1)	9(1)	-2(1)
O(2)	23(1)	34(1)	53(1)	0(1)	6(1)	3(1)
C(1)	42(2)	55(2)	111(3)	17(2)	10(2)	-13(2)
C(2)	25(1)	37(1)	41(2)	-4(1)	7(1)	-3(1)
C(3)	25(1)	37(1)	34(1)	-5(1)	6(1)	4(1)
C(4)	30(1)	41(1)	37(2)	-7(1)	5(1)	4(1)
C(5)	43(2)	35(1)	43(2)	-2(1)	10(1)	11(1)
C(6)	48(2)	31(1)	44(2)	-2(1)	8(1)	11(1)
C(7)	41(2)	30(1)	50(2)	-2(1)	9(1)	0(1)
C(8)	31(1)	33(1)	42(2)	-2(1)	6(1)	1(1)
C(9)	27(1)	31(1)	32(1)	-2(1)	8(1)	2(1)
C(10)	24(1)	30(1)	32(1)	-2(1)	7(1)	-1(1)
C(11)	26(1)	33(1)	40(2)	0(1)	7(1)	-2(1)
C(12)	23(1)	28(1)	32(1)	-1(1)	6(1)	-3(1)
C(13)	27(1)	29(1)	38(1)	3(1)	6(1)	-3(1)
C(14)	29(1)	28(1)	39(2)	2(1)	6(1)	1(1)
C(15)	25(1)	27(1)	34(1)	-1(1)	5(1)	2(1)
C(16)	27(1)	30(1)	34(1)	-3(1)	7(1)	3(1)
C(17)	24(1)	29(1)	35(1)	-4(1)	6(1)	2(1)
C(18)	21(1)	34(1)	42(2)	-3(1)	7(1)	-2(1)
C(19)	23(1)	32(1)	38(1)	-4(1)	7(1)	0(1)

Table 58. Crystal data and structure refinement for 3-(5'-(4,6,8-trimethylazulen-1-yl)-[2,2'-bithiophen]-5-yl)-2-cyanoacrylic acid (**213**).

Identification code	s16sel3	
Empirical formula	C25 H19 N O2 S2	
Formula weight	429.53	
Temperature	150.00(10) K	
Wavelength	1.54184 Å	
Crystal system	Monoclinic	
Space group	$P2_1/c$	
Unit cell dimensions	a = 13.2530(9) Å	a= 90°.
	b = 8.2886(3) Å	b= 103.552(5)°.
	c = 19.6068(9) Å	g = 90°.
Volume	2093.82(19) $Å^3$	
Z	4	
Density (calculated)	1.363 Mg/m^3	
Absorption coefficient	2.480 mm^{-1}	
F(000)	896	
Crystal size	0.050 x 0.040 x 0.010 mm^3	
Theta range for data collection	3.430 to 72.687°.	
Index ranges	-16<=h<=16, -10<=k<=10, -24<=l<=17	
Reflections collected	11375	
Independent reflections	4062 [R(int) = 0.0414]	
Completeness to theta = 67.684°	99.80%	
Absorption correction	Semi-empirical from equivalents	
Max. and min. transmission	1.00000 and 0.91397	
Refinement method	Full-matrix least-squares on F2	
Data / restraints / parameters	4062 / 2 / 282	
Goodness-of-fit on F2	1.04	
Final R indices [I>2sigma(I)]	R1 = 0.0423, wR2 = 0.0971	
R indices (all data)	R1 = 0.0552, wR2 = 0.1039	
Extinction coefficient	n/a	
Largest diff. peak and hole	0.411 and -0.277 $e.Å^{-3}$	

Table 59. Atomic coordinates (x 10^4) and equivalent isotropic displacement parameters ($Å^2$ x 10^3) for 3-(5'-(4,6,8-trimethylazulen-1-yl)-[2,2'-bithiophen]-5-yl)-2-cyanoacrylic acid (**213**). U(eq) is defined as one third of the trace of the orthogonalized U^{ij} tensor.

	x	**y**	**z**	**U(eq)**
S(1)	7908(1)	7669(1)	4250(1)	26(1)
S(2)	5847(1)	3729(1)	4464(1)	28(1)
N	8951(2)	10332(3)	3350(1)	55(1)
O(1)	9774(2)	13669(2)	4322(1)	38(1)
O(2)	9348(1)	13541(2)	5363(1)	36(1)
C(1)	9381(2)	12961(3)	4774(1)	29(1)
C(2)	8938(2)	11339(3)	4590(1)	28(1)
C(3)	8951(2)	10783(3)	3902(1)	35(1)
C(4)	8551(2)	10460(3)	5054(1)	26(1)
C(5)	8081(2)	8909(3)	4984(1)	24(1)
C(6)	7638(2)	8218(3)	5483(1)	28(1)
C(7)	7157(2)	6740(3)	5280(1)	27(1)
C(8)	7237(2)	6258(2)	4619(1)	24(1)
C(9)	6828(2)	4828(2)	4235(1)	23(1)
C(10)	7095(2)	4136(3)	3670(1)	32(1)
C(11)	6517(2)	2743(3)	3422(1)	33(1)
C(12)	5798(2)	2359(3)	3792(1)	24(1)
C(13)	5065(2)	989(3)	3710(1)	24(1)
C(14)	5330(2)	-448(3)	4079(1)	30(1)
C(15)	4503(2)	-1514(3)	3931(1)	29(1)
C(16)	3661(2)	-761(2)	3485(1)	23(1)
C(17)	2674(2)	-1465(3)	3264(1)	25(1)
C(18)	2542(2)	-3177(3)	3501(1)	35(1)
C(19)	1785(2)	-737(3)	2875(1)	29(1)
C(20)	1629(2)	811(3)	2591(1)	29(1)
C(21)	529(2)	1225(4)	2214(1)	44(1)
C(22)	2374(2)	2006(3)	2598(1)	28(1)
C(23)	3441(2)	2059(2)	2891(1)	24(1)
C(24)	3976(2)	3544(3)	2700(1)	34(1)
C(25)	4016(2)	884(2)	3330(1)	22(1)

Table 60. Bond lengths for 3-(5'-(4,6,8-trimethylazulen-1-yl)-[2,2'-bithiophen]-5-yl)-2-cyanoacrylic acid (**213**).

Bond	Length (Å)	Bond	Length (Å)
S(1)-C(8)	1.728(2)	C(13)-C(25)	1.418(3)
S(1)-C(5)	1.740(2)	C(14)-C(15)	1.385(3)
S(2)-C(12)	1.728(2)	C(14)-H(14)	0.95
S(2)-C(9)	1.730(2)	C(15)-C(16)	1.393(3)
N-C(3)	1.145(3)	C(15)-H(15)	0.95
O(1)-C(1)	1.273(3)	C(16)-C(17)	1.405(3)
O(1)-H(1)	0.87(2)	C(16)-C(25)	1.497(3)
O(2)-C(1)	1.261(3)	C(17)-C(19)	1.383(3)
O(2)-H(2)	0.87(2)	C(17)-C(18)	1.516(3)
C(1)-C(2)	1.477(3)	C(18)-H(18A)	0.98
C(2)-C(4)	1.356(3)	C(18)-H(18B)	0.98
C(2)-C(3)	1.430(3)	C(18)-H(18C)	0.98
C(4)-C(5)	1.421(3)	C(19)-C(20)	1.394(3)
C(4)-H(4)	0.95	C(19)-H(19)	0.95
C(5)-C(6)	1.379(3)	C(20)-C(22)	1.397(3)
C(6)-C(7)	1.395(3)	C(20)-C(21)	1.511(3)
C(6)-H(6)	0.95	C(21)-H(21A)	0.98
C(7)-C(8)	1.385(3)	C(21)-H(21B)	0.98
C(7)-H(7)	0.95	C(21)-H(21C)	0.98
C(8)-C(9)	1.440(3)	C(22)-C(23)	1.396(3)
C(9)-C(10)	1.366(3)	C(22)-H(22)	0.95
C(10)-C(11)	1.407(3)	C(23)-C(25)	1.400(3)
C(10)-H(10)	0.95	C(23)-C(24)	1.511(3)
C(11)-C(12)	1.363(3)	C(24)-H(24A)	0.98
C(11)-H(11)	0.95	C(24)-H(24B)	0.98
C(12)-C(13)	1.478(3)	C(24)-H(24C)	0.98
C(13)-C(14)	1.395(3)		

Table 61. Bond angles (°) for 3-(5'-(4,6,8-trimethylazulen-1-yl)-[2,2'-bithiophen]-5-yl)-2-cyanoacrylic acid (**213**).

Bond	Angle (°)	Bond	Angle (°)
C(8)-S(1)-C(5)	91.98(10)	C(13)-C(14)-H(14)	124.9
C(12)-S(2)-C(9)	92.55(10)	C(14)-C(15)-C(16)	108.84(19)
C(1)-O(1)-H(1)	114(7)	C(14)-C(15)-H(15)	125.6
C(1)-O(2)-H(2)	114(4)	C(16)-C(15)-H(15)	125.6
O(2)-C(1)-O(1)	124.7(2)	C(15)-C(16)-C(17)	123.9(2)
O(2)-C(1)-C(2)	118.2(2)	C(15)-C(16)-C(25)	107.03(19)
O(1)-C(1)-C(2)	117.0(2)	C(17)-C(16)-C(25)	129.0(2)
C(4)-C(2)-C(3)	123.3(2)	C(19)-C(17)-C(16)	126.9(2)
C(4)-C(2)-C(1)	121.1(2)	C(19)-C(17)-C(18)	115.7(2)
C(3)-C(2)-C(1)	115.6(2)	C(16)-C(17)-C(18)	117.4(2)
N-C(3)-C(2)	179.3(3)	C(17)-C(18)-H(18A)	109.5
C(2)-C(4)-C(5)	130.3(2)	C(17)-C(18)-H(18B)	109.5
C(2)-C(4)-H(4)	114.8	H(18A)-C(18)-H(18B)	109.5
C(5)-C(4)-H(4)	114.8	C(17)-C(18)-H(18C)	109.5
C(6)-C(5)-C(4)	123.9(2)	H(18A)-C(18)-H(18C)	109.5
C(6)-C(5)-S(1)	110.24(16)	H(18B)-C(18)-H(18C)	109.5
C(4)-C(5)-S(1)	125.80(17)	C(17)-C(19)-C(20)	130.5(2)
C(5)-C(6)-C(7)	113.92(19)	C(17)-C(19)-H(19)	114.8
C(5)-C(6)-H(6)	123	C(20)-C(19)-H(19)	114.8
C(7)-C(6)-H(6)	123	C(19)-C(20)-C(22)	127.6(2)
C(8)-C(7)-C(6)	112.94(19)	C(19)-C(20)-C(21)	116.1(2)
C(8)-C(7)-H(7)	123.5	C(22)-C(20)-C(21)	116.3(2)
C(6)-C(7)-H(7)	123.5	C(20)-C(21)-H(21A)	109.5
C(7)-C(8)-C(9)	128.69(19)	C(20)-C(21)-H(21B)	109.5
C(7)-C(8)-S(1)	110.92(16)	H(21A)-C(21)-H(21B)	109.5
C(9)-C(8)-S(1)	120.38(16)	C(20)-C(21)-H(21C)	109.5
C(10)-C(9)-C(8)	129.2(2)	H(21A)-C(21)-H(21C)	109.5
C(10)-C(9)-S(2)	110.03(16)	H(21B)-C(21)-H(21C)	109.5
C(8)-C(9)-S(2)	120.76(15)	C(23)-C(22)-C(20)	132.2(2)
C(9)-C(10)-C(11)	113.6(2)	C(23)-C(22)-H(22)	113.9
C(9)-C(10)-H(10)	123.2	C(20)-C(22)-H(22)	113.9
C(11)-C(10)-H(10)	123.2	C(22)-C(23)-C(25)	125.7(2)

Table 61 continued

Bond	Angle (°)	Bond	Angle (°)
C(12)-C(11)-C(10)	113.57(19)	C(22)-C(23)-C(24)	114.3(2)
C(12)-C(11)-H(11)	123.2	C(25)-C(23)-C(24)	119.9(2)
C(10)-C(11)-H(11)	123.2	C(23)-C(24)-H(24A)	109.5
C(11)-C(12)-C(13)	130.17(19)	C(23)-C(24)-H(24B)	109.5
C(11)-C(12)-S(2)	110.22(16)	H(24A)-C(24)-H(24B)	109.5
C(13)-C(12)-S(2)	119.57(15)	C(23)-C(24)-H(24C)	109.5
C(14)-C(13)-C(25)	108.48(19)	H(24A)-C(24)-H(24C)	109.5
C(14)-C(13)-C(12)	121.3(2)	H(24B)-C(24)-H(24C)	109.5
C(25)-C(13)-C(12)	130.01(19)	C(23)-C(25)-C(13)	127.27(19)
C(15)-C(14)-C(13)	110.2(2)	C(23)-C(25)-C(16)	127.4(2)
C(15)-C(14)-H(14)	124.9	C(13)-C(25)-C(16)	105.37(18)

Table 62. Anisotropic displacement parameters ($Å^2$ x 10^3) for 3-(5'-(4,6,8-trimethylazulen-1-yl)-[2,2'-bithiophen]-5-yl)-2-cyanoacrylic acid (**213**). The anisotropic displacement factor exponent takes the form: $-2\pi^2[h^2 a^{*2}U^{11} + ... + 2 h k a^* b^* U^{12}]$.

	U11	**U22**	**U33**	**U23**	**U13**	**U12**
S(1)	36(1)	22(1)	24(1)	-6(1)	14(1)	-9(1)
S(2)	36(1)	25(1)	27(1)	-6(1)	16(1)	-9(1)
N	87(2)	43(1)	45(1)	-17(1)	36(1)	-32(1)
O(1)	49(1)	28(1)	39(1)	-3(1)	17(1)	-15(1)
O(2)	49(1)	28(1)	34(1)	-12(1)	13(1)	-13(1)
C(1)	33(1)	24(1)	31(1)	-5(1)	9(1)	-6(1)
C(2)	33(1)	22(1)	30(1)	-7(1)	10(1)	-7(1)
C(3)	49(2)	26(1)	36(1)	-6(1)	18(1)	-16(1)
C(4)	30(1)	23(1)	23(1)	-6(1)	5(1)	-3(1)
C(5)	28(1)	22(1)	24(1)	-4(1)	7(1)	-1(1)
C(6)	38(1)	24(1)	21(1)	-3(1)	8(1)	-1(1)
C(7)	40(1)	21(1)	23(1)	0(1)	12(1)	-3(1)
C(8)	28(1)	20(1)	24(1)	0(1)	8(1)	-2(1)
C(9)	30(1)	19(1)	23(1)	0(1)	10(1)	-5(1)
C(10)	43(1)	24(1)	34(1)	-6(1)	22(1)	-10(1)
C(11)	49(1)	24(1)	32(1)	-9(1)	22(1)	-10(1)
C(12)	31(1)	21(1)	22(1)	-2(1)	7(1)	-3(1)
C(13)	29(1)	19(1)	26(1)	1(1)	10(1)	-1(1)
C(14)	28(1)	26(1)	34(1)	6(1)	2(1)	-1(1)
C(15)	34(1)	18(1)	37(1)	7(1)	9(1)	-1(1)
C(16)	30(1)	18(1)	22(1)	2(1)	9(1)	1(1)
C(17)	32(1)	23(1)	21(1)	-1(1)	10(1)	-2(1)
C(18)	34(1)	27(1)	44(1)	3(1)	9(1)	-7(1)
C(19)	29(1)	35(1)	23(1)	-1(1)	8(1)	-5(1)
C(20)	30(1)	39(1)	21(1)	4(1)	8(1)	5(1)
C(21)	32(1)	60(2)	38(1)	15(1)	6(1)	6(1)
C(22)	40(1)	27(1)	19(1)	6(1)	9(1)	8(1)
C(23)	35(1)	20(1)	19(1)	-1(1)	10(1)	1(1)
C(24)	44(1)	23(1)	33(1)	10(1)	4(1)	1(1)
C(25)	32(1)	16(1)	20(1)	-1(1)	11(1)	-1(1)

Table 63. Crystal data and structure refinement for 3-(5'-(azulen-1-yl)-[2,2'-bithiophen]-5-yl)-2-cyanoacrylic acid (**212**).

Identification code	s16sel4	
Empirical formula	C50 H39 N3 O6 S4	
Formula weight	906.08	
Temperature	150.01(10) K	
Wavelength	1.54184 Å	
Crystal system	Triclinic	
Space group	P-1	
Unit cell dimensions	a = 8.5235(4) Å	a= 84.123(4)°.
	b = 13.4554(7) Å	b= 85.083(4)°.
	c = 18.4321(8) Å	g = 85.917(4)°.
Volume	2090.92(17) $Å^3$	
Z	2	
Density (calculated)	1.439 Mg/m^3	
Absorption coefficient	2.558 mm^{-1}	
F(000)	944	
Crystal size	0.050 x 0.030 x 0.010 mm^3	
Theta range for data collection	3.308 to 72.469°.	
Index ranges	-10<=h<=6, -16<=k<=16, -21<=l<=22	
Reflections collected	13862	
Independent reflections	8075 [R(int) = 0.0238]	
Completeness to theta = 67.684°	99.90%	
Absorption correction	Semi-empirical from equivalents	
Max. and min. transmission	1.00000 and 0.87758	
Refinement method	Full-matrix least-squares on F2	
Data / restraints / parameters	8075 / 0 / 571	
Goodness-of-fit on F2	1.032	
Final R indices [I>2sigma(I)]	R1 = 0.0565, wR2 = 0.1470	
R indices (all data)	R1 = 0.0686, wR2 = 0.1573	
Extinction coefficient	n/a	
Largest diff. peak and hole	0.953 and -0.465 $e.Å^{-3}$	

Table 64. Atomic coordinates (x 10^4) and equivalent isotropic displacement parameters ($Å^2$ x 10^3) for 3-(5'-(azulen-1-yl)-[2,2'-bithiophen]-5-yl)-2-cyanoacrylic acid (**212**). U(eq) is defined as one third of the trace of the orthogonalized U^{ij} tensor.

	x	y	z	U(eq)
S(1)	7456(1)	3084(1)	8732(1)	35(1)
S(2)	9878(1)	2383(1)	10732(1)	38(1)
S(3)	-538(1)	6372(1)	2858(1)	37(1)
S(4)	-2873(1)	6077(1)	877(1)	39(1)
C(1)	5099(4)	5150(2)	6764(2)	37(1)
C(2)	5854(3)	4488(2)	7361(2)	33(1)
C(3)	5795(4)	3433(2)	7328(2)	39(1)
C(4)	6548(3)	4868(2)	7894(2)	34(1)
C(5)	7317(3)	4374(2)	8502(2)	34(1)
C(6)	8005(4)	4846(2)	9012(2)	38(1)
C(7)	8610(4)	4192(2)	9574(2)	39(1)
C(8)	8400(3)	3208(2)	9505(2)	33(1)
C(9)	8792(3)	2327(2)	9991(2)	34(1)
C(10)	8331(4)	1377(2)	9975(2)	42(1)
C(11)	8837(4)	708(2)	10551(2)	43(1)
C(12)	9699(4)	1130(2)	11021(2)	34(1)
C(13)	10371(4)	597(2)	11664(2)	36(1)
C(14)	10328(4)	-460(2)	11808(2)	42(1)
C(15)	11032(4)	-786(2)	12442(2)	44(1)
C(16)	11579(4)	43(2)	12724(2)	39(1)
C(17)	12391(4)	-15(3)	13348(2)	44(1)
C(18)	13048(4)	750(3)	13656(2)	46(1)
C(19)	12993(4)	1757(3)	13431(2)	45(1)
C(20)	12274(4)	2280(3)	12837(2)	43(1)
C(21)	11472(4)	1917(2)	12310(2)	39(1)
C(22)	11146(3)	944(2)	12227(2)	34(1)
C(31)	2420(4)	5031(3)	4918(2)	41(1)
C(32)	1482(4)	5522(2)	4314(2)	38(1)
C(33)	1373(4)	6595(3)	4218(2)	46(1)
C(34)	805(4)	4940(2)	3891(2)	40(1)

Table 64 continued

	x	y	z	U(eq)
C(35)	-80(4)	5182(2)	3268(2)	38(1)
C(36)	-646(4)	4477(3)	2883(2)	44(1)
C(37)	-1422(4)	4879(3)	2275(2)	44(1)
C(38)	-1466(3)	5903(2)	2182(2)	35(1)
C(39)	-2152(3)	6569(2)	1606(2)	35(1)
C(40)	-2352(4)	7579(2)	1530(2)	44(1)
C(41)	-3082(4)	7969(2)	896(2)	41(1)
C(42)	-3456(3)	7253(2)	471(2)	34(1)
C(43)	-4248(3)	7308(2)	-197(2)	35(1)
C(44)	-4916(4)	6480(2)	-437(2)	42(1)
C(45)	-5605(4)	6746(3)	-1083(2)	44(1)
C(46)	-5434(4)	7767(2)	-1283(2)	39(1)
C(47)	-6044(4)	8300(3)	-1890(2)	46(1)
C(48)	-5963(4)	9308(3)	-2132(2)	50(1)
C(49)	-5197(4)	10024(3)	-1835(2)	49(1)
C(50)	-4339(4)	9926(3)	-1218(2)	45(1)
C(51)	-4033(4)	9096(2)	-728(2)	39(1)
C(52)	-4534(3)	8139(2)	-718(2)	35(1)
C(61)	2724(5)	8026(3)	5953(2)	50(1)
C(62)	1296(5)	8715(3)	5917(3)	67(1)
C(63)	1542(6)	9760(4)	5575(3)	72(1)
C(64)	2481(5)	10353(3)	6024(2)	66(1)
C(65)	2925(6)	11366(3)	5633(2)	68(1)
C(66)	3899(5)	11893(3)	6109(2)	54(1)
N(1)	5736(4)	2594(2)	7297(2)	55(1)
N(2)	1303(5)	7444(3)	4151(2)	70(1)
N(3)	4634(4)	12840(3)	5649(2)	66(1)
O(1)	5048(3)	6070(2)	6796(1)	49(1)
O(2)	4573(3)	4700(2)	6272(1)	41(1)
O(3)	2462(3)	4125(2)	5052(1)	56(1)
O(4)	3105(3)	5640(2)	5265(1)	44(1)
O(5)	3863(3)	8064(3)	5506(2)	73(1)
O(6)	2717(4)	7369(2)	6524(2)	63(1)

Table 65. Bond lengths for 3-(5'-(azulen-1-yl)-[2,2'-bithiophen]-5-yl)-2-cyanoacrylic acid (**212**).

Bond	Length (Å)	Bond	Length (Å)
S(1)-C(8)	1.724(3)	C(35)-C(36)	1.377(5)
S(1)-C(5)	1.743(3)	C(36)-C(37)	1.392(4)
S(2)-C(9)	1.724(3)	C(36)-H(36)	0.95
S(2)-C(12)	1.730(3)	C(37)-C(38)	1.369(4)
S(3)-C(38)	1.725(3)	C(37)-H(37)	0.95
S(3)-C(35)	1.733(3)	C(38)-C(39)	1.452(4)
S(4)-C(39)	1.733(3)	C(39)-C(40)	1.352(4)
S(4)-C(42)	1.738(3)	C(40)-C(41)	1.409(4)
C(1)-O(1)	1.242(4)	C(40)-H(40)	0.95
C(1)-O(2)	1.268(4)	C(41)-C(42)	1.372(4)
C(1)-C(2)	1.502(4)	C(41)-H(41)	0.95
C(2)-C(4)	1.351(4)	C(42)-C(43)	1.447(4)
C(2)-C(3)	1.431(4)	C(43)-C(44)	1.412(4)
C(3)-N(1)	1.142(4)	C(43)-C(52)	1.419(4)
C(4)-C(5)	1.428(4)	C(44)-C(45)	1.375(5)
C(4)-H(4)	0.95	C(44)-H(44)	0.95
C(5)-C(6)	1.377(4)	C(45)-C(46)	1.400(5)
C(6)-C(7)	1.398(4)	C(45)-H(45)	0.95
C(6)-H(6)	0.95	C(46)-C(47)	1.386(4)
C(7)-C(8)	1.368(4)	C(46)-C(52)	1.491(4)
C(7)-H(7)	0.95	C(47)-C(48)	1.389(5)
C(8)-C(9)	1.448(4)	C(47)-H(47)	0.95
C(9)-C(10)	1.368(4)	C(48)-C(49)	1.382(5)
C(10)-C(11)	1.397(4)	C(48)-H(48)	0.95
C(10)-H(10)	0.95	C(49)-C(50)	1.393(5)
C(11)-C(12)	1.371(4)	C(49)-H(49)	0.95
C(11)-H(11)	0.95	C(50)-C(51)	1.388(4)
C(12)-C(13)	1.459(4)	C(50)-H(50)	0.95
C(13)-C(22)	1.412(4)	C(51)-C(52)	1.384(4)
C(13)-C(14)	1.423(4)	C(51)-H(51)	0.95
C(14)-C(15)	1.377(4)	C(61)-O(5)	1.219(5)

Table 65 continued

Bond	Length (Å)	Bond	Length (Å)
C(14)-H(14)	0.95	C(61)-O(6)	1.304(4)
C(15)-C(16)	1.402(5)	C(61)-C(62)	1.478(6)
C(15)-H(15)	0.95	C(62)-C(63)	1.503(6)
C(16)-C(17)	1.384(4)	C(62)-H(62A)	0.99
C(16)-C(22)	1.488(4)	C(62)-H(62B)	0.99
C(17)-C(18)	1.397(5)	C(63)-C(64)	1.517(6)
C(17)-H(17)	0.95	C(63)-H(63A)	0.99
C(18)-C(19)	1.374(5)	C(63)-H(63B)	0.99
C(18)-H(18)	0.95	C(64)-C(65)	1.531(6)
C(19)-C(20)	1.402(5)	C(64)-H(64A)	0.99
C(19)-H(19)	0.95	C(64)-H(64B)	0.99
C(20)-C(21)	1.382(4)	C(65)-C(66)	1.515(6)
C(20)-H(20)	0.95	C(65)-H(65A)	0.99
C(21)-C(22)	1.383(4)	C(65)-H(65B)	0.99
C(21)-H(21)	0.95	C(66)-N(3)	1.592(5)
C(31)-O(3)	1.218(4)	C(66)-H(66A)	0.99
C(31)-O(4)	1.289(4)	C(66)-H(66B)	0.99
C(31)-C(32)	1.497(4)	N(3)-H(3A)	0.91
C(32)-C(34)	1.350(4)	N(3)-H(3B)	0.91
C(32)-C(33)	1.434(5)	N(3)-H(3C)	0.91
C(33)-N(2)	1.135(5)	O(1)-H(1)	0.84
C(34)-C(35)	1.425(4)	O(4)-H(4A)	0.84
C(34)-H(34)	0.95		

Table 66. Bond angles for 3-(5'-(azulen-1-yl)-[2,2'-bithiophen]-5-yl)-2-cyanoacrylic acid (**212**).

Bond	Angle (°)	Bond	Angle (°)
C(8)-S(1)-C(5)	92.04(14)	C(37)-C(38)-C(39)	128.0(3)
C(9)-S(2)-C(12)	92.69(15)	C(37)-C(38)-S(3)	111.2(2)
C(38)-S(3)-C(35)	92.00(15)	C(39)-C(38)-S(3)	120.8(2)
C(39)-S(4)-C(42)	92.82(14)	C(40)-C(39)-C(38)	129.9(3)
O(1)-C(1)-O(2)	126.5(3)	C(40)-C(39)-S(4)	110.2(2)
O(1)-C(1)-C(2)	117.8(3)	C(38)-C(39)-S(4)	119.9(2)
O(2)-C(1)-C(2)	115.6(3)	C(39)-C(40)-C(41)	113.9(3)
C(4)-C(2)-C(3)	122.1(3)	C(39)-C(40)-H(40)	123.1
C(4)-C(2)-C(1)	121.9(3)	C(41)-C(40)-H(40)	123.1
C(3)-C(2)-C(1)	116.0(3)	C(42)-C(41)-C(40)	114.0(3)
N(1)-C(3)-C(2)	179.2(3)	C(42)-C(41)-H(41)	123
C(2)-C(4)-C(5)	130.4(3)	C(40)-C(41)-H(41)	123
C(2)-C(4)-H(4)	114.8	C(41)-C(42)-C(43)	132.7(3)
C(5)-C(4)-H(4)	114.8	C(41)-C(42)-S(4)	109.1(2)
C(6)-C(5)-C(4)	125.2(3)	C(43)-C(42)-S(4)	118.1(2)
C(6)-C(5)-S(1)	109.8(2)	C(44)-C(43)-C(52)	107.2(3)
C(4)-C(5)-S(1)	124.9(2)	C(44)-C(43)-C(42)	123.3(3)
C(5)-C(6)-C(7)	113.9(3)	C(52)-C(43)-C(42)	129.5(3)
C(5)-C(6)-H(6)	123.1	C(45)-C(44)-C(43)	110.9(3)
C(7)-C(6)-H(6)	123.1	C(45)-C(44)-H(44)	124.5
C(8)-C(7)-C(6)	113.2(3)	C(43)-C(44)-H(44)	124.5
C(8)-C(7)-H(7)	123.4	C(44)-C(45)-C(46)	108.6(3)
C(6)-C(7)-H(7)	123.4	C(44)-C(45)-H(45)	125.7
C(7)-C(8)-C(9)	129.3(3)	C(46)-C(45)-H(45)	125.7
C(7)-C(8)-S(1)	111.1(2)	C(47)-C(46)-C(45)	124.4(3)
C(9)-C(8)-S(1)	119.5(2)	C(47)-C(46)-C(52)	128.6(3)
C(10)-C(9)-C(8)	127.9(3)	C(45)-C(46)-C(52)	107.0(3)
C(10)-C(9)-S(2)	110.2(2)	C(46)-C(47)-C(48)	129.0(3)
C(8)-C(9)-S(2)	121.8(2)	C(46)-C(47)-H(47)	115.5
C(9)-C(10)-C(11)	113.5(3)	C(48)-C(47)-H(47)	115.5
C(9)-C(10)-H(10)	123.3	C(49)-C(48)-C(47)	128.2(3)

Table 66 continued

Bond	Angle (°)	Bond	Angle (°)
C(11)-C(10)-H(10)	123.3	C(49)-C(48)-H(48)	115.9
C(12)-C(11)-C(10)	114.0(3)	C(47)-C(48)-H(48)	115.9
C(12)-C(11)-H(11)	123	C(48)-C(49)-C(50)	129.3(3)
C(10)-C(11)-H(11)	123	C(48)-C(49)-H(49)	115.3
C(11)-C(12)-C(13)	125.0(3)	C(50)-C(49)-H(49)	115.3
C(11)-C(12)-S(2)	109.7(2)	C(51)-C(50)-C(49)	130.1(3)
C(13)-C(12)-S(2)	125.3(2)	C(51)-C(50)-H(50)	115
C(22)-C(13)-C(14)	107.6(3)	C(49)-C(50)-H(50)	115
C(22)-C(13)-C(12)	131.2(3)	C(52)-C(51)-C(50)	128.6(3)
C(14)-C(13)-C(12)	121.2(3)	C(52)-C(51)-H(51)	115.7
C(15)-C(14)-C(13)	110.3(3)	C(50)-C(51)-H(51)	115.7
C(15)-C(14)-H(14)	124.8	C(51)-C(52)-C(43)	127.8(3)
C(13)-C(14)-H(14)	124.8	C(51)-C(52)-C(46)	126.0(3)
C(14)-C(15)-C(16)	108.6(3)	C(43)-C(52)-C(46)	106.2(3)
C(14)-C(15)-H(15)	125.7	O(5)-C(61)-O(6)	120.7(4)
C(16)-C(15)-H(15)	125.7	O(5)-C(61)-C(62)	124.4(4)
C(17)-C(16)-C(15)	124.2(3)	O(6)-C(61)-C(62)	114.9(3)
C(17)-C(16)-C(22)	128.5(3)	C(61)-C(62)-C(63)	116.1(4)
C(15)-C(16)-C(22)	107.3(3)	C(61)-C(62)-H(62A)	108.3
C(16)-C(17)-C(18)	128.9(3)	C(63)-C(62)-H(62A)	108.3
C(16)-C(17)-H(17)	115.6	C(61)-C(62)-H(62B)	108.3
C(18)-C(17)-H(17)	115.6	C(63)-C(62)-H(62B)	108.3
C(19)-C(18)-C(17)	128.5(3)	H(62A)-C(62)-H(62B)	107.4
C(19)-C(18)-H(18)	115.7	C(62)-C(63)-C(64)	113.2(4)
C(17)-C(18)-H(18)	115.7	C(62)-C(63)-H(63A)	108.9
C(18)-C(19)-C(20)	129.3(3)	C(64)-C(63)-H(63A)	108.9
C(18)-C(19)-H(19)	115.4	C(62)-C(63)-H(63B)	108.9
C(20)-C(19)-H(19)	115.4	C(64)-C(63)-H(63B)	108.9
C(21)-C(20)-C(19)	129.2(3)	H(63A)-C(63)-H(63B)	107.7
C(21)-C(20)-H(20)	115.4	C(63)-C(64)-C(65)	113.5(4)
C(19)-C(20)-H(20)	115.4	C(63)-C(64)-H(64A)	108.9
C(20)-C(21)-C(22)	129.7(3)	C(65)-C(64)-H(64A)	108.9
C(20)-C(21)-H(21)	115.1	C(63)-C(64)-H(64B)	108.9

Table 66 continued

Bond	Angle (°)	Bond	Angle (°)
C(22)-C(21)-H(21)	115.1	C(65)-C(64)-H(64B)	108.9
C(21)-C(22)-C(13)	128.0(3)	H(64A)-C(64)-H(64B)	107.7
C(21)-C(22)-C(16)	125.8(3)	C(66)-C(65)-C(64)	110.1(3)
C(13)-C(22)-C(16)	106.2(3)	C(66)-C(65)-H(65A)	109.6
O(3)-C(31)-O(4)	125.6(3)	C(64)-C(65)-H(65A)	109.6
O(3)-C(31)-C(32)	119.6(3)	C(66)-C(65)-H(65B)	109.6
O(4)-C(31)-C(32)	114.7(3)	C(64)-C(65)-H(65B)	109.6
C(34)-C(32)-C(33)	123.8(3)	H(65A)-C(65)-H(65B)	108.2
C(34)-C(32)-C(31)	118.9(3)	C(65)-C(66)-N(3)	110.1(3)
C(33)-C(32)-C(31)	117.3(3)	C(65)-C(66)-H(66A)	109.6
N(2)-C(33)-C(32)	178.8(4)	N(3)-C(66)-H(66A)	109.6
C(32)-C(34)-C(35)	131.7(3)	C(65)-C(66)-H(66B)	109.6
C(32)-C(34)-H(34)	114.2	N(3)-C(66)-H(66B)	109.6
C(35)-C(34)-H(34)	114.2	H(66A)-C(66)-H(66B)	108.2
C(36)-C(35)-C(34)	123.8(3)	C(66)-N(3)-H(3A)	109.5
C(36)-C(35)-S(3)	109.8(2)	C(66)-N(3)-H(3B)	109.5
C(34)-C(35)-S(3)	126.3(3)	H(3A)-N(3)-H(3B)	109.5
C(35)-C(36)-C(37)	114.2(3)	C(66)-N(3)-H(3C)	109.5
C(35)-C(36)-H(36)	122.9	H(3A)-N(3)-H(3C)	109.5
C(37)-C(36)-H(36)	122.9	H(3B)-N(3)-H(3C)	109.5
C(38)-C(37)-C(36)	112.8(3)	C(1)-O(1)-H(1)	109.5
C(38)-C(37)-H(37)	123.6	C(31)-O(4)-H(4A)	109.5
C(36)-C(37)-H(37)	123.6		

Table 67. Anisotropic displacement parameters ($Å^2$ x 10^3) for 3-(5'-(azulen-1-yl)-[2,2'-bithiophen]-5-yl)-2-cyanoacrylic acid (**212**). The anisotropic displacement factor exponent takes the form: $-2\pi^2[h^2 a^{*2}U^{11} + ... + 2 h k a^* b^* U^{12}]$.

	U11	U22	U33	U23	U13	U12
S(1)	42(1)	38(1)	26(1)	-2(1)	-10(1)	-1(1)
S(2)	44(1)	38(1)	33(1)	2(1)	-16(1)	-7(1)
S(3)	44(1)	38(1)	31(1)	1(1)	-9(1)	-3(1)
S(4)	44(1)	35(1)	40(1)	-3(1)	-15(1)	0(1)
C(1)	38(2)	38(2)	33(2)	4(1)	-6(1)	-1(1)
C(2)	36(2)	35(2)	28(1)	1(1)	-5(1)	0(1)
C(3)	48(2)	42(2)	27(1)	-2(1)	-13(1)	3(1)
C(4)	38(2)	35(2)	30(1)	0(1)	-3(1)	-3(1)
C(5)	35(2)	39(2)	28(1)	0(1)	-4(1)	-3(1)
C(6)	40(2)	41(2)	35(2)	-2(1)	-6(1)	-6(1)
C(7)	41(2)	45(2)	32(1)	-2(1)	-10(1)	-5(1)
C(8)	32(1)	44(2)	25(1)	-4(1)	-4(1)	-3(1)
C(9)	35(2)	43(2)	25(1)	-3(1)	-6(1)	-1(1)
C(10)	52(2)	43(2)	34(2)	-7(1)	-17(1)	-2(1)
C(11)	56(2)	38(2)	37(2)	-6(1)	-13(1)	-3(1)
C(12)	38(2)	33(2)	32(1)	-3(1)	-5(1)	-2(1)
C(13)	40(2)	36(2)	32(1)	-3(1)	-9(1)	-1(1)
C(14)	50(2)	37(2)	41(2)	-4(1)	-12(1)	-6(1)
C(15)	56(2)	35(2)	41(2)	2(1)	-9(2)	-2(1)
C(16)	44(2)	38(2)	34(2)	1(1)	-6(1)	1(1)
C(17)	50(2)	43(2)	37(2)	3(1)	-9(1)	3(1)
C(18)	51(2)	56(2)	33(2)	-2(1)	-13(1)	3(2)
C(19)	49(2)	55(2)	35(2)	-9(1)	-12(1)	-7(2)
C(20)	53(2)	42(2)	35(2)	-3(1)	-9(1)	-9(1)
C(21)	49(2)	37(2)	32(2)	0(1)	-8(1)	-2(1)
C(22)	38(2)	35(2)	27(1)	1(1)	-5(1)	-1(1)
C(31)	42(2)	47(2)	32(2)	6(1)	-7(1)	0(1)
C(32)	40(2)	42(2)	30(1)	4(1)	-4(1)	-1(1)
C(33)	55(2)	49(2)	34(2)	7(1)	-15(1)	-4(2)
C(34)	40(2)	41(2)	36(2)	7(1)	-4(1)	-2(1)
C(35)	37(2)	41(2)	34(2)	5(1)	-4(1)	-4(1)

Table 67 continued

	U11	U22	U33	U23	U13	U12
C(36)	44(2)	39(2)	49(2)	6(1)	-12(1)	-7(1)
C(37)	45(2)	42(2)	48(2)	-1(1)	-16(1)	-7(1)
C(38)	31(1)	42(2)	34(2)	-1(1)	-5(1)	-4(1)
C(39)	34(2)	41(2)	31(1)	-2(1)	-5(1)	-4(1)
C(40)	59(2)	41(2)	33(2)	-1(1)	-12(1)	-8(2)
C(41)	54(2)	33(2)	35(2)	1(1)	-9(1)	-5(1)
C(42)	35(2)	34(2)	33(1)	0(1)	-4(1)	-2(1)
C(43)	32(1)	38(2)	35(2)	-4(1)	-4(1)	-2(1)
C(44)	41(2)	38(2)	46(2)	-5(1)	-7(1)	-3(1)
C(45)	43(2)	46(2)	48(2)	-15(2)	-12(1)	-6(1)
C(46)	36(2)	49(2)	34(2)	-10(1)	-4(1)	0(1)
C(47)	45(2)	62(2)	32(2)	-10(2)	-9(1)	-1(2)
C(48)	55(2)	66(2)	29(2)	0(2)	-9(1)	3(2)
C(49)	57(2)	53(2)	36(2)	4(2)	-5(2)	3(2)
C(50)	52(2)	42(2)	39(2)	-1(1)	-6(1)	-3(1)
C(51)	42(2)	40(2)	35(2)	-3(1)	-7(1)	-2(1)
C(52)	32(1)	40(2)	31(1)	-4(1)	-3(1)	0(1)
C(61)	61(2)	50(2)	41(2)	-1(2)	-7(2)	-9(2)
C(62)	66(3)	62(3)	72(3)	12(2)	-13(2)	-5(2)
C(63)	70(3)	77(3)	68(3)	15(2)	-18(2)	-9(2)
C(64)	66(3)	75(3)	55(2)	8(2)	-9(2)	-2(2)
C(65)	88(3)	69(3)	47(2)	3(2)	-12(2)	-11(2)
C(66)	79(3)	42(2)	41(2)	-3(2)	-9(2)	2(2)
N(1)	83(2)	39(2)	48(2)	-4(1)	-31(2)	5(2)
N(2)	106(3)	48(2)	57(2)	11(2)	-35(2)	-9(2)
N(3)	69(2)	68(2)	70(2)	-42(2)	-42(2)	32(2)
O(1)	61(2)	36(1)	51(1)	6(1)	-25(1)	-2(1)
O(2)	53(1)	39(1)	32(1)	1(1)	-16(1)	-1(1)
O(3)	72(2)	43(1)	53(1)	9(1)	-28(1)	-2(1)
O(4)	56(1)	46(1)	32(1)	4(1)	-14(1)	0(1)
O(5)	60(2)	104(3)	60(2)	-22(2)	4(1)	-21(2)
O(6)	78(2)	56(2)	55(2)	6(1)	-9(1)	-6(1)

Table 68. Crystal data and structure refinement for 3-(5'-(3-methylthioazulen-1-yl)-[2,2'-bithiophen]-5-yl)-2-cyanoacrylic acid (**214**).

Identification code	s16sel5a	
Empirical formula	C23 H15 N O2 S3	
Formula weight	433.54	
Temperature	150(2) K	
Wavelength	1.54184 Å	
Crystal system	Triclinic	
Space group	P-1	
Unit cell dimensions	a = 9.4510(5) Å	a= 76.551(4)°.
	b = 10.3205(4) Å	b= 78.594(5)°.
	c = 21.7815(11) Å	g = 72.217(4)°.
Volume	1949.05(17) $Å^3$	
Z	4	
Density (calculated)	1.477 Mg/m^3	
Absorption coefficient	3.647 mm^{-1}	
F(000)	896	
Crystal size	0.100 x 0.050 x 0.010 mm^3	
Theta range for data collection	4.214 to 68.604°.	
Index ranges	-11<=h<=7, -12<=k<=12, -26<=l<=25	
Reflections collected	12137	
Independent reflections	7089 [R(int) = 0.0631]	
Completeness to theta = 67.684°	99.10%	
Absorption correction	Semi-empirical from equivalents	
Max. and min. transmission	1.00000 and 0.86399	
Refinement method	Full-matrix least-squares on F2	
Data / restraints / parameters	7089 / 2 / 533	
Goodness-of-fit on F2	0.901	
Final R indices [I>2sigma(I)]	R1 = 0.0466, wR2 = 0.0850	
R indices (all data)	R1 = 0.0921, wR2 = 0.1068	
Extinction coefficient	n/a	
Largest diff. peak and hole	0.463 and -0.433 e.$Å^{-3}$	

Table 69. Atomic coordinates (x 10^4) and equivalent isotropic displacement parameters ($Å^2$ x 10^3) for 3-(5'-(3-methylthioazulen-1-yl)-[2,2'-bithiophen]-5-yl)-2-cyanoacrylic acid (**214**). U(eq) is defined as one third of the trace of the orthogonalized U^{ij} tensor.

	x	y	z	U(eq)
S(1)	5252(1)	10582(1)	6548(1)	27(1)
S(2)	5507(1)	12265(1)	7561(1)	29(1)
S(3)	2587(1)	14831(1)	9806(1)	36(1)
N(1)	1801(4)	10870(3)	6359(2)	35(1)
O(1)	1705(3)	8664(3)	5456(1)	31(1)
O(2)	4034(3)	7553(3)	5051(1)	31(1)
C(1)	3167(4)	8375(4)	5386(2)	26(1)
C(2)	3746(4)	9122(4)	5734(2)	24(1)
C(3)	2659(4)	10087(4)	6086(2)	27(1)
C(4)	5254(4)	8896(4)	5708(2)	26(1)
C(5)	6057(4)	9472(4)	6006(2)	24(1)
C(6)	7595(4)	9237(4)	5915(2)	28(1)
C(7)	8119(4)	9935(4)	6259(2)	25(1)
C(8)	6983(4)	10701(4)	6638(2)	24(1)
C(9)	7076(4)	11568(4)	7051(2)	26(1)
C(10)	8264(4)	12027(4)	7092(2)	24(1)
C(11)	7900(4)	12952(4)	7521(2)	26(1)
C(12)	6453(4)	13208(4)	7816(2)	24(1)
C(13)	5662(4)	14043(4)	8296(2)	28(1)
C(14)	4519(4)	13753(4)	8779(2)	28(1)
C(15)	4026(5)	14788(4)	9147(2)	29(1)
C(16)	1114(5)	16267(4)	9472(2)	37(1)
C(17)	4844(4)	15769(4)	8909(2)	27(1)
C(18)	4718(4)	16911(4)	9168(2)	33(1)
C(19)	5426(5)	17971(4)	8930(2)	43(1)
C(20)	6282(5)	18212(4)	8352(2)	40(1)
C(21)	6834(4)	17405(4)	7882(2)	34(1)
C(22)	6682(4)	16092(4)	7894(2)	28(1)
C(23)	5852(4)	15328(4)	8340(2)	26(1)
S(4)	-397(1)	4078(1)	3408(1)	26(1)

Table 69 continued

	x	y	z	U(eq)
S(5)	-441(1)	2120(1)	2477(1)	28(1)
S(6)	3125(1)	-621(1)	387(1)	33(1)
N(2)	3053(4)	3972(3)	3628(2)	34(1)
O(3)	608(3)	7382(3)	4840(1)	33(1)
O(4)	2945(3)	6224(3)	4479(1)	34(1)
C(31)	1494(5)	6516(4)	4535(2)	27(1)
C(32)	950(4)	5711(4)	4200(2)	26(1)
C(33)	2090(5)	4740(4)	3877(2)	28(1)
C(34)	-552(4)	5926(4)	4198(2)	26(1)
C(35)	-1295(4)	5290(4)	3896(2)	25(1)
C(36)	-2830(4)	5543(4)	3941(2)	28(1)
C(37)	-3271(4)	4787(4)	3603(2)	27(1)
C(38)	-2096(4)	3941(4)	3277(2)	25(1)
C(39)	-2106(4)	3019(4)	2870(2)	25(1)
C(40)	-3297(4)	2699(4)	2732(2)	27(1)
C(41)	-2871(4)	1751(4)	2310(2)	27(1)
C(42)	-1364(4)	1328(4)	2126(2)	25(1)
C(43)	-455(4)	406(4)	1697(2)	26(1)
C(44)	802(4)	649(4)	1269(2)	29(1)
C(45)	1497(4)	-469(4)	952(2)	27(1)
C(46)	2476(6)	783(6)	-235(3)	79(2)
C(47)	699(4)	-1470(4)	1177(2)	26(1)
C(48)	1064(4)	-2744(4)	994(2)	31(1)
C(49)	385(5)	-3823(4)	1227(2)	34(1)
C(50)	-800(5)	-3899(4)	1717(2)	36(1)
C(51)	-1636(4)	-2940(4)	2096(2)	32(1)
C(52)	-1532(4)	-1607(4)	2068(2)	27(1)
C(53)	-550(4)	-916(4)	1668(2)	27(1)

Table 70. Bond lengths for 3-(5'-(3-methylthioazulen-1-yl)-[2,2'-bithiophen]-5-yl)-2-cyanoacrylic acid (**214**).

Bond	Length (Å)	Bond	Length (Å)
S(1)-C(8)	1.729(4)	S(4)-C(38)	1.738(4)
S(1)-C(5)	1.740(4)	S(4)-C(35)	1.740(4)
S(2)-C(9)	1.739(4)	S(5)-C(42)	1.733(3)
S(2)-C(12)	1.741(3)	S(5)-C(39)	1.736(4)
S(3)-C(15)	1.770(4)	S(6)-C(45)	1.760(4)
S(3)-C(16)	1.817(4)	S(6)-C(46)	1.785(5)
N(1)-C(3)	1.139(5)	N(2)-C(33)	1.146(5)
O(1)-C(1)	1.307(5)	O(3)-C(31)	1.241(5)
O(1)-H(1A)	0.88(2)	O(4)-C(31)	1.298(5)
O(2)-C(1)	1.245(4)	O(4)-H(4A)	0.88(2)
C(1)-C(2)	1.471(5)	C(31)-C(32)	1.476(5)
C(2)-C(4)	1.364(5)	C(32)-C(34)	1.369(5)
C(2)-C(3)	1.433(5)	C(32)-C(33)	1.424(5)
C(4)-C(5)	1.415(5)	C(34)-C(35)	1.420(5)
C(4)-H(4)	0.95	C(34)-H(34)	0.95
C(5)-C(6)	1.381(5)	C(35)-C(36)	1.381(5)
C(6)-C(7)	1.394(5)	C(36)-C(37)	1.384(5)
C(6)-H(6)	0.95	C(36)-H(36)	0.95
C(7)-C(8)	1.375(5)	C(37)-C(38)	1.373(5)
C(7)-H(7)	0.95	C(37)-H(37)	0.95
C(8)-C(9)	1.439(5)	C(38)-C(39)	1.446(5)
C(9)-C(10)	1.370(5)	C(39)-C(40)	1.368(5)
C(10)-C(11)	1.410(5)	C(40)-C(41)	1.413(5)
C(10)-H(10)	0.95	C(40)-H(40)	0.95
C(11)-C(12)	1.365(5)	C(41)-C(42)	1.362(5)
C(11)-H(11)	0.95	C(41)-H(41)	0.95
C(12)-C(13)	1.453(5)	C(42)-C(43)	1.453(5)
C(13)-C(14)	1.402(5)	C(43)-C(44)	1.407(5)
C(13)-C(23)	1.419(5)	C(43)-C(53)	1.410(5)
C(14)-C(15)	1.395(5)	C(44)-C(45)	1.403(5)
C(14)-H(14)	0.95	C(44)-H(44)	0.95
C(15)-C(17)	1.403(5)	C(45)-C(47)	1.404(5)

Table 70 continued

Bond	Length (Å)	Bond	Length (Å)
C(16)-H(16A)	0.98	C(46)-H(46A)	0.98
C(16)-H(16B)	0.98	C(46)-H(46B)	0.98
C(16)-H(16C)	0.98	C(46)-H(46C)	0.98
C(17)-C(18)	1.385(5)	C(47)-C(48)	1.385(5)
C(17)-C(23)	1.476(5)	C(47)-C(53)	1.496(5)
C(18)-C(19)	1.400(6)	C(48)-C(49)	1.398(5)
C(18)-H(18)	0.95	C(48)-H(48)	0.95
C(19)-C(20)	1.369(6)	C(49)-C(50)	1.393(6)
C(19)-H(19)	0.95	C(49)-H(49)	0.95
C(20)-C(21)	1.390(6)	C(50)-C(51)	1.389(6)
C(20)-H(20)	0.95	C(50)-H(50)	0.95
C(21)-C(22)	1.399(5)	C(51)-C(52)	1.396(5)
C(21)-H(21)	0.95	C(51)-H(51)	0.95
C(22)-C(23)	1.379(5)	C(52)-C(53)	1.387(5)
C(22)-H(22)	0.95	C(52)-H(52)	0.95

Table 71. Bond angles for 3-(5'-(3-methylthioazulen-1-yl)-[2,2'-bithiophen]-5-yl)-2-cyanoacrylic acid (**214**).

Bond	Angle (°)	Bond	Angle (°)
C(8)-S(1)-C(5)	92.05(18)	C(38)-S(4)-C(35)	91.98(18)
C(9)-S(2)-C(12)	92.37(18)	C(42)-S(5)-C(39)	92.51(18)
C(15)-S(3)-C(16)	100.20(19)	C(45)-S(6)-C(46)	100.6(2)
C(1)-O(1)-H(1A)	115(4)	C(31)-O(4)-H(4A)	119(4)
O(2)-C(1)-O(1)	124.5(3)	O(3)-C(31)-O(4)	124.7(3)
O(2)-C(1)-C(2)	121.0(4)	O(3)-C(31)-C(32)	121.4(4)
O(1)-C(1)-C(2)	114.5(3)	O(4)-C(31)-C(32)	113.9(3)
C(4)-C(2)-C(3)	122.9(3)	C(34)-C(32)-C(33)	123.6(3)
C(4)-C(2)-C(1)	120.2(3)	C(34)-C(32)-C(31)	121.1(4)
C(3)-C(2)-C(1)	116.9(3)	C(33)-C(32)-C(31)	115.3(3)
N(1)-C(3)-C(2)	178.9(5)	N(2)-C(33)-C(32)	177.0(4)
C(2)-C(4)-C(5)	130.0(4)	C(32)-C(34)-C(35)	129.7(4)
C(2)-C(4)-H(4)	115	C(32)-C(34)-H(34)	115.1
C(5)-C(4)-H(4)	115	C(35)-C(34)-H(34)	115.1
C(6)-C(5)-C(4)	125.3(3)	C(36)-C(35)-C(34)	125.5(3)
C(6)-C(5)-S(1)	109.6(3)	C(36)-C(35)-S(4)	109.7(3)
C(4)-C(5)-S(1)	125.1(3)	C(34)-C(35)-S(4)	124.8(3)
C(5)-C(6)-C(7)	114.5(3)	C(35)-C(36)-C(37)	114.2(3)
C(5)-C(6)-H(6)	122.7	C(35)-C(36)-H(36)	122.9
C(7)-C(6)-H(6)	122.7	C(37)-C(36)-H(36)	122.9
C(8)-C(7)-C(6)	112.6(3)	C(38)-C(37)-C(36)	113.7(3)
C(8)-C(7)-H(7)	123.7	C(38)-C(37)-H(37)	123.2
C(6)-C(7)-H(7)	123.7	C(36)-C(37)-H(37)	123.2
C(7)-C(8)-C(9)	128.9(3)	C(37)-C(38)-C(39)	129.9(4)
C(7)-C(8)-S(1)	111.2(3)	C(37)-C(38)-S(4)	110.4(3)
C(9)-C(8)-S(1)	119.9(3)	C(39)-C(38)-S(4)	119.7(3)
C(10)-C(9)-C(8)	129.1(4)	C(40)-C(39)-C(38)	129.2(4)
C(10)-C(9)-S(2)	110.5(3)	C(40)-C(39)-S(5)	110.2(3)
C(8)-C(9)-S(2)	120.4(3)	C(38)-C(39)-S(5)	120.6(3)
C(9)-C(10)-C(11)	112.9(4)	C(39)-C(40)-C(41)	113.1(4)
C(9)-C(10)-H(10)	123.5	C(39)-C(40)-H(40)	123.4
C(11)-C(10)-H(10)	123.5	C(41)-C(40)-H(40)	123.4

Table 71 continued

Bond	Angle (°)	Bond	Angle (°)
C(12)-C(11)-C(10)	114.6(3)	C(42)-C(41)-C(40)	114.1(3)
C(12)-C(11)-H(11)	122.7	C(42)-C(41)-H(41)	123
C(10)-C(11)-H(11)	122.7	C(40)-C(41)-H(41)	123
C(11)-C(12)-C(13)	131.6(3)	C(41)-C(42)-C(43)	132.5(3)
C(11)-C(12)-S(2)	109.7(3)	C(41)-C(42)-S(5)	110.0(3)
C(13)-C(12)-S(2)	118.7(3)	C(43)-C(42)-S(5)	117.4(3)
C(14)-C(13)-C(23)	107.8(3)	C(44)-C(43)-C(53)	107.5(3)
C(14)-C(13)-C(12)	125.8(3)	C(44)-C(43)-C(42)	124.1(3)
C(23)-C(13)-C(12)	126.3(4)	C(53)-C(43)-C(42)	128.1(4)
C(15)-C(14)-C(13)	109.5(3)	C(45)-C(44)-C(43)	110.6(3)
C(15)-C(14)-H(14)	125.2	C(45)-C(44)-H(44)	124.7
C(13)-C(14)-H(14)	125.2	C(43)-C(44)-H(44)	124.7
C(14)-C(15)-C(17)	109.2(4)	C(44)-C(45)-C(47)	108.3(4)
C(14)-C(15)-S(3)	124.5(3)	C(44)-C(45)-S(6)	126.1(3)
C(17)-C(15)-S(3)	126.3(3)	C(47)-C(45)-S(6)	125.6(3)
S(3)-C(16)-H(16A)	109.5	S(6)-C(46)-H(46A)	109.5
S(3)-C(16)-H(16B)	109.5	S(6)-C(46)-H(46B)	109.5
H(16A)-C(16)-H(16B)	109.5	H(46A)-C(46)-H(46B)	109.5
S(3)-C(16)-H(16C)	109.5	S(6)-C(46)-H(46C)	109.5
H(16A)-C(16)-H(16C)	109.5	H(46A)-C(46)-H(46C)	109.5
H(16B)-C(16)-H(16C)	109.5	H(46B)-C(46)-H(46C)	109.5
C(18)-C(17)-C(15)	125.9(4)	C(48)-C(47)-C(45)	125.7(4)
C(18)-C(17)-C(23)	127.8(4)	C(48)-C(47)-C(53)	127.7(4)
C(15)-C(17)-C(23)	106.3(3)	C(45)-C(47)-C(53)	106.6(3)
C(17)-C(18)-C(19)	128.5(4)	C(47)-C(48)-C(49)	128.8(4)
C(17)-C(18)-H(18)	115.8	C(47)-C(48)-H(48)	115.6
C(19)-C(18)-H(18)	115.8	C(49)-C(48)-H(48)	115.6
C(20)-C(19)-C(18)	128.2(4)	C(50)-C(49)-C(48)	128.4(4)
C(20)-C(19)-H(19)	115.9	C(50)-C(49)-H(49)	115.8
C(18)-C(19)-H(19)	115.9	C(48)-C(49)-H(49)	115.8
C(19)-C(20)-C(21)	130.2(4)	C(51)-C(50)-C(49)	130.2(4)
C(19)-C(20)-H(20)	114.9	C(51)-C(50)-H(50)	114.9
C(21)-C(20)-H(20)	114.9	C(49)-C(50)-H(50)	114.9

Table 71 continued

Bond	Angle (°)	Bond	Angle (°)
C(20)-C(21)-C(22)	128.0(4)	C(50)-C(51)-C(52)	128.5(4)
C(20)-C(21)-H(21)	116	C(50)-C(51)-H(51)	115.7
C(22)-C(21)-H(21)	116	C(52)-C(51)-H(51)	115.7
C(23)-C(22)-C(21)	129.3(4)	C(53)-C(52)-C(51)	129.1(4)
C(23)-C(22)-H(22)	115.4	C(53)-C(52)-H(52)	115.5
C(21)-C(22)-H(22)	115.4	C(51)-C(52)-H(52)	115.5
C(22)-C(23)-C(13)	126.1(4)	C(52)-C(53)-C(43)	125.5(4)
C(22)-C(23)-C(17)	126.6(3)	C(52)-C(53)-C(47)	127.1(3)
C(13)-C(23)-C(17)	106.9(3)	C(43)-C(53)-C(47)	107.0(3)

Table 72. Anisotropic displacement parameters ($Å^2$ x 10^3) for 3-(5'-(3-methylthioazulen-1-yl)-[2,2'-bithiophen]-5-yl)-2-cyanoacrylic acid (**214**). The anisotropic displacement factor exponent takes the form: $-2\pi^2[h^2 a^{*2}U^{11} + ... + 2 h k a^* b^* U^{12}]$.

	U11	U22	U33	U23	U13	U12
S(1)	23(1)	29(1)	32(1)	-14(1)	-1(1)	-7(1)
S(2)	23(1)	34(1)	36(1)	-17(1)	1(1)	-9(1)
S(3)	38(1)	31(1)	31(1)	-6(1)	4(1)	-4(1)
N(1)	29(2)	33(2)	44(2)	-17(2)	-3(2)	-6(2)
O(1)	25(2)	39(2)	35(2)	-15(1)	-1(1)	-15(1)
O(2)	31(2)	31(2)	36(2)	-16(1)	1(1)	-10(1)
C(1)	27(2)	26(2)	25(2)	-4(2)	-4(2)	-9(2)
C(2)	27(2)	22(2)	24(2)	-5(2)	-3(2)	-6(2)
C(3)	25(2)	27(2)	31(2)	-5(2)	-6(2)	-10(2)
C(4)	30(2)	20(2)	26(2)	-5(2)	-2(2)	-5(2)
C(5)	21(2)	20(2)	30(2)	-8(2)	-2(2)	-2(2)
C(6)	29(2)	24(2)	29(2)	-9(2)	-3(2)	-3(2)
C(7)	17(2)	26(2)	30(2)	-8(2)	2(2)	-5(2)
C(8)	19(2)	21(2)	30(2)	-3(2)	-4(2)	-4(2)
C(9)	23(2)	24(2)	30(2)	-7(2)	-3(2)	-4(2)
C(10)	20(2)	22(2)	29(2)	-5(2)	-4(2)	-4(2)
C(11)	23(2)	23(2)	32(2)	-5(2)	-7(2)	-6(2)
C(12)	19(2)	24(2)	29(2)	-6(2)	-6(2)	-4(2)
C(13)	29(2)	26(2)	30(2)	-4(2)	-7(2)	-6(2)
C(14)	32(2)	22(2)	31(2)	-7(2)	-2(2)	-6(2)
C(15)	29(2)	30(2)	25(2)	-7(2)	1(2)	-7(2)
C(16)	34(3)	37(2)	39(2)	-9(2)	-2(2)	-7(2)
C(17)	25(2)	28(2)	30(2)	-8(2)	-6(2)	-4(2)
C(18)	29(2)	32(2)	39(2)	-15(2)	-6(2)	-2(2)
C(19)	54(3)	31(2)	51(3)	-19(2)	-14(2)	-11(2)
C(20)	43(3)	29(2)	58(3)	-11(2)	-14(2)	-14(2)
C(21)	28(2)	33(2)	44(2)	-5(2)	-6(2)	-11(2)
C(22)	21(2)	28(2)	37(2)	-10(2)	-5(2)	-5(2)
C(23)	22(2)	25(2)	32(2)	-9(2)	-9(2)	-3(2)
S(4)	24(1)	24(1)	31(1)	-12(1)	-2(1)	-6(1)

Table 72 continued

	U11	U22	U33	U23	U13	U12
S(5)	24(1)	28(1)	36(1)	-14(1)	-2(1)	-9(1)
S(6)	31(1)	31(1)	34(1)	-7(1)	4(1)	-8(1)
N(2)	31(2)	31(2)	43(2)	-13(2)	-7(2)	-6(2)
O(3)	37(2)	30(2)	38(2)	-16(1)	-5(1)	-9(1)
O(4)	28(2)	39(2)	41(2)	-18(1)	-2(1)	-12(1)
C(31)	36(2)	25(2)	24(2)	-6(2)	-1(2)	-13(2)
C(32)	30(2)	23(2)	25(2)	-6(2)	-4(2)	-8(2)
C(33)	37(3)	22(2)	28(2)	-7(2)	-3(2)	-12(2)
C(34)	34(2)	20(2)	24(2)	-7(2)	2(2)	-7(2)
C(35)	26(2)	20(2)	27(2)	-7(2)	1(2)	-3(2)
C(36)	26(2)	25(2)	32(2)	-10(2)	2(2)	-5(2)
C(37)	21(2)	26(2)	34(2)	-10(2)	1(2)	-7(2)
C(38)	27(2)	22(2)	28(2)	-5(2)	-1(2)	-10(2)
C(39)	24(2)	23(2)	27(2)	-3(2)	-3(2)	-7(2)
C(40)	15(2)	29(2)	36(2)	-7(2)	-2(2)	-5(2)
C(41)	20(2)	30(2)	35(2)	-10(2)	-6(2)	-8(2)
C(42)	26(2)	25(2)	27(2)	-5(2)	-6(2)	-7(2)
C(43)	26(2)	24(2)	29(2)	-6(2)	-6(2)	-7(2)
C(44)	32(2)	24(2)	32(2)	-7(2)	-9(2)	-6(2)
C(45)	27(2)	28(2)	26(2)	-5(2)	-2(2)	-9(2)
C(46)	70(5)	70(4)	55(4)	21(3)	10(3)	8(3)
C(47)	28(2)	30(2)	24(2)	-9(2)	-5(2)	-9(2)
C(48)	29(2)	34(2)	30(2)	-10(2)	-3(2)	-9(2)
C(49)	47(3)	27(2)	32(2)	-11(2)	-5(2)	-13(2)
C(50)	43(3)	28(2)	41(2)	-5(2)	-8(2)	-18(2)
C(51)	24(2)	35(2)	39(2)	-3(2)	-1(2)	-15(2)
C(52)	24(2)	26(2)	32(2)	-6(2)	-5(2)	-6(2)
C(53)	28(2)	27(2)	28(2)	-6(2)	-9(2)	-7(2)

Compound List

1 – azulene
2 – guaiazulene
3 - 1-formylazulene
4 - 1,3-diformylazulene
5 - triethylorthoformate
6 - 1-acylazulene
7 - 1-bromoazulene
8 - 1,3-dibromoazulene
9 - 1-hydroazulenium
10 - 1-(R-methyl-1-ene)azulenium
11 - 1-nitroazulene
12 - 1,3-dinitroazulene
13 - 5-nitroazulene
14 - 1-nitrosoazulene
15 - 1-(azulen-1-yl)-2-aryldiazene
16 - 1-azulenesulfonic acid
17 - 4-subs-azulene addition intermediate
18 - 4-substituted azulenes
19 – Chamazulene
20 – Vetivazulene
21 – Indane
22 – Ethyldiazoacetate
23 - ethyl 1,1a,3,4,5,6a-hexahydrocyclopropa[f]indene-1-carboxylate
24 - 1,1a,3,4,5,6a-hexahydrocyclopropa[f]indene-1-carboxylic acid
25 – Pyridine
26 - 1-chloro-2,4-dinitrobenzene
27 - 1-(2,4-dinitrophenyl)pyridin-1-ium Zincke salt
28 - (2Z,4E)-N1-(2,4-dinitrophenyl)-N1,N1,N5,N5-tetramethylpenta-2,4-diene-1,1,5-triamine Zeigler-Hafner synth intermediate
29 - N,N,N',N'-tetramethylpenta-1,3-dien-1,5-diamine
30 - unsaturated diaminoaminofulvene
31 - 7-oxocyclohepta-1,3,5-trien-1-yl 4-methylbenzenesulfonate
32 - malonitrile anion
33 - 2-(7-oxocyclohepta-1,3,5-trien-1-yl)malononitrile
34 - 2-imino-2H-cyclohepta[b]furan-3-carbonitrile
35 - (3-cyano-8a-(dicyanomethyl)-8aH-cyclohepta[b]furan-2-yl)amide
36 - (2-amino-3-cyano-8aH-cyclohepta[b]furan-8a-yl)dicyanomethanide
37 - 2-amino-1-cyano-1-(7-(dicyanomethylene)cyclohepta-1,3,5-trien-1-yl)-2-oxoethan-1-ide
38 - (1-carbamoyl-1,3-dicyanoazulen-2(1H)-ylidene)amide
39 - (1,3-dicyano-2-imino-1,2-dihydroazulene-1-carbonyl)amide
40 - (1,3-dicyanoazulen-2-yl)amide
41 - 2-aminoazulene-1,3-dicarbonitrile
42 – diethylmalonate
43 - diethyl 2-hydroxyazulene-1,3-dicarboxylate
44 - 2,4,6-trimethylpyrylium BF_4
45 – cyclopentadienide
46 - TMAz synth intermediate 1
47 - TMAz synth intermediate rearranged
48 - 4,6,8-trimethylazulene, TMAz
49 - 3-phenylpropionylchloride
50 - 1-diazo-4-phenylbutan-2-one
51 - 4-phenylbutan-2-one carbine intermediate
52 - 3a,3b-dihydro-1H-cyclopenta[1,3]cyclopropa[1,2]benzen-3(2H)-one
53 - 2,3-dihydroazulen-1(8aH)-one
54 - 2,3-dihydroazulen-1(4H)-one
55 - 3-bromo-3-phenylpropanoyl chloride
56 - 4-bromo-1-diazo-4-phenylbutan-2-one
57 - 3-bromo-2,3-dihydroazulen-1(8aH)-one
58 - azulen-1-yl acetate
59 - 6-dimethylaminofulvene
60 - 6-acyloxyfulvenes
61 - substituted 2-pyrones
62 - substituted thiophene-1,1-dioxides
63 - thiophene-1,1-dioxide
64 - 6-dimethylaminofulvene
65 - [6 + 4] intermediate with SO2 bridge
66 - [6 + 4] intermediate after SO2 extrusion
67 - 1-diethylaminobutadiene
68 – 6-(4-nitrobenzoyloxy)fulvene
69 - Houk [6 + 4] intermediate A

70 - Houk [6 + 4] intermediate B
71 - [2 + 2] cycloaddition products with four-membered rings
72 - 2,2-dichlorocyclopentanones
73 - cyclopentanone analogues
74 - 4-nitrobenzoic acid
75 - 7-R-cycloheptatriene
76 - a,a-dichlorocyclobutanone mono addition adduct
77 - a,a-dichlorocyclobutanone di addition adduct
78 - 3,3-dichloro-3,3a,8,8a-tetrahydroazulen-2(1H)-ones
79 - 3-chloro-8,8a-dihydroazulen-2(1H)-ones
80 - 3-chloro-1,2,8,8a-tetrahydroazulen-2-ols
81 - 1-chloro-3a,4-dihydroazulenes
82 - 1-chloroazulenes
83 - 2-hydroxyazulene
84 - Az-1-tcaa, 3-(5-(azulen-1-yl)thiophen-2-yl)-2-cyanoacrylic acid
85 - Az-2-tcaa, 3-(5-(azulen-2-yl)thiophen-2-yl)-2-cyanoacrylic acid
86 - Az-6-tcaa, 3-(5-(azulen-6-yl)thiophen-2-yl)-2-cyanoacrylic acid
87 - 5-(azulen-1-yl)thiophene-2-carboxaldehyde
88 - cyanoacetic acid
89 - dimethyl 5-ethynylisophthalate
90 - dimethyl 5-(9-borabicyclo[3.3.1]nonan-9-ylethynyl)isophthalate
91 - dimethyl 5-(azulen-1-ylethynyl)isophthalate
92 - 1-iodoazulene
93 - tetramethylsilylacetylene
94 - (azulen-1-ylethynyl)trimethylsilane
95 - 1-ethynylazulene
96 - dimethyl 5-iodoisophthalate
97 - 6-bromoazulene
98 - 6-(tri-n-butylstannyl)azulenes
99 - 4-halotoluene
100 - Stille 6-azulene x-coupled product
101 - 2-iodoazulene
102 - 2-isopropoxy-4,4,5,5-tetramethyl-1,3,2-dioxaborolane
103 - 2-azulenylboronate
104 - 1-azulene triflate
105 - 1-ethylazulene
106 - 1-(pseudo)haloazulene
107 – 5-metallated-thiophene-2-carboxaldehyde
108 - 1-bromo-4,6,8-trimethylazulene, 1-Br-TMAz
109 - methyl 5-(4,4,5,5-tetramethyl-1,3,2-dioxaborolan-2-yl)thiophene-2-carboxylate
110 - 4-bromo-1-diazo-4-phenylbutan-2-one
111 - azulenyl-1-triflate
112 - 1-chloroazulene
113 - dicyclohexyl(2',6'-dimethoxy-[1,1'-biphenyl]-2-yl)phosphine, SPhos ligand
114 - 1-(azulen-1-yl)-5-hydroxypentane-1,4-dione
115 - (5-(azulen-1-yl)thiophen-2-yl)methanol
116 - 1,4-diketone stetter product
117 - thiazolium salt
118 - Breslow intermediate
119 - Vilsmeier reagent, substituted chloroiminium ion
120 - 4,6,8-trimethylazulene-1-carboxaldehyde, TMAz-CHO
121 – 2-butyne-1,4-diol
122 - 1-hydroxybut-3-en-2-one
123 - methylvinylketone
124 - 3-benzyl-5-(2-hydroxyethyl)-4-methylthiazol-3-ium
125 - 1-(4,6,8-trimethylazulen-1-yl)pentane-1,4-dione
126 - azulen-1-yllithium
127 - 2-(azulen-1-yl)-4,4,5,5-tetramethyl-1,3,2-dioxaborolane
128 - cinnamic acid
129 - 3-bromo-3-phenylpropanoic acid
130 - 3-bromo-3-phenylpropanoyl chloride
131 - 4-bromo-1-diazo-4-phenylbutan-2-one
132 - 1,3-dichloroazulene
133 - thiophene-2-carboxaldehyde
134 - ethane-1,2-diol (ethylene glycol)
135 - 2-(thiophen-2-yl)-1,3-dioxolane
136 – trimethylborate
137 - dimethyl (5-(1,3-dioxolan-2-yl)thiophen-2-yl)boronate
138 - 5-Formyl-2-thiopheneboronic acid
139 – diethanolamine
140 - 8-(5-formylthiophen-2-yl)hexahydro-[1,3,2]oxazaborolo[2,3-b][1,3,2]oxazaborol-4-ium-8-uide
141 - dicyclohexyl(2',4',6'-triisopropyl-[1,1'-biphenyl]-2-yl)phosphine – Xphos

142 - 2-(5-(1,3-dioxolan-2-yl)thiophen-2-yl)-4,4,5,5-tetramethyl-1,3,2-dioxaborolane (thiophene pinacol ester coupling partner)
143 - 2-(5-(azulen-1-yl)thiophen-2-yl)-1,3-dioxolane
144 - 1-chloro-4,6,8-trimethylazulene 1-cl-TMAz
145 - 2-(5-(4,6,8-trimethylazulen-1-yl)thiophen-2-yl)-1,3-dioxolane
146 - 5-(4,6,8-trimethylazulen-1-yl)thiophene-2-carboxaldehyde
147 - TMAz-1-tcaa, 3-(5-(4,6,8-trimethylazulen-1-yl)thiophen-2-yl)-2-cyanoacrylic acid
148 – piperidine
149 - cyanoacetic acid enolate
150 - aldehyde (generic)
151 - dye enolate (generic)
152 - protonated dye enolate (generic)
153 - Knoevenagel condensation product (generic)
154 - Az-1-caa - 3-(azulen-1-yl)-2-cyanoacrylic acid
155 - TMAz-1-caa - 3-(4,6,8-trimethylazulen-1-yl)-2-cyanoacrylic) acid
156 - 1,3-di-tert-butylazulenes
157 - 1,3-bis(methylthio)azulenes
158 - tert-butanol
159 - 1-tert-butylazulene
160 - 1,3-di-tert-butylazulene
161 - tetrahydrothiophene-1-oxide (TMSO)
162 - 1-(3-tert-butylazulen-1-yl)tetrahydrothiophenium PF6
163 - 2-(5-(3-(tert-butyl)azulen-1-yl)thiophen-2-yl)-1,3-dioxolane
164 - 5-(3-(tert-butyl)azulen-1-yl)thiophene-2-carboxaldehyde
165 - DMSO dimethylsulfoxide
166 - triflic anhydride
167 - Tf2O activated DMSO
168 - 1-(dimethylsulfonium)azulene
169 - 1,3-bis(dimethylsulfonium)azulene
170 - 1,3-bis(methylthio)azulene
171 - 5-isopropyl-3,8-dimethylazulene-1-carbonyl bromide
172 - ethyl 5-isopropyl-3,8-dimethylazulene-1-carboxylate
173 - ethyl 3-formyl-5-isopropyl-8-methylazulene-1-carboxylate
174 - N-tert-butylhydroxylamine HCl
175 - N-tert-butyl-alpha-(7-isopropyl-4-methyl-3-ethoxycarbonyl-azulen-1-yl)nitrone
176 - 5-isopropyl-3,8-dimethylazulene-1-oxalyl chloride
177 - ethyl 2-(5-isopropyl-3,8-dimethylazulen-1-yl)-2-oxoacetate
178 – THF
179 - 4-bromobutan-1-ol
180 - 4-bromobutyl 5-isopropyl-3,8-dimethylazulene-1-carboxylate
181 - 1-tert-butylazulene
182 - Az-Pd(2)-tBu complex
183 - isobutene
184 - Az-Pd(2)-H complex
185 - 1-tert-butyl-3-formylazulene
186 - ipso-substitution wheland intermediate
187 - tert-butyl cation
188 - ipso-substitution iminium ion
189 - 1,3-di-tert-butyl-5-formylazulene
190 - azulene de-formylation Wheland intermediate
191 – pyrrole
192 - azulene de-formylation Wheland-pyrrole intermediate
193 - 2-pyrrolecarboxaldehyde
194 - 1,3-di-tert-butyl-4,6,8-trimethylazulene
195 - trifluoroacetic anhydride
196 - dimethylsulfonium ditrifluoroacetate
197 - 1-(dimethylsulfonium)azulene Wheland intermediate
198 - 1-(methylthio)azulene
199 – (3-(5-formylthiophen-2-yl)azulen-1-yl)dimethylsulfonium
200 - 5-(3-(methylthio)azulen-1-yl)thiophene-2-carbaldehyde
201 - (3-(5-formylthiophen-2-yl)-4,6,8-trimethylazulen-1-yl)dimethylsulfonium
202 - 5-(4,6,8-trimethyl-3-(methylthio)azulen-1-yl)thiophene-2-carbaldehyde
203 - 3-(5-(3-(methylthio)azulen-1-yl)thiophen-2-yl)cyanoacrylic acid - MeT-Az-1-tcaa
204 - 3-(5-(4,6,8-trimethyl-3-(methylthio)azulen-1-yl)thiophen-2-yl)cyanoacrylic acid - MeT-TMAz-1-tcaa
205 - 3-(5-(3-(tert-butyl)azulen-1-yl)thiophen-2-yl)-2-cyanoacrylic acid – tBu-Az-1-tcaa
206 - 2-cyano-3-(thiophen-2-yl)acrylic acid
207 - azulenyl-1-tetrahydrothiophenium PF6
208 - 4-tolylboronic acid
209 - 1-(4-tolyl)azulene
210 - 1-(4,6,8-trimethylazulen-1-yl)tetrahydrothiophenium
211 - 2,2-bithiophene
212 - Az-1-ttcaa 3-(5'-(azulen-1-yl)-[2,2'-bithiophen]-5-yl)-2-cyanoacrylic acid

213 – TMAz-1-ttcaa 3-(5'-(4,6,8-trimethylazulen-1-yl)-[2,2'-bithiophen]-5-yl)-2-cyanoacrylic acid
214 – MeTAz-1-ttcaa 3-(5'-(3-methylthioazulen-1-yl)-[2,2'-bithiophen]-5-yl)-2-cyanoacrylic acid
215 – tBuAz-1-ttcaa 3-(5'-(3-tert-butylazulen-1-yl)-[2,2'-bithiophen]-5-yl)2-cyanoacrylic acid
216 - (5'-formyl-[2,2'-bithiophen]-5-yl)boronic acid
217 - 2,2'-bithiophene
218 - 2,2'-bithiophene-2-carboxaldehyde
219 - Neopentyl glycol
220 - 2-([2,2'-bithiophen]-5-yl)-5,5-dimethyl-1,3-dioxane
221 - 3-bromopropan-1-ol
222 - 2-([2,2'-bithiophen]-5-yl)-1,3-dioxane
223 - 5,5-dimethyl-2-(thiophen-2-yl)-1,3-dioxane
224 - 2-([2,2'-bithiophen]-5-yl)-5,5-dimethyl-1,3-dioxane
225 - 2-(5'-(1,3-dioxan-2-yl)-[2,2'-bithiophen]-5-yl)-4,4,5,5-tetramethyl-1,3,2-dioxaborolane
226 - 2-(5'-(5,5-dimethyl-1,3-dioxan-2-yl)-[2,2'-bithiophen]-5-yl)-4,4,5,5-tetramethyl-1,3,2-dioxaborolane
227 - 2-(5'-(azulen-1-yl)-[2,2'-bithiophen]-5-yl)-1,3-dioxane
228 - 2-(5'-(azulen-1-yl)-[2,2'-bithiophen]-5-yl)-5,5-dimethyl-1,3-dioxane
229 - 5'-(azulen-1-yl)-[2,2'-bithiophene]-5-carboxaldehyde
230 - 5'-(4,6,8-trimethylazulen-1-yl)-[2,2'-bithiophene]-5-carboxaldehyde
231 - 5'-(3-(tert-butyl)azulen-1-yl)-[2,2'-bithiophene]-5-carboxaldehyde
232 - 5'-(3-(methylthio)azulen-1-yl)-[2,2'-bithiophene]-5-carboxaldehyde